Chemical Profiling of Five Canadian Haskap Berry Varieties and the Roles of their Phenolic Extracts in Modulating Cellular Stress in Human Fibroblasts

A Thesis Submitted to the College of

Graduate and Postdoctoral Studies

in Partial Fulfillment of the Requirements for the

Degree of Master of Science in the Department of

Food and Bioproduct Sciences

University of Saskatchewan

Saskatoon, Saskatchewan, Canada

By

Lily Zehfus

PERMISSION TO USE

In presenting this thesis in partial fulfillment of the requirements for a Postgraduate degree from the University of Saskatchewan, I agree that the Libraries of this University may make it freely available for inspection. I further agree that permission for copying of this thesis in any manner, in whole or in part, for scholarly purposes may be granted by the professor or professors who supervised my thesis work or, in their absence, by the Head of the Department or the Dean of the College in which my thesis work was done. It is understood that any copying, publication, or use of this thesis or parts thereof for financial gain shall not be allowed without my written permission. It is also understood that due recognition shall be given to me and to the University of Saskatchewan in any scholarly use which may be made of any material in my thesis.

Requests for permission to copy or to make other use of material in this thesis in whole or part should be addressed to:

Head of the Department of Food and Bioproduct Sciences

University of Saskatchewan

Saskatoon, Saskatchewan, S7N 5A8

Canada

Dean

College of Graduate and Postdoctoral Studies

University of Saskatchewan

116 Thorvaldson Building, 110 Science Place

Saskatoon, Saskatchewan S7N 5C9

Canada

ABSTRACT

Interest in plant phenolic structure(s) and their applications has grown due to their potent antioxidant and nutraceutical potential. Many plant species produce phenolics for a variety of functions, with high levels of these compounds often found in berry fruits. When applied to cells and organisms, berry fruit phenolics have shown anti-aging, anticancer, and anti-inflammatory activities. Haskap berries (*Lonicera caerulea*) are an edible honeysuckle species that contain very high levels of phenolics when compared to other commercial fruits. In this study, the chemical and physicochemical composition of five Canadian haskap berry varieties (Aurora, Blizzard, Honey Bee, Indigo Gem, and Tundra) was determined, with a focus on phenolic analysis and the *in vitro* health-promoting potential of these compounds. Total phenolic chromatographic indices (TPCI) using high performance liquid chromatography with photodiode array detection (HPLC-PDA) identified anthocyanins as the major phenolic subclass with cyanidin-3-*O*-glucoside, cyanidin-3,5-*O*-diglucoside, and cyanidin-3-*O*-rutinoside being the most prevalent. HPLC-tandem mass spectrometry (HPLC-MS/MS) was also employed to identify haskap phenolic structures including three previously unreported phenolic compounds. *In vitro* free radical scavenging assays showed that these haskap varieties had higher radical scavenging abilities than many other fruits (e.g. blueberry) with the Tundra variety demonstrating the highest capacity. These experiments led to selection of the Tundra variety for use in tissue culture assays due to its high phenolic content and free radical scavenging abilities. Phenolic extracts and fractions from Tundra haskap berries were produced using solid phase extraction, so as to separate phenolic subclasses for comparative cell line treatments *in vitro*.

In tissue culture assays, phenolic extracts from the Tundra variety slowed the growth of fibroblasts isolated from healthy donors (2DD) and immortalized (NB1 hTERT) fibroblasts without inducing cell death, indicating potential biological impacts similar to resveratrol, a fruit phenolic known to promote cellular health. Tundra phenolic fractions also increased cellular protein and activity levels of Sirtuin-1 (SIRT1), decreased levels of the pro-inflammatory phospho-nuclear factor kappa B (phospho-NF-κB p65) and the phosphorylated mammalian target of rapamycin (phospho-mTOR), and increased nuclear factor erythroid 2 (Nrf2). These observations are significant as these activities have been linked to slowed aging, improved intracellular radical scavenging (resistance to oxidative stress), and decreased inflammatory responses. Tundra phenolic fraction activities were shown to rely primarily on SIRT1 by employing lentiviral and

siRNA SIRT1 knockdown cells, with additional SIRT1-independent mechanism(s) related to Nrf2 upregulation. These fractions also showed the ability to decrease transcript levels of select pro-inflammatory cytokines and antioxidant enzymes, demonstrating further anti-inflammatory activities along with decreased requirements for cellular antioxidant mechanisms. These experimental results indicated that Saskatchewan-bred haskaps have the potential to promote health *in vitro* by mediating cellular stress responses and may be candidates for use as nutraceutical supplements.

ACKNOWLEDGMENTS

TABLE OF CONTENTS

LIST OF TABLES

x

LIST OF FIGURES

LIST OF SYMBOLS AND ABBREVIATIONS

ABTS	2,2′-azinobis-3-ethylbenzthiazoline-sulfonic acid
ABTS$^{\bullet+}$	2,2′-azinobis-3-ethylbenzthiazoline-sulfonic acid radical cation
AMP	Adenosine monophosphate
AMPK	5'-AMP-activated kinase
ANOVA	Analysis of variance
C3G	Cyanidin-3-*O*-glucoside
cDNA	Complementary DNA
ChIP	Chromatin immunoprecipitation assay
cm	Centimetre(s)
CR	Caloric restriction
°C	Degree Celsius
Dalton	Da
DMEM	Dulbecco's Modified Eagle Medium
DPPH	2,2-diphenyl-1-picrylhydrazyl
DW	Dry weight
EFW	Ethanol-formic acid-water
FC	Folin-Ciocalteu
F/G	Fructose/glucose ratio
FW	Fresh weight
FWHM	Full width at half maximum
g	Gram(s)
GAE	Gallic acid equivalents
GI	Gastrointestinal
h	Hour(s)
HP1	Hairpin 1
HP1/2	Hairpin 1 and 2
HP2	Hairpin 2
HPAE	High performance anion exchange chromatography
HPAE-PAD	High performance anion exchange chromatography with pulsed amperometric detection

HPLC	High performance liquid chromatography
HPLC-PDA	High performance liquid chromatography with photodiode array detection
HPLC-MS/MS	High performance liquid chromatography tandem mass spectrometry
HPLC-RI	High performance liquid chromatography with refractive index detection
hTERT	Human telomerase
IC_{50}	Concentration for 50% inhibition
iNOS	Inducible nitric oxide synthase
Kg	Kilogram(s)
L	Litre(s)
LPS	Lipopolysaccharide
M	Molar
mAU	Milli-absorbance units
μg	Microgram(s)
μL	Microlitre(s)
μM	Micromolar
min	Minute(s)
mg	Milligram(s)
mL	Millilitre(s)
mm	Millimetre(s)
mM	Millimolar
mTORC1	Mammalian target of rapamycin complex 1
mTORC2	Mammalian target of rapamycin complex 2
m/z	Mass to charge ratio
N	Normality
NAD	Nicotinamide adenine dinucleotide
NaOH	Sodium hydroxide
NF-κB	Nuclear factor kappa-light-chain-enhancer of activated B cells
nm	Nanometre(s)
NO	Nitric oxide
Nrf2	Nuclear factor erythroid-2 related factor 2
%	Percent

p53	Tumor suppressor protein 53
PAD	Pulsed amperometric detector
PCR	Polymerase chain reaction
PDA	Photodiode array detector
PGC-1α	Peroxisome proliferator-activated receptor gamma coactivator 1-α
PPAR-γ	Peroxisome proliferator-activated receptor-γ
r	Correlation coefficient
RI	Refractive index
ROS	Radical oxygen species
RS	Radical scavenging
RT	Retention time(s)
RT-qPCR	Reverse transcriptase-quantitative PCR
sec	Second(s)
shRNA	Short hairpin RNA
SIR2	Sirtuin-2
siRNA	Small interfering RNA
SIRT1	Sirtuin-1
Sirtuin	Silent mating type information regulation
s/n	Signal-to-noise ratio
TEAC	Trolox equivalence antioxidant capacity
TPC	Total phenolic content
TPCI	Total phenolic chromatographic index/indices
UV	Ultraviolet
UV-vis	Ultraviolet-visible
V	Volts

1. INTRODUCTION

1.1 Summary

Haskap berries (*Lonicera caerulea*) are an edible honeysuckle of the class Caprifoliaceae, native to northern boreal regions of the world, with wild varieties growing naturally in Asia, Europe, and North America (Celli et al., 2014). Haskaps have been an integral part of commercialized horticulture in parts of Japan and Russia for over a century (Celli et al., 2014). In North America, haskaps failed to gain breeder interest until the 1990s (Bors, 2007). In 1998, the University of Saskatchewan's (UofS) Horticulture Field Lab began to pursue haskap breeding and quickly gained traction, developing their first hybrids by 2005. In recent years, the program has released seven varieties to the public, which are being grown and studied locally and internationally. The following Saskatchewan-bred and grown varieties were selected for this work: Aurora, Blizzard, Honey Bee, Indigo Gem, and Tundra.

Primary interest in haskap research began from a nutraceutical perspective, when it was discovered that the berries contain high levels of phenolic compounds (i.e. phenolics) (Celli et al., 2014). Phenolics are ubiquitous secondary metabolites in plants as derivatives of the phenylpropanoid pathway which primarily transforms the amino acid phenylalanine (and to a lesser extent, tyrosine) through the pentose phosphate and shikimate pathways (Lin et al., 2016). Phenolics can act as antioxidants within biological systems to neutralize reactive oxygen species (ROS) which can cause oxidative stress and inflammation, known contributors to many diseases such as cancer and diabetes (Aruoma et al., 2006). Phenolics have also exhibited anticancer properties in trials using human cancer cell lines and rat models (Vuong et al., 2014; Gruia et al., 2008). The mechanisms responsible for this activity beyond free radical scavenging have not been well-explored, which leads to this investigation of alternative biochemical pathways employing haskap phenolics and their possible unique composition.

Although many berry species contain phenolics, those that were previously considered to be high in these compounds have significantly less than haskaps; one popular species, blueberries,

have approximately one-third of the phenolic content of many haskap berry varieties (You et al., 2011). As the consumer market for haskaps grows, chemical and physicochemical data on these berries has become important for the development of haskap products. An in-depth knowledge of a berry's chemical composition can be instrumental to attract growers and industrial food processors to a promising new crop. The recently developed Canadian varieties have readily gained momentum in international markets strictly based on their taste and size, yet actual chemical compositional data remains limited (Bors, 2018). Access to scientific information could positively influence potential growers and processors as haskaps enter into North American berry markets and industries. Biological data could also promote haskaps for medical and nutraceutical applications, providing additional consumer appeal and demand.

1.2 Hypotheses and Objectives

The overarching goal of this research was to identify the chemical composition and physicochemical properties of five Canadian haskap berry varieties with a focus on their phenolic composition, and to employ a structure-function-mechanism approach to identify the impact of these compounds on cellular stress mechanisms. The central hypotheses of this research were as follows: (1) physicochemical and chemical analyses will identify unique compositional information about these Saskatchewan-bred and grown varieties; (2) phenolic compounds can be effectively extracted from haskap berries and can be fractionated based on their structures; and (3) phenolic extracts/fractions will have *in vitro* antioxidant activities and activate cellular pathways promoting cellular stress mediation.

In addressing these hypotheses, the following objectives were investigated: (1) determine the physicochemical (i.e. colour, pH, size, and °Brix) and chemical composition (i.e. carbohydrates/polyols, moisture, and organic acids/ascorbic acid) of five Saskatchewan-bred and grown haskap varieties (Aurora, Blizzard, Honey Bee, Indigo Gem, and Tundra); (2) extract and fractionate haskap phenolics from the five varieties employing ethanol:formic acid:water (70:2:28 (v:v:v)) and Amberlite® XAD16N resin; (3) determine the phenolic subclasses, concentrations, and antioxidant potentials of haskap phenolic extracts and fractions; and (4) examine the effects that haskap phenolic extracts and fractions have on cellular functions (e.g. antioxidant activity,

inflammation, and proliferation) in normal and immortalized human cell lines and explore their mechanism(s) of action.

2. LITERATURE REVIEW

2.1 Phenolic Compounds in Plants

Phenolic compounds (phenolics) are ubiquitous secondary metabolites in plant tissues that have a multitude of biological functions (Giada, 2013; Cheynier, 2012). These include but are not limited to roles in structural integrity, protection against ultraviolet (UV) radiation, and defensive mechanisms against pathogens (Bhattacharya et al., 2010; Pandey and Rizvi, 2009). Phenolics also contribute to a plant's sensory qualities such as colour, flavour, and odour (Pandey and Rizvi, 2009). These features attract pollinators and seed distributors, which are fundamental for plant reproductive success (Giada, 2013).

The basic structure of a phenolic is an aromatic ring with at least one hydroxyl group directly attached (Vermerris and Nicholson, 2006). A polyphenol refers to the direct linkage of more than one hydroxyl group to one or more aromatic rings (Vermerris and Nicholson, 2006). Within plant tissues, phenolics often exist as glycosides, esters, or as protein conjugates, due to the toxicity of their free forms (Giada, 2013; Vermerris and Nicholson, 2006). Though they all arise from the common intermediate phenylalanine (or the closely related tyrosine), phenolics are a structurally diverse group, with more than 8000 identified in the kingdom Plantae (Pandey and Rizvi, 2009).

2.2 Phenolic Classes/Subclasses

Phenolics are classified based on twelve different carbon skeleton structures which are shown in Table 2.1. Of these classes, the phenolic acids (e.g. hydroxybenzoic and hydroxycinnamic acids) and flavonoids are considered to be the most abundant in fruits (Haminiuk et al., 2012).

Table 2.1 Carbon chains of major phenolic classes.

Phenolic Class	Structure
Simple phenol, benzoquinones	C_6
Hydroxybenzoic acids	$C_6\text{-}C_1$
Acethophenones, phenylacetic acids	$C_6\text{-}C_2$
Hydroxycinnamic acids, phenylpropanoids	$C_6\text{-}C_3$
Napthoquinones	$C_6\text{-}C_4$
Xanthones	$C_6\text{-}C_1\text{-}C_6$
Stilbenes, anthraquinones	$C_6\text{-}C_2\text{-}C_6$
Flavonoids, isoflavonoids	$C_6\text{-}C_3\text{-}C_6$
Lignans, neolignans	$(C_6\text{-}C_3)_2$
Biflavonoids	$(C_6\text{-}C_3\text{-}C_6)_2$
Lignins	$(C_6\text{-}C_3)_n$
Tannins	$(C_6\text{-}C_3\text{-}C_6)_n$

2.2.1 Phenolic Acids

Phenolic acids are estimated to make up approximately one-third of the phenolics consumed in the average human's diet (Yang et al., 2001). They are defined by the presence of a carboxylic acid functional group which is generally esterified (Vermerris and Nicholson, 2006). There are two major subclasses of phenolic acids, the hydroxybenzoic and hydroxycinnamic acids, which are shown in Figure 2.1. Hydroxybenzoic acids have a 7-carbon ($C_6\text{-}C_1$) structure and usually occur as esters with those commonly found in fruits being gallic, syringic, and vanillic acids (Haminiuk et al., 2012). Hydroxycinnamic acids have a 9-carbon ($C_6\text{-}C_3$) structure with caffeic, chlorogenic, and *p*–coumaric acids being those most commonly found in fruits (Haminiuk et al., 2012). In a survey of ten haskap genotypes grown in the USA (Oregon), the concentration of hydroxycinnamates ranged from 30.4-156.2 mg/100 g FW (Chaovanalikit et al., 2004).

Hydroxybenzoic	Substituents				Hydroxycinnamic	Substituents			
Acid Derivatives	R_1	R_2	R_3	R_4	Acid Derivatives	R_1	R_2	R_3	R_4
Gallic Acid	OH	OH	OH	H	Caffeic Acid	H	OH	OH	H
Syringic Acid	OCH_3	OH	OCH_3	H	Ferulic	H	OCH_3	OH	H
Vanillic Acid	OCH_3	OH	OH	H	*p*-Coumaric Acid	H	H	OH	H
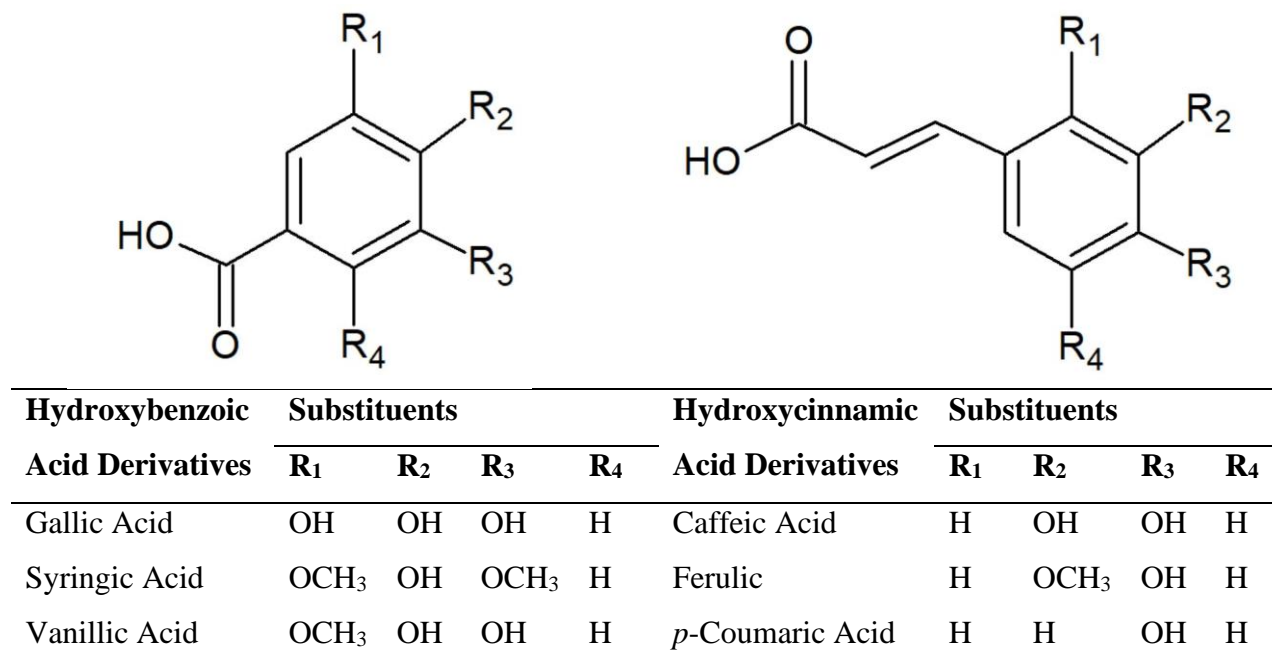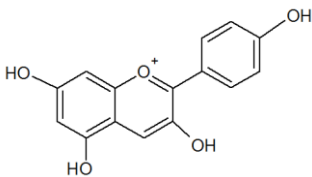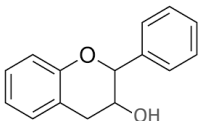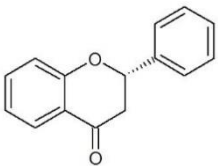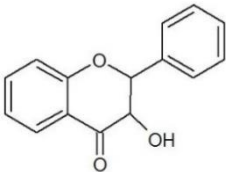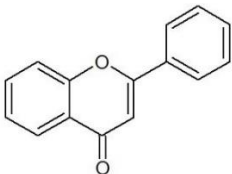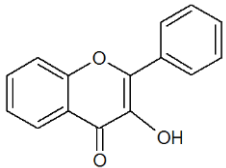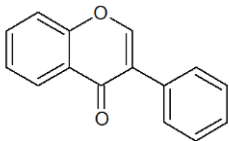
Figure 2.1 Basic phenolic acid structures.

2.2.2 Flavonoids

Flavonoids are the most abundant class of plant phenolics, constituting more than half of those naturally present (Balasundram et al., 2006). They exist primarily as glycosides, and are the main bioactive phenolic compounds found in fruits (Haminiuk et al., 2012; Heim et al., 2002). The basic structure of a flavonoid is C_6-C_3-C_6, with two aromatic rings joined by a 3-carbon bridge (Table 2.1). The flavonoids are further divided into 13 subclasses based on structural modifications (i.e. acylation, hydrogenation, hydroxylation) of the 3-carbon bridge (Giada, 2013; Vermerris and Nicholson, 2006). The most prominent flavonoid subclasses in fruits are the anthocyanidins, flavanols, flavanones, flavanonols, flavones, flavonols, and isoflavones (Table 2.2). In addition, flavonoids (e.g. flavonols) in fruits are often polymerized and are present as tannins (Pandey and Rizvi, 2009).

Table 2.2 Major subclasses of flavonoids and their dietary sources (Giada, 2013; Kumar and Pandey, 2013; United States Department of Agriculture, 2013; Heim et al., 2002).

Subclass	Basic Structure	Dietary Sources
Anthocyanidin		Bilberry, elderberry, haskap, red cabbage, wine
Flavanol		Apples, bananas, beer, black tea, blueberries
Flavanone		Citrus fruits, grapes, oregano, raw artichoke
Flavanonol		Apples, beer, broccoli, olive oil, onion, tea
Flavone		Celery seed, juniper berries, kumquats, parsley, pepper, radicchio, wine
Flavonol		Arugula, beer, capers, chokeberry, saffron, sea buckthorn, tea
Isoflavone		Soybeans

2.2.3 Anthocyanins

In many fruits, including haskap berries, the most abundant subclass of flavonoids is the anthocyanins. Anthocyanins are derivatives of anthocyanidins and result from glycosylation with a group of carbohydrates that can include galactose, gentiobiose, glucose, rhamnose, and rutinose (Corradini et al., 2011; Welch et al., 2008; Vermerris and Nicholson, 2006). Anthocyanin structures can vary by hydroxylation, methylation, position of carbohydrate attachment, as well as acylation of the associated carbohydrate(s) (Prior and Wu, 2006). Seventeen anthocyanidins have been identified in nature, with the most common in plants being cyanidin, delphinidin, malvidin, pelargonidin, peonidin, and petunidin, which are shown in Figure 2.2 (Del Rio et al., 2010; Ozga et al., 2006).
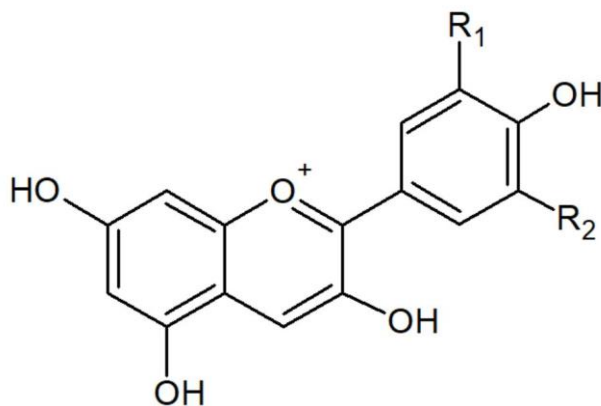
Anthocyanidins	R_1	R_2
Cyanidin	OH	H
Delphinidin	OH	OH
Malvidin	OCH_3	OCH_3
Pelargonidin	H	H
Peonidin	OCH_3	H
Petunidin	OCH_3	OH

Figure 2.2 Structures of the most common anthocyanidins found in plants.

Anthocyanins are water-soluble pigments that are generally stored in the vacuoles of coloured plant cells, such as in flower petals and fruits (Kong et al., 2003). Visible colouration may vary due to plant chemical properties such as anthocyanin content and concentration, pH, and

the presence of metal ions (Vermerris and Nicholson, 2006). In addition to colour, anthocyanins have other important plant functions such as antimicrobial, cold tolerance, and photoinhibition activities (Kong et al., 2003).

2.3 Phenolic Composition of Haskap Berries

The phenolic content of haskaps has been reported as 0.4% of the fresh weight (FW), with variation based on geographic origin (Palíková et al., 2008). In a review that included data on genotypes from six geographic regions (Canada, Czech Republic, Norway, Poland, Russia, USA), the most abundant phenolic classes reported in haskap berries were the flavonoids and phenolic acids, with anthocyanins as the major subclass of flavonoids (Celli et al., 2014).

The major anthocyanin reported in the fruit of ten Polish cultivars was cyanidin-3-*O*-glucoside, which accounted for 84-92% of the concentration of this subclass (Kusznierewicz et al., 2012). Other chromatographically identified anthocyanins and their concentrations in ten haskap genotypes (Oregon, USA) included cyanidin-3,5-*O*-diglucoside (2.2-6.4%), cyanidin-3-*O*-rutinoside (1-11%), peonidin-3-*O*-glucoside (0.3-1.3%), and pelargonidin-3-*O*-glucoside (0.2-1%) (Chaovanalikit et al., 2004). For the flavonols, the major constituents were quercetin derivatives, which included quercetin-3-*O*-galactoside, quercetin-3-*O*-glucoside, and quercetin-3-*O*-rutinoside (Kusznierewicz et al., 2012; Chaovanalikit et al., 2004).

The most abundant phenolic acids found in haskaps (two Russian varieties; ten varieties from Oregon, USA) were hydroxycinnamic acid derivatives, specifically, chlorogenic and neochlorogenic acids (Caprioli et al., 2016; Chaovanalikit et al., 2004). In addition, 4-aminobenzoic acid and gallic acid, both hydroxybenzoic acid derivatives, have been reported in two varieties of wild Eastern Russian haskaps at concentrations of 170 and 600 mg/kg FW, respectively (Gazdik et al., 2008). The aforementioned qualitative phenolic results are relatively consistent across haskap berry varieties from a range of geographic origins including Eastern Russia, Poland, and Western Canada (Caprioli et al., 2016; Jurikova et al., 2012a; Kusznierewicz et al., 2012).

The majority of analytical work on haskap phenolics has focused on wild and domesticated Eurasian varieties, with limited research conducted on those developed and grown in Canada. One

of the few studies on Canadian haskaps (Borealis, Indigo Gem, and Tundra varieties) compared their total phenolic content (TPC) and antioxidant capacities with blackberries, lowbush blueberries, partridgeberries, raspberries, red grapes, and strawberries, and showed that the Borealis haskap variety had the highest TPC at 622.52 mg gallic acid equivalents (GAE)/100 g FW (Rupasinghe et al., 2012).

2.4 Phenolics as Antioxidants

2.4.1 Antioxidant Mechanisms

Phenolics can act as antioxidants through the donation of electrons or hydrogen atoms (H-atom) to a free radical molecule (i.e. ROS) (Wright et al., 2001). During H-atom transfer, a compound loses a hydrogen atom followed by reaction with an O_2 molecule to produce an alkoperoxyl radical ($RO_2\bullet$). The alkoperoxyl radical can then participate in H-atom transfer resulting in a propagation reaction. An example of H-atom transfer is lipid peroxidation, where RH is an unsaturated fatty acid:

A. Initiation: $RH \rightarrow R\bullet$

B. Propagation: $R\bullet + O_2 \rightarrow RO_2\bullet$

$RO_2\bullet + RH \rightarrow ROOH + R\bullet$
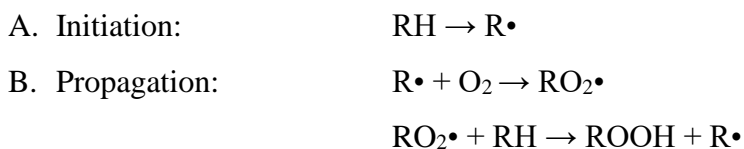
As antioxidants, phenolics can actively participate in H-atom transfer, where ArOH is a phenolic:

H-atom transfer: $RO_2\bullet + ArOH \rightarrow ROOH + ArO\bullet$
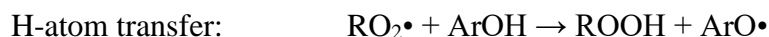
The resulting phenoxyl radical (ArO•) is much more stable than R•, which delays the overall oxidation reaction.

Phenolic compound antioxidant activity by electron transfer (steps A-E) involves chemical compound (e.g. unsaturated lipids) deprotonation in solution. Upon formation of the alkoperoxyl radical ($RO_2\bullet$), the phenolic donates an electron to form RO_2^-. In solution, the resulting positively charged phenolic is then deprotonated by the solvent (H_2O), after which the hydronium ion donates a proton to the ROS. The final products of the electron transfer process are peroxides (ROOH), H_2O, and the relatively stable phenoxyl radical (ArO•) (Wright et al., 2001):

A. Initiation: $RH \rightarrow R\bullet$

B. Propagation: $R\bullet + O_2 \rightarrow RO_2\bullet$

C. Electron Transfer: $RO_2\bullet + ArOH \rightarrow RO_2^- + ArOH^+$

D. Deprotonation: $ArOH^+ + H_2O \leftrightarrow ArO\bullet + H_3O^+$

E. Peroxide Formation: $RO_2^- + H_3O^+ \leftrightarrow ROOH + H_2O$

Both antioxidant mechanisms rely on the relative stability of phenoxyl radicals, which are less likely to participate in propagation reactions due to resonance of the unpaired electron in the aromatic ring(s), coupled with the steric hindrance of substituents on these rings. In addition to the aforementioned antioxidant mechanisms, phenolics have the ability to chelate trace metal ions, preventing them from contributing to ROS formation (i.e. Fenton reaction) and have been shown to upregulate cellular antioxidant defense mechanisms (Kumar and Pandey, 2013).

2.4.2 Phenolic Structure and Free Radical Scavenging

Research on how differences in phenolic structure impact reaction kinetics and free radical scavenging (RS) potential often employ one or more *in vitro* system (e.g. ABTS, DPPH, ORAC). Sample performance in different RS assays can be highly variable, as results depend on the assay (i.e. free radical) and experimental conditions. These issues make it difficult to summarize phenolic RS abilities without focusing on mechanisms that are applicable to a specific assay. With recent emphasis on the RS abilities of naturally occurring phenolics from plant extracts, comparative analyses (e.g. blueberry *vs.* saskatoon berry) have become more complicated, as diverse combinations of phenolics are found in any given plant extract.

Though phenolics can have a wide range of potential structures, RS efficiency is highly dependent on common features present in these compounds. In general, the number of hydroxyl groups on the aromatic ring(s) is the most significant structural feature in determining free radical scavenging potential, with more hydroxyl groups increasing antioxidant activity (Heim et al., 2002; Rice-Evans et al., 1996). Phenolic compound RS efficiency is also impacted by other factors such as proximity and position (i.e. *ortho-* or *para-*) of other functional groups (e.g. alkyl groups on neighboring carbons), conjugation, and the amount and position of glycosylation (Wang et al., 1997).

The use of *in vitro* assays for measuring phenolic activity is convenient and provides useful antioxidant data particularly when coupled with chromatographic methods. However, data obtained from *in vivo* experiments must be obtained to establish biochemical mechanism(s) of action for phenolics (Granato et al., 2018).

2.4.2.1 Phenolic Acid Free Radical Scavenging

The two main phenolic acid subclasses in fruits are the hydroxybenzoic and hydroxycinnamic acids (Figure 2.1). Hydroxybenzoic acids usually exhibit lower RS activity than hydroxycinnamic acids which is proposed to be due to the CH=CH-COOH side chain (found in hydroxycinnamic acids), which leads to greater stability as a phenoxyl radical (Mathew et al., 2015; Yamagami et al., 2005). Phenolic acid RS activity can also be enhanced by the presence of methoxy groups found in the *ortho-* position in relation to hydroxyl groups, and by additional hydroxyl groups (Mathew et al., 2015). Select hydroxycinnamic and hydroxybenzoic acids are commonly used as standards for RS comparisons (e.g. gallic acid, a hydroxybenzoic acid; and caffeic acid, a hydroxycinnamic acid) (Todorova et al., 2010).

2.4.2.2 Flavonoid Free Radical Scavenging

Flavonoids are a major polyphenol class in fruits, which encompass many of the subclasses (e.g. anthocyanins, flavanols, flavonols) prevalent in haskaps and other berry species. Many individual flavonoids are well known for their RS abilities such as: catechin, a flavanol; and quercetin and rutin, both flavonols (Kähkönen et al., 2003). Antioxidant activity of flavonoids has been linked to hydroxylation of the B-ring, especially for 3'4'-*ortho*-positioned hydroxylation (Figure 2.3) (Kumar and Pandey, 2013; Rice-Evans et al., 1996). This configuration is especially important for flavonoids with a saturated 2,3-bond in the C-ring (e.g. flavanols and flavanones; Table 2.2) (Wang et al., 1997).
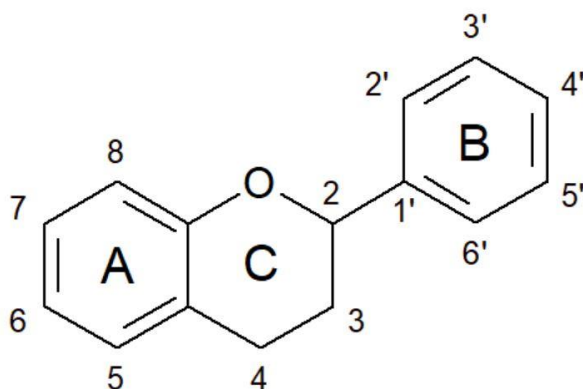
Figure 2.3 Numbering system of a basic flavonoid.

Although it is generally accepted that RS activity increases with the number of hydroxyl groups, the anthocyanin subclass, particularly the aglycones (i.e. anthocyanidins), can violate this norm. As an example, for delphinidin, the presence of an additional hydroxyl group at the 5' position decreased RS activity in comparison to cyanidin, which has an equivalent structure but lacks the 5' hydroxyl (Figure 2.2) (Wang et al., 1997). In addition, RS activity results for anthocyanins have led to literature controversy, with increased values being reported for malvidin (the aglycone) *vs.* malvidin-3-*O*-glucoside (Rice-Evans et al., 1996) and decreased values for petunidin (the aglycone) *vs.* petunidin-3-*O*-glucoside (Kähkönen et al., 2003) depending on the assay. It has also been shown that carbohydrate structure of the anthocyanin (e.g. cyanidin-3-*O*-glucoside and cyanidin-3-*O*-galactoside) can have a significant impact on compound RS activities (Wang et al., 1997). These results show how important phenolic structural features are in RS reactions, with the position of a single hydroxyl group on the aromatic ring(s) altering a compound's activity (Wang et al., 1997).

2.5 Analysis of Phenolics

2.5.1 Extraction and Fractionation

The most common methods of phenolic extraction from plant tissues employ solvents and are based on liquid-liquid and solid phase (i.e. solid-liquid) mechanisms (Ignat et al., 2011). Liquid-liquid extraction involves the treatment of a liquid sample (e.g. berry macerate) with a solvent that has a strong affinity for the molecules of interest, resulting in an extract that is rich in

these compounds (e.g. phenolic rich). Solid phase extraction employs an insoluble stationary phase (e.g. hydrophobic resin) that has a strong affinity for the molecules of interest in the liquid sample resulting in the molecules of interest being bound to the stationary phase (Ignat et al., 2011). Fractionation is an extension of the solid phase methodology, which involves the stationary phase (i.e. the solid to which the molecules of interest have been bound) being treated with progressively more nonpolar solvents, so as to elute molecules of interest sequentially based on their structure.

Typically, these extraction techniques employ an acidified organic solvent, which can damage/destroy cell membranes to improve phenolic extraction, and dissolve and stabilize phenolics (García-Salas et al., 2010). Use of these solvents can also chemically denature enzymes (i.e. polyphenol oxidase) that would otherwise degrade phenolic compounds. Some commonly used solvents are acetone, acidified ethanol or methanol (e.g. 2% formic acid), ethyl acetate, and propanol, though food grade ethanol-based solvents are preferred for food industry applications (Ignat et al., 2011; García-Salas et al., 2010). Other factors impacting extraction efficiency include temperature, light exposure, length of time for solvent contact, and characteristics of the specific berry (e.g. fruit pectin content). In addition to these phenolic extraction techniques, it has also been reported that the application of additional sample preparation steps such as boiling, freeze-drying (often followed by grinding), pH adjustment, and sonication of fruit tissues can improve phenolic extraction efficiency (Auzanneau et al., 2018; Kusznierewicz et al., 2012; Merken and Beecher, 2000).

2.5.2 High Performance Liquid Chromatography (HPLC)

Analytical procedures for phenolics include chromatography, spectroscopy, electrophoresis, and high performance liquid chromatography (HPLC), with the latter being the technique most widely used (Khattab et al., 2016). Phenolic separation by HPLC is generally achieved using reverse-phase chromatography systems (i.e. hydrophobic stationary phase), typically employing C_{18} as the stationary phase (Merken and Beecher, 2000). Columns with a range of physical properties have been published for phenolic analysis including: C_{18} columns of 2.1-4.6 mm in diameter, 100-300 mm in length, with stationary phase particle sizes of 2.5-10 µm, and pore sizes of 80-100 Å (Auzanneau et al., 2018; Caprioli et al., 2016; Kusznierewicz et al., 2012; Merken and Beecher, 2000). Mobile phases coupled with these stationary phases typically employ

gradient systems using an acidified aqueous phase (e.g. acetic, formic, perchloric, or phosphoric acids) and an organic phase (e.g. acetonitrile or methanol), which is often acidified (Auzanneau et al., 2018; Ignat et al., 2011; Merken and Beecher, 2000).

The most common detector used in conjunction with HPLC for phenolics is photodiode array (PDA) which has the ability to monitor multiple wavelengths simultaneously (Khattab et al., 2016). Phenolics absorb in the ultraviolet (UV) range and have varying lambda max values (λ_{max}) determined by their structural features and conjugation (Khattab et al., 2016). Published methods report monitoring over a wide range of wavelengths based on the target phenolics such as: 210-350 nm/hydroxycinnamic acids (Caprioli et al., 2016); 500 nm/anthocyanins (Auzanneau et al., 2018; Caprioli et al., 2016); and 250-500 nm/all major phenolic classes/subclasses (Auzanneau et al., 2018). Monitoring at different wavelengths improves detection (i.e. higher sensitivity and lower detection limits) of target phenolics and also aids in quantification accuracy as both standards and samples can be measured at or close to their λ_{max}.

Other parameters (e.g. flow rate, gradient system, run time) are highly varied based on the sample being analyzed, its phenolic composition, and the goal of the analysis (i.e. compound identification or quantitation). Many HPLC methods for phenolic analysis have run times in the realm of 60 min, though some as high as 340 min have been reported, specifically for isoflavone separation (Merken and Beecher, 2000). Many HPLC methods are now run in tandem with mass spectrometry for a more detailed structural analysis of phenolics, which will be described in the next section.

2.5.3 Mass Spectrometry (MS)

An alternate system for phenolic analysis that is becoming more widely reported in literature is mass spectrometry (MS). The principle of mass spectrometry is the creation and isolation of gas-phase ions so as to obtain their molecular ion mass-to-charge (*m/z*) ratio which can be used for structural identification (El-Aneed et al., 2009). This analytical technique can also be used to break down ions of a particular *m/z* (precursor ion) into their smaller structural components (product ions), which yields the unique molecular fingerprint of the molecule. The results of these ion fragmentations can then be used for detailed analysis and compositional identification of a sample.

The coupling of HPLC with MS is becoming the standard for analysis of fruit phenolics. However, there are many considerations that must be observed to effectively combine these techniques (Ribeiro de Souza et al., 2019; Khoddami et al., 2013; Welch et al., 2008). Many MS systems are not compatible with certain mobile/stationary phase combinations (e.g. mobile phases employing buffers, high acid, or salt) and flow rates commonly used for HPLC alone. For the latter, many MS systems have a maximum flow intake rate of 0.2-0.3 mL/min, which is much lower than the flow rates generally used in HPLC phenolic methods of 0.8-1.5 mL/min (Merken and Beecher, 2000). Therefore, in order to successfully meld these techniques, method adjustments are often necessary to overcome potential system incompatibilities between HPLC and MS.

Another important consideration is selecting the proper MS configuration (e.g. ionization method and mass analyzer) to meet the research goal. The most common method of sample ionization for phenolics is electrospray ionization (ESI), a soft ionization technique that minimizes the amount of energy transferred to the analyte molecule (El-Aneed et al., 2009). ESI applies a high voltage to a liquid spray, creating an aerosol of ionized molecules without the structural damage that may result from harsher ionization methods such as electron impact (EI), which bombards analyte molecules with high energy electrons (El-Aneed et al., 2009; Welch et al., 2008). ESI can be used in either positive or negative ion mode, so as to maximize ionization efficiency, which is dependent on the structure of the molecules of interest (e.g. negative ion for phenolic acids and positive ion for anthocyanins).

Following ionization, charged molecules enter the mass analyzer which separates these ions based on their m/z values. Many types of mass analyzers are commercially available which have different resolutions (i.e. ion separation) and sensitivities (i.e. detection limits) and must be selected appropriately to meet the goal of the analysis. One commonly used analyzer is time of flight (ToF), which separates ions in a long vacuum tube under an electric field and can have a resolution >30,000 FWHM (full width at half maximum; Balogh, 2004). FWHM describes mass spectrometer resolving power based on peak width where narrower peaks yield higher FWHM values (i.e. superior ion separation/resolution). ToF instruments also have impressive mass accuracy capabilities up to four decimal places (seven significant figures for masses 100-999 Da; Brenton and Godfrey, 2010).

Quadrupole analyzers are also common in mass spectrometers and consist of four parallel rods with oscillating electrical fields that can filter ions of a particular m/z and have a resolution <10,000 FWHM (Balogh, 2004). Quadrupole analyzers are often selected for targeted analyte quantification because of their filtering abilities despite the lower resolution. Phenolic methods have been developed using both of these analyzers including ToF for anthocyanin analysis (Caprioli et al., 2016) and a triple quadrupole (QqQ) for anthocyanin and flavonol analysis (Kusznierewicz et al., 2012). Phenolic methods have also employed a quadrupole paired with a ToF (qToF) to combine the filtering power of the quadrupole with the mass accuracy and resolution of the ToF (Wojdylo et al., 2013).

Following sample analysis, the resulting analyte fragmentation patterns are used to determine the structure of the corresponding phenolic compounds with the aid of literature. For example, the mass difference between a precursor and product ion can identify the presence and structure of a carbohydrate moiety (e.g. hexose or pentose) or other functional group (e.g. methoxy) attached to a phenolic. A significant limitation of MS analysis is the inability to distinguish between phenolics that may have the same precursor and product m/z values (e.g. cyanidin-3-*O*-glucoside and cyanidin-3-*O*-galactoside). The addition of HPLC separation can negate this issue if these compounds have different elution times and available standards. Another potential solution is the use of ion mobility MS (IMS), which can separate ions based on shape and size in addition to m/z values (Armenta et al., 2011). IMS has been successfully used to separate and identify fruit phenolic isomers, specifically, chlorogenic acids in apple and pear juices (Willems et al., 2016).

2.6 Health Potential of Phenolics

The basic unit of eukaryotic life, the cell, possess many mechanisms to respond to different types of stress which can include heat shock, osmotic changes, low cellular energy, and oxidative stress. Oxidative stress occurs when high concentrations of cellular ROS cannot be effectively neutralized, leading to a defensive inflammatory response that can be harmful over time (i.e. chronic inflammation). Cells employ protein-based antioxidant mechanisms to counteract the production of ROS resulting from cellular metabolism; however, these mechanisms are not always sufficient. Oxidative stress and inflammation have been implicated in the onset and progression of

many human diseases, including but not limited to cancer, neurodegenerative diseases, diabetes, cardiovascular disease, as well as aging (Li et al., 2014; Aruoma et al., 2006). The nutraceutical value of plant phenolics has been widely attributed to their RS abilities, which can aid cells in their natural defensives (Li et al., 2017; Seeram, 2008). The consumption of phenolic rich fractions from berry fruits could mitigate oxidative stress by reducing ROS levels and limiting cell damage (e.g. membrane and mitochondrial), leading to decreased stress responses (e.g. inflammation), a lower incidence of the aforementioned diseases, and even slower aging. Additional mechanisms and activities (e.g. anticancer) are also being explored to assess the full potential of fruit phenolics.

2.7 Phenolic Activities *in vitro* and *in vivo*

2.7.1 Anticancer Activity

Initial trials of candidate drug treatments often begin with viability testing *in vitro*. These experimental protocols use cultured cells to determine if and at what concentration a treatment is lethal, in addition to its functional range. A number of scientific studies have been conducted on the viability of healthy/normal and cancer cells treated with a range of phenolic extracts. Phenolic rich fruit extracts have shown a variety of anticancer properties including inhibition of proliferation and metastasis, induction of apoptosis, and cytotoxicity, with minimal negative impact on normal cells (Seeram, 2008).

Select examples of the *in vitro* anticancer properties of fruit phenolics include: (a) a phenolic rich blueberry extract (150 µg/mL) was found to induce caspase-dependent apoptosis in HT29 colon cancer cells (Srivastava et al., 2007); (b) blueberry phenolic extracts (25-100 µg/mL) caused growth arrest in G2/M phase and cell death in two high-risk acute lymphoblastic leukemia-derived cell lines (SEM and RS4;11) (Zunino et al., 2010); (c) cervical cancer (HeLa) cells showed less than 20% cell survival after 72 h treatment with lingonberry phenolic extracts (40 µg GAE/mL) (McDougall et al., 2008); and (d) lowbush blueberry flavonoid extracts were able to inhibit metastasis by downregulating proteins required for cellular/matrix adhesion (matrix metalloproteinases) (Matchett et al., 2006; Kleiner and Stetler-Stevenson, 1999).

If the primary bioactive role of fruit phenolics was free radical scavenging, these compounds would in theory promote the health and growth of all cells, both normal and cancerous.

The observed anticancer results go beyond RS for fruit phenolics, evidence that additional phenolic mechanisms are at play.

2.7.2 Anti-inflammatory Activity

Another major research focus is the effects of phenolic compounds on inflammatory responses, as inflammation is one of the major drivers contributing to the development/onset of many common diseases. The pro-inflammatory process involves many molecules with a wide range of functions including: (a) enzymes (e.g. inducible nitric oxide synthase (iNOS)) that can produce nitric oxide (NO) or other chemicals to promote vasodilation and recruit immune cells (e.g. leukocytes); (b) cytokines (e.g. interleukins) which can activate immune cells; and (c) other mediators (e.g. histamine and prostaglandins) which can contribute to many of the common symptoms of inflammation such as pain (Abdulkhaleq et al., 2018; Ambriz-Pérez et al., 2016; Hassimotto et al., 2013). The ability of phenolic extracts to decrease the inflammatory response can be assessed by monitoring levels of a selection of these molecules such as iNOS, interleukin-6 (IL-6), prostaglandin E2 (PGE$_2$), and tumor necrosis factor (TNF-α) (Hassimotto et al., 2013).

A multitude of anti-inflammatory activities have been reported for fruit phenolics including: (a) reduced serum levels of iNOS and TNF-α in male Wistar rats after treatment with cyanidin-3-O-glucoside (0.9 mmole/kg body weight) (Tsuda et al., 2002); (b) lower levels of lipopolysaccharide (LPS)-induced NO production were observed for a murine macrophage cell line (RAW 264.7) treated with 50 µg/mL of a grapefruit phenolic extract (García-Martínez et al., 2017); and (c) LPS-stimulated murine macrophage cells (RAW 264.7) treated with 250 µg/mL of a blueberry phenolic extract showed suppressed IL-6 and IL-1β transcript levels by greater than 50% relative to untreated controls (Grace et al., 2019). Multiple studies have shown that other berry (e.g. raspberry and strawberry) phenolic treatments can lead to decreased levels of many of the aforementioned pro-inflammatory molecules, ameliorating cellular inflammatory responses (Giampieri, et al., 2017; Li et al., 2017; Costamagna et al., 2016; Taverniti et al., 2014). These anti-inflammatory abilities demonstrate an important aspect of cellular stress mediation that can have widespread health-promoting effects in cells and organisms.

2.8 Healthy Aging

Aging is a complex process that results in accumulated damage (e.g. DNA mutations) at the cellular level, which ultimately leads to a decline in function and death of the organism. Although all lifeforms are subject to this process, the rate of biological aging can vary significantly amongst individuals of the same chronological age, dependent on genetics and environmental exposures. Healthy aging is the concept that through external factor control (e.g. diet, exercise, limiting exposure to harmful chemicals/UV rays), the biological aging process can be slowed, resulting in a decrease or later onset of age-related pathologies (e.g. cardiovascular disease, cancer, diabetes) and delayed loss of function (e.g. hearing, sight loss) over time.

The free radical theory of aging suggests that cumulative free radical damage is a major contributor to biological aging and gradually leads to disease and deterioration (Buehler, 2012). If this injurious cycle can be controlled, theoretically, the aging process could be slowed, resulting in healthy aging. Because of their role in cellular RS and modulation of responses to oxidative stress (i.e. inflammation), phenolics could potentially have a significant role in the regulation of the biological aging process.

A method that has been well-documented in improving health and extending lifespan of model organisms is caloric restriction (CR), which is the reduction (typically 20-40%) of nutrient intake without causing malnutrition (Gillespie, et al. 2016; Taormina and Mirisola, 2014). CR is theorized to drive the upregulation of autophagy, a cellular process where old, damaged proteins and organelles are recycled for energy and protein biosynthesis (Escobar et al., 2019; Taormina and Mirisola, 2014). Although several CR strategies (i.e. decreased amino acid levels) are associated with autophagy activation, other environmental/dietary conditions are being investigated to determine whether they could have similar impacts, leading to increased cellular health and slower aging.

2.8.1 Caloric Restriction (CR) Mimetics: The Sirtuin Proteins

Though the benefits of CR are well-recognized and replicable, long-term CR for humans is not considered a feasible strategy to promote healthy aging, as it would require both indefinite self-control and significant nutritional knowledge to be safely and successfully implemented. As a result, there is scientific interest in discovering a treatment or dietary supplement that could

mimic the effects of CR without requiring diet reduction. In order to achieve this, cellular targets must be identified that are involved in the health and aging processes.

One of the targets for CR mimicry is Sirtuin-1 (SIRT1). Initial interest in the Sirtuin (silent mating type information regulation) protein family arose due to studies in yeast (*Saccharomyces cerevisiae*) which showed that the homolog, Sirtuin-2 (SIR2), was important in mechanisms of health-promotion and aging pathways (Guarente, 2007; Wood et al., 2004). Overexpression of SIRT1 has been shown to significantly extend lifespan in yeast and fruit flies, and it has become a popular focus in human studies, particularly for age-related pathologies (e.g. Alzheimer's disease, type 2 diabetes) (Kaeberlein, 2010; Rogina and Helfand, 2004). SIRT1 also gained interest for phenolic studies when resveratrol, a commonly studied grape phenolic, was shown to increase its activities (Azorín-Ortuño et al., 2012; Kaeberlein, 2010). SIRT1's importance in mechanisms of stress mediation (e.g. inflammation), health-promotion, and aging, along with its activation by other fruit phenolics, make it a cellular target for phenolic extracts from haskaps.

2.8.2 SIRT1 Cellular Functions

SIRT1 functions as a protein deactetylase that removes acetyl groups from lysine residues of cellular proteins in the presence of nicotinamide adenine dinucleotide (NAD) (Rahman and Islam, 2011). SIRT1 has been found to act on many different substrates (e.g. histones, transcription factors, and cofactors) and is vital in a wide range of biological processes including aging, metabolic function, and stress response regulation (e.g. inflammation) (Rahman and Islam, 2011; Guarente, 2007; De Boer et al., 2006). Its activities are also intertwined with many other biological pathways, increasing the complexity and importance of its roles in cellular function. Examples of SIRT1 substrates and their functions include: (a) tumor suppressor protein 53 (p53) for regulation of the cell cycle and suppression of tumor formation (Rahman and Islam, 2011); (b) transcription factors of the Forkhead box (FOX) family (e.g. FOXO1 and FOXO3) for DNA repair and metabolic signaling (Maiese et al., 2008); and (c) the Nuclear factor kappa-light-chain-enhancer of activated B cells (NF-κB) protein complex for cytokine production and DNA transcription regulation (Rahman and Islam, 2011; Guarente, 2007).

SIRT1 levels and activity are dependent on many intracellular conditions and relationships. One of the primary feedback loops for SIRT1 regulation involves NAD and nicotinamide (NAM),

a product of the deacetylation reaction (Imai, 2009). SIRT1 activity increases with NAD levels and decreases as NAM increases. SIRT1 has a positive reciprocal relationship with adenosine monophosphate (AMP)-activated protein kinase (AMPK) which is vital for metabolic regulation such as glucose uptake control (Giovannini and Bianchi, 2017). Increases in AMPK (and SIRT1) repress the mammalian target of rapamycin complexes 1 and 2 (mTORC1 and mTORC2) which has been investigated as an anticancer mechanism (Giovannini and Bianchi, 2017). SIRT1 has also been shown to upregulate nuclear factor erythroid-2 related factor 2(Nrf2), a transcription factor that modulates the expression of antioxidant enzymes (Zhang et al., 2018). If a treatment and/or dietary supplement alters SIRT1 levels/activity, it could be doing so through any one of these relationships, making determination of the exact mechanistic pathway a challenge. A visual of these selected SIRT1 relationships is shown in Figure 2.4.
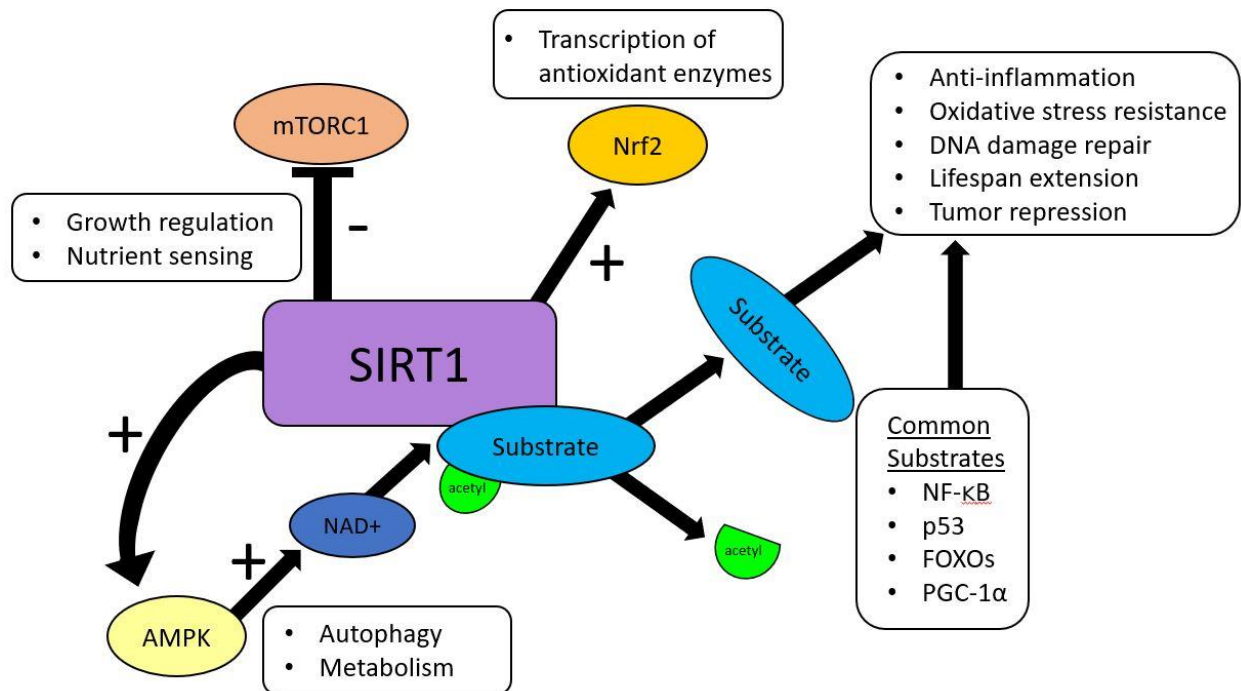
Figure 2.4 The relationships and roles of SIRT1, AMPK, mTORC1 (mTORC2 not shown), Nrf2 and select common substrates.

2.8.3 Phenolics and SIRT1

SIRT1's biological importance in aging, cellular stress mediation, and metabolism, coupled with current data linking phenolics (e.g. resveratrol) to its activities, has made it a research

focus for phenolic treatments. Research examples include: (a) treatment with the anthocyanin, delphinidin-3-*O*-glucoside (50-200 µM), showed protective effects against LPS-induced injury in human umbilical vein endothelial cells (HUVECs) with concentration-dependent increases in SIRT1 levels (by Western blot) and LC3ii (a marker of autophagy) (Jin et al., 2014); (b) paeonol (methoxybenzene), a phenolic found in peonies, caused elevated levels of SIRT1 (by Western blot) and downstream proteins in the kidneys of diabetic mice, ameliorating the progression of renal fibrosis, a buildup of scar tissue that can lead to renal failure (Zhang et al., 2018); and (c) strawberry (Alba cultivar) phenolics reduced biomarkers of inflammation (e.g. NF-κB) and increased SIRT1 (by Western blot) in murine macrophages (RAW 264.7), demonstrating protective effects against DNA damage and oxidative stress in response to LPS treatment (Gasparrini et al., 2017).

Potential synergistic effects of phenolics on SIRT1 expression have also been explored using human cervical cancer (HeLa) cells exposed to treatments between 1 and 50 µM of varying phenolic compounds (Giovannini and Bianchi, 2017). Phenolics that showed the greatest individual SIRT1 increases (by Western blot) included tyrosol (phenylethanoid; greater activity than resveratrol) and catechin and malvidin (flavonoids; activity equal to resveratrol). Phenolic combinations were also tested, and two synergistic pairs were identified: quercetin and ferulic acid (25 and 50 µM, respectively); and tyrosol and ferulic acid (20 and 25 µM, respectively). As individual treatments, 20 µM tyrosol had ~2x the densitometry of the control (for SIRT1) and 25 µM ferulic acid had ~1.6x the control, meaning the combination treatment would be predicted to cause a change of ~3.6x the control. However, when these phenolics (at these concentrations) were combined in treatment, the actual change was higher at ~4x the control (for SIRT1) (Giovannini and Bianchi, 2017). The aforementioned demonstrates how synergy of phenolic structures may be important for the *in vitro* mechanism(s) of an extract.

2.9 Bioactivity of Haskap Phenolics

Research focused on phenolic rich haskap extracts in animal/cell line models has spanned a wide range of topics. In studies on haskap phenolic anticancer abilities, results have varied significantly. As an example, in an *in vivo* study, 120 Wistar albino rats were implanted with Walker 256 carcinoma cells to induce localized tumor growth and were then fed a dietary

supplement of 1 mL of a haskap macerate extract (water-extracted; 0.24 g FW/mL) each day for 17 days (Gruia et al., 2008). After this treatment period, unsupplemented controls showed an average tumor size 2.21x larger than that of the concurrently extract-supplemented groups (Gruia et al., 2008). However, when haskap extract supplementation began three weeks prior to grafting, tumor growth was accelerated, with a final tumor size approximately 1.6x that of the unsupplemented controls (Gruia et al., 2008). With such varied results, further studies on the anticancer abilities and mechanism(s) of action of haskap phenolics are required to clarify their effects and elucidate their structure-function-mechanisms.

In a study on inflammation, three Canadian haskap cultivars (Borealis, Indigo Gem, and Tundra) were investigated (Rupasinghe et al., 2015). When applied to human THP-1 monocytes, the Borealis phenolic extract at 100 µg/mL inhibited TNF-α and IL-6 by 55 and 50%, respectively (Rupasinghe et al., 2015). This extract also had the highest total phenolic content (TPC) and cyanidin-3-O-glucoside concentration of the three varieties studied. In a study using haskap fruit native to Hokkaido, Japan, phenolic extracts (100 µg/mL) inhibited the LPS-dependent elevation of TNF-α levels in mouse RAW 264.7 macrophages (Jin et al., 2006). Further testing occurred using three individual phenolic compounds (cyanidin-3-O-glucoside, cyanidin-3-O-rutinoside, and chlorogenic acid) and demonstrated no reduction in this inflammatory marker. In some cases, the concentration of pro-inflammatory cytokines increased after exposure to the isolated compounds (Jin et al., 2006). These results strongly suggest that anti-inflammatory activity is dependent on both phenolic composition (i.e. structure) and synergy among active components (Giovannini and Bianchi, 2017; Li et al., 2017).

Additional literature examples of bioactivity in response to haskap phenolics include: (a) potential for use against non-alcoholic fatty liver disease (NAFLD) as demonstrated by decreased expression of adipogenic gene transcripts (e.g. peroxisome proliferator activated receptor gamma (PPAR-γ)) in colon cancer (HepG2) cells treated with 250-1000 µg/mL haskap phenolics (Park et al., 2019); (b) mice fed a high-fat diet with 0.5-1% haskap phenolics showed lower levels of lipid peroxidation and cytokines (e.g. IL-1β, IL-6, and IL-10) following exposure to carbon tetrachloride (CCl_4) (Wu et al., 2016); and (c) male adults (aged 62-81 years) who ate 400 mg of haskap anthocyanins daily displayed improved measurements of working memory including higher word recall and improved word recognition; these subjects also showed significantly lower

diastolic blood pressure (~3 mmHg lower than untreated control subjects) and heart rate (~3 beats per minute less) (Bell and Williams, 2018). With such a wide range of *in vitro* and *in vivo* effects, further exploration into haskap phenolic activities is needed.

3. MATERIALS AND METHODS

3.1 Samples

Haskap berry samples of Aurora, Blizzard, Honey Bee, Indigo Gem, and Tundra varieties (2017 and 2018 crop) were obtained from the University of Saskatchewan Horticulture Field Lab (Saskatoon, SK). All samples were stored at -30 ± 2°C until analysis.

3.2 Chemicals

All solvents used in this research were of American Chemical Society (ACS) grade or higher. The following chemicals were obtained from Sigma-Aldrich Canada Ltd. (Oakville, ON): Amberlite® XAD16N resin; 3-aminophthalhydrazide (luminol); α-amylase solution (Cat #: A-3306); amyloglucosidase solution (Cat #: A-9913); arabitol; arbutin; 2,2'-azinobis(3-ethylbenzothiazoline-6-sulfonic acid) (ABTS); caffeic acid; catechin; celite; citric acid; chlorogenic acid; *p*-coumaric acid; cyanidin chloride, cyanidin-3-*O*-rutinoside; cyanidin-3,5-*O*-diglucoside; 2,2'-diphenyl-1-picrylhydrazyl (DPPH); egtazic acid; epicatechin; ethidium bromide; ethylenediaminetetraacetic acid (EDTA) disodium salt; ferulic acid; Folin-Ciocalteu reagent (FC); D-fructose (fructose); fucitol; D-galactose (galactose); gallic acid; D-glucose (glucose); hydrogen peroxide; 4-hydroxybenzoic acid; 4-(2-hydroxyethyl)-1-piperazineethanesulfonic acid (Hepes); isomaltose; lactitol; L-malic acid; malonic acid; maltose; 2-mercaptoethanol; naringenin; nonidet P-40; phloridzin; phosphatase inhibitor cocktail 2 (Cat #: P-5726); phytic acid; protease enzyme solution (Cat #: P-3910); protease inhibitor cocktail 2 (Cat #: P-8340); quercetin; quercetin-3-*O*-rutinoside (rutin); quinic acid; raffinose; shikimic acid; sorbitol; succinic acid; sucrose; and D-tagatose (tagatose).

Chemicals obtained from Fisher Scientific (Edmonton, AB) were: acetone; acetonitrile; ammonium persulfate; bromophenol blue; chloroform; dimethyl sulfoxide; formic acid; glycerol; glycine; hydrochloric acid; isopropanol; magnesium chloride; methanol; 2-(4-N-morpholino)ethanesulfonic acid; oxalic acid; phosphoric acid; RNaseOUT™ recombinant ribo-

nuclease inhibitor (Cat#: 10777019); sodium acetate; sodium carbonate; sodium hydroxide solution (50% (w:w)); trifluoroacetic acid; tris base; tris hydrochloride (Tris-HCl); tris(hydroxymethyl)aminomethane; and Tween™ 20. Chemicals obtained from BDH (Edmonton, AB) were acetic acid, ascorbic acid, disodium hydrogen phosphate, and potassium chloride, potassium hydroxide (KOH). Maleic acid was obtained from Acros Organics (NJ, USA). Inositol was obtained from MP Biomedicals, LLC (Solon, OH, USA). Sodium dodecyl sulfate was obtained from ICN Biomedicals (Irvine, CA, USA). Polyacrylamide was obtained from Bio-Rad Laboratories (Hercules, CA, USA), and sodium chloride was obtained from EM Sciences (Hatfield, PA, USA). Acid phenol:chloroform was purchased from Ambion (Foster City, CA, USA). Agarose was obtained from Melford Laboratories, Ltd. (Chelsworth, UK).

The following chemicals were obtained from Santa Cruz Biotechnology (Dallas, TX, USA): 6-hydroxy-2,5,7,8-tetramethylchroman-2-carboxylic acid (Trolox), control siRNA (Cat #: sc-37007), SIRT1 siRNA (Cat #: sc-40986), and vanillic acid. Cyanidin-3-*O*-xyloside was provided by Toronto Research Chemicals Inc. (Toronto, ON). Apigenin, cyanidin-3-*O*-arabinoside, cyanidin-3-*O*-glucoside, isorhamnetin-3-*O*-rutinoside, pelargonidin-3-*O*-glucoside, peonidin-3-*O*-glucoside, and quercetin-3-*O*-galactoside were purchased from Extrasynthese S. A. (Genay, France).

Quercetin-3-*O*-glucoside and isorhamnetin-3-*O*-glucoside were obtained from Indofine Chemical Company, Inc. (NJ, USA). 1,2-Dithio-DL-threitol was purchased from Fluka Chemie GmbH (Buchs, Switzerland). The water used in this research was produced from a Millipore Milli-Q™ water system (Millipore Corporation, Milford, MA, USA). Lipofectamine® 3000 reagent, nuclease free water, and P3000™ reagent were obtained from Invitrogen (Carlsbad, CA, USA). Ethanol (95% (v:v) and anhydrous) was obtained from Commercial Alcohols Inc. (Brampton, ON) through the College of Agriculture and Bioresources chemical stores (Saskatoon, SK). Carbon dioxide was obtained from Praxair (Mississauga, ON).

Dulbecco's Modified Eagle Medium (DMEM) was obtained from Corning Cellgro Mediatech, Inc. (Manassas, VA, USA). Penicillin-streptomycin 100X solution and bovine calf serum were obtained from HyClone™, GE Healthcare Life Sciences (Logan, UT, USA). TrypLE Express and Opti-Mem reduced serum media were obtained from Gibco™ (Dun Laoghaire, Ireland). Trypan blue dye was obtained from VWR International (Edmonton, AB). TRIzol™

reagent was obtained from Life Technologies (Carlsbad, CA, USA). PerfeCTa® SYBR® Green SuperMix was obtained from Quantabio (Beverley, MA, USA).

A DNase treatment kit was obtained from New England Biolabs (Ipswich, MA, USA, Cat #: B03035) including 10X DNase I reaction buffer and DNase I. A OneScript® Plus Reverse Transcriptase kit (Cat #: G237) was purchased from Applied Biological Materials, Inc. (Richmond, BC) including deoxynucleotide triphosphate solution, 5X RT buffer, OneScript® Plus Reverse Transcriptase, and random primers (10 µM). A SIRT1 activity assay kit was obtained from Abcam (Cambridge, MA, USA, Cat #: ab156065) including developer solution, fluoro-substrate peptide, nicotinamide adenine dinucleotide (NAD), SIRT1 assay buffer, and recombinant SIRT1. Trichostatin A (10 mM DMSO solution) was also obtained from Abcam (Cambridge, MA, USA).

Primary antibodies used were mouse anti-NRF2 antibody (Santa Cruz, Dallas, TX, USA, Cat #: sc-365949), mouse anti-phospho-mTOR (Ser 2448) antibody (Santa Cruz, Dallas, TX, USA, Cat #: sc-293133), mouse anti-SIRT1 antibody (Abcam, Cambridge, MA, USA, Cat #: ab110304), rabbit anti-β-actin antibody (Abcam, Cambridge, MA, USA, Cat #: ab8227), and rabbit anti-phospho-NF-κB p65 (Ser536) antibody (Cell Signaling Technology, Danvers, MA, USA, Cat #: 3033). Secondary antibodies used were goat anti-rabbit horse radish peroxidase (HRP) (Abcam, Cat #: ab97069) or goat anti-mouse HRP (Jackson Scientific, West Grove, PA, USA, Cat #: 715-035-150).

3.3 Physicochemical Analysis

3.3.1 Sample Preparation

Haskap berry samples were thawed at $4 \pm 2°C$ for 24 h, then macerated (Osterizer™, Sunbeam Canada, Toronto, ON) on the blend setting for 2 min. Juice was obtained by pressing berry macerate between four layers of cheesecloth (Fisher Scientific, Edmonton, AB). Juice samples were centrifuged on autotransformer setting 30 (Sorvall Superspeed, Newtown, CT, USA; Staco Inc., Dayton, OH, USA) to remove particulates. The supernatants were transferred to foil wrapped plastic vials and stored at $-30 \pm 2°C$ until analysis. All samples were prepared in triplicate.

3.3.2 Colour

Juice color was assessed using a ColorFlex EZ colourimeter (Hunterlab Labscan 6000, Hunter Associates Laboratory Inc., Reston, VA, USA). The colourimeter was standardized using a white tile (standard no. LS-13903) with colour coordinates: $L^* = 92.81$, $a^* = -1.25$, and $b^* = 1.06$. Colour parameters (L^*: lightness/darkness; a^*: red/green; b^*: yellow/blue) were determined for 20 mL aliquots of haskap berry juice for each variety. Hue and chroma were determined by calculating tan^{-1} (b^*/a^*) and the square root of $(a^*)^2 + (b^*)^2$, respectively. The observed angle was set at 10°, and three separate measurements were taken following rotation of the sample cup by ~30°. All samples were analyzed in triplicate.

3.3.3 pH

Juice pH was measured using a SympHony SP70P pH meter (VWR International, Edmonton, AB). Prior to measurement, the pH meter was calibrated using a three-point standard with pH buffers of 2.00, 4.00, and 7.00 (Fisher Scientific). All samples were analyzed in triplicate.

3.3.4 Size

Freshly picked (never frozen) ripe haskap berries (2018 crop) were measured using an electronic digital caliper (VWR International). Fruit length and diameter were measured on ten randomly selected berries of each variety.

3.3.5 Total Soluble Solids (°Brix)

Sample total soluble solids (°Brix) was determined using an Auto Abbe Refractometer (Model 10504, Leica Inc, Buffalo, USA) with temperature compensation, according to AOAC method 932.12 (AOAC, 2000). All samples were analyzed in triplicate.

3.4 Chemical Composition

3.4.1 Carbohydrates/Polyols

Major carbohydrate concentrations in haskap berry juices were determined by high performance liquid chromatography with refractive index detection (HPLC-RI) on an Agilent 1100 series HPLC system (Agilent Technologies Canada Inc., Mississauga, ON). The components of the HPLC system were the solvent degasser, quaternary pump, auto sampler, column heater, refractive index detector (RI), and system control by Chemstation LC-3D software (Revision B.04.01). Carbohydrate separation was achieved on a Capcell-Pak 5 µm NH2 UG-80S5 column, 250 x 4.6 mm, with a CapCell guard cartridge (Phenomenex, Torrance, CA, USA). An isocratic mobile phase of acetonitrile:water (75:25 (v:v)) at a flow rate of 1.0 mL/min was used for major carbohydrate analysis. Sample injection volume was 5.0 µL. The refractive index detector was maintained at a temperature of 35 ± 1°C. Juice samples were diluted 1:1 with water to yield carbohydrate concentrations that fell well within the linear range of standards, with sample values ranging from 6.0-9.0 °Brix. The diluted samples were syringe filtered (nylon, 0.2 µm pore size; 13 mm diameter; Chromatographic Specialties, Brockville, ON) into 2 mL amber HPLC vials (Chromatographic Specialties). Standards used were fructose, galactose, glucose, inositol, isomaltose, maltose, raffinose, sorbitol, and sucrose. After spiking experiments and comparison of retentions times, standard curves were made for fructose and glucose at concentrations ranging from 5.00-50.00 g/L in water. Standard curves had correlation coefficients ≥0.990. All samples were analyzed in triplicate.

Haskap juice polyol content and concentrations were determined using high performance anion exchange chromatography coupled with pulsed amperometric detection (HPAE-PAD). A Dionex 5000 HPAE-PAD system (Thermo Fisher, Waltham, MA, USA) equipped with a Dionex AS autosampler and an ICS 5000 electrochemical cell with a disposable gold electrode was used for analysis. The potentials and durations of the gold electrode were as follows: $E1 = 0.10$ V, $t1 = 0.00$ sec; $E2 = -2.00$ V, $t2 = 0.41$ sec; $E3 = 0.60$ V, $t3 = 0.43$ sec; $E4 = -0.10$ V, $t4 = 0.44$ sec; $E5 = -0.10$ V, $t5 = 0.50$ sec, and data acquisition was carried out using Dionex Chromeleon 7.0 software (Revision B.04.01). Carbohydrate separation was accomplished employing a Dionex CarboPac PA1 column (4 x 250 mm) in series with a CarboPac PA1 guard column (4 x 50 mm) at room temperature. An isocratic mobile phase of 80 mM NaOH was used at a flow rate of 1.0 mL/min and the sample injection volume was 20.0 µL. Juice samples were diluted with water so

as to fall well within the linear range for each compound. Dilutions were in the following ranges based on sample concentration of the analyte: arabitol, 1/10 to 1/20; inositol, 1/20 to 1/50; and sorbitol, 1/50 to 1/70. The diluted samples were syringe filtered into 2 mL amber HPLC vials. Standards used were arabitol, fucitol, galactose, inositol, lactitol, sorbitol, sucrose, and tagatose. After spiking experiments and comparison of retention times, calibration curves for arabitol, inositol, and sorbitol were prepared at concentrations ranging from 1-125 mg/L. Standard curves had correlation coefficients ≥0.990. All samples were analyzed in triplicate.

3.4.2 Moisture

Sample moisture content was determined gravimetrically by forced-air oven drying according to AOAC Method 925.10 (AOAC, 2000). Moisture analysis was conducted on macerated berry samples. Whole berries were thawed at $4 \pm 2°C$ for 24 h, then macerated (Osterizer™, Sunbeam Canada, Toronto, ON) on the blend setting for 2 min. Aluminum dishes (70 mm, Fisher Scientific) were pre-dried in a forced-air draft oven at 105ºC for 12 h, then cooled in a desiccator for 1 h. Aluminum dishes were then weighed, and berry macerate (3-4 g) was accurately added $(\pm 0.0001\ g)$, followed by drying at 105ºC for 18 h. The dried samples were then cooled in a desiccator for 1 h before weighing. All samples were analyzed in triplicate. Sample moisture content was determined as follows:

$$\% \text{ Moisture} = \left[1 - \left[\frac{\text{(weight of dried sample + dish) - dish weight}}{\text{weight of sample before drying}}\right]\right] *100$$

3.4.3 Organic Acids and Ascorbic Acid

The organic acid and ascorbic acid contents of haskap berry juices were determined by high performance liquid chromatography with photodiode array detection (HPLC-PDA) on an Agilent Technologies 1100 Series HPLC system. Organic acid separation was achieved on a Restek Allure organic acids column (250 x 4.6 mm, 5 µm, 60 Å; Chromatographic Specialties) using an isocratic mobile phase of 100 mM K_2HPO_4 (adjusted to pH 2.5 with 50 mM phosphoric

acid) at a flow rate of 0.7 mL/min. The sample injection volume was 50 µL. Organic acids were monitored at 226 nm with reference at 360 nm. Prior to analysis, samples were diluted 1 in 3 with water and syringe filtered into 2 mL amber HPLC vials. The reducing agent 1,2-Dithio-DL-threitol was added (to achieve a concentration of 0.75 mg/mL sample) to ensure that any ascorbic acid present in the sample would be in the reduced state. The following standards were selected based on common organic acids in fruits and those reported to be present in haskaps: acetic, ascorbic, citric, fumaric, maleic, malic, malonic, oxalic, phytic, quinic, shikimic, and succinic acids. Organic acid identification was afforded by retention time comparison to standards and spiking experiments. Sample organic acid quantification was determined by comparison to standard curves that ranged in concentration from 5-1200 mg/L and had correlation coefficients ≥0.990. All samples were analyzed in triplicate.

3.4.4 Total Dietary Fibre

Sample total dietary fibre content was determined by enzymatic digestion according to AOAC Method 991.43 (AOAC, 2000). Pre-dried and defatted samples (1 g) were accurately weighed (±0.0001 g) and transferred into a 400 mL beaker followed by the addition of 50 mL of 0.05 M MES-TRIS buffer (19.52 g of 2-(4-N-morpholino)ethanesulfonic acid and 14.2 g of tris(hydroxymethyl)aminomethane in 1.7 L of water, followed by pH adjustment to 8.2 with the dropwise addition of 6.0 N NaOH). An α-amylase enzyme solution was added (50 µL), and the beaker was covered and placed in a water bath (Haake D1, Berlin, Germany) at 95-100°C for 30 min. The resulting mixture was cooled to <60°C followed by the addition of 100 µL of protease enzyme solution and the covered beaker was placed in a shaking/agitating water bath at 60°C for 30 min. This was followed by the addition of 5.0 mL of 3.0 M acetic acid solution and 100 µL of amyloglucosidase solution followed by incubation in the same water bath at 60°C for 30 min.

Following enzymatic hydrolysis, 200 mL of 95% ethanol was added, and the solution was reheated to 60°C for 10 min. The beaker was then covered with aluminum foil and kept static at room temperature for 10-12 h. The resulting precipitate was collected by vacuum filtration using a dried and pre-weighed (±0.0001 g) filtration crucible (Pyrex no. 32940, coarse ASTM 40~60 µm, 50 mL; Fisher Scientific) containing ~0.5 g of celite, followed by sequential treatment with 8 mL portions of 78% ethanol, 95% ethanol, and acetone. The filtration crucible plus residue was

transferred to a forced-air oven and dried at 105°C for 10-12 h and was then cooled in a desiccator for 1 h followed by gravimetric analysis. Total dietary fibre was determined as follows:

% Total dietary fibre = $\underline{\text{crucible with residue weight - crucible and celite weight}}$ x 100

$$\text{sample weight}$$

3.5 Phenolics Extraction

3.5.1 Ethanol-Formic Acid-Water (EFW) Extracts

Ethanol-formic acid-water extracts (EFW, 70:2:28% (v:v:v)) were prepared for each variety using 25 g (±0.03 g) of the berry macerate (Section 3.3.1). The berry macerate was weighed into a 250 mL beaker and 50 g (±0.03 g) of EFW was added. The resulting mixture was covered with parafilm and aluminum foil and stirred at 700 rpm/4 ± 2°C on a hot plate/stirrer (IKAMAG REO) for 2 h. The mixture was then vacuum filtered (VWR-413, 12.5 cm), and the remaining sediment and filter paper was resuspended in another 50 g (±0.03 g) of EFW. This mixture was stirred at 4 ± 2°C for 2 h as outlined above. Following the second filtration, the filtrates were combined and quantitatively transferred to a 200 mL volumetric flask and brought to volume with EFW. Haskap berry EFW extracts were transferred to sealed plastic containers, covered with aluminum foil, and stored at -30 ± 2°C until analysis. All samples were prepared in triplicate.

3.5.2 Phenolic Rich (PR) Extract Production

The EFW extracts (Section 3.5.1) were used to produce phenolic rich (PR) extracts employing Amberlite® XAD16N resin (i.e. stationary phase). The resin was hydrated in 50% (v:v) ethanol for at least 30 min prior to use. Sufficient hydrated resin was packed into a glass column (50 x 2.0 cm) to produce a resin bed of approximately 75 mL. The stationary phase was pre-conditioned with sequential treatment of 90 mL of water, 90 mL of 100% ethanol, and 90 mL of water at a flow rate of 2.5 mL/min.

Individual 10.0 mL aliquots of each of the haskap EFW extracts (Section 3.5.1) were evaporated (35°C) (BUCHI Labortechnik AG, Switzerland), re-dissolved in 5.0 mL of water, and quantitatively transferred to the resin column. The stationary phase was then treated with 135 mL

33

of water to remove nonphenolics, followed by phenolics elution with 135 mL of 100% ethanol. The resulting PR extracts were then concentrated to ~1 mL by rotary evaporation, quantitatively transferred to a 10 mL volumetric flask and brought to volume with EFW. Samples were transferred to foil wrapped plastic vials and stored at -30 ± 2°C until analysis. All PR samples were prepared in triplicate.

3.5.3 Phenolic Fractionation

The EFW extracts (Section 3.5.1) were fractionated employing solid phase extraction using Amberlite® XAD16N resin as the stationary phase. Stationary phase/column preparation and EFW extract concentration was afforded as described previously (Section 3.5.2). For fractionation, 5.0 mL of the concentrated sample was loaded on the stationary phase, which was treated sequentially with 60 mL of water (fraction 1), 60 mL of 20% ethanol (v:v, fraction 2), 60 mL of 40% ethanol (v:v, fraction 3), 60 mL of 70% ethanol (v:v, fraction 4) and 60 mL of 100% ethanol (v:v, fraction 5). The aqueous ethanol solutions (e.g. 20, 40, and 70% ethanol) were sonicated for 5 min at 4 ± 2°C to remove dissolved gases before they were applied to the column. The mobile phase flow rate was 1.0 mL/min. Following fractionation, 3.0 mL of each fraction was individually removed and freeze-dried (Heto-Holten A/S, Allerod, Denmark). Each freeze-dried sample was dissolved in 250 μL EFW prior to HPLC-PDA analysis. The remaining volumes of each fraction were concentrated by rotary evaporation (35°C) (BUCHI Labortechnik AG, Switzerland) and freeze-dried. Freeze-dried fractions were stored in lightproof containers at -30 ± °2C. Five fractionation experiments were conducted for each variety.

3.6 Phenolic Analysis

Total phenolic content (TPC) by the Folin-Ciocalteu method and total chromatographic index (TPCI) by HPLC-PDA were determined for EFW and PR extracts, and fractions of all five haskap varieties.

3.6.1 Total Phenolic Content (TPC) by the Folin-Ciocalteu Method

The total phenolic content (TPC) for all samples was determined using the Folin-Ciocalteu (FC) method. Sample dilutions were made with water to ensure that all spectroscopic results were well within standard curves. For EFW and PR extracts, dilutions ranged from 1/15 to 1/30. The freeze-dried material obtained from five fractionation replicates per variety was combined and dissolved in EFW for a total volume of 1 mL. Fraction dilutions were made with water as follows: water fraction, 1/10; 20% ethanol fraction, 1/8 to 1/10; 40% ethanol fraction, 1/150 to 1/250; 70% ethanol fraction, 1/200; and the 100% ethanol fraction, 1/20 to 1/30. A 250 µL aliquot of each of the diluted samples was quantitatively transferred to individual 13 x 100 mm glass test tubes (VWR International), followed by the addition of 1.25 mL of 0.2 N of FC solution and 1.0 mL of a 15% (w:v) aqueous sodium carbonate solution. The resulting mixture was vortexed at setting 6 for 10-15 sec, and then placed in the dark for 2 h at room temperature ($22 \pm 2°C$), followed by spectroscopic analysis (Genesys 10S UV-visible; Fisher Scientific) at 765 nm. Blanks were prepared as described above with water instead of the diluted sample. Standard curves were prepared using 250 µL aliquots of an aqueous gallic acid solution at concentrations ranging from $10.0\text{-}50.0 \pm 0.1$ mg/L. Standard curves had minimum correlation coefficients ≥ 0.990. All samples and standards were analyzed in triplicate and sample results were reported as mg gallic acid equivalents (GAE)/100 g of fresh fruit weight (FW).

3.6.2 Total Phenolic Chromatographic Indices (TPCI)

Sample total phenolic chromatographic indices (TPCI) were determined on EFW and PR extracts (Sections 3.5.1-2) and fractions (Section 3.5.3) employing high performance liquid chromatography with photodiode array detection (HPLC-PDA). Phenolics were identified and placed into specific phenolic subclasses (e.g. hydroxybenzoic acids, hydroxycinnamic acids, flavanols) based on their UV-visible spectra comparison to reference standards. The concentration for each subclass was determined by chromatographic peak area comparison to reference standards. Sample TPCI was determined by the summation of all subclass concentrations.

Chromatography was performed on an 1100 series HPLC system (Agilent Technologies Canada Incorporated, Mississauga, ON) with separation achieved using a 250 x 4.6 mm Prodigy ODS-3 5 µm, 100 Å, C_{18} column (Phenomenex) in series with a C_{18} guard cartridge (Phenomenex)

at 25.0 ± 1.0°C. The gradient mobile phase system used for phenolic compound separation consisted of: solvent A was 10 mM formic acid and solvent B was 70% acetonitrile:30% solvent A (v:v). The linear gradient program was as follows: 100% A for 3 min, to 4% B at 6 min, to 10% B at 15 min, to 15% B at 30 min, to 20% B at 35 min, to 23% B at 50 min, to 25% B at 60 min, to 30% B at 66 min, to 50% B at 80 min, to 80% B at 85 min, which was held at 80% B for 5 min. For EFW and PR extracts, the injection volume was 20 μL; for fractions, the injection volume was 50 μL. The mobile phase flow rate was 0.8 mL/min. All samples were syringe filtered prior to HPLC analysis. Phenolic compound detection was achieved employing a PDA detector with monitoring at 254, 280, 360, and 520 nm, with reference at 360, 400, 700, and 700 nm, respectively. Phenolic standards, apigenin, arbutin, caffeic acid, catechin, chlorogenic acid, cyanidin-3-*O*-glucoside, cyanidin-3-*O*-rutinoside, epicatechin, ferulic acid, 4-hydroxybenzoic acid, gallic acid, naringenin, *p*-coumaric acid, phloridzin, quercetin, rutin, and vanillic acid, were prepared at 100.0 (± 0.2) mg/L and were used to identify sample spectral (i.e. UV-visible profiles), retention time, and quantitation parameters. For quantification, the following representative compounds for each subclass (of the two major classes: flavonoids and phenolic acids) were selected: anthocyanins, cyanidin-3-*O*-glucoside; flavanols, catechin; flavanones, naringenin; flavonols, rutin; hydroxybenzoic acids, gallic acid; and hydroxycinnamic acids, chlorogenic acid. Standard curves were prepared with concentrations ranging from 0.5 to 2500 mg/L and had correlation coefficients ≥0.980. All samples were analyzed in triplicate.

3.6.3 Phenolic Analysis by HPLC-MS/MS

Sample analysis was performed with the previously described phenolic HPLC method (Section 3.6.2) in tandem with an API QSTAR XL MS/MS hybrid QqToF tandem mass spectrometer (MS) equipped with an ESI source (Applied Biosystems Inc., CA, USA). The ESI source was operated in the negative ion mode with mass spectra recorded from 100-750 *m/z* (mass to charge) with an accumulation time of 0.5 s. The following parameters were used: ion source temperature 450°C, needle voltage -3200 V, declustering potential (DP) -40 V, and collision-induced dissociation (CAD) 5 V. The drying and ESI-nebulizing gas was nitrogen and were set at 70 and 50°C, respectively. The system continually corrected for mass drifts by passing Agilent reference solutions (+ve mode ion: HP-0921, 922.009798 m/z; -ve mode ion: HP-0921-TFA

adduct, 1033.988109 m/z) through the reference nebulizer. MS/MS spectra were acquired using collision energies of -30, -45, and -55 v and analyzed using Analyst software (QS 1.1).

The HPLC mobile phase flow rate was 0.8 mL/min. During the first and final 10 min of the HPLC method, the mobile phase flow was diverted to waste. Phenolic compound detection was achieved employing a photodiode array (PDA) detector with monitoring at 254, 280, 360, and 520 nm, with reference at 360, 400, 700, and 700 nm, respectively. The 40%, 70%, and 100% ethanol fractions of the Tundra variety were analyzed employing a 20 μL injection volume. All samples were syringe filtered prior to HPLC-MS/MS analysis and each sample was injected once.

3.6.4 Anthocyanin Analysis by HPLC

Sample EFW extracts (Section 3.5.1) were analyzed to determine anthocyanin content and concentration. Samples were analyzed by high performance liquid chromatography with photodiode array detection (HPLC-PDA). Anthocyanin separation was afforded using the previously described analytical column (Section 3.6.2) with a mobile phase system consisting of aqueous 4.0% (v:v) phosphoric acid at pH 1.4 (solvent A) and acetonitrile (solvent B) with the following gradient conditions: initial, 6% B for 12 min, followed by a linear gradient to 20% B at 66 min, and then held at 20% B for 18 min. The mobile phase flow rate was 0.8 mL/min. Undiluted EFW extracts and 1 in 50 dilutions in EFW were used for analysis. The sample injection volume was 20 μL and all samples were syringe filtered prior to analysis. Analyte detection was achieved using a PDA detector with monitoring at 520 nm and reference at 700 nm. Anthocyanin standards used for identification were: cyanidin-3-*O*-galactoside (ideain), cyanidin-3-*O*-glucoside (kuromanin), cyanidin-3,5-*O*-diglucoside, cyanidin-3-*O*-rutinoside (keracyanin), cyanidin-3-*O*-xyloside, pelargonidin-3-*O*-glucoside, and peonidin-3-*O*-glucoside. Sample anthocyanin identification was afforded by retention time comparison to standards and spiking experiments, and standard curves (0.5-2500 mg/L; correlation coefficients ≥0.980) were employed to determine their concentrations.

3.6.5 Anthocyanin Analysis by HPLC-MS/MS

Anthocyanin separation was afforded using the previously described stationary phase (Section 3.6.2) with a mobile phase system (described in Palíková et al., 2008) consisting of aqueous 0.12% (v:v) trifluoroacetic acid with 5% (v:v) acetonitrile (solvent A) and 0.12% (v:v) trifluoroacetic acid in 100% acetonitrile (solvent B) with the following gradient conditions: initial, 5% B for 5 min, to 14% B at 50 min, to 20% at 55 min, to 5% B at 60 min, and held at 5% to 65 min. This separation method was used in tandem with the MS instrumentation described previously (Section 3.6.3). The following parameters were used: ion source temperature 500°C, needle voltage 5500 V, declustering potential (DP) 60 V, and collision-induced dissociation (CAD) 5 V. The ESI source was operated in the positive ion mode with mass spectra recorded from 100-1000 m/z with an accumulation time of 1 s. The drying and ESI-nebulizing gas was nitrogen and were set at 90 and 65°C, respectively. MS/MS spectra were acquired using collision energies of 20, 25, and 30 V and analyzed using Analyst software (QS 1.1).

The HPLC mobile phase flow rate was 0.8 mL/min. Anthocyanin detection was achieved employing a photodiode array (PDA) detector with monitoring at 520 nm and reference at 700 nm. Freeze-dried aliquots (3 mL) of the Tundra variety 70% ethanol fraction (Section 3.5.3) were resuspended in 100 μL of solvent A and were analyzed with a 20 μL injection volume. All samples were syringe filtered prior to HPLC-MS/MS analysis and samples were injected once.

3.7 *In vitro* Radical Scavenging Assays

ABTS and DPPH *in vitro* radical scavenging assay experiments were conducted on all haskap EFW extracts (Section 3.5.1), PR extracts (Section 3.5.2), and fractions (Section 3.5.3).

3.7.1 ABTS (2.2-azino-bis-3-ethylbenzthiazoline-6-sulfonic acid)

Radical cation (ABTS$^{\bullet+}$) solutions were prepared by mixing 2.00 mL of 7.0 mM ABTS and 1.00 mL of 7.0 mM of aqueous potassium persulfate. This mixture was maintained at room temperature for 12 h in the dark to promote ABTS$^{\bullet+}$ formation. The resulting solution was diluted approximately 1 in 50 with 70% methanol:water (v:v) to achieve an absorbance of 0.75 ± 0.05 at 734 nm. Testing showed that the original concentration of EFW could inflate RS results due to the

presence of formic acid; sample dilutions with 70% methanol were made to negate these impacts and to provide five data points for curves centered around the equivalent scavenging of 1 mM Trolox. Sample EFW and PR extracts were diluted from 1/2 to 1/10 with 70% methanol. The freeze-dried material obtained from five fractionation (Section 3.5.3) replicates per variety was combined and dissolved in EFW for a total volume of 1 mL, and the following dilutions were made with 70% methanol: 40% fraction, 1/20 to 1/100, 70% fraction, 1/20 to 1/100, and the 100% fraction from 1/2 to 1/10.

The Trolox standard was prepared in 70% methanol at the following concentration range: 0.1 mg/mL (0.47 mM) to 0.5 mg/mL (2.06 mM). To perform the assay, 20 μL of each sample dilution was added to 2.00 mL of ABTS$^{\bullet+}$ solution. A blank was prepared using 20 μL of 70% methanol in 2.00 mL ABTS$^{\bullet+}$ solution. Samples and blanks were vortexed for 10 to 15 sec, then stored in the dark for 6 min, followed by spectroscopic analysis at 734 nm. Percent ABTS radical scavenging activity was calculated as follows:

$$\% \text{ ABTS radical scavenging activity} = [1- (A_{734}\text{ sample}/A_{734}\text{ control})]*100$$

A_{734} sample = sample absorbance at 734 nm

A_{734} control = control absorbance at 734 nm

The % ABTS$^{\bullet+}$ inhibition was plotted as a function of sample concentration and linear regression equations were determined. Correlation coefficients of the linear regression equations were ≥0.960. The sample concentration equivalent to the inhibition activity of 1.0 mM Trolox was calculated. The Trolox equivalent antioxidant capacity (TEAC) was expressed as the equivalent activity of Trolox (mM)/100 mg sample as follows:

$$\text{TEAC} = 100/Y_{TE}$$

TEAC = Trolox equivalent antioxidant capacity ((Trolox equivalents in 100 mg sample/mL), where 100 is the conversion factor to standardize the sample to 100 mg/mL

Y_{TE} = sample concentration (mg/mL) producing an ABTS$^{\bullet+}$ inhibition equivalent to 1.0 mM Trolox.

3.7.2 DPPH (2,2-diphenyl-1-picrylhdrazyl)

A 500 µM DPPH solution was prepared by dissolving 9.8 ± 0.2 mg of DPPH in a 50 mL volumetric flask with 70% methanol:water (v:v) followed by sonication for 60 min ($4 \pm 2°C$; Bransonic, Danbury, CT, USA). Fresh DPPH was prepared daily. EFW was found to falsely inflate RS results for DPPH RS as described for ABTS in Section 3.7.1; sample dilutions with 70% methanol were made to negate these impacts and to provide for curves ranging from approximately 10 to 85% inhibition (centered around 50% inhibition). Sample EFW and PR extracts were diluted from 1/4 to 1/20. The freeze-dried material obtained from five fractionation (Section 3.5.3) replicates per variety was combined and dissolved in EFW for a total volume of 1 mL, and the following dilutions were then made with 70% methanol: 40% fraction, 1/50 to 1/200, 70% fraction, 1/40 to 1/300, and the 100% fraction, 1/5 to 1/20.

Diluted sample aliquots of 250 µL were added to 1.00 mL of DPPH solution in 13 x 100 mm glass test tubes. A control sample was prepared using 250 µL of 70% methanol and the spectrometer blank was 70% methanol. Samples, control, and blank were vortexed for 10 to 15 sec followed by storage in the dark at room temperature for 15 min before their absorbance was measured at 517 nm. Percent DPPH radical scavenging activity was calculated as follows:

% DPPH radical scavenging activity= [1-(A_{517} sample/A_{517} control)]*100

A_{517} sample = sample absorbance at 517 nm

A_{517} control = control absorbance at 517 nm

The 50% radical inhibition concentration (IC_{50}) was determined by plotting the % DPPH radical scavenging versus the concentration for each sample. The IC_{50} value was expressed as mg solids/mL of DPPH solution and antioxidant activity was reported as $1/IC_{50}$. Regression equations had correlation coefficients ≥ 0.950. All samples were analyzed in triplicate.

3.8 Tissue Culture

3.8.1 Cell Culture

A normal human fibroblast cell line (designated 2DD; described in Bridger et al., 1993) and human telomerase immortalized fibroblasts (designated NB1 hTERT; described in Bodnar et al., 1998) were grown in high glucose (4.5 mg/mL) Dulbecco's Modified Eagle Medium (DMEM;

pH 7.7) supplemented with 10% (v:v) bovine calf serum (CS) and 1% (v:v) penicillin-streptomycin 10X solution. Cells were plated at an initial density of 3000/cm^2 and were not grown past 80% confluency. Cells were incubated (Fisher Scientific, Marietta, OH, USA) at 37°C in a humidified environment with 5% carbon dioxide (CO_2).

When cells reached ~70% confluency, they were passaged (i.e. harvested and reseeded) by first aspirating the media and adding an appropriate volume of TrypLE Express to dissociate the cells from the plate surface (3-5 mL). Plates were then incubated for 5 min at 37°C or until the cells were fully dissociated. An appropriate (~5 mL) volume of media was used to rinse the surface of the plate and transfer the cell/media suspension to a 15 mL conical tube. The cells were pelleted by centrifuging at 174 relative centrifugal force (rcf) for 3 min (Eppendorf, Hamburg, Germany). Following centrifugation, the media was aspirated. The pellet was resuspended in 10 mL of media and 20 µL of this suspension was pipetted onto a hemocytometer (Tiefe 0.100 mm, 0.0025 mm^2; Neubauer Improved, EM Sciences, Hatfield, PA, USA). Cells in 5 of the 9 squares were counted using 10x magnification (Leica DMi1, Leica Microsystems, Concord, ON). Total cell number was calculated using the following formula:

$$\text{Total cells} = \frac{\text{number of cells}}{5} \times \text{volume of suspension (mL)} \times 10{,}000$$

Cells were reseeded at 3000/cm^2 using the total number of cells and surface area of the vessel. Cells from passage numbers 12 to 18 were used in subsequent experiments. As cells grew, their media was changed every 2-3 days if passaging was not required. To prevent contamination, all handling of cell cultures (i.e. passaging, media changes, etc.) was performed in a sterile environment (Labconco, Kansas City, MO, USA).

3.8.2 Cell Treatment

Tundra variety phenolic extracts and fractions (Sections 3.5.1-3) were individually freeze-dried and resuspended in dimethyl sulfoxide (DMSO) to produce stock solutions. Phenolic solutions were added to supplemented DMEM (Section 3.8.1) to achieve final concentrations of

5.0 and 50.0 µg phenolics/mL media. Cyanidin-3-*O*-glucoside (C3G) DMSO solutions were also prepared and added to supplemented DMEM (Section 3.8.1) to achieve final concentrations of 2.4 and 23.7 µg C3G/mL media. The volume of total DMSO added to create each treatment concentration was consistent and the vehicle control was prepared by adding that same volume of DMSO to supplemented DMEM. Volumes of DMSO never exceeded 0.05% (v:v) in the media. For the purposes of these experiments, multiple plates or wells of cells (from the same stock) were treated and as such, are biological replicates due to variability in cellular populations; numbers of replicates performed for each experiment are reported in the respective section(s).

3.8.3 Cell Counts and Cell Viability

Cells were seeded in 6-well plates (Thermo Fisher, Rochester, NY, USA) at a density of $3000/cm^2$ as described previously (Section 3.8.1) and left for 24 h to adhere to the plate surface. After this period, fresh DMEM was prepared with the phenolic treatments and C3G (Section 3.8.2) and added to cells which were incubated at 37°C for 72 h. Sample analysis was performed with three biological replicates.

At the end of the treatment period, the culture media was aspirated and TrypLE Express (1 mL for 2DD cells or 2 mLs for NB1 hTERT cells) was added to each well to dissociate the cells. Plates were then incubated for 5 min at 37°C or until the cells were fully dissociated. Following dissociation, 20 µL of the suspension was pipetted onto a hemocytometer and counted as described previously (Section 3.8.1). Population doubling times were calculated using the following formula:

$$\text{Population doubling time (h)} = \text{incubation time (h) x } \frac{\log(2)}{\log\left(\frac{\text{final cell count}}{\text{initial cell count}}\right)}$$

To assess cell viability, plate media was individually collected from each of the 6-wells by pipetting and transferred to 15 mL conical tubes. Cell dissociation was achieved as described above, and the cell/TrypLE Express suspension from each well was added to its corresponding 15 mL conical tube to ensure all cells (living and dead) were collected. The conical tubes were centrifuged at 174 rcf for 3 min, and the supernatant was aspirated to leave behind the pellet. The pellet was resuspended in 250 µL of DMEM, and 50 µL of this suspension was transferred to a 1.5 mL centrifuge tube. The resulting suspension was mixed 1:1 with 0.4% (v:v) trypan blue dye

and incubated for 7 min at room temperature. Stained and unstained cells were then counted using a hemocytometer, with dark blue stained cells considered nonviable. Percentage cell survival was calculated as follows:

$$\% \text{ Cell survival} = 100\% \text{ x } \frac{\text{total counted cells} - \text{nonviable cells}}{\text{total counted cells}}$$

3.8.4 Protein Extraction and Quantification

Cells were plated in 10-cm (diameter) dishes (Sarstedt, Nümbrecht, Germany) and treated as described previously (Section 3.8.2) in duplicate. At the end of the treatment period, cells were dissociated from the plate surface using 1.5 mL TrypLE Express and incubated until fully dissociated. This volume was transferred to 1.5 mL centrifuge tubes and centrifuged at 174 rcf for 5 min. Following centrifugation, the supernatant was removed and the pellet was resuspended in 100 µL Laemmli lysis buffer (62.5 mM Tris-HCl pH 6.8, 2% sodium dodecyl sulfate (SDS; w:v), 10% glycerol (v:v), and 5% 2-mercaptoethanol (v:v)) containing protease inhibitor cocktail 2 and phosphatase inhibitor cocktail 2 in a ratio of 100:1:1 (v:v:v). All protein extracts were vortexed well and stored at -20 ± 2°C until analysis. Proteins were quantified employing UV spectroscopy at 280 nm using a NanoDrop™ 2000 Spectrophotometer (Thermo Fisher, Wilmington, DE, USA). Laemmli buffer was used as a blank and a volume of 1.5 µL was used for each sample.

3.8.5 Western Blot

Prior to analysis, protein extracts were diluted to working concentrations using NanoDrop™ quantification (Section 3.8.4); all extracts were diluted to the same concentration achieving a final concentration of 1x Laemmli buffer. A small volume (8 µL/100 µL protein extract) of 5x Laemmli buffer with 1% bromophenol blue (w:v) was also added to increase the density of the diluted sample and for gel visualization.

Protein samples were denatured for 5 min at 95°C prior to sample loading using a Dry Bath Incubator (Thermo Fisher). Protein samples were loaded (30-60 µg per well; loading volume was dependent on the concentration of the working sample) and separated on a 5% polyacrylamide stacking gel in conjunction with a 6-12% polyacrylamide resolving gel in 1X running buffer (25

43

mM Tris base, 192 mM glycine, and 0.1% SDS) at 125 V. Proteins were transferred from the gel to a nitrocellulose membrane (Bio-Rad Laboratories) using 1X transfer buffer (25 mM Tris base, 192 mM glycine, and 20% methanol (v:v)) with a Trans-Blot® SD semi-dry transfer cell (Bio-Rad Laboratories) at 25 V. Membranes were then blocked by incubating in 5.0% skim milk powder (w:v) in phosphate-buffered saline with Tween™ 20 (PBST; 8% sodium chloride (w:v), 0.2% potassium chloride (w:v), 0.76% disodium hydrogen phosphate (w:v), and 0.05% Tween™ 20 (v:v)) for 30 min at room temperature.

Membranes were then incubated with primary antibody diluted in 5.0% skim milk powder in PBST at $4 \pm 2°C$ overnight. Primary antibodies were diluted as follows: β-actin, 1:2000 (Abcam, Cambridge, MA, USA); phospho-NF-κB p65, 1:1000 (Cell Signaling Technology, Danvers, MA, USA); Nrf2, 1:200 (Santa Cruz, Dallas, TX, USA); phospho-mTOR, 1:500 (Santa Cruz, Dallas, TX, USA); and SIRT1, 1:1000 (Abcam, Cambridge, MA, USA). Following primary antibody incubation, membranes were treated with approximately 15 mL of 5.0% skim milk powder in PBST 3 times each for 5 min. Membranes were then incubated with secondary antibody diluted in 5 mL of 2.5% skim milk powder in PBST at $4 \pm 2°C$ overnight. Secondary antibodies (goat anti-rabbit HRP and goat anti-mouse HRP) were diluted 1:2000. Membranes were then treated with approximately 15 mL of 5.0% skim milk powder in PBST 3 times each for 5 min, followed by approximately 15 mL of PBST once for 5 min, and approximately 15 mL of PBS once for 5 min. Protein bands were imaged using enhanced chemiluminescence (ECL) reagent (100 mM Tris-HCl pH 8.5, 0.2 mM p-coumaric acid, 1.25 mM luminol, and 0.1% hydrogen peroxide (H_2O_2 (v:v))). Following imaging, densitometry measurements were taken for each protein band using Image J software (64-bit Java 1.8.0_112). All protein measurements were normalized first to the loading control β-actin, and then to the control sample (untreated) for data presentation. Western blots of two biological replicates of each treatment and cell line were performed.

3.8.6 RNA Extraction

Cells were plated in 10-cm (diameter) dishes and treated as described previously (Section 3.8.2) in duplicate. Following the treatment period, cells were dissociated with 1.5 mL TrypLE Express and incubated until fully dissociated. This volume was transferred to 1.5 mL centrifuge tubes and centrifuged at 174 rcf for 5 min. Following centrifugation, the supernatant was removed

and the pellet was resuspended in 1 mL TRIzol™ reagent and incubated at room temperature for 10 min. Chloroform was then added (200 µL) and each sample was vortexed well. Samples were incubated at room temperature for 5 min and then centrifuged at 21130 rcf for 10 min at 4°C. The top layer (aqueous phase; ~300 µL) was transferred to a new 1.5 mL centrifuge tube. RNA was then precipitated by first adding 1/10 of the aqueous phase volume of 3M sodium acetate (pH 5.2) and vortexing. An equal volume (to the aqueous phase) of isopropanol was then added and tubes were vortexed. Samples were incubated for 30 min on ice and then centrifuged at 21130 rcf for 10 min at 4°C. The supernatant was carefully removed to prevent disruption of the RNA pellet. A wash step was performed by adding 1 mL of cold 70% ethanol (v:v) and centrifuging at 21130 rcf for 10 min at 4°C. The ethanol was removed, and the pellet was air-dried for 10 min.

To remove DNA from the sample and isolate the RNA, a DNase treatment was performed by resuspending the dried pellet in 88 µL of nuclease free water, followed by the addition of 1 µL RNaseOUT™, 10 µL 10X DNase I reaction buffer, and 1 µL DNase I. This solution was mixed well and incubated for 20 min at 37°C and 100 µL of acid phenol:chloroform (5:1 (v:v); pH 4.5) was added. Samples were vortexed and then centrifuged at 21130 rcf for 15 min at 4°C. The upper aqueous phase (~100 µL) was transferred to a new 1.5 mL centrifuge tube, and 1/10 the volume of the aqueous phase of 3M sodium acetate (pH 5.2) was added to the RNA pellet followed by vortexing. Cold 100% ethanol was then added to each sample (3x aqueous phase volume) followed by vortexing, and RNA was precipitated for a second time by placing samples on ice for 30 min.

Samples were centrifuged at 21130 rcf for 30 min at 4°C and the ethanol was removed, and the pellet was air-dried for 10 min. Sample RNA was dissolved in 30.5 µL of nuclease free water and 1 µL of RNaseOUT™ was added to inhibit RNase activity that could otherwise degrade the sample. To determine whether the extraction was successful, 5 µL of each sample was run on a 1% agarose gel and only those with clear 18S and 28S rRNA bands were used for cDNA synthesis. Sample RNA was quantified using a NanoDrop™ 2000 Spectrophotometer (Thermo Fisher, Wilmington, DE, USA) at 260 nm and aliquots of 2 µg per 12.5 µL of nuclease free water were transferred to centrifuge tubes for cDNA synthesis. All sample aliquots were stored at -80 ± 2°C until cDNA synthesis.

3.8.7 cDNA Synthesis

For cDNA synthesis, 1 µL of random primers (10 µM), and 1 µL deoxynucleotide triphosphate solution (10 mM) were added to the 2 µg (in 12.5 µL water) RNA aliquots (Section 3.8.6) after thawing on ice and incubated at 65°C for 5 min. Samples were then placed on ice and 0.5 µL RNaseOUT™, 1 µL EasyScript RTase (200 U/µL), and 4 µL 5X RT buffer was added. Samples were then incubated at 25°C for 10 min, 42°C for 60 min, 85°C for 15 min, and were then brought to 4°C using a thermocycler (Bio-Rad Laboratories, Hercules, CA, USA). Samples were stored at -20 ± 2°C until analysis.

3.8.8 Reverse-Transcriptase-quantitative PCR (RT-qPCR)

RT-qPCR was performed following cDNA synthesis (Section 3.8.7). Triplicate 10 µL reactions were prepared for each primer pair with two biological replicates per treatment. Each reaction used 5 µL PerfeCTa® SYBR® Green SuperMix, 2 µL cDNA template, 1 µL nuclease free water, and 1 µL primer mix (forward and reverse each at 3 µM). Reactions were conducted using a Rotor-Gene® Q qPCR (Qiagen, Germantown, MD, USA), and non-template controls were included for each primer pair. Melt curve analyses were performed to ensure that single products were produced in each reaction. Results were quantified using the ΔΔCt method to produce fold changes based on five normalizing genes: *EFEMP2, FAU, FKBP10, PRDX5,* and *SPARC.* Primers were designed using Primer 3 Software (version 0.4.0) and sequences are shown in Table 3.1 (Wang and Eskiw, 2019).

Fold changes were calculated as follows:

$\Delta Ct_{\text{treatment sample}} = Ct_{\text{target gene}}$ in treatment sample - $Ct_{\text{normalizing gene}}$ in treatment sample

$\Delta Ct_{\text{control sample}} = Ct_{\text{target gene}}$ in control sample - $Ct_{\text{normalizing gene}}$ in control sample

$\Delta\Delta Ct = \Delta Ct_{\text{treatment sample}} - \Delta Ct_{\text{control sample}}$ $\qquad$ Fold change $= 2^{-\Delta\Delta Ct}$

Table 3.1 RT-qPCR primer sequences (Wang and Eskiw, 2019).

Target Gene	Forward Primer Sequence (5'→3')	Reverse Primer Sequence (5'→3')
EFEMP2	CGGTTCTCAGAGACCTGGATG	GCCCAAACCTGTGTCAACTTC
FAU	CGCATGCTTGGAGGTAAAGTC	TTCTCCTGTTTGGCCACCTTA
FKBP10	GCCGTGCTAATCTTCAACGTC	GGTGGTCTCATTGCAGGTCTC
PRDX5	GGGGTGGAGGAAGTAATCTG	GCATAGTGAAGGCCCTGAATG
SPARC	TACATCGGGCCTTGCAAATAC	GGTGACCAGGACGTTCTTGAG
CAT	TGCAAGCTAGTGGCTTCAAAA	TCCAATCATCCGTCAAAACAA
GPx1	CCTCCCCTTACAGTGCTTGTT	GAGAAGGCATACACCGACTGG
GSS	AGCTTTCCATCTGAGGACCAG	TCCTATCCCAAGTCAGGCACT
HMOX1	AAAGGAGGAAGGAGCCTATGG	AGCTGCCACATTAGGGTGTCT
SOD1	GGCAAAGGTGGAAATGAAGAA	GGGCCTCAGACTACATCCAAG
IL-1β	GCTACGAATCTCCGACCACCA	AACCAGCATCTTCCTCAGCTTG
IL-6	CGTCCGTAGTTTCCTTCTAGCTT	CAAAGGAGGACCTTGTGGCA
IL-8	TGCAGTTTTGCCAAGGAGTG	TGATAAATTTGGGGTGGAAAGG
TNF-α	CAATGGCGTGGAGCTGAGAG	TCTGGTAGGAGACGGCGATG

3.8.9 SIRT1 Activity Assay

To prepare 2DD cell lysates, cells were plated in 10-cm (diameter) dishes and treated as described previously (Section 3.8.2). The 50.0 µg/mL concentration was used for all haskap phenolic treatments, and 23.7 µg/mL was used for C3G. Additional untreated control plates were also grown to collect enough material for experiments using exclusively untreated cell lysate. At the end of the treatment period, cells were dissociated from the plate surface using 1.5 mL TrypLE Express and incubated until fully dissociated. This volume was transferred to 1.5 mL centrifuge tubes and centrifuged at 174 rcf for 5 min. Following centrifugation, the supernatant was removed leaving behind the cell pellet. Pellets were resuspended in 100 µL non-denaturing lysis buffer (50 mM Hepes KOH (pH 7.5), 420 mM NaCl, 0.5 mM EDTA disodium salt, 0.1 mM egtazic acid, and 10% glycerol (v:v)). Proteins were quantified employing UV spectroscopy at 280 nm using a NanoDrop™ 2000 Spectrophotometer (Thermo Fisher, Wilmington, DE, USA). Non-denaturing

lysis buffer was used as a blank and a volume of 1.5 µL was used for each sample. Samples were then diluted to be the same concentration using non-denaturing lysis buffer. All protein extracts were vortexed well and stored at -80 ± 2°C until analysis.

SIRT1 activity was measured fluorometrically using an assay kit (Abcam, Cat #: ab156065). All reactions were prepared in a 96-well black microtiter plate. To test direct activation of SIRT1 by phenolics, an initial mixture was prepared of 20 µL water, 5 µL SIRT1 assay buffer, 5 µL 2 mM NAD, 5 µL 500 µg/mL haskap phenolic extract in DMSO (237 µg/mL for C3G), and 5 µL fluoro-substrate peptide. Developer was then added (5 µL) to each reaction and mixed well, followed by the addition of 5 µL recombinant SIRT1 (diluted 1 in 10 with water). The plate was immediately placed in the plate reader and fluorescence was measured at (350 nm excitation/460 nm emission) every 2 min for 60 min. Negative controls were run with no NAD and no SIRT1.

To test SIRT1 activity in untreated lysates in the presence of haskap phenolics and C3G, the initial mixture was prepared with 25 µL water (no NAD was added), 5 µL SIRT1 assay buffer, 5 µL 500 µg/mL phenolic extract in DMSO (237 µg/mL for C3G), and 5 µL fluoro-substrate peptide. After the addition of the developer, 5 µL of untreated cell lysate was added and fluorescence was measured. To test SIRT1 activity in haskap phenolic and C3G-treated lysates, the initial mixture was prepared with 25 µL water, 5 µL SIRT1 assay buffer, 5 µL Trichostatin A (10 µM in DMSO), and 5 µL 2 mM NAD. Developer was then added (5 µL) to each reaction and mixed well, followed by the addition of 5 µL treated cell lysates. Fluorescence was measured as described.

Total reaction volumes in all cases were 50 µL. After fluorescence was measured for all wells, an arbitrary timepoint was selected and the fluorescence at that time was recorded for each reaction. These values were then normalized by dividing the fluorescence of the treated sample by the fluorescence of the untreated control sample and reported as normalized fluorescence (in arbitrary units).

3.8.10 siRNA Knockdown of SIRT1

Cells were plated in 10-cm dishes and grown to ~80% confluence. To begin siRNA reactions, 1.5 mL centrifuge tubes were prepared for each plate containing 50 µL of

Lipofectamine® 3000 reagent and 575 µL of Opti-Mem (reduced serum media). Another set of centrifuge tubes were prepared (one for each plate) containing 50 µL of siRNA at 10 µM (SIRT1 or control), 25 µL P3000™ reagent, and 550 µL Opti-Mem. Each tube was mixed by pipetting and then tubes were combined (one tube containing Lipofectamine® 3000 reagent mixture and one tube containing siRNA mixture). Centrifuge tubes were incubated at room temperature for 15 min.

During this incubation time, cell plates were prepared by aspirating media and washing with 5 mLs cold 1X PBS followed by washing with 2 mLs Opti-Mem per plate. After the 15 min, 1.25 mL Opti-Mem was added to each plate along with the respective siRNA mixture (1.25 mLs). Plates were incubated at 37°C for 4 h and then 2.5 mLs 2X DMEM (20% (v:v) bovine calf serum (CS) and 2% (v:v) penicillin-streptomycin 10X solution) was added. Plates were incubated at 37°C for 18 h and then media was aspirated and cells were treated as described previously (Section 3.8.2). Untreated cells exposed to control (scramble) siRNA and untreated cells exposed to SIRT1 siRNA were used as controls. The 50.0 µg/mL concentration was used for all Tundra variety haskap phenolic treatments, and 23.7 µg/mL was used for C3G.

Following the 72 h treatment period, the media was aspirated and cells were dissociated with 1.5 mL TrypLE Express at 37°C for 5 min or until fully dissociated. A scraper (Thermo Fisher, Rochester, NY, USA) was used to ensure removal of as many cells from the plate as possible, and this volume was transferred to a 1.5 mL centrifuge tube. Protein extraction and Western blotting were then performed as described previously (Section 3.8.4-5).

3.9 Statistical Analysis

Statistical analysis of chemical experimental data was performed using SPSS for Windows version 22.0 (IBM SPSS Inc., Chicago, IL, USA) for one-way analysis of variance (ANOVA). Difference between means ($p<0.05$) was determined using the multiple-comparison Tukey's HSD (honestly significant difference) multiple comparison. Statistical analysis for biological experiments was performed using Microsoft Excel for Office 365 MSO (16.0.11727.20222) 32-bit for student t-tests with a significance cutoff of $p<0.10$.

4. RESULTS AND DISCUSSION

4.1 Physicochemical Analysis

Physicochemical analyses (colour, pH, size, total soluble solids (°Brix)) are important for evaluating the quality of berries and their juices and for identifying the best potential uses for different haskap varieties. Due to the limited information available on the physicochemical properties of haskap berries, this data will be an important addition to our scientific knowledge for future research and for commercialization purposes. Mean and standard deviation physicochemical and moisture analysis results for juices, fresh berries, and macerate of Aurora, Blizzard, Honey Bee, Indigo Gem, and Tundra haskap varieties are shown in Table 4.1.

Table 4.1 Mean and standard deviation physicochemical and moisture results for juices, fresh berries, and macerate from Aurora, Blizzard, Honey Bee, Indigo Gem, and Tundra haskap varieties.[1]

Physicochemical Parameter		Variety				
		Aurora	Blizzard	Honey Bee	Indigo Gem	Tundra
Colour[2]	L*	8.34 ± 0.22^{d}	5.03 ± 0.14^{a}	6.67 ± 0.12^{c}	6.14 ± 0.11^{b}	4.89 ± 0.12^{a}
	a*	11.94 ± 0.25^{e}	2.45 ± 0.52^{a}	9.06 ± 0.07^{d}	7.07 ± 0.07^{c}	3.68 ± 0.09^{b}
	b*	4.95 ± 0.26^{e}	0.44 ± 0.04^{a}	2.92 ± 0.09^{d}	2.13 ± 0.10^{c}	1.06 ± 0.03^{b}
	Chroma (C*)	12.92 ± 0.33^{e}	2.49 ± 0.51^{a}	9.52 ± 0.09^{d}	7.39 ± 0.10^{c}	3.83 ± 0.09^{b}
	Hue angle (Θ)	22.49 ± 0.68^{c}	10.61 ± 2.56^{a}	17.78 ± 0.35^{b}	16.73 ± 0.63^{b}	16.10 ± 0.37^{b}
pH[2]		3.11 ± 0.02^{b}	3.31 ± 0.03^{c}	3.17 ± 0.04^{b}	3.18 ± 0.04^{b}	2.99 ± 0.02^{a}
Length[3]		23.49 ± 3.23^{b}	23.31 ± 3.13^{b}	19.28 ± 1.61^{a}	18.79 ± 1.58^{a}	17.41 ± 1.65^{a}
Diameter[3,4]		10.04 ± 1.04^{ab}	11.97 ± 0.96^{d}	9.35 ± 0.73^{a}	11.64 ± 1.13^{cd}	10.62 ± 1.06^{bc}
°Brix[2]		13.91 ± 0.49^{a}	14.59 ± 0.19^{b}	13.70 ± 0.08^{a}	17.05 ± 0.03^{d}	15.96 ± 0.07^{c}
Moisture (%)[5]		86.21 ± 0.04^{d}	86.04 ± 0.10^{c}	86.05 ± 0.05^{cd}	84.10 ± 0.04^{a}	85.53 ± 0.07^{b}

[1]Mean ± standard deviation results of triplicate sample analysis.
[2]Measured on juices.
[3]Measurements (mm) made on fresh berries from the 2018 crop.
[4]Measured at the widest point of the fresh berry.
[5]Measured on berry macerate.
[a-e]Mean values in the same row followed by a common letter were not statistically different ($p < 0.05$) by Tukey's HSD multiple range test between the varieties.

The Hunterlab system measures sample colour mathematically, and these results are often used for quality control and raw material selection by commercial food processors and producers. The L* measurement refers to the lightness of a juice on a scale of 0-100, with 0 being black and 100 white. The other two measurements, a* and b*, describe the juice on a colour scale: for a*, green to red (-100 to 100); and for b*, blue to yellow (-100 to 100). Once these measurements are obtained, sample chroma and hue angle can be calculated using $\tan^{-1}$ (b*/a*) and the square root of $(a*)^2 + (b*)^2$, respectively. Hue angle indicates the predominant colour of the sample, and the intensity of this colour is represented by the chroma value (Green and Low, 2013).

Sample L* values ranged from 4.89-8.34 (Table 4.1) with Tundra and Blizzard being significantly darker than the other varieties analyzed, and Aurora significantly lighter. However, even the lightest value (8.34), found for Aurora, indicates a very dark juice. These values were considerably lower than those reported for haskaps grown in Poland and Korea, which ranged from 20 to 30 (Lee et al., 2015; Ochmian, et al., 2012). These observed differences in results could be due to many factors with the major being fruit ripeness. For example, it has been reported that significant decreases in the lightness of the juice produced from Polish 'Wojtek' haskaps were observed from early to late fruit ripeness, with the L* value changing from 41.15 to 21.08, although the exact timeframe was not defined (Ochmian et al., 2012). This data suggests that the time of harvest has a significant effect on juice L* value. Berry harvest for this study was based on input from Dr. Bob Bors, director of UofS Horticulture Field Laboratory so as to obtain fruit at near optimum ripeness based on estimated °Brix values of approximately 15. Other factors that can impact fruit/juice lightness measurements include variety, environmental growing conditions, fruit damage, phenolic composition, and phenolic degradation due to storage/polyphenol oxidase activity.

Sample hue angle results ranged from 10.61 to 22.49° (Table 4.1), indicating a predominant juice colour of deep red for all samples, shifting slightly towards red-orange with increasing b* values. Aurora displayed the largest hue angle of 22.49° and Blizzard the least at 10.61°, which was significantly lower than all other varieties analyzed.

Aurora and Honey Bee juices had the highest chroma values of 12.92 and 9.52 (Table 4.1), respectively, indicating the most saturated colouration. Blizzard and Tundra had significantly lower chroma values of 2.49 and 3.83, respectively, meaning that the intensity or purity of the

colouration was much lower for these juices, more gray/black than red, which aligned with their low L* values.

Within the literature, the limited data on colour varies, with no published datasets in agreement for measurements of both a* and b*. The a* values of the haskap varieties analyzed in this study ranged from 2.45-11.39 and were significantly lower than those reported in literature of ~20 for a Korean variety (Lee et al., 2015); these results were generally higher or similar to those reported for two Polish varieties of 1.43 and 4.27 (Ochmian et al., 2012). Furthermore, the peel of the Japanese variety 'Nakai,' grown in Hokkaido, was reported to have an a* value of 0 (Yamamoto et al., 2014).

Literature b* values for Nakai and an unidentified Korean variety were reported as -5 and ~10, respectively (Lee et al., 2015; Yamamoto et al., 2014). These results are very different from each other and also from the results obtained in this study of 0.44 to 4.95. As with L*, this variation is related to factors such as fruit ripeness, variety, environmental growing conditions, phenolic composition, peel *vs*. juice or whole berry measurement, and phenolic degradation due to storage/polyphenol oxidase activity.

The colour analysis results from this study are important to producers and growers who need to make educated decisions about which variety to use and for what purpose. These Saskatchewan-grown varieties produced dark purple to purple-red juices, with Aurora and Honey Bee the lightest of those studied. The strength of haskap juice pigments in food product formulations (e.g. ice cream, yogurt) has been demonstrated, but must be carefully assessed by manufacturers as haskap juices often create strong visual colouration long before any noticeable haskap flavour is achieved (Bors, 2018).

The analysis of pH is important for assessing the flavour profile and potential uses of a berry juice. Results for all haskap varieties analyzed in this study indicated acidic juices with values ranging from 2.99 to 3.31 (Table 4.1). Tundra had the lowest pH of 2.99 and Blizzard the highest of 3.31, with Aurora, Honey Bee, and Indigo Gem showing no significant differences between their values. A study of seven haskap varieties (including Indigo Gem and Tundra) grown in Switzerland over three harvesting years (2014-2016) reported pH values of juices ranging from 2.7 to 3.3 (Auzanneau et al., 2018). The three-year pH range observed for Tundra was 2.8-3.1 and Indigo Gem was 2.9-3.3, which are in agreement with the values obtained for these varieties in

this study. The pH values observed in this study are similar to blackberries (2.99) but are more acidic than blueberries (3.64) and saskatoon berries (3.95-4.10) (Ribeiro de Souza, 2017; Rios de Souza et al., 2014).

Total soluble solid (TSS) measurement is defined as the grams of sucrose per 100 g of sample (i.e. % carbohydrate) and is reported as degrees Brix (ºBrix). ºBrix measurements are often used to appraise the quality of fruit juices, with better quality and value realized for higher ºBrix values. Government regulations on the minimum required ºBrix values exist for most commercial fruit juices (Government of Canada Food and Drug Regulations, 2018). These measurements are also key for fruit processing industries, where carbohydrate content significantly impacts the production of fruit/berry products (e.g. fermentation for berry wines) (Wang, 2017).

The observed ºBrix values in this study ranged from 13.70-17.05 ºBrix (Table 4.1) for Honey Bee and Indigo Gem, respectively, with a mean of 15.04. These results demonstrated that the berries were well-ripened based on the ºBrix criteria used at the UofS Horticulture Field Laboratory, and were within the range of values reported in literature for haskaps (Bors, 2007). As an example, a study of seven varieties including three from the UofS (Indigo Gem, Indigo Treat, and Tundra) reported a ºBrix range of 9.74-18.30, demonstrating the wide range of values for this fruit (Auzanneau et al., 2018). The aforementioned literature values also showed a high variation based on harvest year, with Tundra values ranging from 14.8 in 2014 to 10.8 ºBrix in 2016 (Auzanneau et al., 2018). Total soluble solids analysis of haskap fruit over a five-year period at the UofS Horticulture Field Lab has also shown high variability in values between varieties ranging from 10-20 ºBrix (Bors, 2018). During this timeframe, Tundra, specifically, had a range from 12.5 to 17.0 ºBrix (Bors, 2018). Based on the significant variation in ºBrix seen between varieties grown in the same geographical area/season, and also the differences seen for a single variety in different harvest years, it can be hypothesized that the differences found in ºBrix values are related to variety and also their growing conditions.

In foods, ºBrix measures soluble solids in a sample, not only carbohydrates, which can be seen when comparing carbohydrate analytical data (measured via high performance liquid chromatography with refractive index detection (HPLC-RI)) to these values. Of the haskap varieties analyzed, Indigo Gem had the highest ºBrix value of 17.05 (Table 4.1) and the highest carbohydrate content (12.67%; Table 4.2), whereas Honey Bee had the lowest ºBrix of 13.70

54

(Table 4.1) and also the lowest carbohydrate content (9.04%; Table 4.2). For these varieties, the °Brix values were respectively 1.3 and 1.5x higher than the total carbohydrate content, showing the presence of other water-soluble solids (e.g. organic acids or complex carbohydrates such as soluble fibre). A value of 8.34% fibre has been reported for haskap berries of a wild Russian variety, which could explain the differences observed between carbohydrate content and °Brix values, as soluble fibre contributes to TSS measurements (Caprioli et al., 2016; Brown, 1967). To determine if fibre was a major contributor to the observed °Brix of the samples analyzed in this study, total dietary fibre analysis was conducted on the Indigo Gem variety. Results showed a total dietary fibre content of $2.30 \pm 0.06\%$, suggesting that fibre was not completely responsible for the observed °Brix/total carbohydrate disparity. The °Brix, carbohydrate, and fibre values for the Indigo Gem variety (17.05 °Brix; 12.67% total carbohydrates; 2.3% fibre) were similar to reports for other berry species such as blueberry (14.67 °Brix; 10.0% total carbohydrates; 2.4% fibre) and sweet cherry (18.67 °Brix; 12.8% total carbohydrates; 2.1% fibre) (United States Department of Agriculture, 2018; Rios de Souza et al., 2014).

Haskap berry size will be presented and discussed in the phenolics section of this report (Section 4.3.2), and moisture will be discussed with chemical composition results (Section 4.2.2).

4.2 Chemical Composition

4.2.1 Carbohydrates and Polyols

Carbohydrates in fruits provide sweetness, one of the most important factors in flavour determination and consumer appeal. Carbohydrate (fructose, glucose, and sucrose) content of haskap samples was determined using HPLC-RI. Carbohydrates were qualitatively and quantitatively analyzed by comparison of sample retention times to external standards, spiking experiments, and peak area/height comparison to standard curves. Mean and standard deviation results for the carbohydrate content of Aurora, Blizzard, Honey Bee, Indigo Gem, and Tundra haskap varieties are shown in Table 4.2. Representative HPLC-RI chromatograms of carbohydrate standards (fructose, glucose, and sucrose) and each of the five varieties are shown in Figures 4.1 and 4.2 (A-E), respectively.

Table 4.2 Mean and standard deviation results for fructose, glucose, and sucrose concentrations in Aurora, Blizzard, Honey Bee, Indigo Gem, and Tundra haskap varieties.[1,2]

	Variety				
Carbohydrate	Aurora	Blizzard	Honey Bee	Indigo Gem	Tundra
Fructose (F)	5.23 ± 0.16^b	5.61 ± 0.29^{bc}	4.31 ± 0.18^a	6.10 ± 0.24^c	5.12 ± 0.15^b
Glucose (G)	4.95 ± 0.27^b	5.28 ± 0.25^b	4.09 ± 0.12^a	5.88 ± 0.20^c	4.88 ± 0.13^b
Sucrose	ND[3]	ND	ND	ND	ND
Total[4]	10.81 ± 0.43^{bc}	11.53 ± 0.55^c	9.04 ± 0.30^a	12.67 ± 0.42^d	10.43 ± 0.15^b
F/G[5]	1.06	1.06	1.06	1.04	1.05

[1] g/100 g fresh weight (FW).
[2] Mean ± standard deviation results of triplicate sample analysis.
[3] ND, not detected <0.07% (HPLC-RI detection limit for sucrose).
[4] Includes polyols from Table 4.3.
[5] Fructose/glucose ratio.
[a-d] Mean values in the same row followed by a common letter were not statistically different ($p < 0.05$) by Tukey's HSD multiple range test between the varieties.
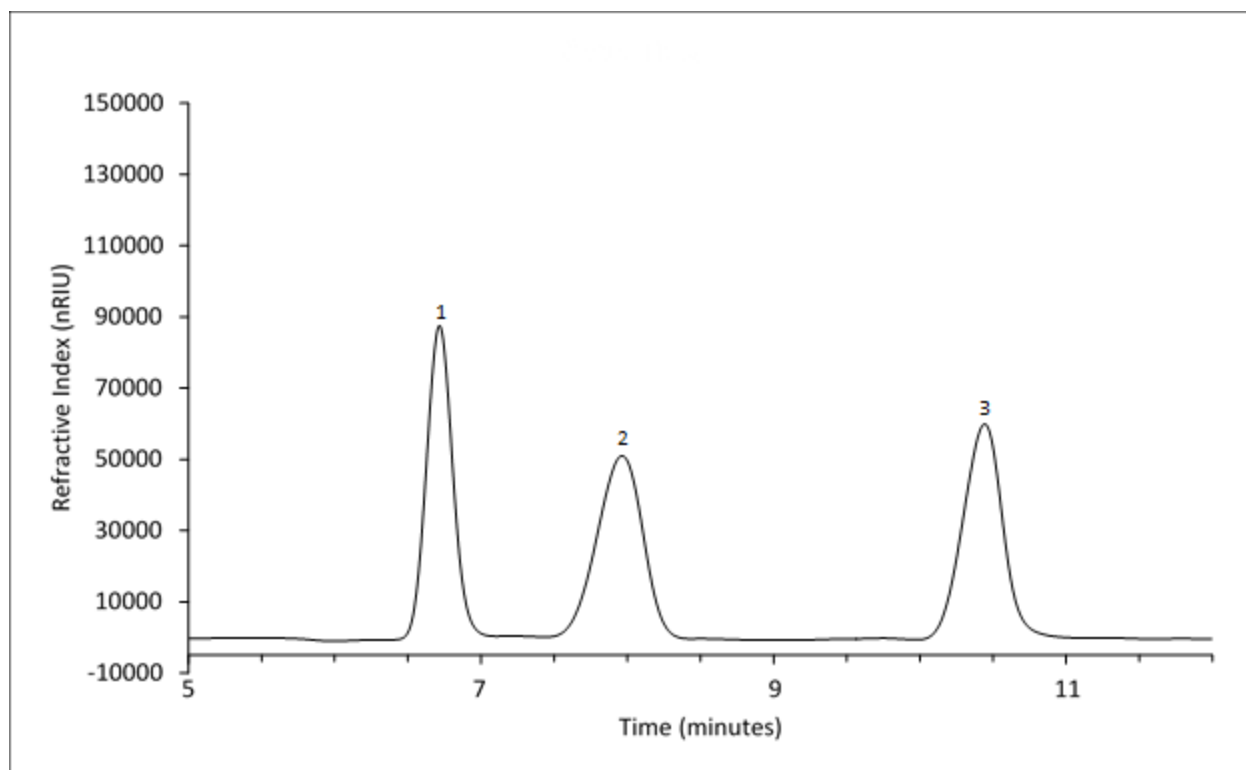
Figure 4.1 HPLC-RI chromatogram of a carbohydrate standard. Peak identities: 1. fructose; 2. glucose; and 3. sucrose (all at 2.5% (w:v)).
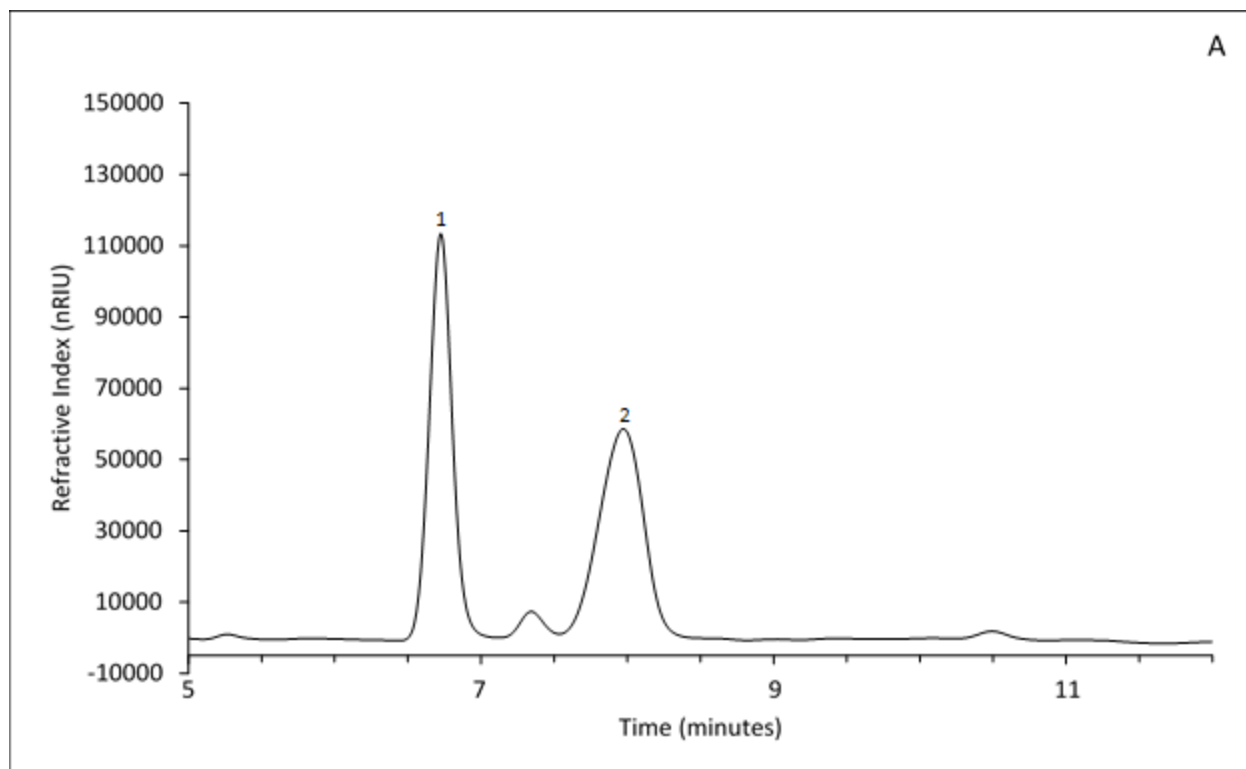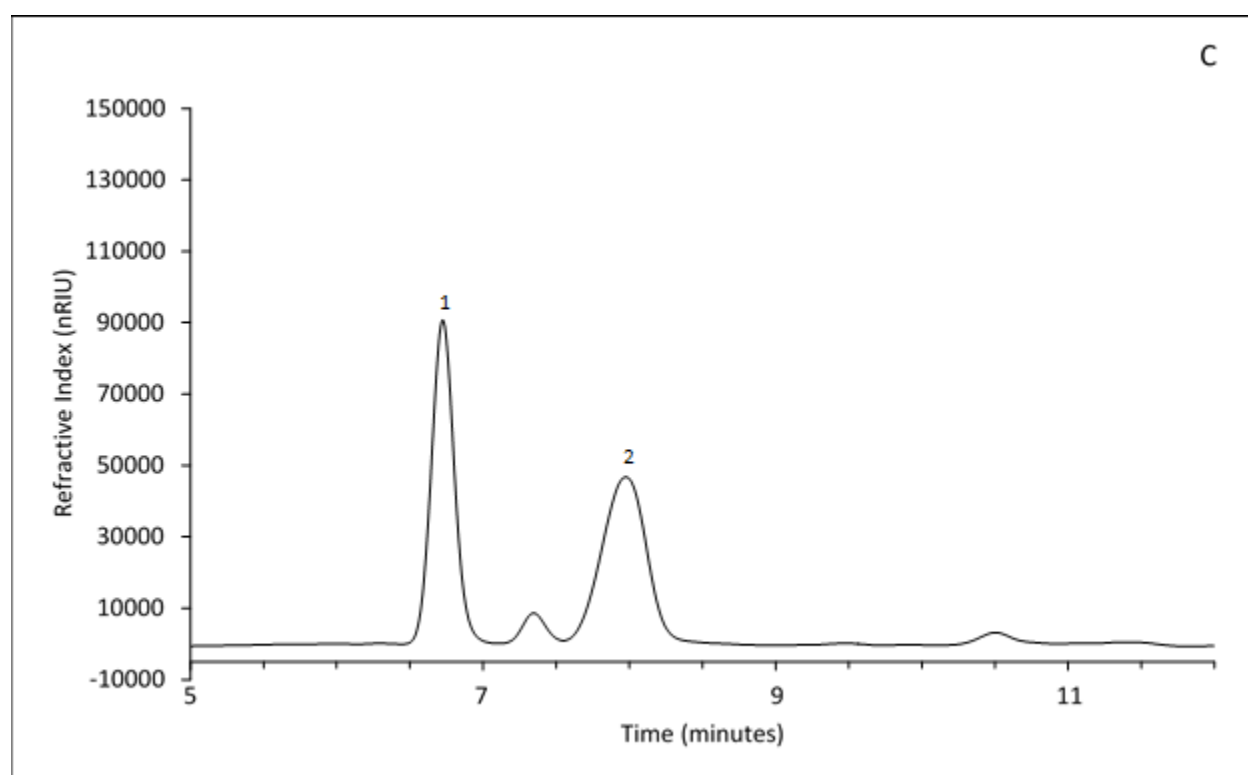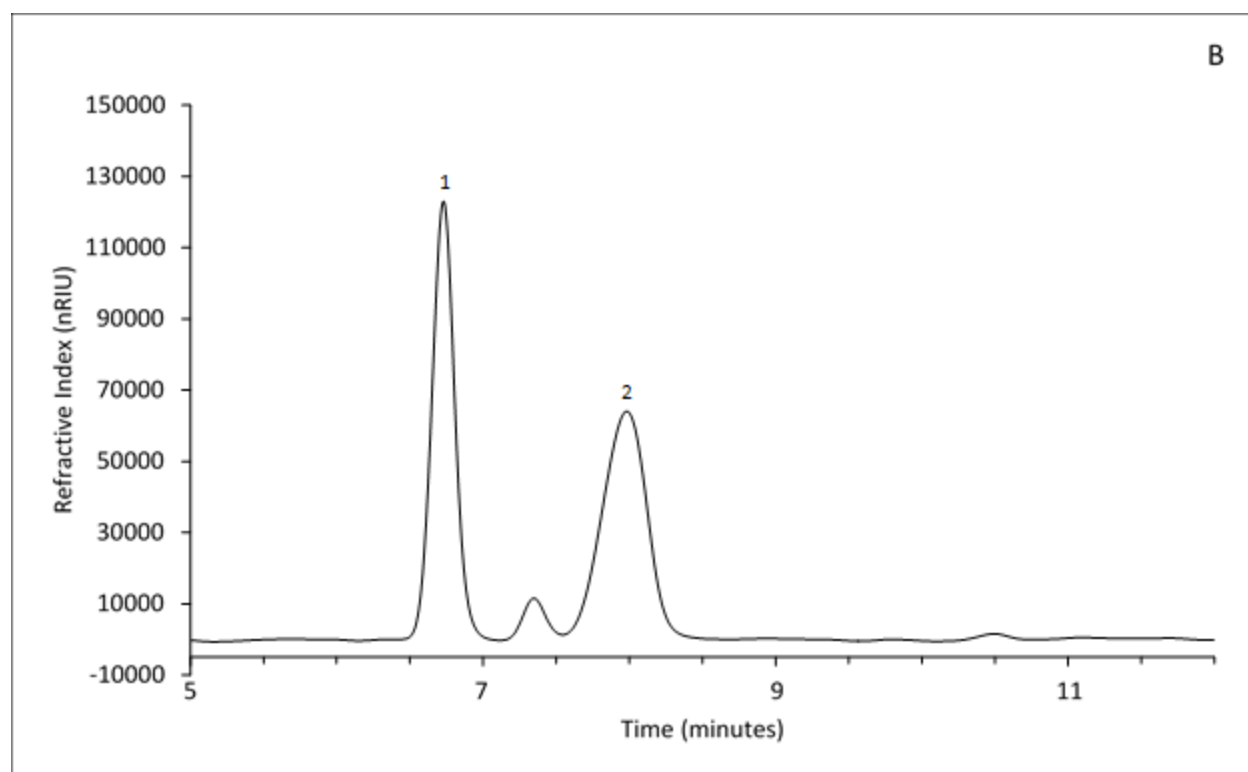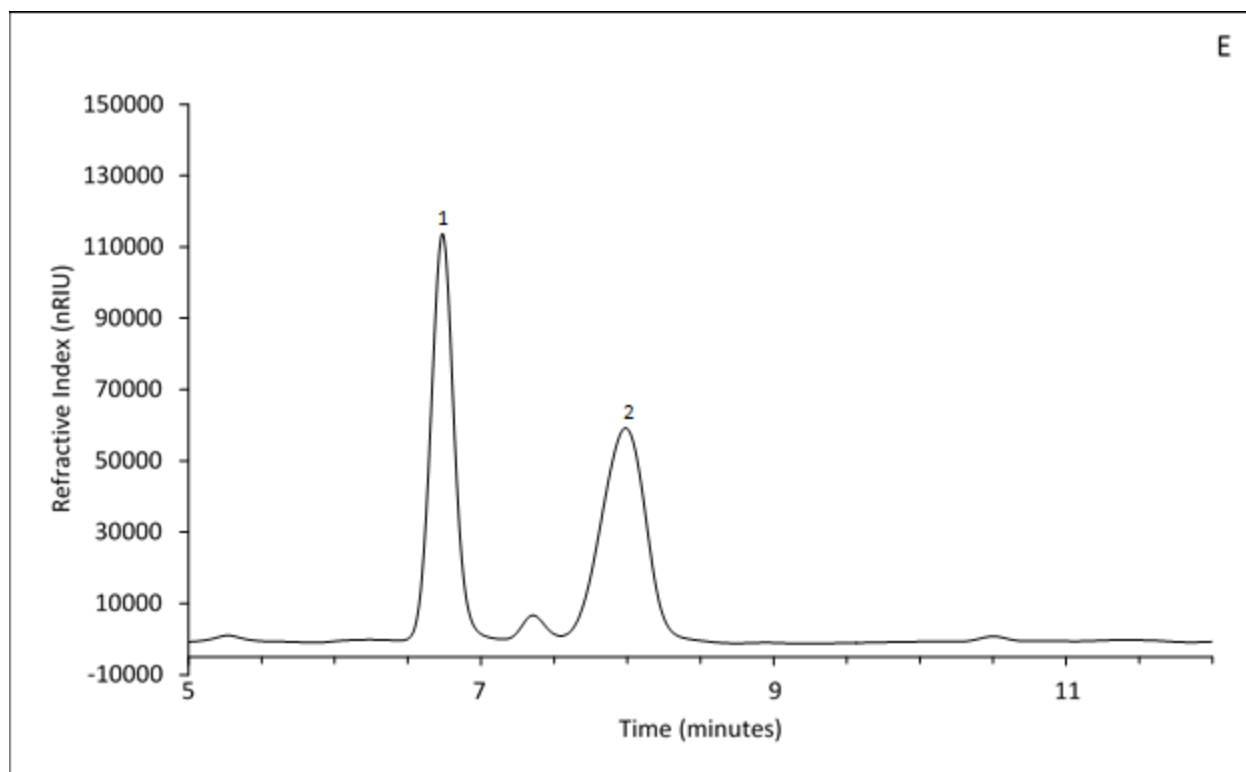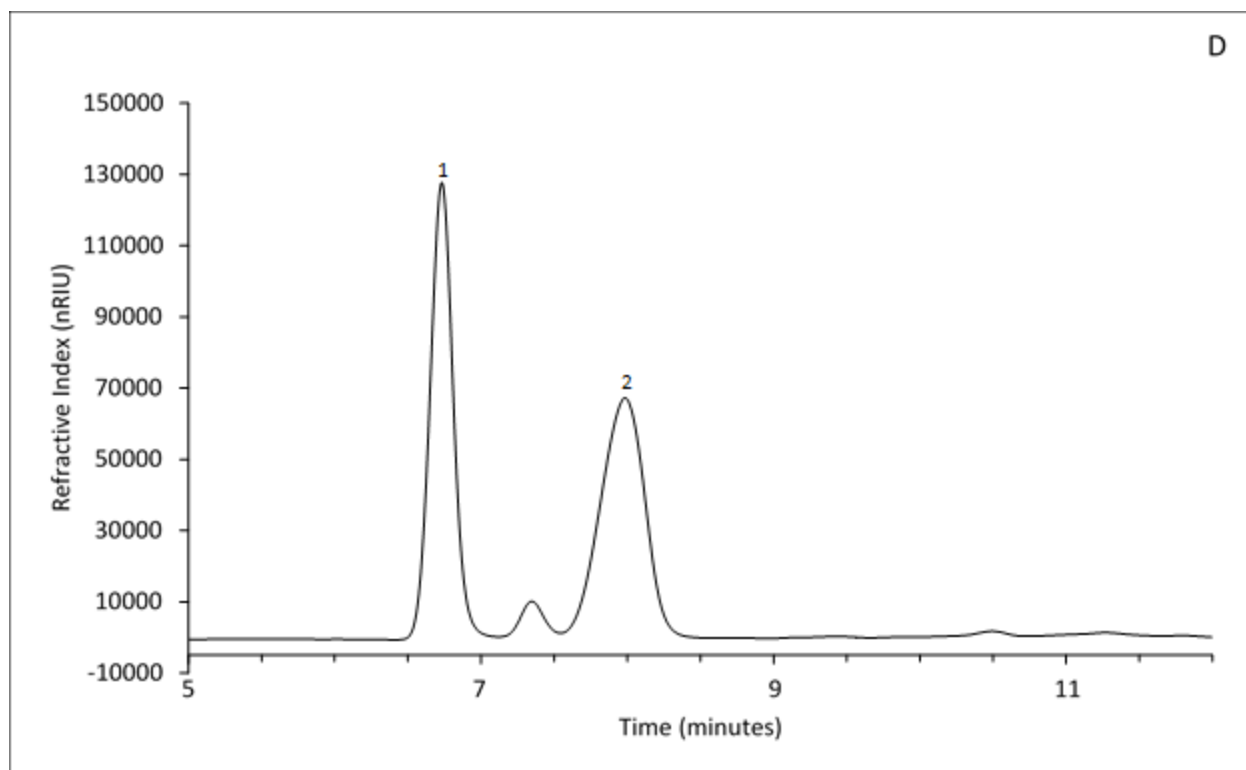
Figure 4.2 HPLC-RI chromatograms of the carbohydrates in haskap juice samples. Chromatogram identification: A. Aurora; B. Blizzard; C. Honey Bee; D. Indigo Gem; and E. Tundra. Peak identities: 1. fructose; and 2. glucose.

Fructose and glucose were found to be the major carbohydrates in the haskap juice samples analyzed, and sucrose was not detected (0.07% detection limit) in any sample. In addition to the two major carbohydrate peaks with approximate retention times (RT) of 8.0 min (glucose) and 6.7 min (fructose), HPLC-RI chromatographic results showed two additional peaks with RT values of approximately 7.3 min, tentatively identified as sorbitol, and 10.6 min, which could not confidently be identified as sucrose. Sucrose showed a consistent RT of ~10.4 min in standards, and spiking experiments resulted in two closely eluting peaks, demonstrating that the unknown peak at ~10.6 min was not sucrose.

As the presence of inositol and sorbitol (polyols; Lee et al., 2015; Wojdylo et al., 2013), other hexoses (e.g. galactose; Lee et al., 2015), and low (trace to 0.11g/100 g FW; Senica et al., 2018; Oszmianski et al., 2016; Rupasinghe et al., 2015) levels of sucrose have been reported in haskaps, an alternative chromatographic method employing high performance anion exchange chromatography with pulsed amperometric detection (HPAE-PAD) was used to investigate the remaining unidentified compounds in the haskap juice samples. This carbohydrate analytical technique has the ability to separate structurally similar carbohydrates and polyols and has much lower detection limits for these compounds when compared to HPLC-RI (Willems and Low, 2012). A series of standards were used for this purpose that included arabitol, fucitol, galactose, inositol, lactitol, sorbitol, sucrose, and tagatose. This second analytical platform was used to identify and quantitate arabitol, inositol, and sorbitol in the haskap samples using retention time comparison to standards, spiking experiments, and standard curves (Table 4.3). The HPAE-PAD results also confirmed the absence of sucrose in all samples (detection limit of 5 mg/L or 0.0005%), and the identification of the HPLC-RI peaks at approximately 7.3 min as sorbitol, and 10.6 min as inositol. Representative HPAE-PAD chromatograms of a polyol (arabitol, inositol, and sorbitol) standard, and the five haskap varieties are shown in Figures 4.3 (A-F).

Table 4.3 Mean and standard deviation results for arabitol, inositol, and sorbitol concentrations in Aurora, Blizzard, Honey Bee, Indigo Gem, and Tundra haskap varieties.[1,2]

	Variety				
Polyol	Aurora	Blizzard	Honey Bee	Indigo Gem	Tundra
Arabitol	<0.01[a]	<0.01[a]	0.02 ± <0.01[c]	0.01 ± <0.01[b]	ND[3]
Inositol	0.15 ± <0.01[a]	0.08 ± <0.01[b]	0.15 ± <0.01[a]	0.07 ± <0.01[b]	0.06 ± <0.01[a]
Sorbitol	0.47 ± 0.02[b]	0.55 ± 0.03[c]	0.47 ± <0.01[b]	0.61 ± 0.03[c]	0.37 ± 0.02[a]

[1] g/100 g FW.
[2] Mean ± standard deviation results of triplicate sample analysis.
[3] ND, <0.5 mg/L (detection limit of arabitol).
[a-c] Mean values in the same row followed by a common letter were not statistically different ($p<0.05$) by Tukey's HSD multiple range test between the varieties.

61
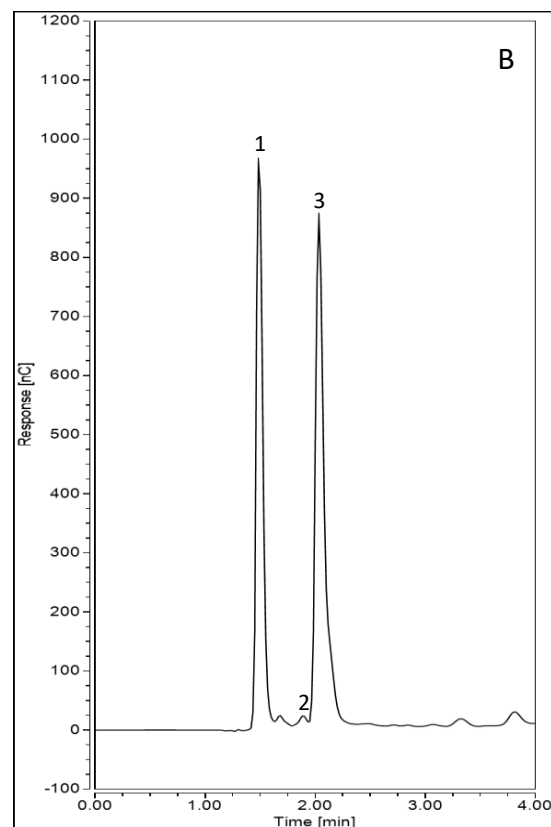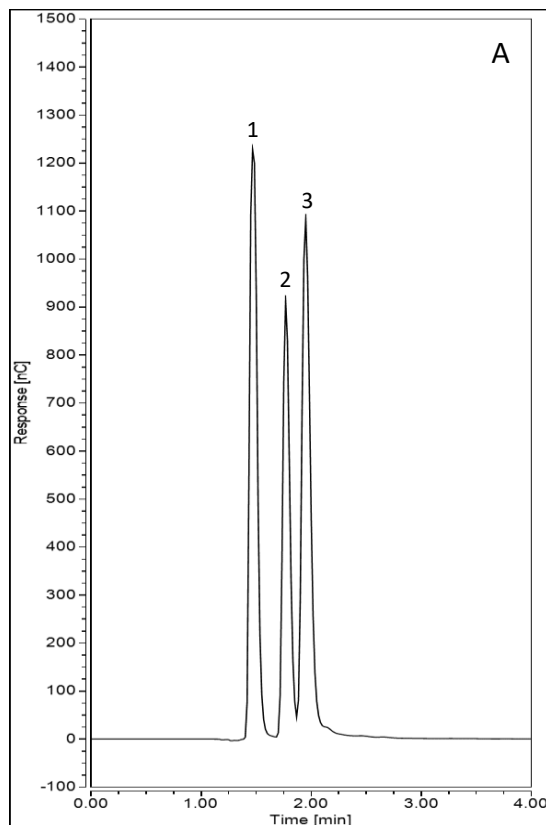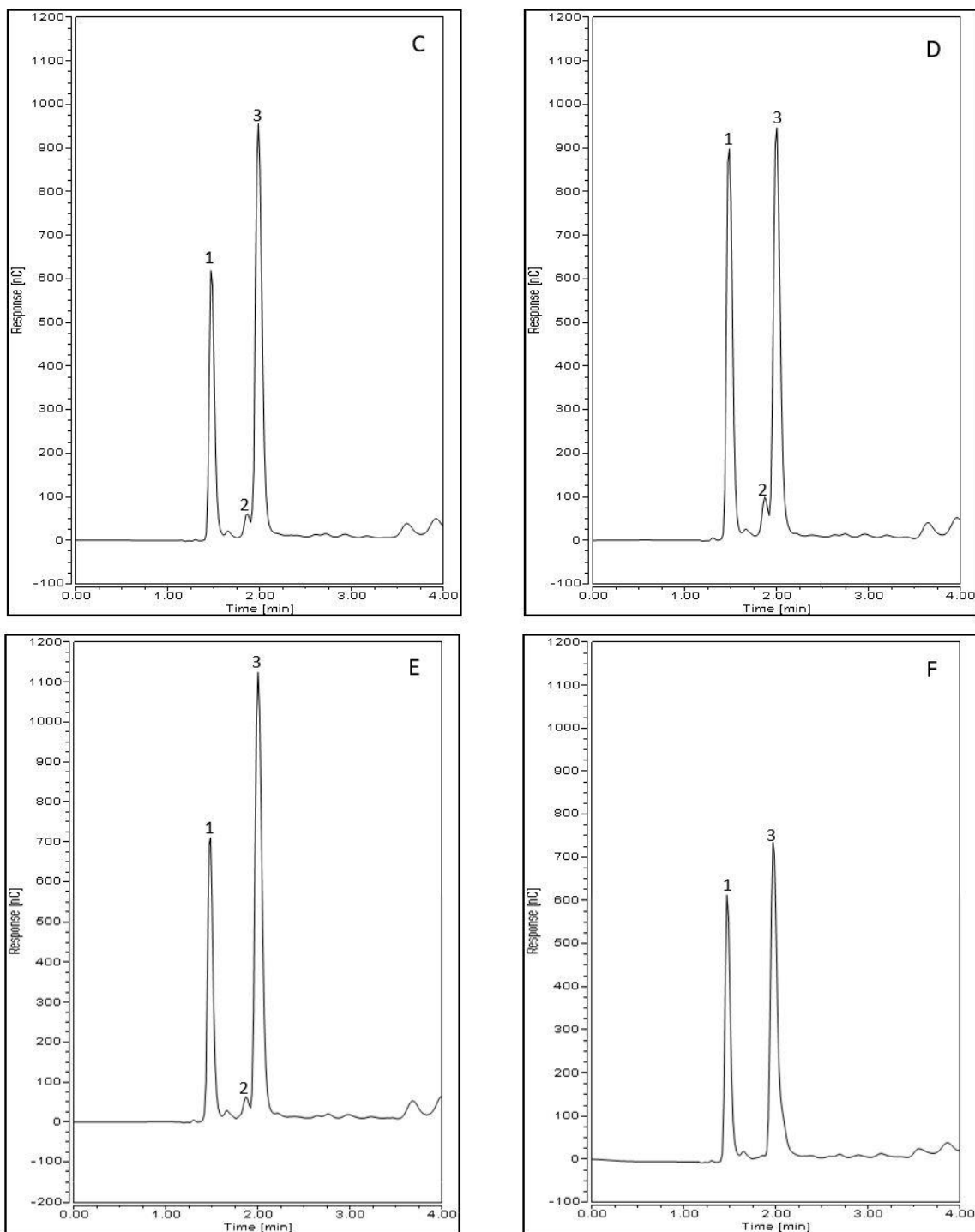
Figure 4.3 HPAE-PAD chromatograms of a polyol standard and haskap juice samples. Chromatogram identification: A. Polyol standard (concentrations ranged from 50 to 150 mg/L); B. Aurora; C. Blizzard; D. Honey Bee; E. Indigo Gem; and F. Tundra. Peak identities: 1. inositol; 2. arabitol; and 3. sorbitol.

The HPAE-PAD results showed that sucrose (RT of ~7.9 min) was not present in any of the haskap varieties studied (detection limit of 5 mg/L or 0.0005%) as clearly indicated by comparison of the carbohydrate standard (Figure 4.4A) to the Honey Bee variety (representative sample; Figure 4.4B), which showed no peak in the sample matching this RT.
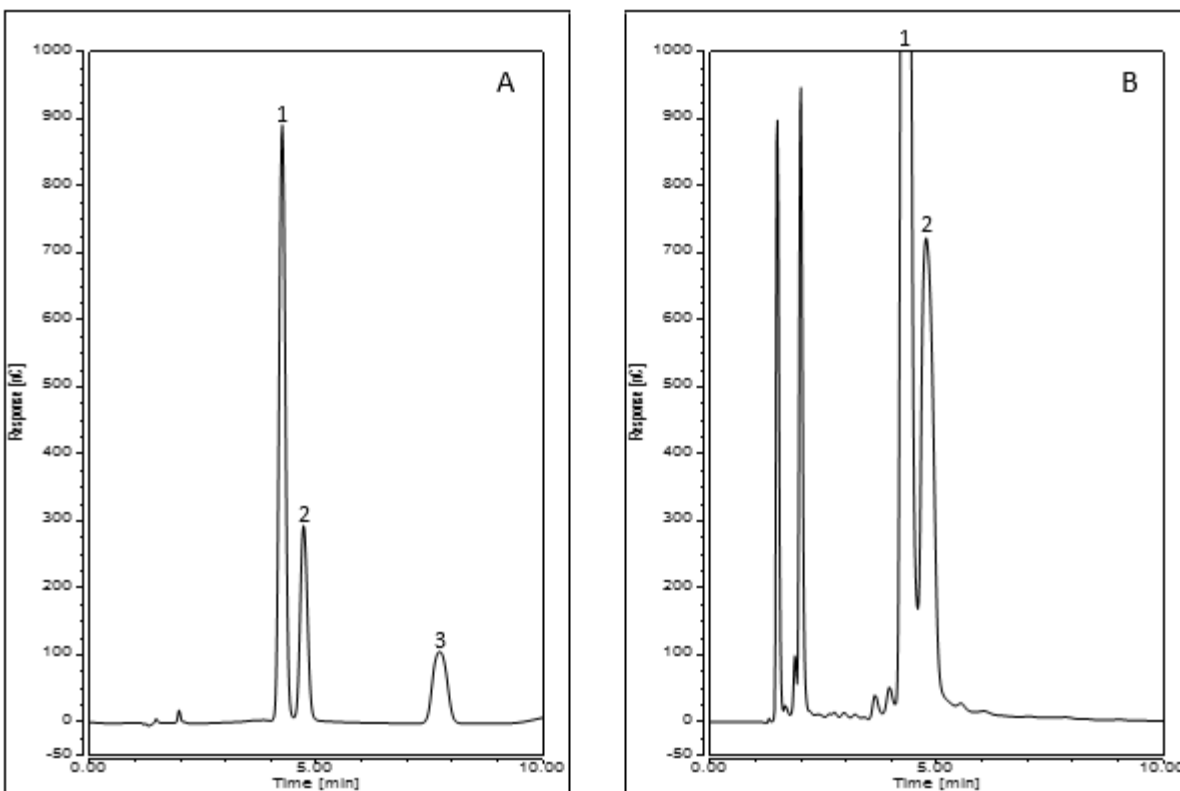
Figure 4.4 HPAE-PAD chromatograms of a carbohydrate standard (concentrations of 100 mg/L; A) and the Honey Bee haskap variety (B). Peak identities: 1. glucose; 2. fructose; and 3. sucrose.

Based on these results, a new carbohydrate/polyol mixed standard containing fructose, glucose, inositol, and sorbitol was prepared, and representative HPLC-RI chromatograms of this standard and the Blizzard variety are shown in Figures 4.5A and B, respectively. Arabitol was not included in this standard, as the concentration of this polyol in the haskap samples was below the determined refractive index detection limit for the equipment used for analysis.
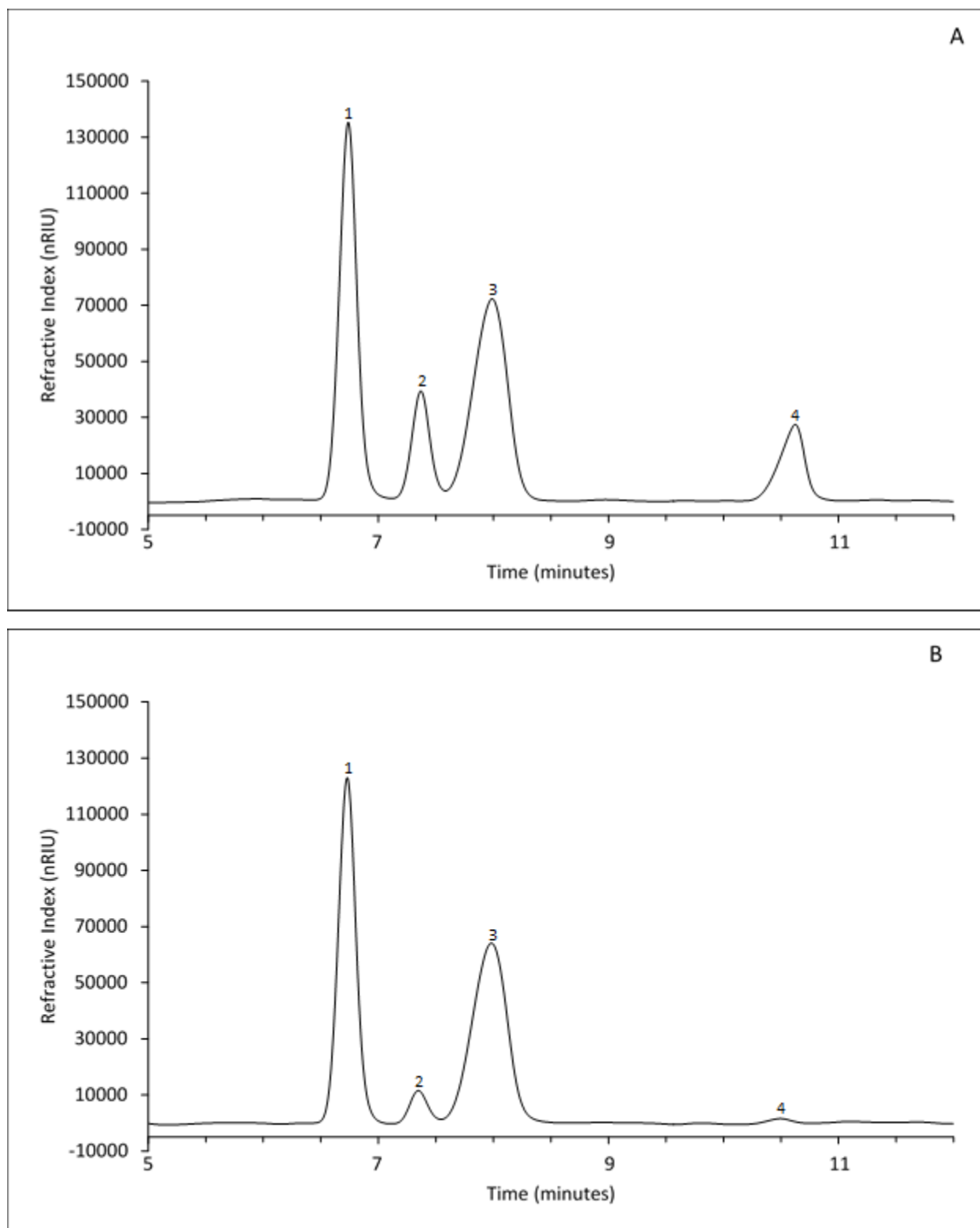
Figure 4.5 HPLC-RI chromatograms of carbohydrates/polyols in a mixed standard (concentrations of 2.5% (w:v); A) and the haskap variety Blizzard (B). Peak identities: 1. fructose; 2. sorbitol; 3. glucose; and 4. inositol.

Haskap sample fructose concentrations ranged from 4.31 (Honey Bee) to 6.10 g/100 g FW (Indigo Gem), with a mean value of 5.27 g/100 g FW. For glucose concentration, the range was 4.09 (Honey Bee) to 5.88 (Indigo Gem) g/100 g FW, with a mean value of 5.02 g/100 g FW. Total carbohydrate concentrations followed the pattern of Indigo Gem (12.67 g/100 g FW) > Blizzard (11.53 g/100 g FW) > Aurora (10.81 g/100 g FW) > Tundra (10.43 g/100 g FW) > Honey Bee (9.04 g/100 g FW). All varieties had similar fructose/glucose (F/G) ratios, ranging from 1.04 to 1.06.

The carbohydrate results from this study are significantly higher than those previously reported, which include: (a) 1.56 to 2.59 g/100 g FW for four Slovenia-grown Canadian varieties (Aurora, Borealis, Honey Bee, and Tundra), where distilled water was used as the extraction solvent (Senica et al. 2018); (b) 6.48 g/100 g FW for the Wojtek variety, where 1% phosphoric acid was used as the extraction solvent (Oszmianski et al., 2016); and (c) 7.2 g/100 g FW for a wild Moravian cultivar with distilled water extraction (Palíková et al., 2008). In each of these studies, HPLC was the analytical approach with either RI or evaporative light scattering detection (ELSD). The mobile phase used for carbohydrate separation was either acetonitrile:water (75:25 (v:v)) or 100% water, and all stationary phases were designated as suitable (e.g. $-NH_2$) for carbohydrate analysis. In two instances, a C_{18} clean-up step prior to carbohydrate analysis was used (Oszmianski et al., 2016; Palíková et al., 2008). Based on this information, it is unlikely that the analytical techniques employed for carbohydrate analysis could account for the large variation observed in these results. Factors that could significantly impact carbohydrate content include fruit maturity, variety, environmental growing conditions, and geographical location. In comparison to other berries, results from this study show that haskaps have a carbohydrate content that is slightly lower (9.04-12.67 g/100 g FW) than blueberry (10.8-14.3 g/100 g FW) and very similar to saskatoon berry (10.94-11.98 g/100 g FW) (Ribeiro de Souza, 2017; Wang et al., 2008).

A number of references indicate low (trace to 0.11g/100 g FW) sucrose concentrations in select haskap varieties (e.g. Borealis; Senica et al., 2018; Oszmianski et al., 2016; Rupasinghe et al., 2015). Initially, HPLC-RI results were inconclusive for the presence of sucrose in these varieties due to similar retention times of the sucrose standard (~10.4 min) and a sample peak (~10.6 min). However, HPAE-PAD was successfully used to identify the sample peak (10.6 min) as inositol and to verify the absence of sucrose in these samples. Because the majority of literature

sources reporting the presence of sucrose in haskaps employed only HPLC-RI analysis (with similar stationary/mobile phase combinations) and did not analyze for inositol, it can be hypothesized that inositol was misidentified as sucrose.

With respect to polyols, the highest concentration in all varieties was found for sorbitol, followed by inositol, and arabitol. The highest sorbitol content was found in the Indigo Gem and Blizzard varieties of 0.61 and 0.55 g/100 g FW, respectively, and the lowest in the Tundra variety of 0.37 g/100 g FW. The mean values for arabitol, inositol, and sorbitol in the five haskap varieties were 0.01, 0.10, and 0.49 g/100 g FW, respectively. Polyols have rarely been reported in literature for haskaps. A single reference reported sorbitol quantification in four Polish haskap varieties with an average of 0.68 mg/g dry weight (DW), which is significantly lower than the values observed in this study (Wojdylo et al., 2013). Inositol and sorbitol were identified in the Korean variety 'Venulosa' by gas chromatography-time of flight mass spectrometry (GC-ToF), however, their concentrations were not reported (Lee et al., 2015). To the best of the author's knowledge, this is the first reporting of these polyols in haskap and their concentrations and is the only work that has identified the presence of arabitol (in all varieties except Tundra).

4.2.2 Moisture

The moisture content of a berry is an important chemical property, as it influences quality (i.e. TSS measurements), storage, and processing practices. In this study, the percent moisture was found to be similar for all five varieties, ranging from 84.10-86.21% (Table 4.1). The highest moisture content values of ~86% were observed for Aurora, Blizzard, and Honey Bee, with Indigo Gem being the lowest at 84.10%. Moisture content values obtained in this study were consistent with those reported in literature of 85.95% for Indigo Gem and 86.0% for an unnamed Polish variety (Khattab et al., 2016; Zadernowski et al., 2005). These values are high when compared to other berry fruits such as blackberry (80.5%), blueberry (81.2%), and saskatoon berry (~81%) (Ribeiro de Souza, 2017; Zadernowski et al., 2005).

4.2.3 Organic Acids and Ascorbic Acid

In berries, the organic acid profile and ratio of carbohydrates to organic acids will determine flavour characteristics (i.e. sourness *vs*. sweetness). Organic acid (and ascorbic acid) analysis was performed on haskap berry juices using high performance liquid chromatography with photodiode array detection (HPLC-PDA). Individual compounds were identified and quantified in haskap juice samples using a comparison of retention times to external standards, spiking experiments, and peak area/height comparison to standard curves. Following their identification, standard solutions were used to quantify the three major (>80 mg/100 g FW) organic acids (citric, malic, and quinic) and ascorbic acid in haskap juice samples. Ascorbic acid (RT of ~9.3 min) was quantitated as an exception (i.e. <80 mg/100 g FW) based on its detector response (i.e. high extinction coefficient) and free radical scavenging ability. Approximate retention times of these compounds were 15.2, 7.3, and 5.6 min, for citric, malic, and quinic acids, respectively. Mean and standard deviation results for ascorbic, citric, malic, and quinic acid concentrations in Aurora, Blizzard, Honey Bee, Indigo Gem, and Tundra haskap varieties are shown in Table 4.4. Figure 4.6 shows a representative HPLC-PDA chromatogram of ascorbic acid and organic acids commonly identified in fruits, and those for the haskap varieties are shown in Figures 4.7 (A-E).

Table 4.4 Mean and standard deviation results for select organic acids and ascorbic acid in Aurora, Blizzard, Honey Bee, Indigo Gem, and Tundra haskap varieties.[1,2]

	Variety				
Organic Acid	Aurora	Blizzard	Honey Bee	Indigo Gem	Tundra
Ascorbic Acid	3.2 ± 0.2^a	4.5 ± 0.2^b	5.3 ± 0.2^b	6.9 ± 0.4^c	9.5 ± 0.7^d
Citric Acid	1879.2 ± 40.0^a	1836.8 ± 28.4^a	1729.8 ± 96.3^a	1796.3 ± 50.9^a	2543.1 ± 51.7^b
Malic Acid	512.6 ± 20.1^b	343.6 ± 5.9^a	988.6 ± 33.7^d	499.1 ± 22.5^b	573.9 ± 14.2^c
Quinic Acid	112.0 ± 0.4^c	83.4 ± 1.1^a	95.9 ± 4.4^b	113.2 ± 4.9^c	81.6 ± 1.8^a
Total	2507.0 ± 59.6^b	2268.2 ± 35.0^a	2819.6 ± 134.2^c	2415.5 ± 77.8^{ab}	3208.2 ± 64.2^d

[1]mg/100 g FW.
[2]Mean ± standard deviation results of triplicate sample analysis.
[a-d]Mean values in the same row followed by a common letter were not statistically different ($p < 0.05$) by Tukey's HSD multiple range test.
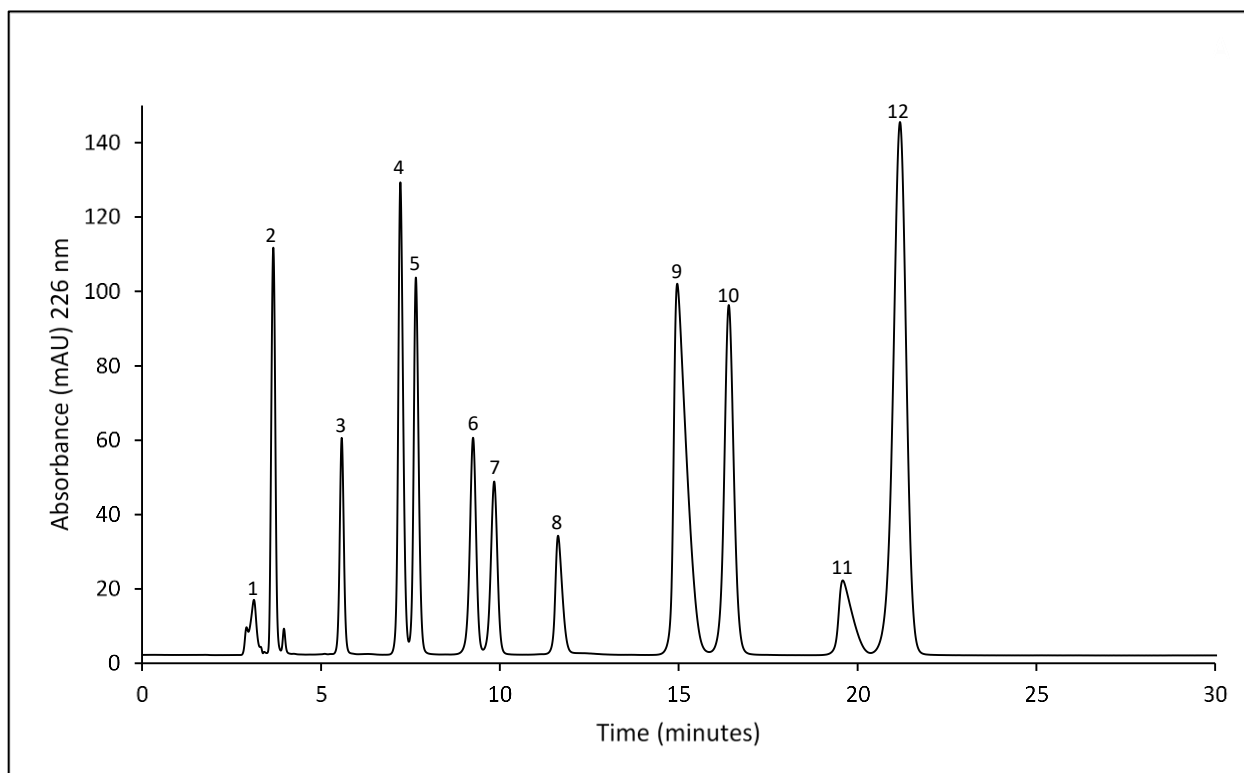
Figure 4.6 HPLC-PDA chromatogram of ascorbic acid and organic acids commonly reported in fruits. Peak identities: 1. phytic acid; 2. oxalic acid; 3. quinic acid; 4. malic acid; 5. malonic acid; 6. ascorbic acid; 7. shikimic acid; 8. acetic acid; 9. citric acid; 10. maleic acid; 11. succinic acid; and 12. fumaric acid (concentrations ranged from 20 to 3000 mg/L).
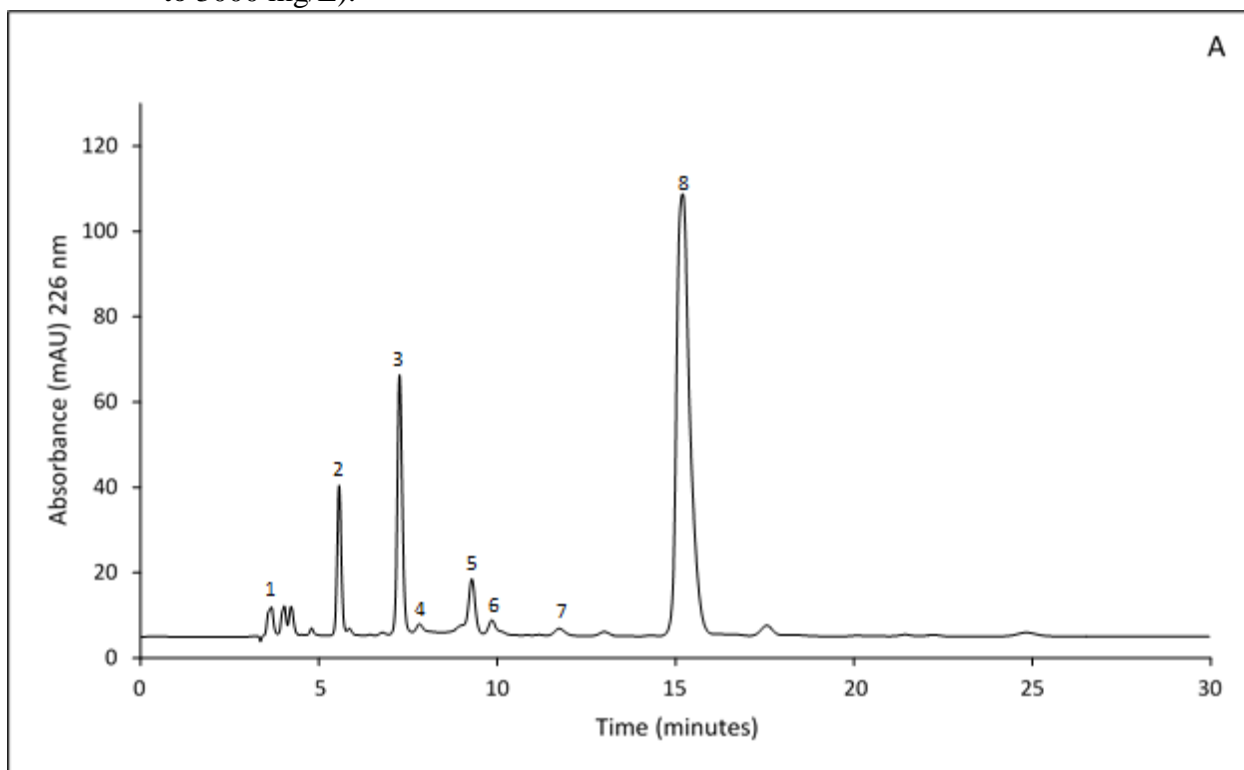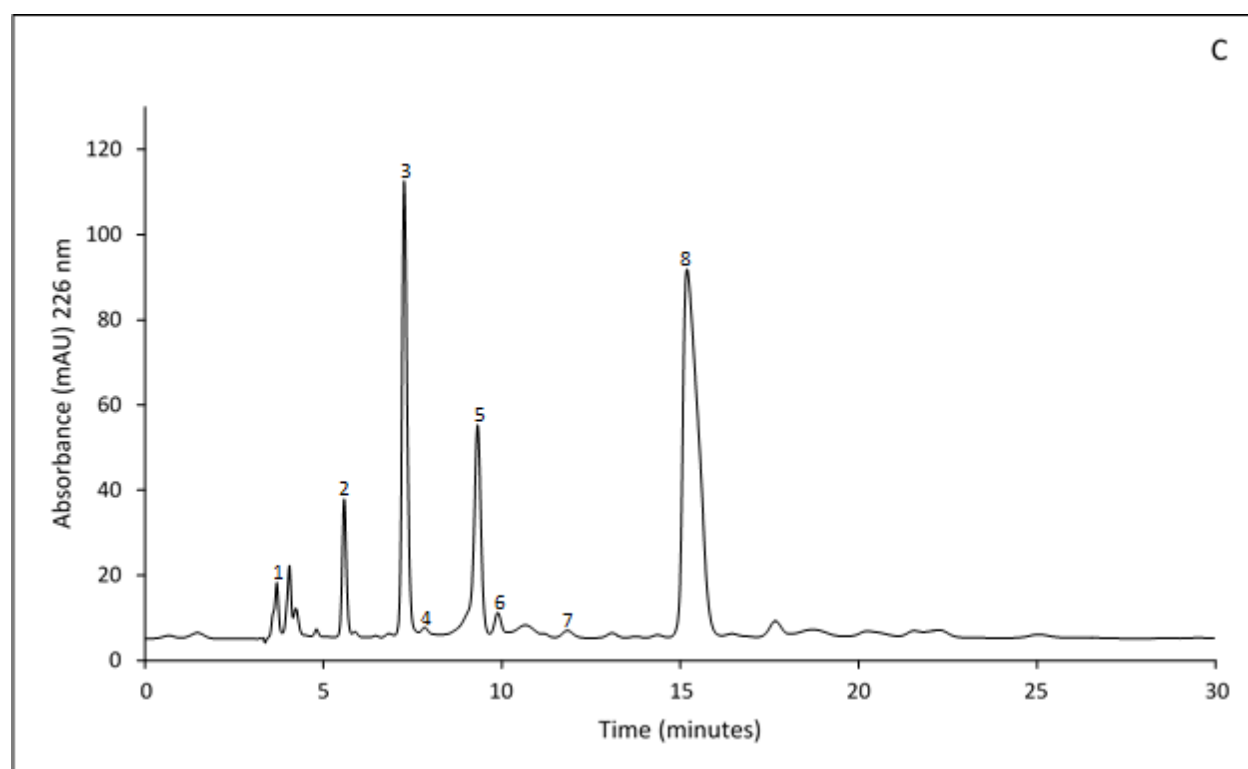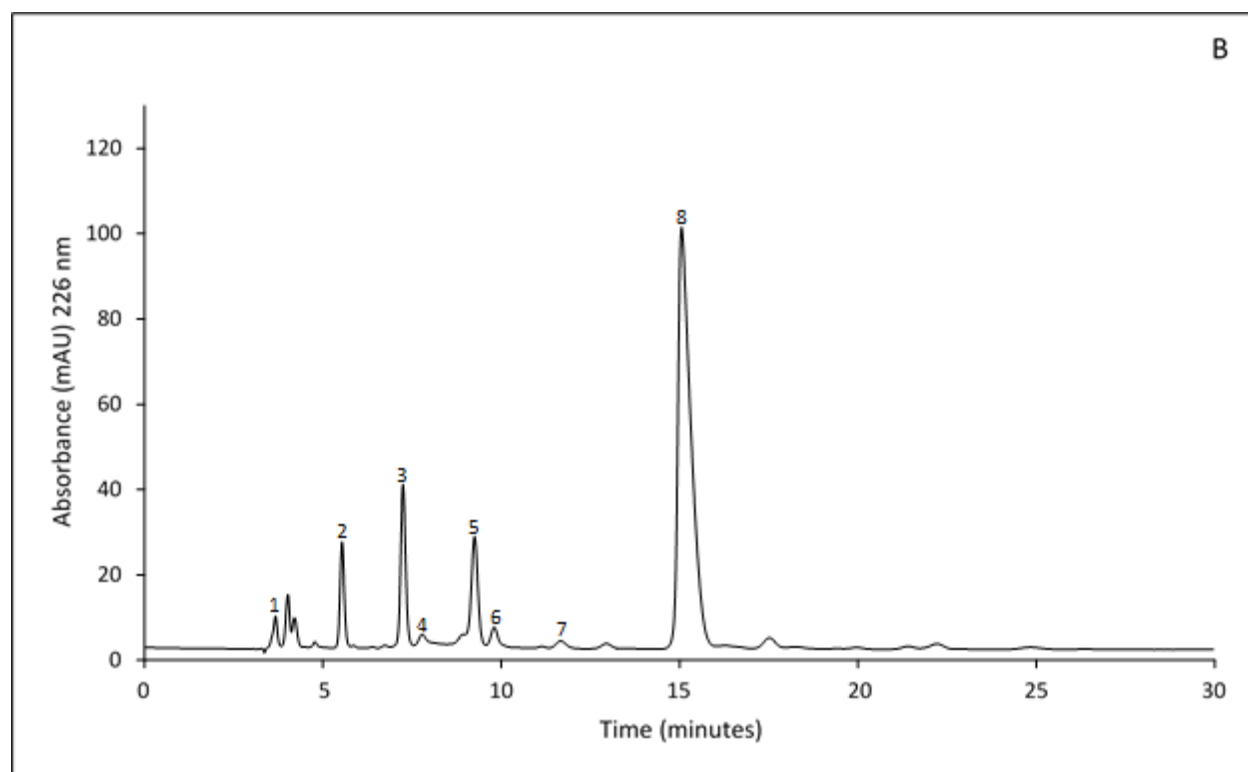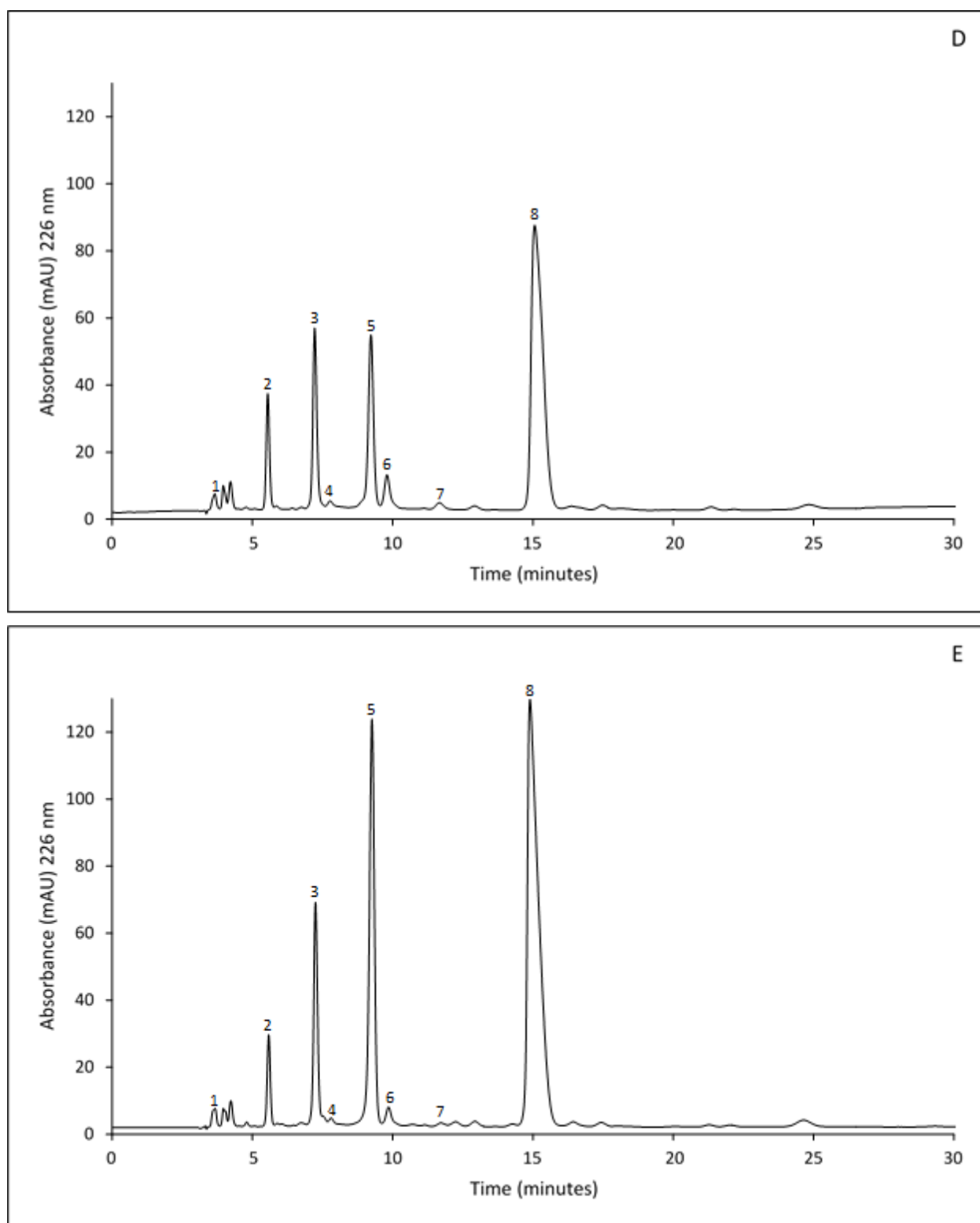
Figure 4.7 HPLC-PDA chromatograms of the organic acids in haskap samples. Chromatogram identification: A. Aurora; B. Blizzard; C. Honey Bee; D. Indigo Gem; and E. Tundra. Peak identities: 1. oxalic acid; 2. quinic acid; 3. malic acid; 4. malonic acid; 5. ascorbic acid; 6. shikimic acid; 7. acetic acid; and 8. citric acid.

The major organic acid present in these haskap varieties was citric acid, with a concentration range of 1729.8-2543.1 and a mean of 1957.0 mg/100 g FW. Tundra and Honey Bee had the highest and lowest concentrations of 2543.1 and 1729.8 mg/100 g FW, respectively. The second most abundant organic acid was malic acid, with a range of 343.6-988.6 and a mean of 583.6 mg/100 g FW. Blizzard had a significantly lower malic acid concentration (343.6 mg/100 g FW) than all other varieties, whereas Honey Bee (988.6 mg/100 g FW) had ~1.7x the concentration of the next highest variety (Tundra with 573.9 mg/100 g FW). Quinic acid concentrations ranged from 81.6-113.2 with a mean of 97.2 mg/100 g FW. Indigo Gem and Tundra had the highest and lowest concentrations of this organic acid, respectively. Ascorbic acid concentrations ranged from 3.2-9.5 with a mean of 5.9 mg/100 g FW.

Previous observations of organic acids in haskap support those found in this study with respect to the major components being citric, malic, and quinic acids (Senica et al., 2018; Rupasinghe et al., 2015). Specific values for citric acid have been reported as: (a) 430.9-807.4 mg/100 g FW for four Canadian varieties (Aurora, Borealis, Honey Bee, and Tundra) grown in Slovenia (Senica et al., 2018); and (b) ~300-1000 mg/100 g FW for four Canadian varieties (Berry Blue, Borealis, Indigo Gem, and Tundra) grown in Nova Scotia (Rupasinghe et al., 2015). These results are much lower than those found in this study where the samples were juices, and in the latter case, may be explained by the extraction solvent (100% methanol). When ethanol-formic acid-water extracts (EFW, 70:2:28% (v:v:v)) of haskap berry macerate were analyzed for organic acids in this study, their HPLC-PDA concentration results were reduced by approximately 60% when compared to the values reported in Table 4.4 for juices. It is unclear why the citric acid results reported by Senica et al. (2018) were much lower than those found in this study, as the extraction solvent used by these authors was distilled water; however, these authors also reported much lower total carbohydrate values and possible explanations for this difference have been addressed in this thesis.

Minor organic acids identified in these samples included acetic, malonic, oxalic, and shikimic acids, which align with oxalic and shikimic acids being commonly reported in haskaps (Rupasinghe et al., 2018; Lee et al., 2015; Wojdylo et al., 2013). Additional organic acids have been reported at low concentrations in haskaps including fumaric (0.06-0.24 mg/100 g FW) and tartaric (1.28-7.56 mg/100 g FW) for Aurora, Borealis, Honey Bee, and Tundra grown in Slovenia

(Senica et al., 2018). To the best of the author's knowledge, this work is the first to report the presence of acetic acid in haskaps.

Ascorbic acid (i.e. vitamin C) is a particularly important organic compound due to its free radical scavenging ability and can be assessed using the HPLC-PDA method (Section 3.4.3) used in this study based on its separation and absorption at 226 nm (λ_{max} of 289 nm) (Raudsepp et al., 2013; Maniyar et al., 2012). The ascorbic acid concentration range for these haskap varieties was 3.2-9.5 with a mean of 5.9 mg/100 g FW. These results were much lower than those reported in literature for this fruit of: (a) 17.75-19.45 mg/100 g FW for Aurora, Borealis, Honey Bee, and Tundra varieties (Senica et al., 2018); (b) 3.19-32.12 with a mean of 14.64 mg/100 g FW for eight Polish varieties (Wojdylo et al., 2013); and (c) 28.56-86.95 mg/100 g FW for two Russian varieties (Jurikova et al., 2007). Haskap ascorbic acid content has shown significant variation based on harvest year, ranging from a low of 36.21 (2003) to 86.95 mg/100 g FW (2001) for the same variety (Jurikova et al., 2007). As such, the lower ascorbic acid concentration results observed for these samples may be explained by environmental growing conditions. Although haskaps have been reported to have ascorbic acid concentrations much higher than other common fruits such as strawberries (58.8 mg/100 g FW) and raspberries (26.2 mg/100 g FW) (Rupasinghe et al., 2018), this study found much lower results, more aligned with berry fruits such as blueberries (9.7 mg/100 g FW) and sweet cherries (6.0 mg/100 g FW) (United States Department of Agriculture, 2018).

Total organic acid results (i.e. for ascorbic, citric, malic, and quinic acids; Table 4.4) are often reported on a % basis and ranged from 2.27-3.21% (2268.2-3208.2 mg/100 g FW) with a mean value of 2.64% (2643.7 mg/100 g FW) for these five varieties. This concentration range and mean were similar to those reported for haskaps of: (a) 1.46-2.94% for six Slovakian varieties, mean of 2.19% (Jurikova et al., 2012b); and (b) 2.7-3.4% for two Polish varieties with a mean of 3.1% (Ochmian et al., 2012). Total organic acid concentration results for other berry fruits such as raspberry (1.17%) and strawberry (1.03%) were much lower, while those for less common species such as lingonberry (2.23%) and rowanberry (3.15%) were similar (Mikulic-Petkovsek et al., 2012).

When comparing total organic acid results (Table 4.4) to pH data (Table 4.1), the highest and lowest organic acid contents were consistent with the pH results found for Tundra (pH of 2.99; 3.21% organic acids) and Blizzard (pH of 3.31; 2.27% organic acids), respectively. The other three

varieties analyzed did not have significantly different pH values (3.11-3.18), and two of these (Aurora and Indigo Gem) did not have significantly different organic acid contents (2.51 and 2.42%, respectively). The Honey Bee variety was the outlier with a similar pH of 3.17 and a significantly higher organic acid content (2.82%) when compared to Aurora and Indigo Gem. A closer review of specific organic acid contents of these three varieties showed that Honey Bee had a significantly higher malic acid concentration of 988.6 mg/100 g FW, with no significant difference in citric acid content. Malic is a weaker acid (pKa1 of 3.51) than citric (pKa1 of 2.79), and as such, it can be hypothesized that in the case of Honey Bee, the concentration of citric acid was more important in its pH determination than total organic acid content (National Center for Biotechnology Information, 2018).

Analysis of the carbohydrate and organic acid results both alone and in combination (Tables 4.2-4) provides an indication of flavour characteristics and commercial applications for these five haskap varieties. As examples: (a) the Blizzard variety, which had low organic acid (2.27 g/100 g FW) and high carbohydrate (11.53 g/100 g FW) contents would have a high carbohydrate/acid ratio, resulting in an improved (i.e. sweeter) taste perception. This hypothesis is supported by this variety winning an international taste test in Austria (Bors, 2018); (b) the Tundra variety had the highest organic acid (3.21 g/100 g FW) and citric acid (2.54 g/100 g FW) contents and also the lowest pH (2.99). This variety could be used as a natural acidulant (i.e. additive) in food formulations to adjust taste (i.e. tartness), and as a contributor to microbial control; and (c) the carbohydrate concentration of the Indigo Gem variety (12.67 g/100 g FW) was higher than that observed for apple (10.39 g/100 g FW) and pear (9.75 g/100g FW), which are both used in commercial fruit juice production (United States Department of Agriculture, 2018). Therefore, it can be postulated that this variety would be a candidate for juice production either as a stand-alone juice or as a blending agent.

4.3 Phenolic Profiling

4.3.1 Total Phenolic Content by the Folin-Ciocalteu Method

Total phenolic content (TPC) of samples was determined using the Folin-Ciocalteu (FC) method. The FC method is a colourimetric assay that measures the reducing capacity of a sample, shown by a colour change that is most likely due to reversible electron reduction reactions that

74

lead to the formation of a blue species (Huang et al., 2005; Folin and Ciocalteu, 1927). The FC method is nonspecific to phenolics, however, it has been tailored to TPC analysis with the creation of basic conditions (using a sodium carbonate solution), which promotes phenolic compound dissociation to form anions capable of reducing the FC solution (Huang et al., 2005). The FC method measures the total reducing ability of a sample, which will be affected by the presence of other reducing compounds (e.g. ascorbic acid), which can impact results (Huang et al., 2005). To quantify total phenolics, the absorbance of the blue species formed is measured at 765 nm with comparison to standards (e.g. gallic acid) of known concentration. Results are then expressed as mg of gallic acid equivalents (GAE)/100 g FW. Mean and standard deviation TPC results as determined by the FC method for EFW and PR extracts, and phenolic fractions of Aurora, Blizzard, Honey Bee, Indigo Gem, and Tundra haskap varieties are shown in Table 4.5.

Table 4.5 Mean and standard deviation total phenolic content results for extracts (EFW and PR) and phenolic fractions from Aurora, Blizzard, Honey Bee, Indigo Gem, and Tundra haskap varieties.[1,2]

Extract or Fraction	Variety				
	Aurora	Blizzard	Honey Bee	Indigo Gem	Tundra
EFW extract	451.5 ± 8.0[a]	549.1 ± 11.2[c]	495.5 ± 4.7[b]	597.4 ± 12.9[d]	778.9 ± 10.4[e]
PR extract	376.2 ± 7.6[a]	482.4 ± 6.8[c]	399.9 ± 6.8[b]	544.7 ± 7.7[d]	640.7 ± 12.6[e]
Water fraction	5.9 ± 0.1[d]	4.9 ± 0.1[b]	4.2 ± 0.2[a]	5.4 ± 0.1[c]	4.0 ± 0.2[a]
20% ethanol fraction	3.5 ± 0.1[d]	1.6 ± <0.1[a]	2.8 ± <0.1[c]	2.3 ± 0.1[b]	4.6 ± 0.1[e]
40% ethanol fraction	106.1 ± 3.9[a]	123.0 ± 5.1[b]	110.1 ± 2.7[ab]	161.8 ± 5.9[d]	147.2 ± 6.1[c]
70% ethanol fraction	199.2 ± 7.3[a]	247.6 ± 16.7[bc]	228.5 ± 15.0[ab]	266.9 ± 11.1[c]	335.6 ± 12.2[d]
100% ethanol fraction	16.9 ± 0.4[b]	11.1 ± 0.4[a]	19.5 ± 1.0[c]	16.8 ± 1.0[b]	20.3 ± 0.2[c]

[1]mg GAE/100 g FW.
[2] Mean ± standard deviation results of triplicate sample analysis.
[a-e]Mean values in the same row followed by a common letter were not statistically different ($p<0.05$) by Tukey's HSD multiple range test between the varieties.

The TPC values of EFW extracts ranged from 451.5-778.9 with a mean of 574.5 mg GAE/100 g FW. These TPC results were in agreement with those reported for this fruit as shown by the following examples: (a) Borealis, Indigo Gem, and Tundra varieties with TPC values of 622.5, 500.8, and 528.1 mg GAE/100 g FW, respectively (Rupasinghe et al., 2012); and (b) Indigo Gem and Tundra with a TPC range of 617-842 mg GAE/100 g FW (Khattab, et al., 2015). The highest TPC extract values (EFW/PR) were observed for the Tundra variety and the lowest for the Aurora variety, with 778.9/640.7 and 451.5/376.2 mg GAE/100 g FW, respectively. Potential factors impacting TPC results include variety, environmental growing conditions, and geographical location (Ozga et al., 2006). The TPC results for the five haskap varieties in this study were significantly higher than those reported for blueberry (300-384 mg GAE/100 g FW) and saskatoon berry (296.2-526.8 mg GAE/100 g FW) (Ribeiro de Souza et al., 2019; You et al., 2011).

Phenolic rich (PR) extracts and phenolic fractions were created using solid phase extraction with Amberlite® XAD16N resin employing water as the initial mobile phase. These experiments were conducted on EFW extracts so as to remove the majority of nonphenolics (e.g. carbohydrates and organic acids) in the case of PR extracts, and to produce fractions containing a narrower range of phenolic structures by eluting with increasing concentrations of aqueous ethanol. Analytical results (i.e. HPAE-PAD and HPLC-PDA) showed carbohydrate and organic acid contents in the PR extract of <0.03% and <0.2%, respectively. During PR production, the loss of polar reducing compounds (e.g. ascorbic acid) and some of the more polar phenolics (e.g. anthocyanins) occurred as shown by the lower TPC values found for the PR extracts when compared to the EFW extracts. As an example, the TPC results for the Tundra EFW and PR extracts were ~779 and ~641 mg GAE/100 g FW, respectively, which corresponded to a reduction of ~18%. The TPC values of PR extracts ranged from 376.2 to 640.7 with a mean of 488.8 mg GAE/100 g FW. The PR extracts were produced to remove compounds that can negatively impact sample analysis by mass spectrometry and to increase the purity of samples for cell line studies.

The TPC results for phenolic fractions produced from EFW extracts showed increasing values concomitant with ethanol concentration to 70%. The lowest TPC values were found for the 20% ethanol fractions, ranging from 1.6-4.6 mg GAE/100 g FW, and the highest for the 70% ethanol fractions, ranging from 199.2-336.6 mg GAE/100 g FW. The low TPC values observed

for the 100% ethanol fraction (11.1-20.3 mg GAE/100 g FW) can be explained by almost complete elution of sample phenolics occurring within the 40-70% ethanol fractions. Phenolic loss as shown by lower TPC values also occurred during the fractionation of the EFW extracts. As an example, the EFW TPC value for the Tundra variety of 778.9 decreased to 511.7 (combined TPC values of water and ethanol (20-100%) fractions) mg GAE/100 g FW, a 34% reduction. This is the first report of TPC values for PR extracts and phenolic fractions produced from haskap EFW extracts.

4.3.2 HPLC-PDA Analysis: Total Phenolic Chromatographic Indices (TPCI)

4.3.2.1 EFW Extract TPCI

The classification of haskap sample phenolics was afforded by high performance liquid chromatography with photodiode array detection (HPLC-PDA). For the purposes of this analysis, all sample compounds with a detector response at 280 nm (i.e. chromatographic peaks with a signal to noise ratio $\geq$6x) and a UV-visible spectrum that matched those of phenolic standard subclasses, were assumed to be phenolics. The total phenolic chromatographic index (TPCI) of a sample is defined as the sum of all extracted phenolics as analyzed by HPLC-PDA and is calculated by the summation of all identified phenolic subclasses found in the sample (Escarpa and Gonzalez, 2001). Initially, the phenolic subclass for each peak was identified by UV-visible spectrum comparison to standards (Figures 4.8A-F), followed by subclass concentration determination using peak area summation and comparison with the phenolic standard of that subclass through linear regression (i.e. concentration *vs*. peak area).
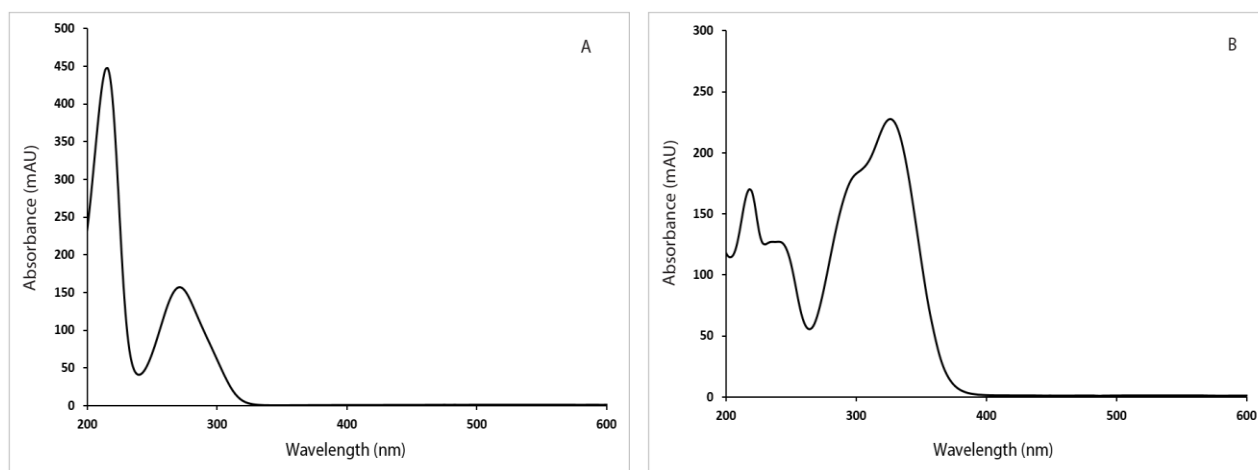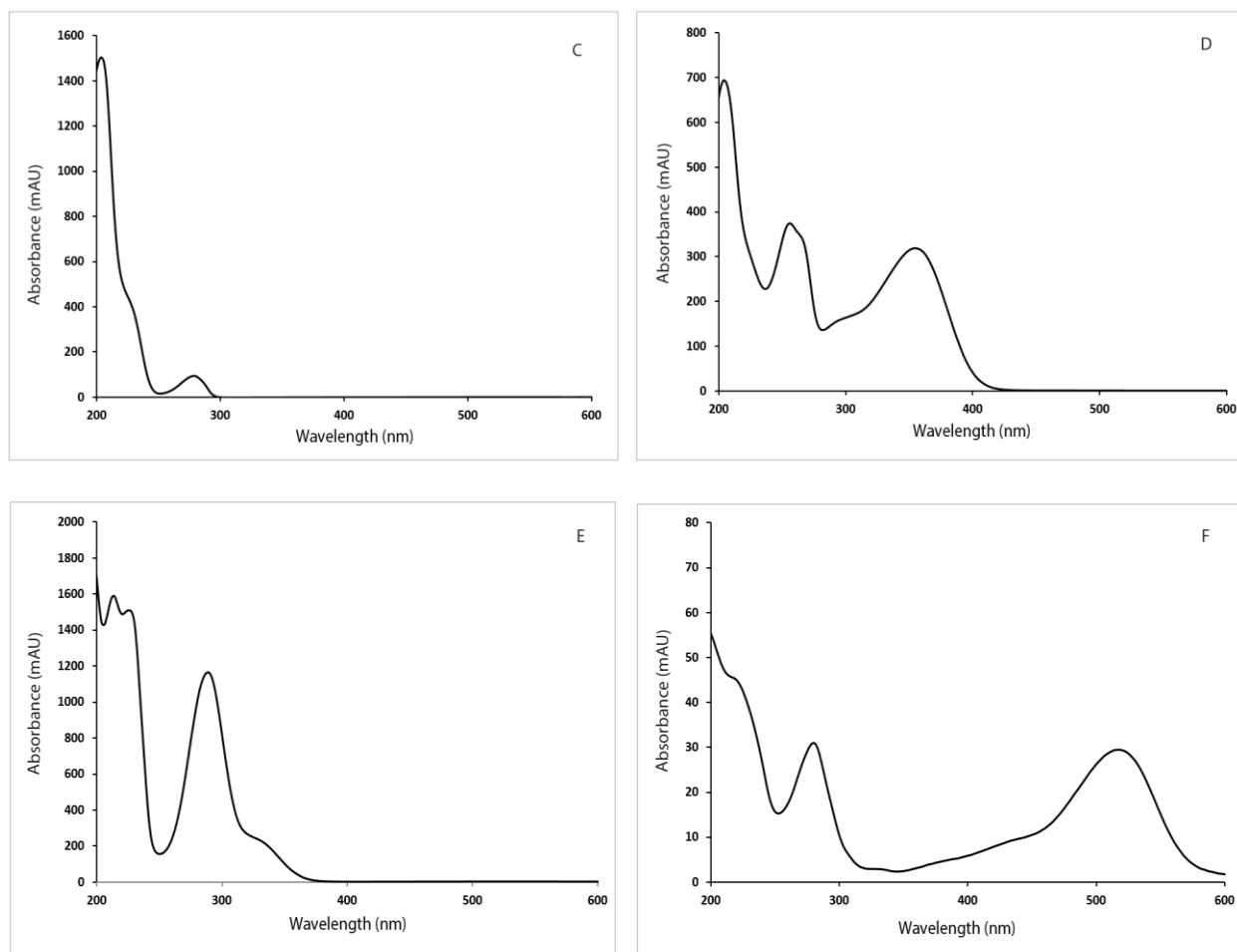
Figure 4.8 UV-visible spectra profiles of phenolic standards. Spectrum identification: A. gallic acid, a hydroxybenzoic acid; B. chlorogenic acid, a hydroxycinnamic acid; C. catechin, a flavanol; D. rutin, a flavonol; E. naringenin, a flavanone; and F. cyanidin-3-*O*-glucoside, an anthocyanin.

Representative compounds for phenolic subclasses were selected based on literature reports of those identified in haskaps and those that are commonly identified in berry fruits. These included catechin, chlorogenic acid, cyanidin-3-*O*-glucoside, gallic acid, naringenin, and rutin, which were representatives of the flavanol, hydroxycinnamic acid, anthocyanin, hydroxybenzoic acid, flavanone, and flavonol subclasses, respectively. Representative HPLC-PDA chromatograms of the mixed standard for the six major phenolic subclasses in haskaps are shown in Figures 4.9A and B, and representative chromatograms with appropriate subclass identification for each of the five haskap varieties are shown in Figures 4.10 (A-E). Mean and standard deviation total phenolic

chromatographic index (TPCI) results for the EFW extracts of Aurora, Blizzard, Honey Bee, Indigo Gem, and Tundra haskap varieties are shown in Table 4.6.

Table 4.6 Mean and standard deviation TPCI results for the six major phenolic subclasses for EFW extracts of Aurora, Blizzard, Honey Bee, Indigo Gem, and Tundra haskap varieties.[1,2]

Phenolic Subclass	Variety				
	Aurora	Blizzard	Honey Bee	Indigo Gem	Tundra
Hydroxybenzoic acids	7.5 ± 0.3^{ab}	14.9 ± 0.7^{c}	19.3 ± 2.2^{d}	4.7 ± 0.2^{a}	9.8 ± 0.2^{b}
Flavanols	71.6 ± 2.2^{c}	23.6 ± 0.7^{a}	143.1 ± 1.9^{e}	49.5 ± 1.2^{b}	130.9 ± 4.0^{d}
Hydroxycinnamic acids	46.5 ± 1.7^{a}	58.2 ± 1.7^{b}	56.4 ± 1.5^{b}	56.6 ± 1.6^{b}	80.2 ± 1.2^{c}
Flavonols	60.3 ± 6.3^{b}	29.8 ± 1.1^{a}	38.1 ± 1.2^{a}	90.7 ± 2.7^{c}	68.9 ± 1.6^{b}
Flavanones	7.4 ± 0.3^{b}	10.6 ± 0.5^{d}	0.6 ± 0.1^{a}	9.9 ± 0.2^{c}	7.8 ± 0.1^{b}
Anthocyanins	249.2 ± 8.3^{a}	315.9 ± 1.8^{b}	253.5 ± 4.4^{a}	447.8 ± 5.9^{d}	429.4 ± 6.3^{c}
TPCI[3]	442.5 ± 14.5^{a}	453.1 ± 3.0^{a}	511.2 ± 3.3^{b}	659.2 ± 10.5^{c}	727.0 ± 3.6^{d}

[1] mg/100 g FW.
[2] Mean ± standard deviation results of triplicate sample analysis.
[3] Total Phenolic Chromatographic Index = sum of all identified and quantified phenolic peaks.
[a-e] Mean values in the same row followed by a common letter were not statistically different ($p<0.05$) by Tukey's HSD multiple range test between the varieties.

Figure 4.9 HPLC-PDA chromatograms of the standards representing the six major phenolic subclasses in haskap for TPCI classification at 280 (A) and 520 nm (B). Peak identities (compound/subclass): 1. gallic acid/hydroxybenzoic acids; 2. catechin/flavanols; 3. chlorogenic acid/hydroxycinnamic acids; 4. rutin/flavonols; 5. naringenin/flavanones; and 6. cyanidin-3-*O*-glucoside/anthocyanins (standard concentrations ranged from 100-300 mg/L).
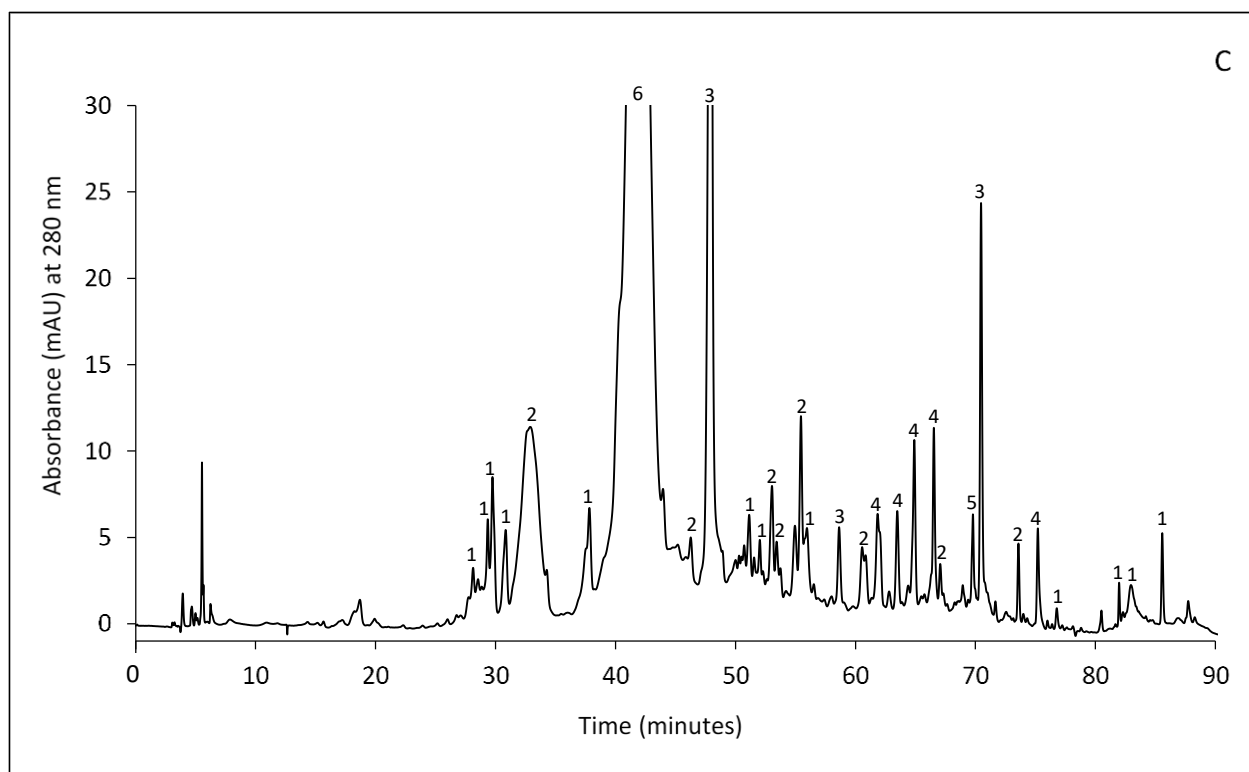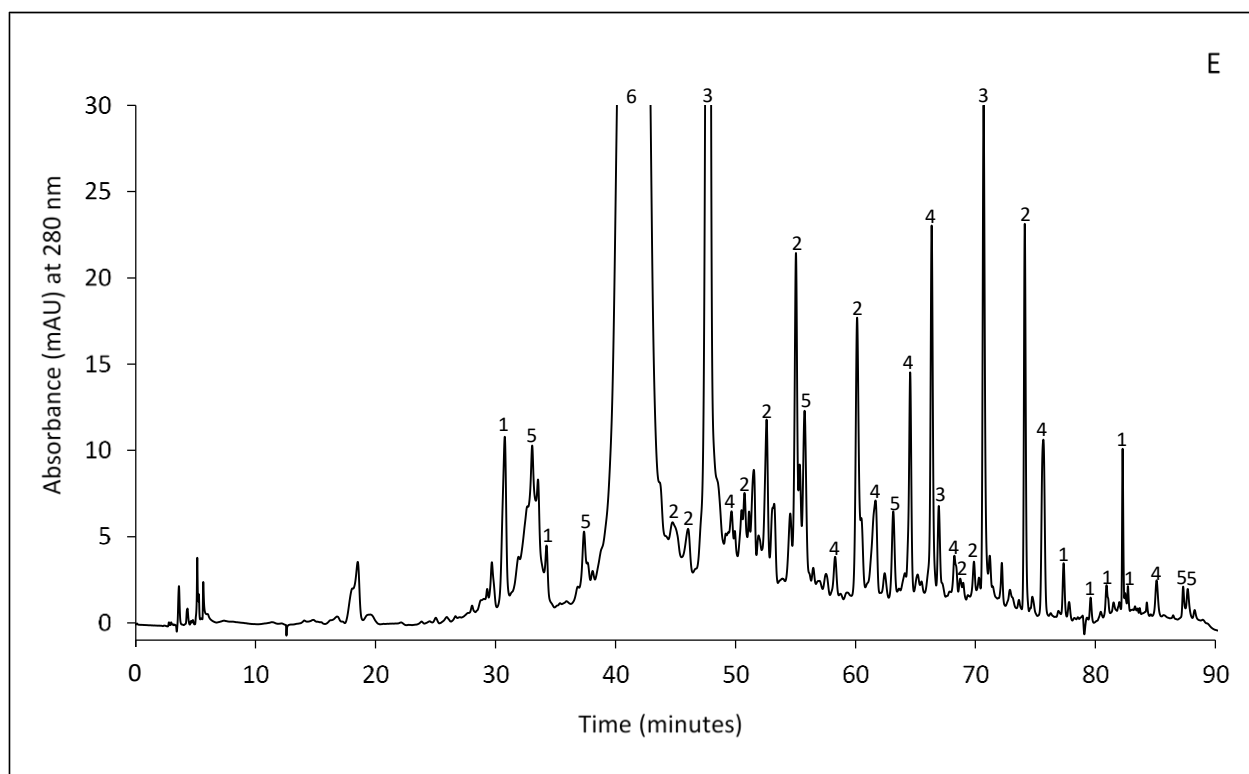
Figure 4.10 HPLC-PDA chromatograms of haskap EFW extracts showing the identification of sample phenolic subclasses. Chromatogram identification: A. Aurora; B. Blizzard; C. Honey Bee; D. Indigo Gem; and E. Tundra. Peak phenolic subclass assignments: 1. hydroxybenzoic acids; 2. flavanols; 3. hydroxycinnamic acids; 4. flavonols; 5. flavanones; and 6. anthocyanins.

The TPCI values for the EFW extracts of the five haskap samples ranged from 442.5-727.0 with a mean of 558.6 mg/100 g FW. Tundra and Aurora were found to have the highest and lowest TPCI concentrations, respectively. The TPCI results for these samples were in general agreement with those found for their TPC values (Table 4.5) of Tundra>Indigo Gem>Blizzard/Honey Bee>Aurora. However, Blizzard>Honey Bee was observed for TPC and Honey Bee>Blizzard for TPCI. To the best of the author's knowledge, this is the first time that TPCI has been used for the identification and quantitation of phenolic subclasses in haskap berries. When compared to literature value results for other berries, these results were higher than: (a) EFW extracts of three commercially-grown saskatoon berry varieties of 215.5-504.2 with a mean of 338.0 mg/100 g FW (Ribeiro de Souza et al., 2019); and (b) 425.5 mg/100 g FW for EFW extracts of wild chokecherry (Green, 2007).

As phenolics are mainly found in the skin/peel of fruits and berries, their size (i.e. surface area:volume) will have a significant impact on total phenolic content (Ribeiro de Souza, 2017). In this work, EFW extract TPCI values were directly related to berry size, with Tundra (length (L): 17.41 mm; diameter (D): 10.62 mm) being the smallest of the five varieties and having the highest TPCI value of 727.0 mg/100 g FW (Tables 4.1 and 4.6). Concomitantly, the Aurora variety (L: 23.49 mm; D: 11.97 mm) had the largest size and the lowest TPCI value of 442.5 mg/100 g FW (Tables 4.1 and 4.6). A similar relationship for EFW extract TPC values and size was also observed for Tundra (778.9 mg GAE/100 g FW) and Aurora (451.5 mg GAE/100g FW) (Table 4.5).

The most abundant phenolic subclass identified by TPCI results in these samples was the anthocyanins (peak at ~42 min; Figures 4.10A-E), which ranged from 249.2-447.8 with a mean of 339.2 mg/100 g FW. The highest anthocyanin content (447.8) was found for Indigo Gem, with Tundra slightly lower, but significantly different at 429.4 mg/100 g FW. The lowest anthocyanin concentrations were observed for Aurora and Honey Bee (not statistically different) of 253.5 and 249.2 mg/100 g FW, respectively. Total anthocyanin results in literature for haskaps vary as illustrated by the following: (a) a study of 30 Polish cultivars (HPLC-PDA) ranged from 150.3-655.2 with a mean of 312.1 mg/100 g FW (Kucharska et al., 2017); and (b) a study of 11 Canadian-grown varieties (LC-MS/MS) ranged from 83.7-223.9 with a mean of 114.0 mg/100 g FW (Rupasinghe et al., 2015). In the latter study, Indigo Gem and Tundra were analyzed and their reported anthocyanin concentrations were 178.9 and 214.5 mg/100 g FW, respectively, which were significantly lower than results for those varieties in this study (447.8 and 429.4, respectively) (Rupasinghe et al., 2015).

Anthocyanin concentration results for the samples in this study fell in a narrower range with the highest value (447.8 mg/100 g FW for Indigo Gem) about 1.8x the lowest value (249.2 mg/100 g FW for Honey Bee), when compared to some ranges in literature with one report of the highest being ~4.2x the lowest value for 30 Polish varieties (range of 150.0-654.0 mg/100 g FW for Karina and Amur cultivars, respectively) (Kucharska et al., 2017). This smaller difference in anthocyanin concentration is most likely due to fruit variety, since fruit maturity, environmental conditions, and geographical location for the fruits in this study were the same. In this work, anthocyanins comprised 49.5-70.0% of the TPCI values, which was lower than literature reports of: (a) 76% of the total phenolic content for a wild Moravian cultivar (Palíková et al., 2008); and

(b) 73-83% for a selection of haskap varieties (Berry Blue, Indigo Gem, and Tundra) grown in Nova Scotia (Khattab et al., 2015). As discussed previously for fruit phenolics in general, anthocyanin content in haskaps is dependent upon variety, growing and environmental conditions, and geographical location.

Flavanols were the next major phenolic subclass identified in three (Aurora, Honey Bee, and Tundra) of the five haskap varieties with a range of 23.6-143.1 and a mean of 83.7 mg/100 g FW. In the other two varieties, Blizzard and Indigo Gem, hydroxycinnamic acids and flavonols were the second major phenolic subclasses, respectively. The flavanol results from this study were similar to those reported for eight Swiss varieties (range of 357-681, mean of 484 mg/100 g DW) (Wojdyło et al., 2013), but were lower than those reported for seven Russian varieties (range of 244-625, mean of 363 mg/100 g FW) (Jurikova et al., 2012a).

In general, the remaining phenolic subclass concentration results from this study showed the following trend: hydroxycinnamic acids>flavonols>hydroxybenzoic acids>flavanones. The concentrations of these less abundant subclasses were generally in line with previously reported values (Senica et al., 2018; Kucharska et al., 2017; Jurikova et al., 2012b). The latest eluting peaks in the TPCI chromatograms had UV-vis spectra corresponding most closely to the hydroxybenzoic acids subclass (Figure 4.10A). This classification would not have been predicted based on the hydrophilic structures of these molecules. Structural identification of these compounds via HPLC-MS/MS could not be accomplished as mobile phase from 80-90 minutes had to be diverted to waste.

A number of nonanthocyanin phenolics (anthocyanins will be discussed in Section 4.3.4) that have been specifically identified in haskaps include: (a) gallic acid (hydroxybenzoic acid; LC with electrochemical detection) (Gazdik et al., 2008); (b) caffeic, chlorogenic, *m*-coumaric, *p*-coumaric, and neochlorogenic acids (hydroxycinnamic acids; HPLC-PDA, LC-MS/MS) (Jurikova et al., 2012a; Ochmian et al., 2012; Chaovanalikit et al., 2004); and (c) isoquercetin, luteolin-7-*O*-glucoside, quercetin-3-*O*-rhamnoside, and rutin (flavonols; HPLC-PDA, LC-MS/MS) (Rupasinghe et al., 2018; Khattab et al., 2015; Celli et al., 2014; Wojdyło et al., 2013).

4.3.2.2 PR Extract TPCI

As described previously (Section 3.5.2), PR extracts were produced from EFW extracts using Amberlite® XAD16N resin so as to remove the majority of nonphenolics in these samples. During this process, the majority of water-soluble compounds (e.g. carbohydrates, minerals, and organic acids) were removed from the EFW extracts via water treatment, followed by phenolic elution with 100% ethanol. The PR extracts were specifically produced for use in cell line studies (Objective 4) to aid in the elucidation of the *in vitro* mechanism(s) of haskap phenolics.

Mean and standard deviation results of total phenolic chromatographic indices (TPCI) for the PR extracts of Aurora, Blizzard, Honey Bee, Indigo Gem, and Tundra haskap varieties are shown in Table 4.7. A representative HPLC-PDA chromatogram of the PR extract for the Tundra haskap variety, with peaks labeled by phenolic subclass, is shown in Figure 4.11 (chromatograms for the remaining samples can be found in Figure 8.1 of the Appendix).

Table 4.7 Mean and standard deviation TPCI results for the six major phenolic subclasses for PR extracts of Aurora, Blizzard, Honey Bee, Indigo Gem, and Tundra haskap varieties.[1,2]

Phenolic Subclass	Aurora	Blizzard	Honey Bee	Indigo Gem	Tundra
			Variety		
Hydroxybenzoic acids	10.8 ± 0.1^b	12.6 ± 0.5^c	10.2 ± 0.5^b	4.8 ± 0.2^a	13.8 ± 0.1^d
Flavanols	69.1 ± 2.4^a	71.2 ± 2.6^a	126.2 ± 5.6^c	73.8 ± 4.0^a	103.4 ± 4.0^b
Hydroxycinnamic acids	42.3 ± 2.1^a	47.4 ± 2.0^b	45.4 ± 1.6^a	46.0 ± 1.8^{ab}	69.4 ± 0.6^c
Flavonols	49.8 ± 0.7^c	30.2 ± 0.1^a	45.5 ± 0.9^b	70.8 ± 1.5^d	72.0 ± 1.0^d
Flavanones	6.9 ± 0.2^a	8.6 ± 0.4^b	ND[3]	9.8 ± 0.5^c	ND
Anthocyanins	202.7 ± 1.8^a	252.1 ± 7.9^b	217.5 ± 8.8^a	385.1 ± 4.9^c	404.7 ± 14.1^c
TPCI[4]	381.7 ± 3.1^a	422.1 ± 11.8^b	444.8 ± 8.2^b	590.2 ± 6.0^c	663.3 ± 11.8^d

[1] mg/100 g FW.
[2] Mean ± standard deviation results of triplicate sample analysis.
[3] ND represents no phenolic subclass peak with a height above the qualitative detection limit (<3 x s/n).
[4] Total Phenolic Chromatographic Index = sum of all identified and quantified phenolic peaks.
[a-d] Mean values in the same row followed by a common letter were not statistically different ($p<0.05$) by Tukey's HSD multiple range test between the varieties.
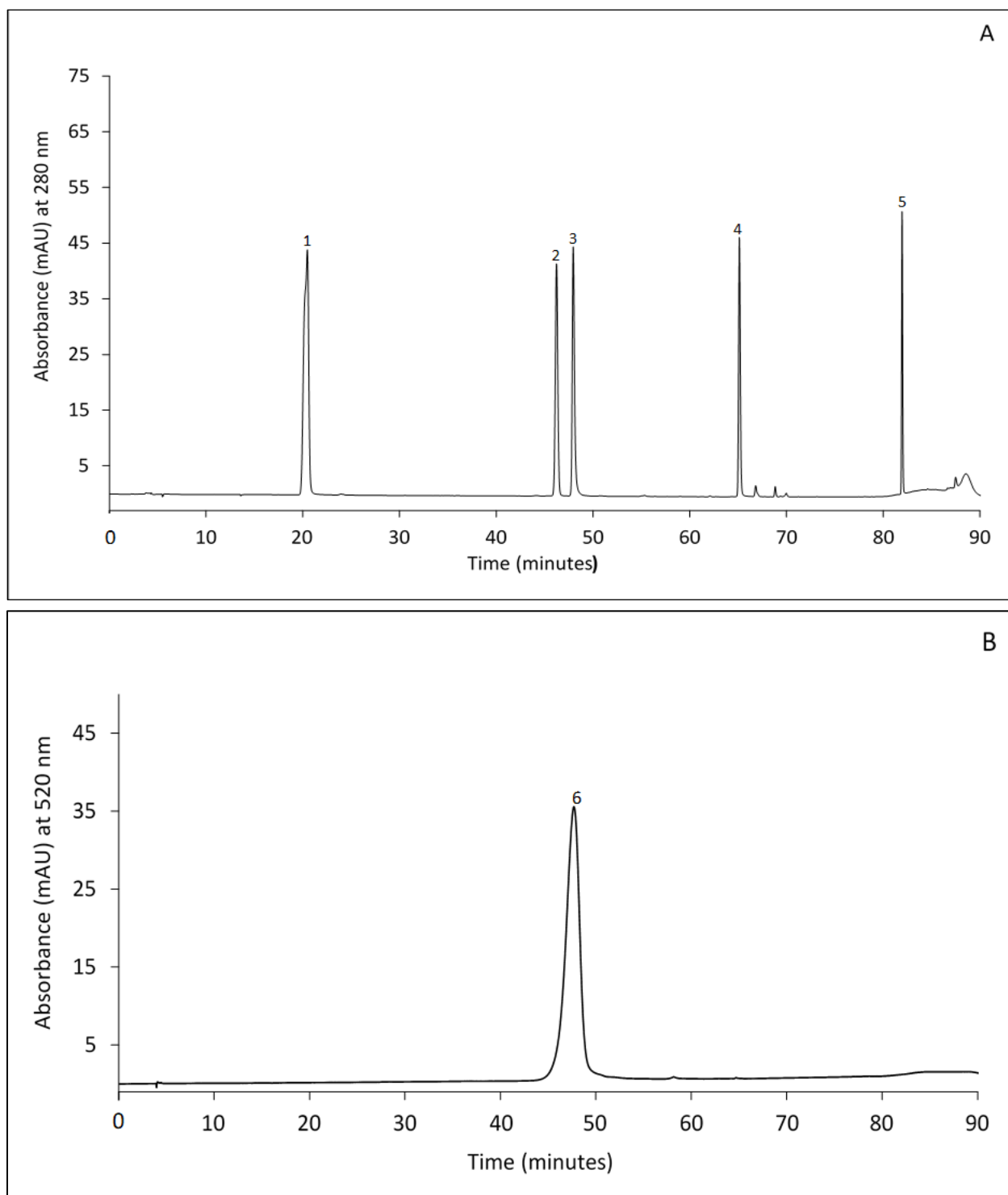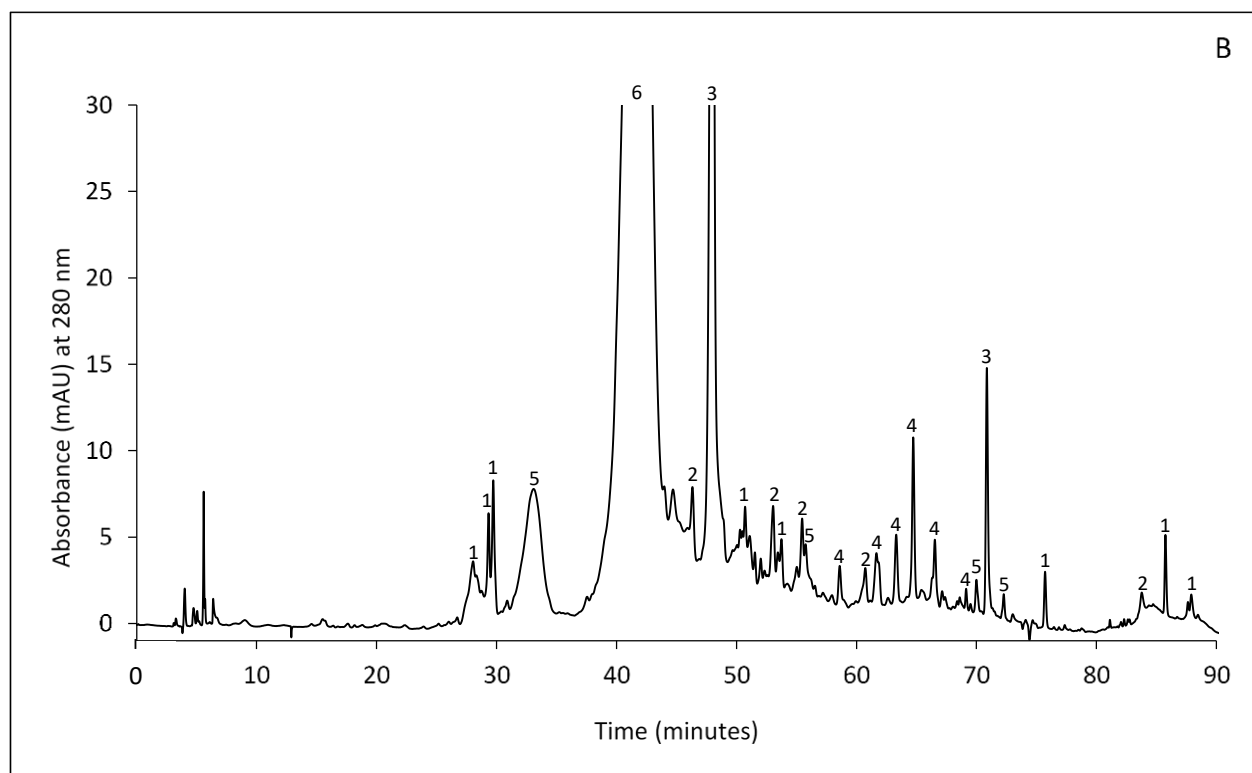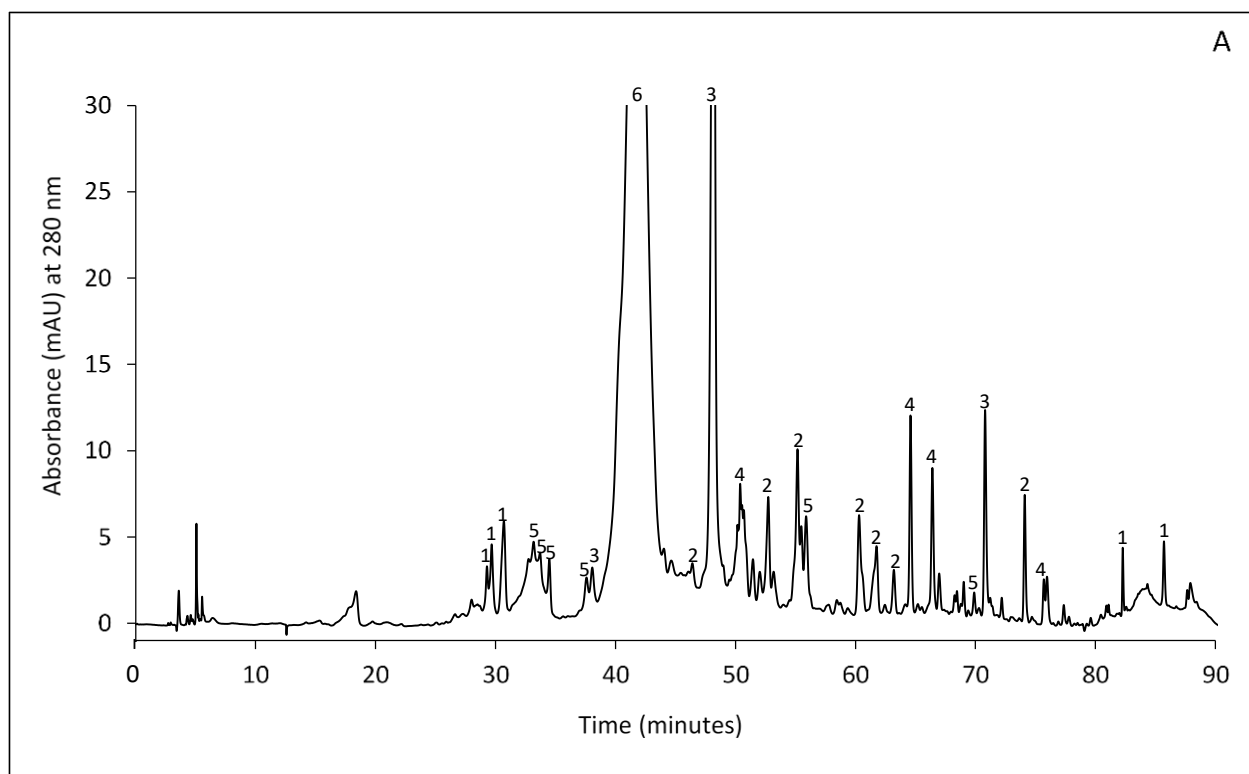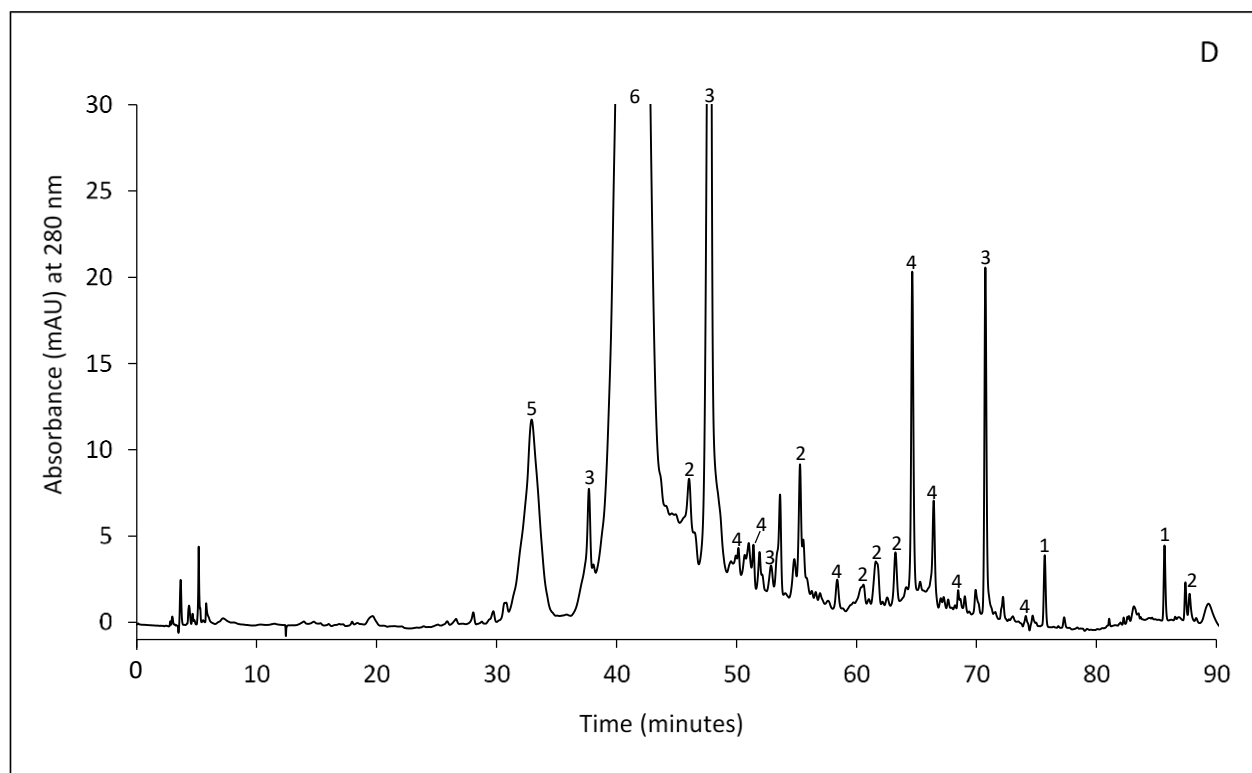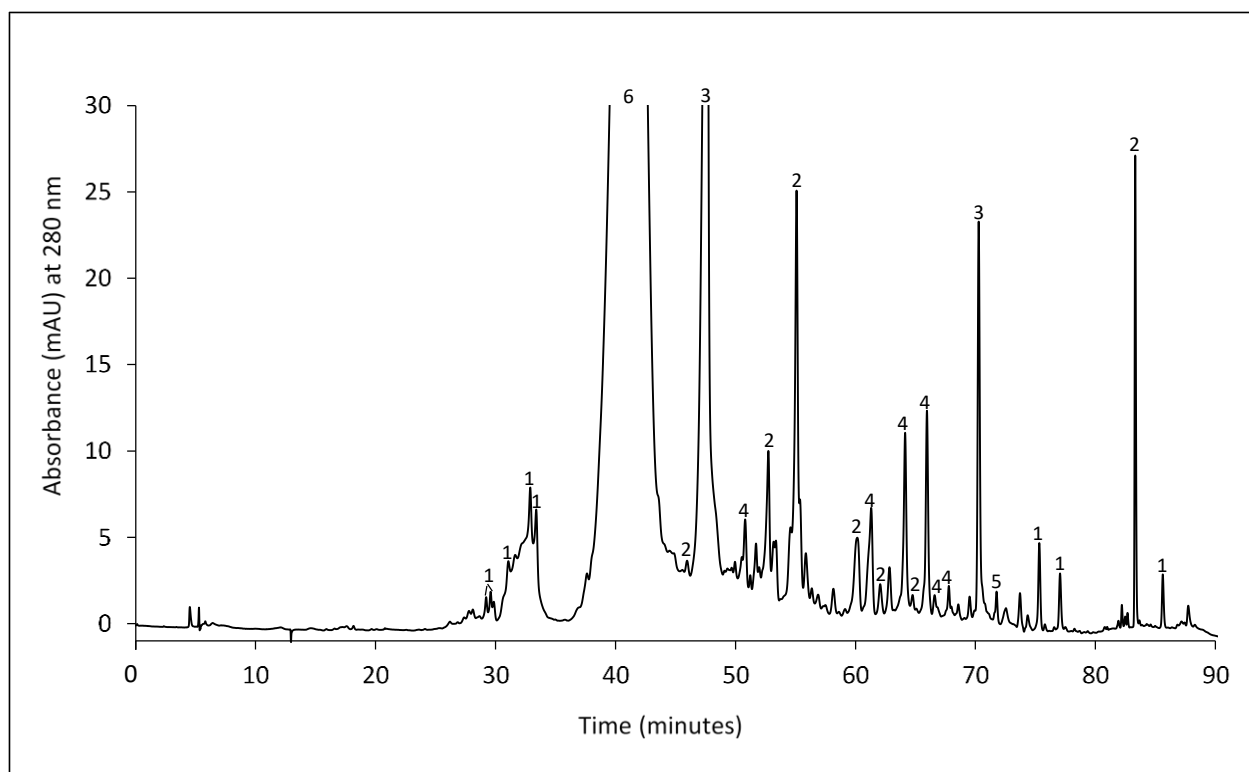
Figure 4.11 HPLC-PDA chromatogram of the PR extract of the Tundra variety showing the identification of phenolic subclasses. Peak phenolic subclass assignments: 1. hydroxybenzoic acids; 2. flavanols; 3. hydroxycinnamic acids; 4. flavonols; 5. flavanones; and 6. anthocyanins.

TPCI results for PR extracts ranged from 381.7-663.3 with a mean of 500.4 mg/100 g FW. The phenolic recovery from this process as determined by TPC (EFW *vs.* PR; Table 4.5) and TPCI (EFW (Table 4.6) *vs.* PR (Table 4.7)) ranged from 81-91% and 86-93%, respectively. Results followed the same varietal pattern for overall phenolic concentration as seen in the EFW extracts (Tundra>Indigo Gem>Honey Bee>Blizzard> Aurora), which was expected due to the similar recovery (EFW compared to PR) in all varieties.

Subclass concentrations showed some differences from EFW extracts. Anthocyanin concentrations ranged from 202.7-404.7 with a mean of 232.4 mg/100 g FW (compared to 249.2-447.8, mean of 339.2 in EFW; Table 4.6). Most varieties showed a loss of flavanols (average ~13%) compared to EFW extracts; however, Blizzard and Indigo Gem showed significant increases in concentration (e.g. Indigo Gem PR-73.8; EFW-49.5 mg/100 g FW). All PR extracts showed a loss of hydroxycinnamic acids resulting in a mean concentration of 50.1 compared to

59.6 mg/100 g FW for EFW extracts. Flavonols showed a similar decrease with a mean of 53.7 (PR) compared to 57.6 mg/100 g FW (EFW). Flavanones showed a mean change from 7.3 (EFW) to 5.1 mg/100 g FW (PR). Indigo Gem and Honey Bee showed no concentration change, while Tundra showed a total loss, from 7.8 mg/100 g FW to no detection (ND) for this subclass.

These TPCI results showed variations in recovery for different phenolic subclasses from EFW to PR extracts. In most cases, this meant a lower concentration of a subclass, but for some subclasses/varieties, an increase was seen in the PR *vs.* EFW extract. A potential explanation for this phenomenon is that the removal of certain nonphenolic compounds may reduce interference, allowing better resolution of the remaining phenolics via HPLC-PDA. This could provide better separation and/or more clear UV-vis spectra, allowing more peaks/compounds to be accurately classified. The decreases in concentration generally seen are explained by the loss of some compounds that are not recovered from the stationary phase in the ethanol elution process. The largest % loss was seen for the anthocyanins (31.5%), likely due to their chemical structure (glycosylated), which makes them more polar than many other phenolics, and therefore, more likely to be lost in the water wash.

4.3.2.3 Phenolic Fraction TPCI

Fractionation of EFW extracts using Amberlite® XAD16N resin (stationary phase) with an aqueous mobile phase containing increasing concentrations of ethanol (i.e. water, 20, 40, 70, and 100% ethanol), was used with the goal of producing samples containing different phenolic subclasses. Representative HPLC-PDA chromatograms of each of the sample fractions for the Tundra variety, with peaks labeled by phenolic subclass, are shown in Figures 4.12 (A-E). Mean and standard deviation TPCI results for each of the phenolic fractions for each of the five haskap varieties are shown in Tables 4.8-12.

Table 4.8 Mean and standard deviation TPCI results for the six major phenolic subclasses for water fractions of Aurora, Blizzard, Honey Bee, Indigo Gem, and Tundra haskap varieties.[1,2]

	Variety				
Phenolic Subclass	Aurora	Blizzard	Honey Bee	Indigo Gem	Tundra
Hydroxybenzoic acids	1.2 ± <0.1[c]	0.9 ± <0.1[b]	1.6 ± <0.1[d]	1.3 ± 0.1[c]	0.6 ± <0.1[a]
Flavanols	0.2 ± <0.1[a]	0.6 ± <0.1[b]	3.8 ± 0.2[d]	4.2 ± 0.1[e]	3.3 ± <0.1[c]
Hydroxycinnamic acids	ND[3]	ND	ND	ND	ND
Flavonols	ND	ND	ND	ND	ND
Flavanones	ND	ND	ND	ND	ND
Anthocyanins	ND	ND	ND	ND	ND
TPCI[4]	1.4 ± <0.1[a]	1.6 ± <0.1[a]	5.4 ± 0.1[c]	5.5 ± 0.2[c]	3.9 ± <0.1[b]

[1]mg/100 g FW.
[2] Mean ± standard deviation results of triplicate sample analysis.
[3]ND represents no phenolic subclass peak with a height above the qualitative detection limit ($<3 \times$ s/n).
[4]Total Phenolic Chromatographic Index = sum of all identified and quantified phenolic peaks.
[a-d]Mean values in the same row followed by a common letter were not statistically different ($p<0.05$) by Tukey's HSD multiple range test between the varieties.

Table 4.9 Mean and standard deviation TPCI results for the six major phenolic subclasses for 20% ethanol fractions of Aurora, Blizzard, Honey Bee, Indigo Gem, and Tundra haskap varieties.[1,2]

Phenolic Subclass	Variety				
	Aurora	Blizzard	Honey Bee	Indigo Gem	Tundra
Hydroxybenzoic acids	1.8 ± 0.1^b	$1.2 \pm {<}0.1^a$	$1.1 \pm {<}0.1^a$	1.1 ± 0.1^a	$1.0 \pm {<}0.1^a$
Flavanols	$0.6 \pm {<}0.1^a$	$0.5 \pm {<}0.1^a$	3.9 ± 0.2^{bc}	4.3 ± 0.4^c	3.5 ± 0.1^b
Hydroxycinnamic acids	ND[3]	ND	ND	ND	ND
Flavonols	ND	ND	ND	ND	ND
Flavanones	ND	ND	ND	ND	ND
Anthocyanins	ND	ND	ND	ND	ND
TPCI[4]	2.4 ± 0.1^a	$1.7 \pm {<}0.1^a$	5.0 ± 0.3^{bc}	5.4 ± 0.5^c	$4.4 \pm {<}0.1^b$

[1] mg/100 g FW.
[2] Mean ± standard deviation results of triplicate sample analysis.
[3] ND represents no phenolic subclass peak with a height above the qualitative detection limit ($<$3 x s/n).
[4] Total Phenolic Chromatographic Index = sum of all identified and quantified phenolic peaks.
[a-c] Mean values in the same row followed by a common letter were not statistically different ($p<0.05$) by Tukey's HSD multiple range test between the varieties.

Table 4.10 Mean and standard deviation TPCI results for the six major phenolic subclasses for 40% ethanol fractions of Aurora, Blizzard, Honey Bee, Indigo Gem, and Tundra haskap varieties.[1,2]

Phenolic Subclass	Variety				
	Aurora	Blizzard	Honey Bee	Indigo Gem	Tundra
Hydroxybenzoic acids	5.1 ± 0.2^c	6.3 ± 0.6^d	4.9 ± 0.2^c	1.1 ± 0.1^a	2.0 ± 0.1^b
Flavanols	9.9 ± 0.2^b	6.6 ± 0.9^a	27.4 ± 0.7^c	11.7 ± 0.8^b	11.2 ± 1.0^b
Hydroxycinnamic acids	4.0 ± 0.2^{ab}	4.2 ± 0.3^b	3.5 ± 0.5^{ab}	3.1 ± 0.1^a	6.1 ± 0.4^c
Flavonols	2.3 ± 0.1^a	2.2 ± 0.2^a	2.3 ± 0.1^a	4.0 ± 0.3^b	6.9 ± 0.2^c
Flavanones	ND[3]	<0.1	$0.2 \pm <0.1^a$	<0.1	2.0 ± 0.1^b
Anthocyanins	58.9 ± 3.1^a	54.0 ± 3.4^a	48.5 ± 4.4^a	105.0 ± 4.0^c	92.7 ± 5.7^b
TPCI[4]	80.2 ± 3.2^{ab}	73.4 ± 3.2^a	86.8 ± 4.2^b	125.0 ± 4.6^c	120.7 ± 5.6^c

[1] mg/100 g FW.
[2] Mean ± standard deviation results of triplicate sample analysis.
[3] ND represents no phenolic subclass peak with a height above the qualitative detection limit (<3 x s/n).
[4] Total Phenolic Chromatographic Index = sum of all identified and quantified phenolic peaks.
[a-d] Mean values in the same row followed by a common letter were not statistically different ($p < 0.05$) by Tukey's HSD multiple range test between the varieties.

Table 4.11 Mean and standard deviation TPCI results for the six major phenolic subclasses for 70% ethanol fractions of Aurora, Blizzard, Honey Bee, Indigo Gem, and Tundra haskap varieties.[1,2]

Phenolic Subclass	Variety				
	Aurora	Blizzard	Honey Bee	Indigo Gem	Tundra
Hydroxybenzoic acids	1.8 ± 0.1^b	$1.2 \pm <0.1^a$	3.3 ± 0.1^c	1.8 ± 0.1^b	1.8 ± 0.1^b
Flavanols	18.5 ± 0.4^c	14.9 ± 1.5^b	8.3 ± 0.5^a	18.7 ± 0.2^c	29.5 ± 1.2^d
Hydroxycinnamic acids	18.8 ± 0.8^b	14.8 ± 0.2^a	20.8 ± 1.1^c	16.3 ± 0.3^a	18.2 ± 0.4^b
Flavonols	21.5 ± 0.9^b	17.0 ± 0.7^a	17.7 ± 1.2^a	23.4 ± 0.8^b	27.9 ± 1.3^c
Flavanones	$0.3 \pm <0.1^a$	$0.2 \pm <0.1^a$	ND[3]	$0.9 \pm <0.1^b$	ND
Anthocyanins	111.4 ± 10.7^a	154.6 ± 7.8^b	132.6 ± 14.1^{ab}	215.6 ± 5.3^c	227.4 ± 11.3^c
TPCI[4]	172.3 ± 10.8^a	202.7 ± 8.9^a	182.6 ± 16.0^a	276.6 ± 5.9^b	304.7 ± 11.5^b

[1]mg/100 g FW.
[2] Mean ± standard deviation results of triplicate sample analysis.
[3]ND represents no phenolic subclass peak with a height above the qualitative detection limit (<3 x s/n).
[4]Total Phenolic Chromatographic Index = sum of all identified and quantified phenolic peaks.
[a-d]Mean values in the same row followed by a common letter were not statistically different ($p<0.05$) by Tukey's HSD multiple range test between the varieties.

Table 4.12 Mean and standard deviation TPCI results for the six major phenolic subclasses for 100% ethanol fractions of Aurora, Blizzard, Honey Bee, Indigo Gem, and Tundra haskap varieties.[1,2]

Phenolic Subclass	Variety				
	Aurora	Blizzard	Honey Bee	Indigo Gem	Tundra
Hydroxybenzoic acids	1.1 ± 0.1[a]	2.1 ± 0.3[b]	2.3 ± 0.2[b]	2.0 ± 0.1[b]	4.5 ± 0.5[c]
Flavanols	15.9 ± 0.6[b]	18.9 ± 0.6[c]	12.6 ± 1.1[a]	12.4 ± 0.7[a]	14.1 ± 0.8[ab]
Hydroxycinnamic acids	0.9 ± <0.1[b]	<0.5	0.6 ± <0.1[a]	<0.5	ND[3]
Flavonols	3.2 ± 0.1[a]	4.0 ± 0.2[a]	5.0 ± 0.3[b]	6.7 ± 0.3[c]	10.9 ± 0.6[d]
Flavanones	ND	0.1 ± <0.1[a]	<0.1	0.2 ± <0.1[a]	ND
Anthocyanins	0.7 ± <0.1[a]	<0.2	<0.2	1.0 ± <0.1[b]	0.9 ± <0.1[b]
TPCI[4]	22.0 ± 0.8[a]	25.0 ± 0.8[b]	20.4 ± 1.0[a]	22.8 ± 1.1[a]	30.5 ± 1.8[c]

[1] mg/100 g FW.
[2] Mean ± standard deviation results of triplicate sample analysis.
[3] ND represents no phenolic subclass peak with a height above the qualitative detection limit (<3 x s/n).
[4] Total Phenolic Chromatographic Index = sum of all identified and quantified phenolic peaks.
[a-d] Mean values in the same row followed by a common letter were not statistically different ($p < 0.05$) by Tukey's HSD multiple range test between the varieties.
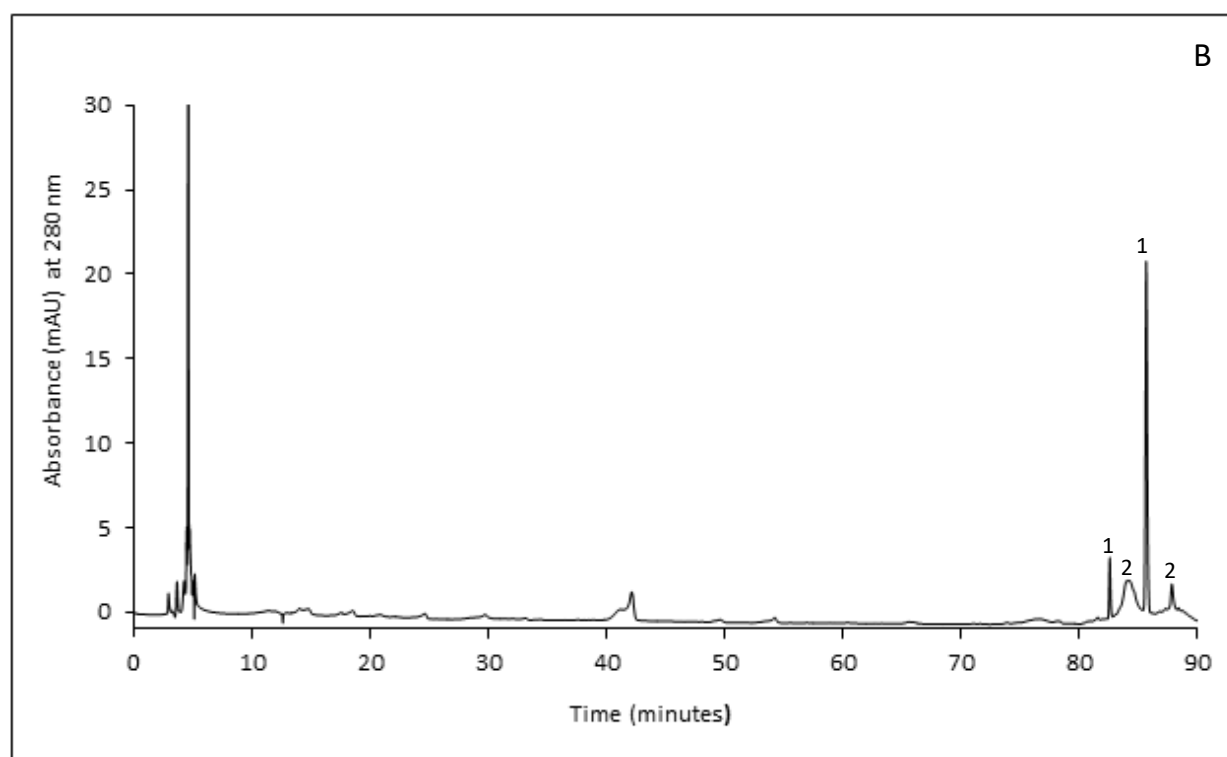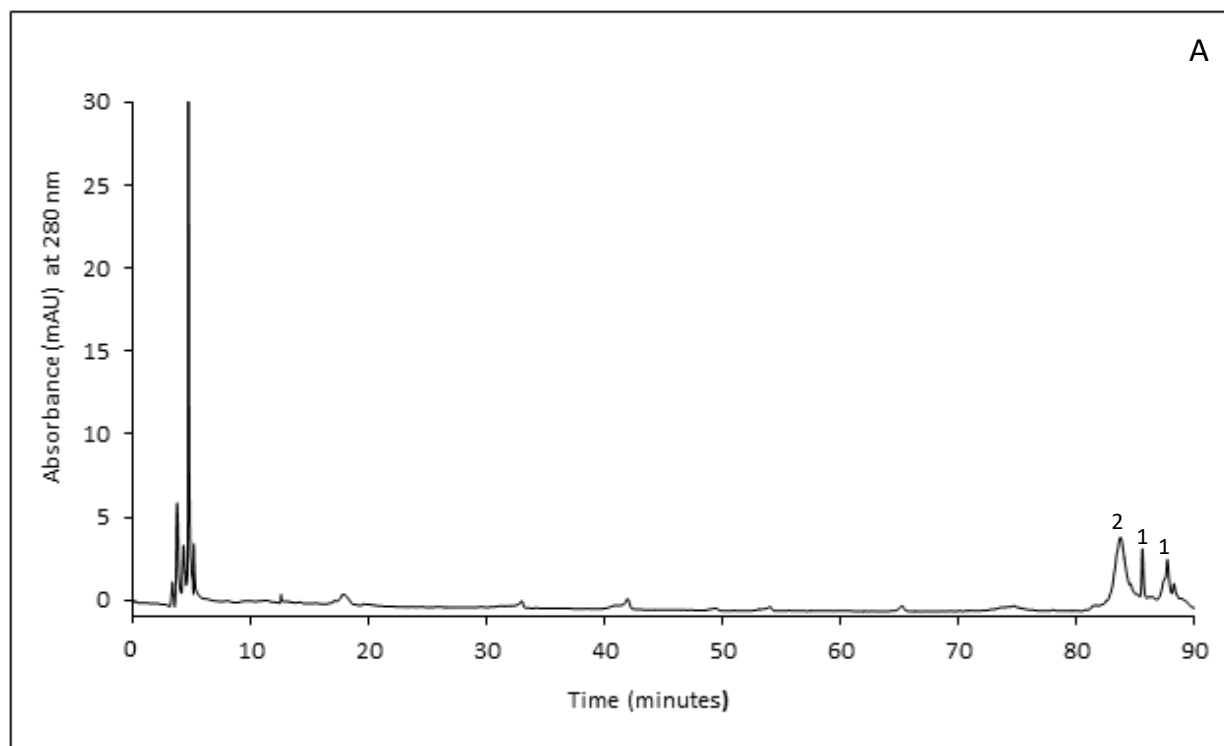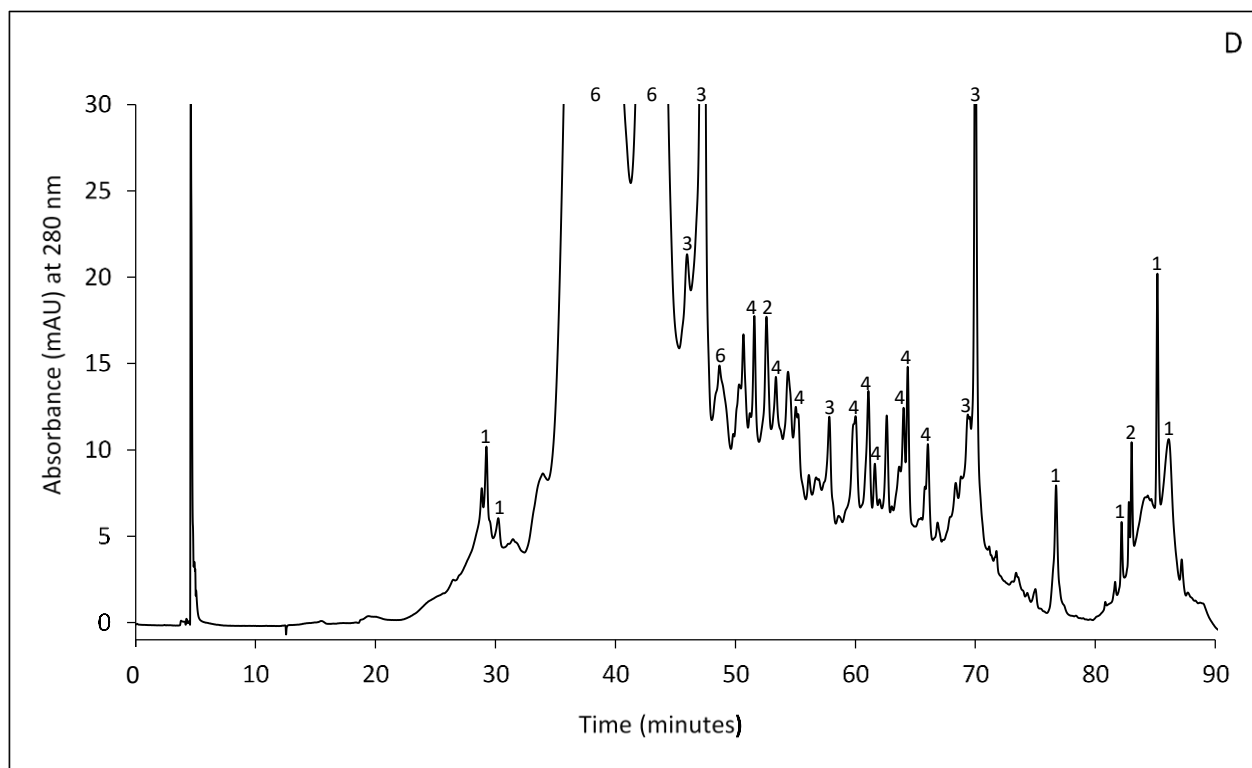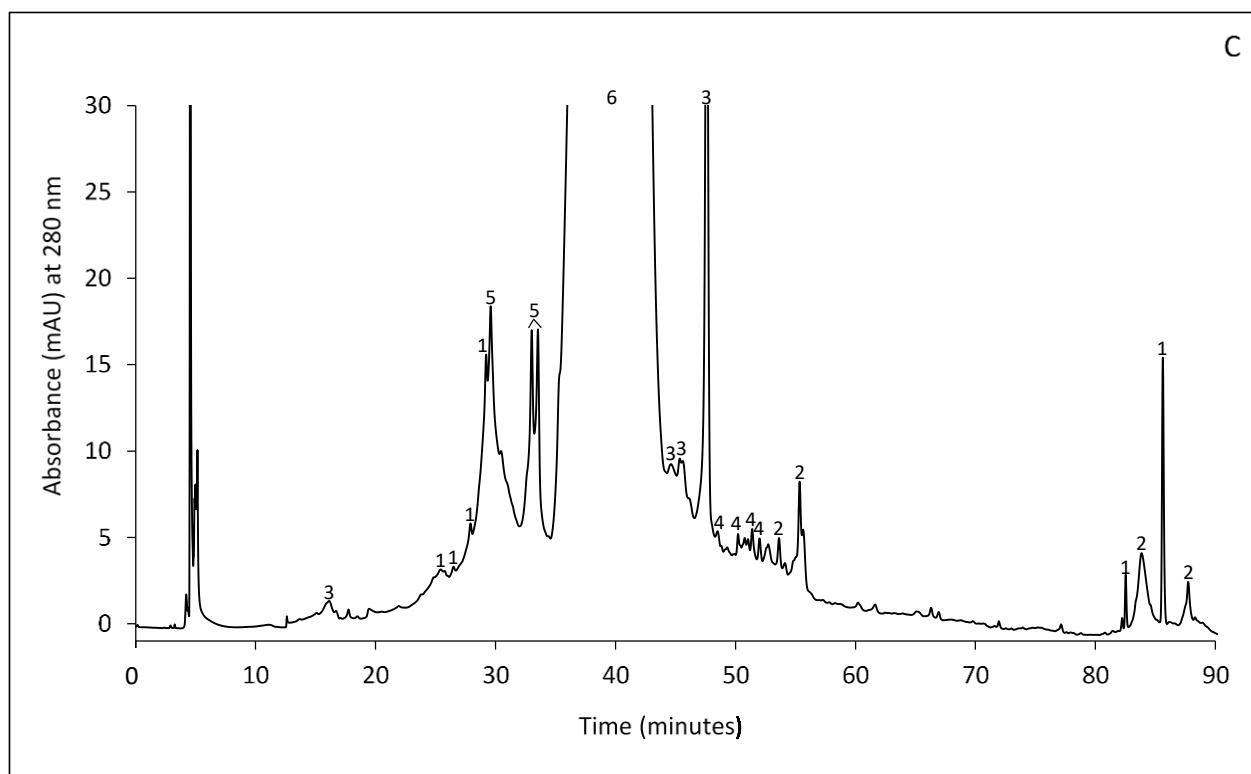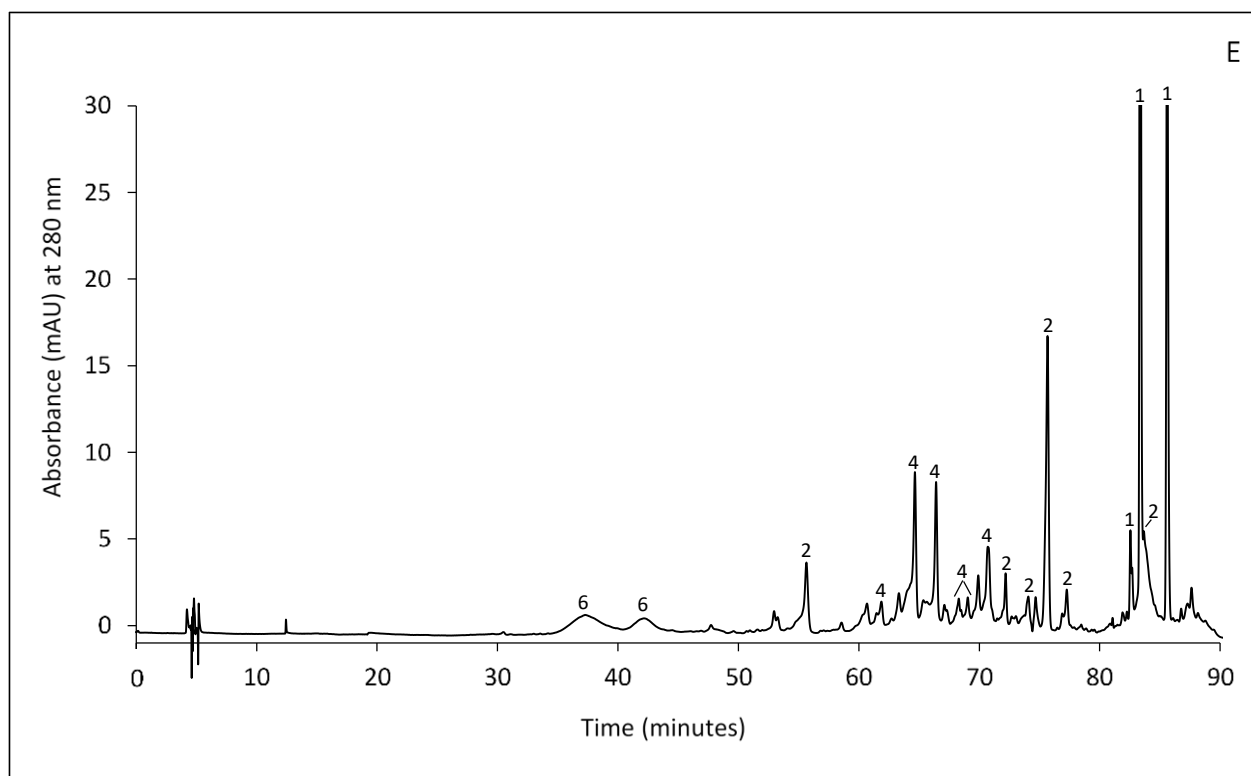
Figure 4.12 HPLC-PDA chromatograms of Tundra phenolic fractions. Chromatogram identification: A. water; B. 20% ethanol; C. 40% ethanol; D. 70% ethanol; and E. 100% ethanol. Peak phenolic subclass assignments: 1. hydroxybenzoic acids; 2. flavanols; 3. hydroxycinnamic acids; 4. flavonols; 5. flavanones; and 6. anthocyanins.

The water and 20% ethanol fractions had low phenolic concentrations compared to the other fractions as shown by their low TPCI values (<5.6 mg/100 g FW; Tables 4.8-9). The two phenolic subclasses identified in these fractions were hydroxybenzoic acids and flavanols. The unlabeled peaks eluting between 4-7 min (e.g. Figure 4.12A) had an absorbance at 280 nm but did not have UV-visible spectra that matched those of the identified phenolic subclasses. One of these compounds is likely to be ascorbic acid based on its RT of ~6.1 min and λ_{max} of 289 nm (Maniyar et al., 2012).

Sample 40% ethanol fractions (Table 4.10) contained an average of 27.4% of the combined TPCI (based on the combined TPCI values of the water, 20, 40, 70, and 100% ethanol fractions), with anthocyanins being the major phenolic subclass, accounting for an average of 72.7% of the 40% fraction TPCI values. The other major phenolic subclass was the flavanols with an average of 14.3% of the fraction TPCI. Indigo Gem had the highest 40% fraction TPCI (125.0 mg/100 g

FW; Table 4.10) and anthocyanin content (105.0 mg/100 g FW; Table 4.10); this variety also had the highest anthocyanin content in its EFW extract (Table 4.6).

Sample 70% ethanol fractions (Table 4.11) contained an average of 63.8% of the combined TPCI, with anthocyanins being the major phenolic subclass, accounting for an average of 73.2% of the 70% fraction TPCI values. The other major phenolic subclasses were the flavonols, hydroxycinnamic acids, and flavanols with averages of 9.7, 8.3, and 7.8% of the fraction TPCI, respectively. The Tundra variety had the highest 70% fraction TPCI (304.7 mg/100 g FW; Table 4.11), along with the highest concentrations of the anthocyanin, flavanol, and flavonol subclasses.

Based on the above results, both the 40% and 70% ethanol fractions could be described as anthocyanin rich. This is based on an increase in the % anthocyanins (i.e. anthocyanin concentration/TPCI concentration) when compared to the starting material (EFW extracts). In the EFW extracts, anthocyanins made up an average of 60.5% of the TPCIs (Table 4.6). The anthocyanin content in the 40% and 70% fractions were 72.7 and 73.2% on average (Tables 4.10-11), respectively. The anthocyanin content of the Tundra variety's EFW extract was 59.0%, which increased to 76.8% and 74.6% in its 40 and 70% fractions, respectively. Of these two anthocyanin rich fractions, the 40% was the best candidate for cell line studies as it had the most successful separation of phenolic subclasses, demonstrated by fewer later eluting peaks in its chromatogram (Figure 4.12C) in comparison to the 70% fraction (Figure 4.12D).

The 100% ethanol fractions (Table 4.12) had low TPCI contents/concentrations (maximum TPCI of 30.5 mg/100 g FW for Tundra) with an average of 6.8% of the combined TPCI. The most abundant phenolic subclasses were the flavanols, accounting for an average of 62.1% of the 100% fraction TPCI values, and the flavonols, with 24.0% of the fraction TPCI. These fractions contained very low levels of anthocyanins (<0.2-1.0 mg/100 g FW; Table 4.12). Based on these results, the 100% ethanol fraction was used in cell line studies to determine the impact of these two phenolic subclasses. Comparison of cell line results between the 40 and 100% fractions showed impacts of a primarily anthocyanin treatment *vs.* a flavanol/flavonol treatment and are discussed in Section 4.5.

TPCI chromatograms of the 40, 70, and 100% ethanol fractions from the Aurora, Blizzard, Honey Bee, and Indigo Gem varieties can be found in Figure 8.2 of the Appendix.

4.3.3 HPLC-MS/MS Phenolic Analysis

To increase the specificity of sample phenolic identification, tandem mass spectrometry (MS/MS) was used in conjunction with HPLC separation. The MS analysis yielded unique mass to charge (*m/z*) values of precursor and product ions (i.e. fragments) that were then used for phenolic compound identification. This allowed for more accurate phenolic compound identification and confirmation of compounds previously identified by HPLC-PDA using standards. The HPLC-MS/MS results with compound identification of the Tundra variety 100% ethanol fraction are shown in Table 4.13. Figure 4.13 shows a representative HPLC-PDA chromatogram of the Tundra 100% ethanol fraction which has been labeled with a combination of HPLC-PDA and HPLC-MS/MS results to show both subclass and specific compound identification. The labeled chromatograms and MS/MS tables of the 40% and 70% ethanol fractions of the Tundra variety are presented in Tables 8.1 and 8.2 and Figure 8.3 of the appendix, as no new phenolic compound identifications were found for these fractions.

Table 4.13 HPLC-MS/MS precursor and product ion *m/z* values and phenolic identification for the Tundra variety 100% ethanol fraction.

Peak Label[1]	RT[2]	Precursor [M-H]⁻ *m/z* values	Product Ion *m/z* values	Phenolic Identification
4a	61.88	595.1	301.0, 271.0, 255.0	Quercetin-vicianoside
4b	64.67	609.2	300.0, 271.0, 255.0	Quercetin-3-*O*-rutinoside[3]
4c/d	66.46	463.1	300.0, 257.0	Quercetin-3-*O*-galactoside[3]/glucoside[3]
4e	68.27	433.1	300.0, 271.0, 255.0	Quercetin-pentoside
4f	68.41	593.2	285.1, 255.0, 227.0	Kaempferol-rutinoside
4g	68.84	623.2	315.1, 300.0, 271.0, 151.0	Isorhamnetin-3-*O*-rutinoside[3]
4h	69.81	447.1	284.0, 255.0, 27.0, 151.0	Kaempferol-hexoside
4i	70.07	477.1	315.1, 271.1, 256.0	Isorhamnetin-3-*O*-glucoside[3]
4j	70.63	505.1	300.0, 271.0, 255.0	Quercetin-acetyl-hexoside
2a	72.00	435.1	273.1, 167.0	Phloridzin[3]
4k	72.38	463.3	417.0, 301.0, 271.0, 255.0	Quercetin-hexoside
4l	74.65	519.2	314.0, 285.0. 271.0, 243.0	Isorhamnetin-acetyl-hexoside

[1]Peak number designates phenolic subclass (2. flavanols; and 4. flavonols), while peak letter identifies individual compounds; peak labels are matched to the chromatogram in Figure 4.13.
[2] Retention time (min).
[3]Compound identification confirmed using standards.
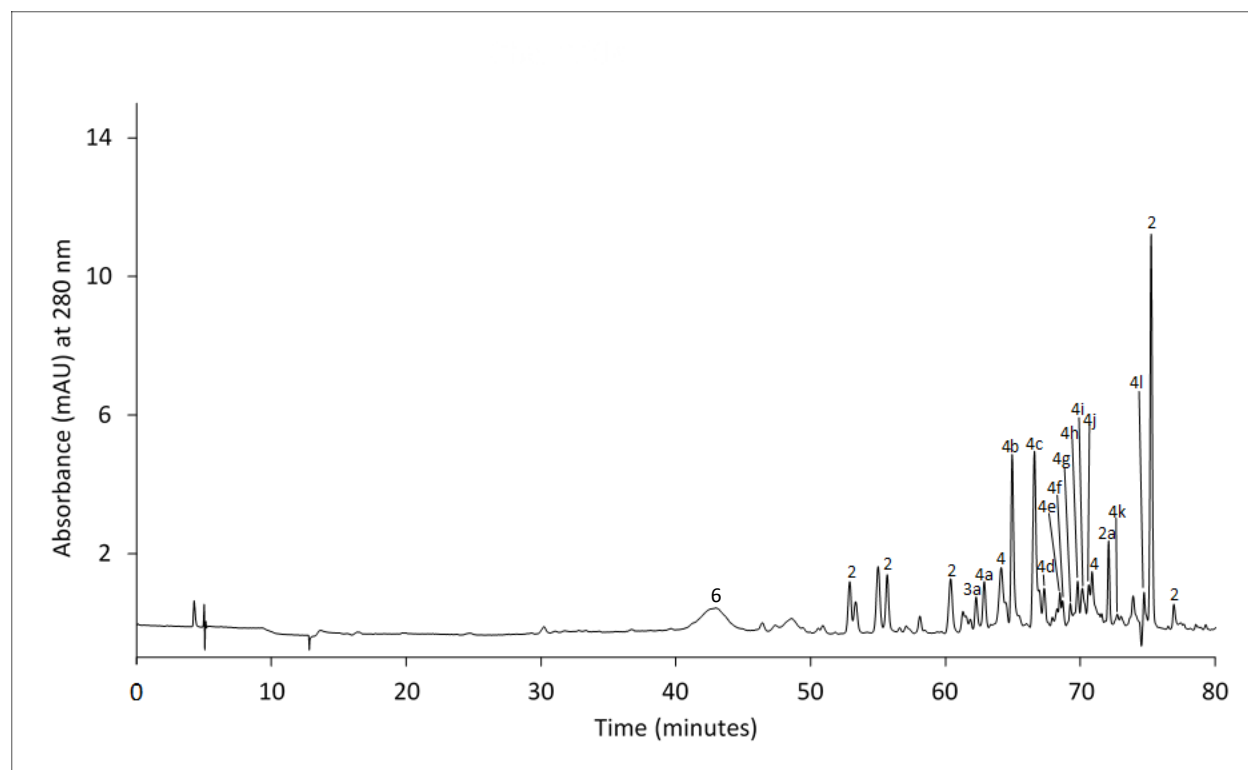
Figure 4.13 HPLC-PDA chromatogram of the Tundra 100% ethanol fraction. Phenolic subclass assignments: 2. flavanols; 3. hydroxycinnamic acids; 4. flavonols; 5. flavanones; and 6. anthocyanins. Compound identification: 3a. ferulic acid*; 4a. quercetin-vicianoside; 4b. quercetin-3-*O*-rutinoside*; 4c. quercetin-3-*O*-glucoside*; 4d. quercetin-3-*O*-galactoside*; 4e. quercetin-pentoside; 4f. kaempferol-rutinoside; 4g. isorhamnetin-3-*O*-rutinoside*; 4h. kaempferol-hexoside; 4i. isorhamnetin-3-*O*-glucoside*; 4j. quercetin-acetyl-hexoside; 2a. phloridzin*; 4k. quercetin-hexoside; and 4l. isorhamnetin-acetyl-hexoside. *confirmed using standards.

Based on both HPLC-PDA and HPLC-MS/MS results, the Tundra variety 100% ethanol fraction contained primarily flavonols, particularly isorhamnetin and quercetin derivatives. The 100% ethanol fraction was also found to contain a previously unreported (to the best of the author's knowledge) phenolic compound: kaempferol-rutinoside. All other identified phenolic compounds have been reported in haskaps (Kucharska et al., 2017; Senica et al., 2017; Khattab et al., 2015; Wojdylo et al., 2013). These HPLC-MS/MS results provided detailed analytical data on the phenolic composition of these haskap berries, and also yielded important information about the specific phenolic compounds that were applied to cell lines (Section 4.5) as part of the 100% fraction treatments.

4.3.4 HPLC-PDA Anthocyanin Analysis

Sample anthocyanins were determined for EFW extracts using high performance liquid chromatography with photodiode array detection (HPLC-PDA). Compounds absorbing at 520 nm and eluting in the timeframe observed with standards (~30-60 min) were assumed to be anthocyanins. Individual anthocyanins were identified and quantified using a comparison of retention times to external standards, spiking experiments, and peak area/height comparison to standard curves. Standards were selected based on anthocyanins that have been identified in haskaps. Analytical results for anthocyanin content in Aurora, Blizzard, Honey Bee, Indigo Gem, and Tundra haskap varieties are shown in Table 4.14. A mixed anthocyanin standard is shown in Figure 4.14, and representative sample chromatograms are shown in Figures 4.15 (A-E).

Table 4.14 Mean and standard deviation anthocyanin results for the EFW extracts of Aurora, Blizzard, Honey Bee, Indigo Gem, and Tundra haskap varieties.[1,2]

Anthocyanin	Variety				
	Aurora	Blizzard	Honey Bee	Indigo Gem	Tundra
Cyanidin-3,5-O-diglucoside	17.5 ± 0.3[a]	34.2 ± 0.5[c]	48.1 ± 1.4[d]	47.3± 1.8[d]	30.3 ± 1.6[b]
Cyanidin-3-O-galactoside	<0.8	<0.8	<0.8	<0.8	<0.8
Cyanidin-3-O-glucoside	227.8 ± 4.8[a]	269.4 ± 1.3[b]	227.3 ± 1.9[a]	396.3 ± 12.4[d]	361.6 ± 11.9[c]
Cyanidin-3-O-rutinoside	13.2 ± 0.4[a]	28.6 ± 0.9[c]	22.7 ± <0.1[b]	32.4 ± 0.8[d]	26.3 ± 1.7[c]
Pelargonidin-3-O-glucoside	2.3 ± 0.1[b]	1.1 ± <0.1[a]	1.1 ± 0.1[a]	4.9 ± 0.2[c]	1.0 ± 0.1[a]
Peonidin-3-O-glucoside	15.4 ± 0.1[b]	20.9 ± 0.8[c]	11.8 ± 0.2[a]	20.4 ± 0.3[c]	31.8 ± 0.9[d]
Total	276.2 ± 5.0[a]	354.3 ± 2.7[c]	311.0 ± 1.0[b]	501.3 ± 13.5[e]	451.0 ± 13.5[d]

[1]mg/100 g FW.
[2] Mean ± standard deviation results of triplicate sample analysis.
[a-d]Mean values in the same row followed by a common letter were not statistically different ($p<0.05$) by Tukey's HSD multiple range test between the varieties.
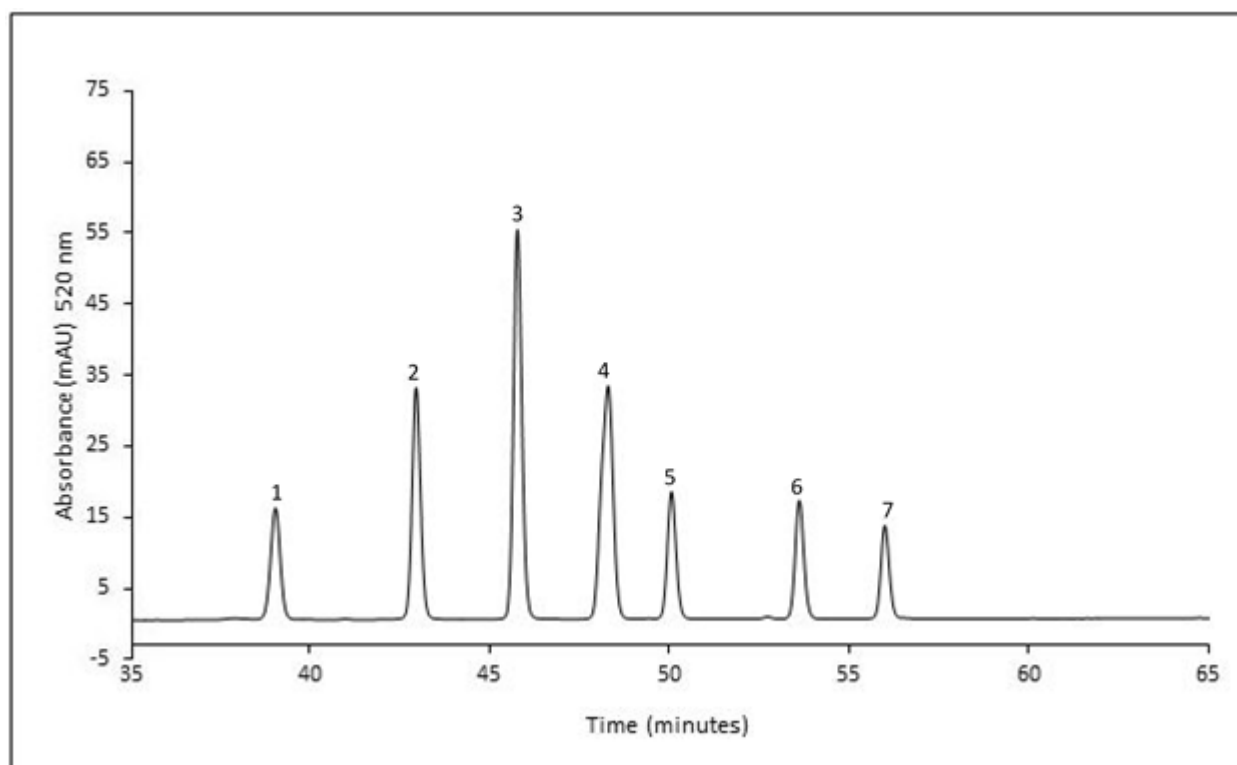
Figure 4.14 HPLC-PDA chromatogram of anthocyanin standards. Peak identities: 1. cyanidin-3,5-*O*-diglucoside; 2. cyanidin-3-*O*-galactoside; 3. cyanidin-3-*O*-glucoside; 4. cyanidin-3-*O*-rutinoside; 5. pelargonidin-3-*O*-glucoside; 6. peonidin-3-*O*-glucoside; and 7. cyanidin-3-*O*-xyloside.
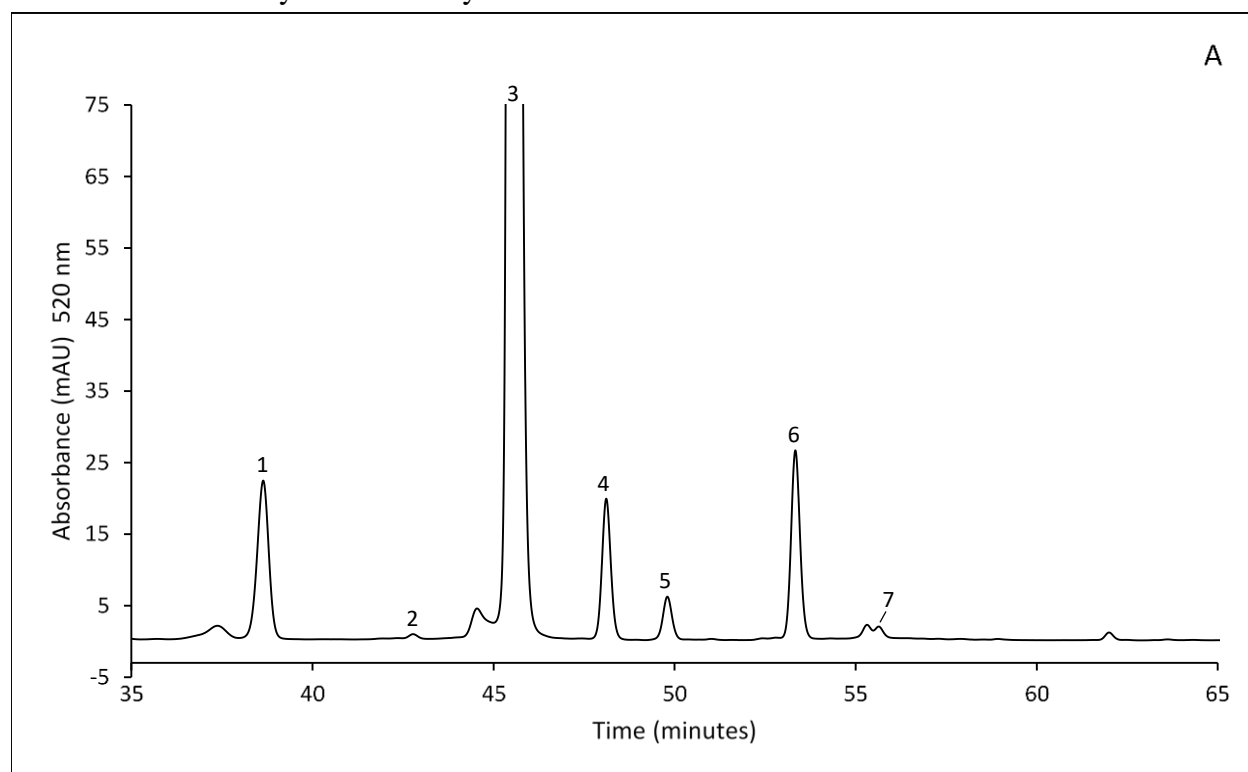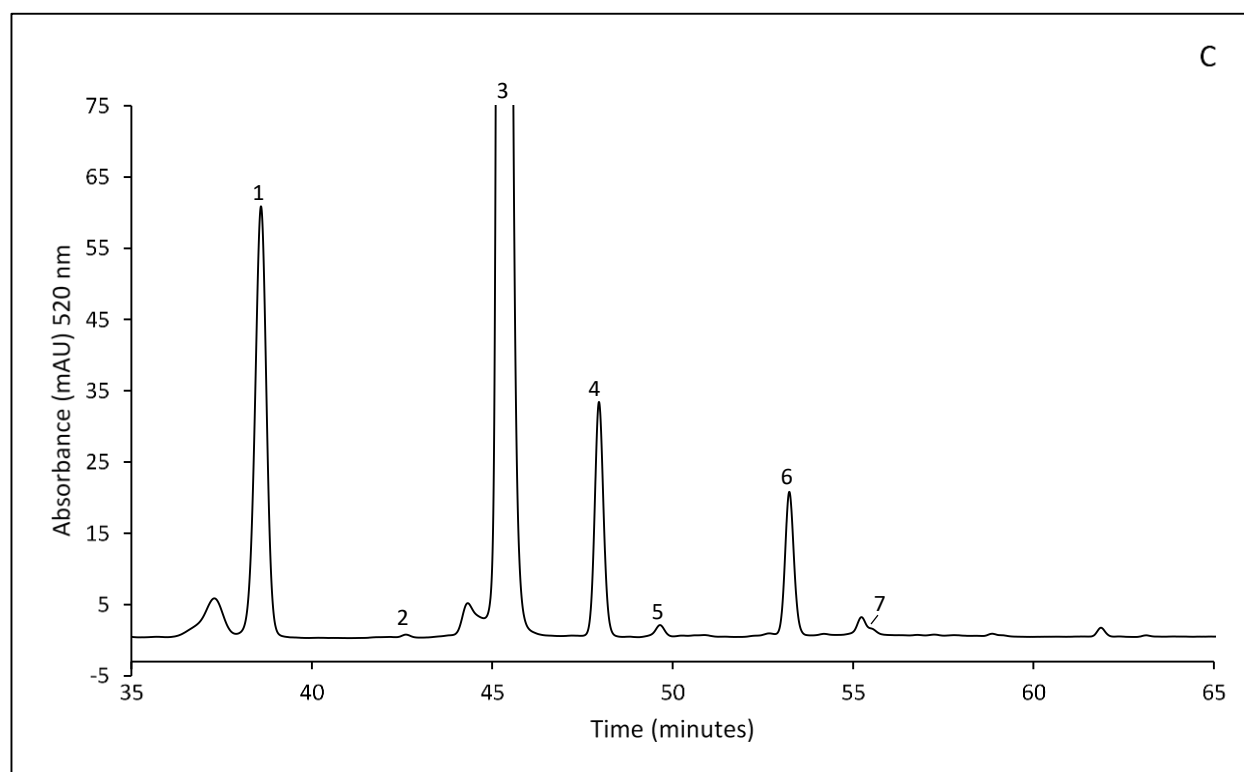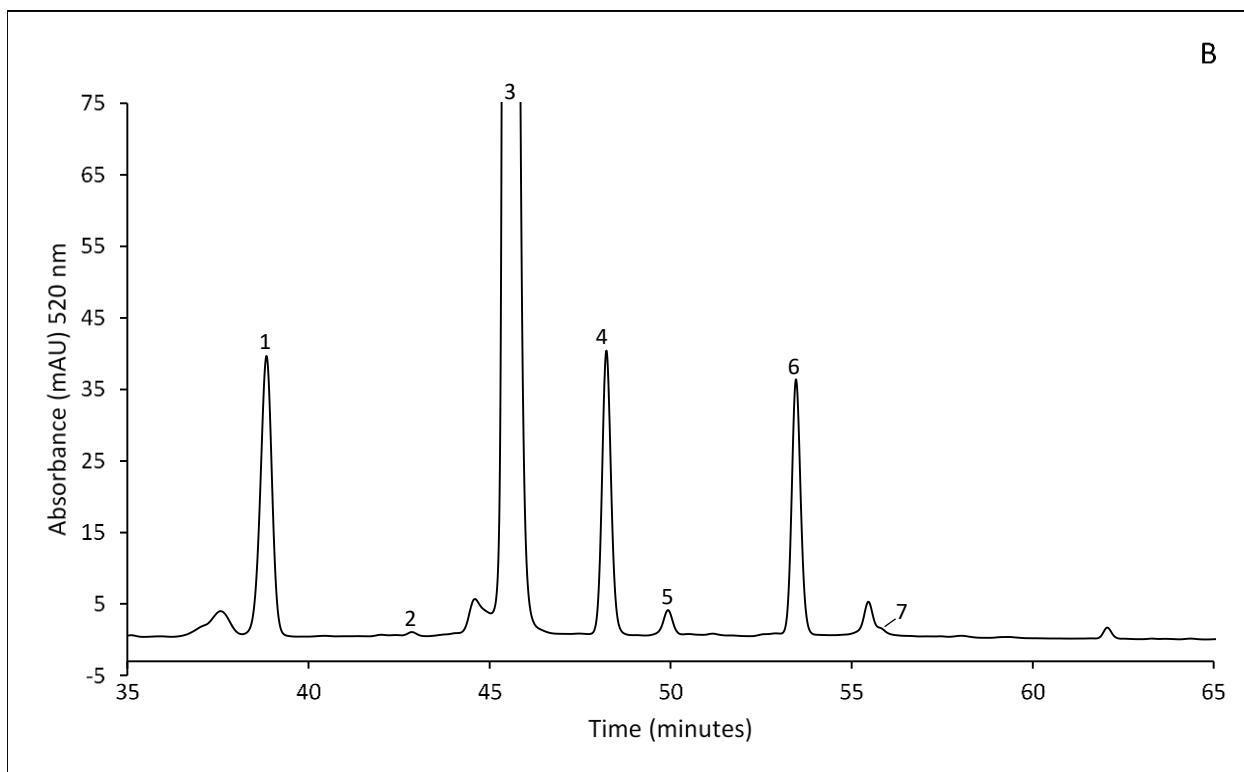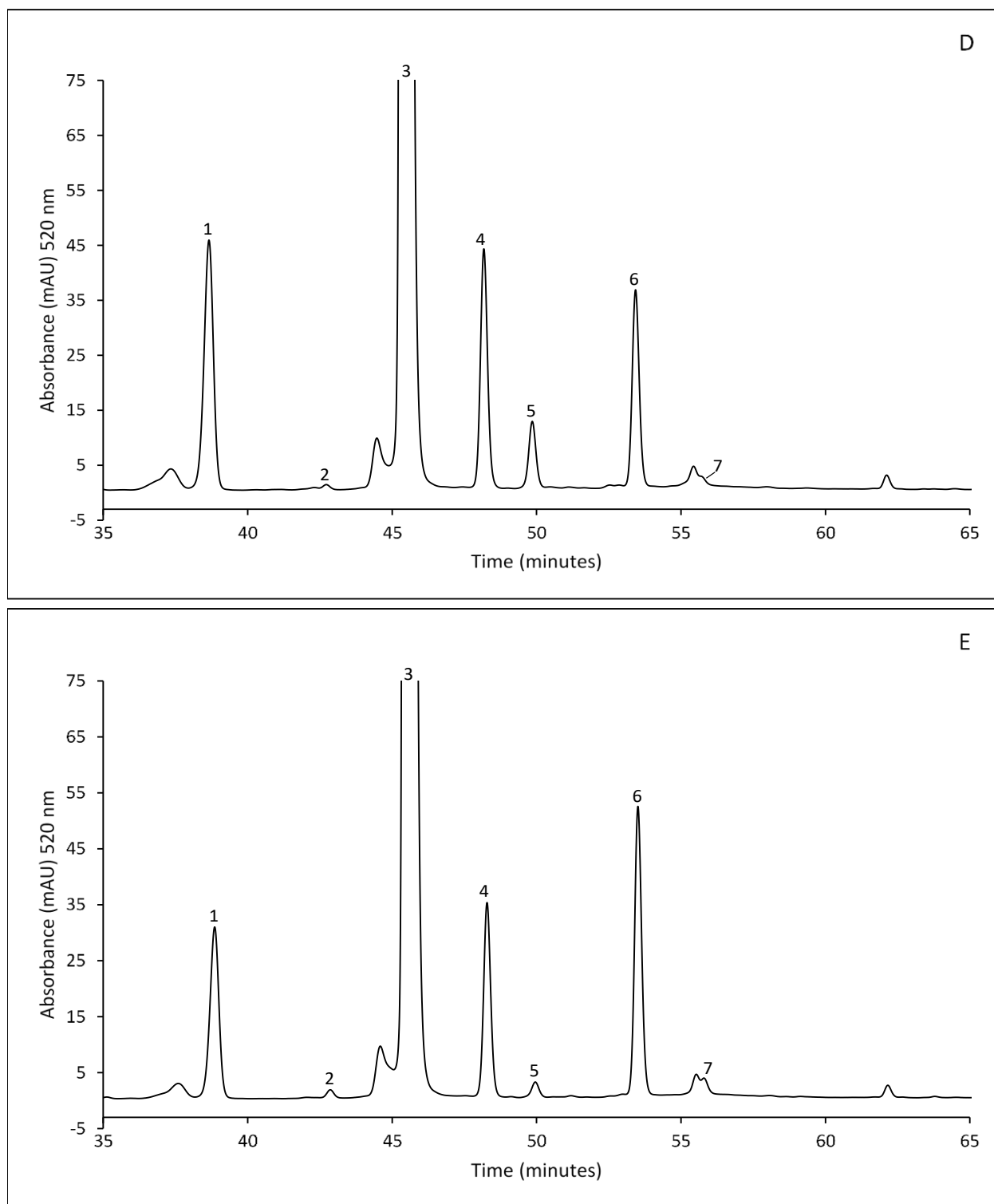
Figure 4.15 HPLC-PDA chromatograms of anthocyanins in the EFW extracts of haskap samples. Chromatogram identification: A. Aurora; B. Blizzard; C. Honey Bee; D. Indigo Gem; and E. Tundra. Peak identities: 1. cyanidin-3,5-O-diglucoside; 2. cyanidin-3-O-galactoside; 3. cyanidin-3-O-glucoside; 4. cyanidin-3-O-rutinoside; 5. pelargonidin-3-O-glucoside; 6. peonidin-3-O-glucoside; and 7. cyanidin-3-O-xyloside.

108

Total anthocyanin content for the five varieties ranged from 276.2-501.3 (Aurora and Indigo Gem, respectively) with a mean of 378.8 mg/100 g FW. These values were higher than those found for anthocyanins by the TPCI method for EFW extracts of 249.2-447.8 mg/100 g FW (mean of 339.2; Table 4.6). This may be due to the use of a representative anthocyanin (cyanidin-3-*O*-glucoside) for TPCI quantitation, which did not account for varying detector responses by individual compounds. When compared to literature results, the anthocyanin concentrations found for these five haskap varieties were: (a) lower than those reported for Indigo Gem and Tundra grown in Nova Scotia of 709 and 640 mg/100 g FW, respectively (HPLC-PDA) (Khattab et al., 2016); and (b) higher than those reported for Indigo Gem and Tundra grown in Saskatchewan of 178.9 and 214.5 mg/100 g FW, respectively (HPLC-PDA) (Rupasinghe et al., 2015).

Haskap anthocyanin content was dominated by cyanidin-3-*O*-glucoside, which made up 72.5-82.1% of the total anthocyanin content. Cyanidin-3-*O*-glucoside content ranged from 227.3-393.3 (Honey Bee and Indigo Gem, respectively) with a mean of 296.5 mg/100 g FW. Literature results for cyanidin-3-*O*-glucoside content in haskaps vary considerably as illustrated by the following: (a) range of 104.7-649.0 with a mean of 306.8 mg/100 g FW for four Canadian varieties (Berry Blue, Borealis, Indigo Gem, and Tundra) (Khattab et al., 2016; Rupasinghe et al., 2015); and (b) range of 81.7-142.0 with a mean of 116.5 mg/100 g FW for two Polish varieties (Brazowa and Wojtek) (Ochmian et al., 2012).

In general, the remaining anthocyanins in order of abundance (after cyanidin-3-*O*-glucoside) were: cyanidin-3,5-*O*-diglucoside, cyanidin-3-*O*-rutinoside, peonidin-3-*O*-glucoside, pelargonidin-3-*O*-glucoside, and cyanidin-3-*O*-galactoside/cyanidin-3-*O*-xyloside. Cyanidin-3-*O*-xyloside (Peak 7; Figures 4.15A-E) was identified, but not quantified due to its coelution with an unidentified anthocyanin peak. The concentrations of these less abundant compounds were generally similar to literature values.

HPLC-PDA analysis was employed primarily for the identification and quantification of major anthocyanin components. To explore in more detail, particularly for identification of uncharacterized peaks (Figures 4.15A-E), HPLC-MS/MS was employed and will be discussed in the next section.

4.3.5 HPLC-MS/MS Anthocyanin Analysis

To investigate haskap anthocyanin structural composition in more detail, MS was used in tandem with HPLC employing an anthocyanin-specific method. The HPLC method used for anthocyanin quantification (Section 3.6.4) employed a mobile phase of 4% phosphoric acid which is incompatible with MS analysis as it can suppress ionization of the analyte. The new method (Section 3.6.5) was developed employing MS-compatible acid at a much lower concentration (solvent A- 0.12% trifluoroacetic acid (TFA)/5% acetonitrile; solvent B- 0.12% TFA in acetonitrile) and had a significantly shorter analysis time (65 min *vs*. 95 min) with a similar linear gradient to the original method. The concentration of the sample was also increased (2.5x more concentrated) to improve analyte detection. Table 4.15 shows the HPLC-MS/MS results with anthocyanin identification for the Tundra variety 70% ethanol fraction. An HPLC-MS/MS chromatogram labeled with the coinciding HPLC-MS/MS data is shown in Figure 4.16.

Table 4.15 HPLC-MS/MS precursor and product ion *m/z* values and anthocyanin identification for the Tundra 70% ethanol fraction

Peak Number[1]	RT[2]	Precursor [M+H]$^+$ *m/z* values	Product Ion [M+H]$^+$ *m/z* values	Anthocyanin Identification
1	22.47	611.2	449.1, 287.1	Cyanidin-3,5-*O*-diglucoside[3]
2	30.42	625.2	463.1, 301.1	Peonidin-dihexoside
3	34.50	449.1	287.1	Cyanidin-3-*O*-galactoside[3]
4	36.90	449.1	287.1	Cyanidin-3-*O*-glucoside[3]
5	40.09	595.2	287.1	Cyanidin-3-*O*-rutinoside[3]
6	43.89	433.1	271.1	Pelargonidin-3-*O*-glucoside[3]
7	47.43	463.1	301.1	Peonidin-3-*O*-glucoside[3]
8	49.45	609.2	463.1, 301.1	Peonidin-rutinoside
9	50.78	597.1	303.1	Delphinidin-sambubioside
10	51.40	419.1	287.1	Cyanidin-3-*O*-xyloside[3]
11	56.47	611.2	465.1, 303.1	Delphinidin-rutinoside
12	58.17	465.1	303.1	Delphinidin-hexoside
13	59.14	433.1	301.1	Peonidin-pentoside

[1]Peak number matched to the chromatogram shown in Figure 4.16.
[2] Retention time (min).
[3]Compound identification confirmed using standards.
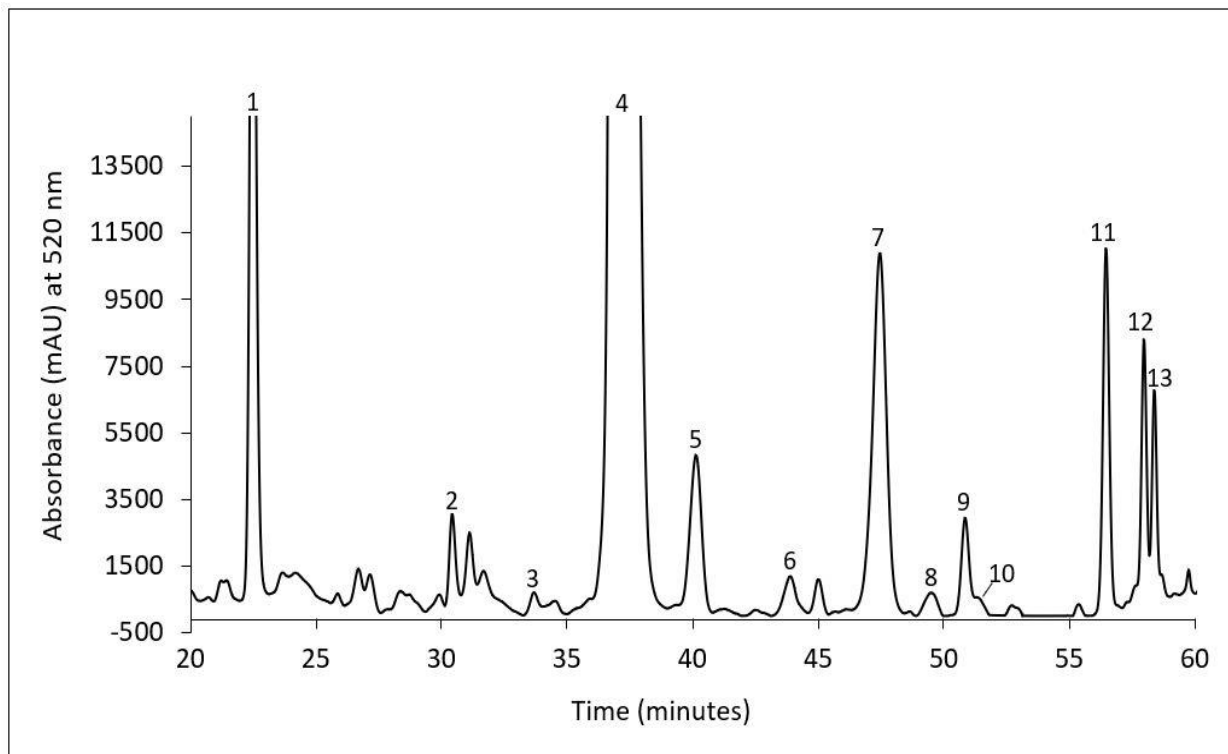
Figure 4.16 HPLC-PDA chromatogram of anthocyanins in Tundra 70% ethanol fraction. Peak identification: 1. cyanidin-3,5-*O*-diglucoside*; 2. peonidin-dihexoside; 3. cyanidin-3-*O*-galactoside*; 4. cyanidin-3-*O*-glucoside*; 5. cyanidin-3-*O*-rutinoside*; 6. pelargonidin-3-*O*-glucoside*; 7. peonidin-3-*O*-glucoside*; 8. peonidin-rutinoside; 9. delphinidin-sambubioside; 10. cyanidin-3-*O*-xyloside*; 11. delphinidin-rutinoside; 12. delphinidin-hexoside; and 13. peonidin-pentoside. *confirmed using standards.

Anthocyanin HPLC-MS/MS results confirmed the presence of the seven previously identified (i.e. by HPLC-PDA) anthocyanins (Peaks 1, 3, 4, 5, 6, 7, and 10; Figure 4.16). Six of these anthocyanins (Peaks 2, 8, 9, 11, 12, 13) were not confirmed with standards due to their cost, limited commercial availability, and/or their relatively low concentrations in the haskap samples analyzed in this study. Of the identified anthocyanins, 11 have been reported for haskaps in literature (Kucharska et al., 2017; Caprioli et al., 2016; Khattab et al., 2016; Rupasinghe et al., 2015; Kusznierewicz et al., 2012) with delphinidin-sambubioside (sambubioside is β-D-xylosyl-(1→2)-β-D-glucose) and peonidin-pentoside being identified for the first time (to the best of the author's knowledge) in this work (Peaks 9 and 13, respectively; Figure 4.16). The successful application of HPLC-PDA and HPLC-MS/MS provided additional analytical data on the phenolic

112

composition of these haskap berries and also detailed information about the contents of the haskap phenolic treatments *in vitro* (Section 4.5).

4.4 Free Radical Scavenging

4.4.1 ABTS (2,2-azino-bis-3-ethylbenzthiazoline-6-sulfonic acid) Radical Scavenging Assay

The ABTS free radical scavenging or Trolox equivalent antioxidant capacity (TEAC) results for EFW and PR extracts, and 40, 70, and 100% ethanol phenolic fractions are reported in Table 4.16.

Table 4.16 Mean and standard deviation for ABTS assay results of extracts (EFW and PR) and selected phenolic fractions of Aurora, Blizzard, Honey Bee, Indigo Gem, and Tundra haskap varieties.[1,2]

Extract or Fraction	Variety				
	Aurora	Blizzard	Honey Bee	Indigo Gem	Tundra
EFW extract	131.4 ± 5.9[a]	158.5 ± 2.5[b]	146.3 ± 3.0[b]	207.0 ± 5.2[c]	225.9 ± 5.8[d]
PR extract	98.7 ± 1.8[a]	117.5 ± 3.8[b]	105.5 ± 4.9[a]	153.1 ± 2.1[c]	186.1 ± 3.1[d]
40% ethanol fraction	33.2 ± 0.9[a]	37.1 ± 0.8[a]	33.9 ± 1.9[a]	63.4 ± 3.2[c]	56.2 ± 1.5[b]
70% ethanol fraction	77.2 ± 3.7[a]	105.1 ± 6.9[b]	97.4 ± 5.1[b]	132.4 ± 8.4[c]	145.0 ± 4.6[c]
100% ethanol fraction	4.0 ± 0.2[b]	3.1 ± 0.1[a]	5.1 ± 0.4[c]	4.5 ± 0.1[b]	6.4 ± 0.1[d]

[1]Reported as mM Trolox activity equivalent (TEAC)/100 mg FW.
[2] Mean ± standard deviation results of triplicate sample analysis.
[a-d]Mean values in the same row followed by a common letter were not statistically different ($p < 0.05$) by Tukey's HSD multiple range test between the varieties.

The ABTS radical scavenging results for EFW extracts ranged from 131.4-225.9 TEAC/100 mg (Aurora and Tundra, respectively) with a mean of 173.8. ABTS results for varietal EFW extracts closely mirrored those for TPCI of Tundra>Indigo Gem>Blizzard>Honey Bee>Aurora with the exception of the Honey Bee/Blizzard inversion in the latter (Table 4.16). It was hypothesized that ABTS results would mirror varietal anthocyanin content, however, this pattern was only observed for Aurora (i.e. the lowest in both cases; Tables 4.14 and 4.16). Based on these results, it is postulated that anthocyanin structure and the concentrations/compound structures of other phenolic subclasses play an important role in the overall ABTS RS ability of extracts.

These results are much higher than a literature report of 9.55 TEAC/100 g FW for an unidentified haskap variety grown in Alberta (Bakowska-Barzcak et al., 2007). These results are similar to those reported in literature for other fruits of: (a) 159.8-177.1 TEAC/100 mg FW (mean 168.5) for EFW extracts of Martin and Pembina saskatoon berry (Ribeiro de Souza et al., 2019); and (b) higher than 122.8 TEAC/100 mg FW for an EFW chokecherry extract (Green, 2007). Differences in results can be explained by variations in analytical methods (i.e. reaction time and temperature), phenolic extraction technique (e.g. solvent), and sample phenolic content, which is dependent on variety, environmental growth conditions, and geographical origin.

The ABTS radical scavenging results for PR extracts ranged from 98.7-186.1 TEAC/100 mg FW with a mean of 132.0, and followed the same varietal pattern observed for EFW extracts. On average, PR extracts showed 75.5% of the RS ability of the EFW extracts, which was lower than the values observed (i.e. PR *vs*. EFW) for TPC (81-91%; Table 4.5) and TPCI (86-98%; Tables 4.6-7). The difference between ABTS RS for the EFW and PR extracts may be explained by the elution of ascorbic acid (i.e. water and 20% ethanol fractions), some hydroxybenzoic acids, and flavanols during the preparation of the latter (i.e. water treatment prior to phenolic elution with 100% ethanol). Additionally, this indicates that the majority of the radical scavenging abilities of these extracts is a result of their phenolic content.

With respect to phenolic fractions, ABTS RS results followed the pattern of: 70%>40%>100% ethanol. These results can be explained by the relationship between fraction phenolic concentration and free radical scavenging, that is, the majority of phenolics were eluted

employing 70% ethanol. Analytical data was gathered for the water and 20% fractions, however, the results were low (TEAC values <1.5) and showed poor replication.

4.4.2 DPPH (2,2-diphenyl-1-picrylhydrazyl) Radical Scavenging Assay

The DPPH free radical scavenging assay results were determined for EFW and PR extracts, and 40, 70, and 100% ethanol phenolic fractions. Results are expressed as $1/IC_{50}$ (1/100 mg of sample weight for 50% DPPH radical inhibition) and are reported in Table 4.17.

Table 4.17 Mean and standard deviation for DPPH assay results of extracts (EFW and PR) and selected phenolic fractions of Aurora, Blizzard, Honey Bee, Indigo Gem, and Tundra haskap varieties.[1,2]

Extract or Fraction	Variety				
	Aurora	Blizzard	Honey Bee	Indigo Gem	Tundra
EFW extract	23.7 ± 1.0[a]	24.8 ± 0.7[a]	23.6 ± 0.4[a]	31.3 ± 0.8[b]	32.7 ± 1.3[b]
PR extract	15.5 ± 0.6[a]	18.9 ± 0.3[b]	17.1 ± 0.8[a]	22.4 ± 0.7[c]	26.9 ± 0.4[d]
40% ethanol fraction	7.2 ± 0.3[a]	9.1 ± 0.6[b]	7.6 ± 0.7[a]	12.3 ± 0.2[c]	9.4 ± 0.6[b]
70% ethanol fraction	8.8 ± 0.1[a]	13.4 ± 0.7[b]	10.3 ± 0.6[a]	13.2 ± 1.0[b]	14.8 ± 1.3[b]
100% ethanol fraction	0.8 ± <0.1[a]	0.8 ± <0.1[a]	1.1 ± <0.1[b]	1.1 ± <0.1[b]	1.3 ± <0.1[c]

[1]Reported as $1/IC_{50}$ (1/100 mg FW sample for 50% DPPH radical inhibition).
[2] Mean ± standard deviation results of triplicate sample analysis.
[a-d]Mean values in the same row followed by a common letter were not statistically different ($p<0.05$) by Tukey's HSD multiple range test between the varieties.

EFW extract $1/IC_{50}$ results ranged from 23.6-32.7 (Honey Bee and Tundra, respectively) with a mean of 27.2. These results were not as closely correlated to TPCI as in the ABTS assay.

The lowest scavenging values were found for Aurora, Blizzard, and Honey Bee (not significantly different), and the highest for Indigo Gem and Tundra (not significantly different). The results of this study are higher than literature reports for Borealis, Indigo Gem, and Tundra haskaps with $1/IC_{50}$ results ranging from 12.8-17.2 with a mean of 15.2 (Rupasinghe et al., 2012). These results are also higher than those reported for a selection of saskatoon berry varieties (Martin, Northline, and Pembina) with $1/IC_{50}$ values of 12.1-23.1 and a mean of 16.6 (Ribeiro de Souza et al., 2019).

PR extract $1/IC_{50}$ results ranged from 15.5-26.9 with a mean of 27.2. These results followed the same varietal pattern observed for TPCI and ABTS results of: Tundra>Indigo Gem>Blizzard>Honey Bee>Aurora. On average, these PR extract values were 73.0% of the EFW $1/IC_{50}$ values and also showed more significant differences between varieties than EFW extracts. The most likely explanation for these differences is due to the nonphenolic components (e.g. ascorbic acid, minerals) which can affect/interfere with the DPPH scavenging assay.

DPPH results for phenolic fractions followed the pattern of 70%>40%>100% ethanol. However, the 40 and 70% fraction results showed more similar scavenging abilities (for some varieties) than would be predicted based on phenolic content. As an example, the 40 and 70% fractions of Indigo Gem had similar $1/IC_{50}$ values of 12.3 and 13.2, respectively (Table 4.15). The reason for this is unclear, as these fractions were very low in nonphenolics (which appear to have affected EFW DPPH results), and a clear relationship between TPCI and DPPH scavenging abilities was seen in the PR extracts. Analysis of water and 20% fractions results mirrored ABTS, with very low scavenging ($1/IC_{50}$ values <0.3) and poor replication.

4.5 The Impact of Haskap Phenolics and Cyanidin-3-*O*-glucoside (C3G) on the Mediation of Cellular Stress

Based on previous findings from our *in vitro* free radical scavenging assays and that of literature examples, we hypothesized that haskap phenolics would have cellular stress mediation abilities (Wang and Eskiw, 2019; Buachan et al., 2014; Taormina and Mirisola, 2014; Pacholec et al., 2010). To test this hypothesis, we used an *in vitro* model of cultured dermal fibroblasts to assess changes in population doubling times and cell viability, protein levels, and mRNA levels (i.e. transcript levels), with a focus on Sirtuin-1 (SIRT1) which has been reported as a mechanistic target for other phenolics. Tundra variety haskaps were selected as their extracts had the highest

phenolic contents and *in vitro* RS abilities. Treatments included: ethanol:formic acid:water phenolic extract (EFW); phenolic rich extract (PR); 40% ethanol fraction (40%); and 100% ethanol fraction (100%). To investigate the role of the primary compound found in haskap phenolic extracts, treatments with cyanidin-3-*O*-glucoside (C3G) were also included.

Dermal (fibroblast) cells were selected due to the ease with which they can be obtained, and because they are a common *in vitro* model when experiments do not require emphasis on responses of specific organs (e.g. liver or kidney cells). Additionally, they can be found throughout the lining of the human gastrointestinal (GI) tract, making them an appropriate experimental model for nutraceutical treatments which would interact with these cell types after consumption and throughout the digestive process (Roulis and Flavell, 2016; Higuchi et al., 2015). A primary fibroblast line which was isolated directly from healthy human donors (2DD), and a line (NB1) that was immortalized with human telomerase (hTERT) were used. Immortalization involves a stable transfection with cDNA coding for the catalytic subunit hTERT (Bonifacio and Jarstfer, 2010). Continuous expression of hTERT prevents telomere shortening and blocks the onset of senescence, the stage at which cells enter permanent growth arrest and stop dividing (Lee et al., 2004). By protecting telomeres from damage (i.e. shortening), the cells can be prevented from entering senescence even after many divisions, allowing study of immortalized cells for many generations (Bonifacio and Jarstfer, 2010; Lee et al., 2004). For this reason, immortalized cell lines are used more frequently than primary cells for *in vitro* tissue culture experiments.

Tundra phenolic samples were first freeze-dried to prevent unknown impacts that could result from the presence of the extraction/fractionation solvent on cellular function. Phenolic samples were then resuspended in DMSO, a common treatment vehicle for *in vitro* cellular work, and added to Dulbecco's Modified Eagle Medium (DMEM) which was applied to the fibroblasts for 72 h. Untreated control cells were exposed to DMEM containing the same volume of DMSO as a vehicle control. This treatment period was selected, as short-term responses (e.g. 6-24 hours) address issues in primary response while our research questions focused on the longer term impacts on gene expression and cellular function. Treatment concentrations of 5.0 and 50.0 µg dry weight (DW)/mL DMEM were selected based on literature (García-Martínez et al., 2017; Jin et al., 2014; Zunino et al., 2010; McDougall et al., 2008) and on initial tests showing that 5.0 µg/mL EFW was the lowest concentration to show an impact on cellular growth profiles. For the second

concentration, 50.0 µg/mL was selected after results from higher concentration tests (from 50.0 to 200.0 µg/mL EFW) showed similar impacts on population doubling time (data not shown). The C3G concentrations selected for *in vitro* assays were 2.4 µg/mL and 23.7 µg/mL, which was based on the amount of C3G present in the Tundra EFW extract (~47.4% C3G; HPLC-PDA anthocyanin analysis; Table 4.14) for the 5.0 and 50.0 µg/mL treatments, respectively. Following the treatment period, cell counts and assessment of cell viability (using trypan blue dye) were performed along with extractions (e.g. protein and RNA) to assess protein level changes (via Western blot densitometry) and transcript level changes (via RT-qPCR).

The protein SIRT1 was selected as one of the focal points of this study, as literature strongly supports the relationship between SIRT1 and cellular stress mediation, health, and aging in mammals (Rahman and Islam, 2011; Maiese et al., 2008; Guarente, 2007; De Boer et al., 2006). Furthermore, published observations demonstrated that phenolics likely modulate SIRT1 function through interactions with upstream regulators of SIRT1 and not SIRT1 itself (Pacholec et al., 2010; Tang, 2010; Beher et al., 2009). SIRT1 modulates gene expression and numerous biological pathways by deacetylating a wide range of protein substrates, leading to either repression or enhancement of their function. For the purpose of this thesis, SIRT1 targets of interest were (a) nuclear factor kappa B (NF-κB), a transcription factor that promotes inflammatory responses and is a substrate for SIRT1 (Rahman and Islam, 2011; Maiese et al., 2008; Guarente, 2007); (b) mammalian target of rapamycin complexes 1 and 2 (mTORC1 and mTORC2) which have repressed signaling due to upstream SIRT1 activities, and are involved in metabolism and nutrient signaling, along with potential anticancer therapies (through repression) (Giovannini and Bianchi, 2017; Ghosh et al., 2010); and (c) nuclear factor erythroid 2 (Nrf2), which regulates antioxidant enzyme transcription triggered by oxidative stress or injury (Zhang et al., 2018). These targets/pathways are linked to cellular health through the mediation of cellular stress (i.e. inflammatory and antioxidant responses); in this case, the primary stressor of interest was oxidative stress caused by excess ROS.

Initial analyses focused on measurement of SIRT1 and Nrf2 protein levels and phosphorylation (which marks increased activity) of NF-κB p65 (phospho-NF-κB p65) and mTOR (phospho-mTOR) by Western blot. Since protein level changes observed via Western blot do not always coincide with changes in enzymatic activity, SIRT1 activity was also explored using a

SIRT1 assay kit which could measure levels of enzymatic activity through the deacetylation of a synthetic peptide attached to a fluorescent marker. The role of SIRT1 was further explored by performing knockdown of SIRT1 using lentiviral and/or siRNA mechanisms; if phenolic treatment mechanisms were dependent on cellular levels of this protein, they would no longer have an impact in its absence.

Due to our interest in stress mediation through anti-inflammatory and antioxidant activities, additional experiments were performed employing RT-qPCR (Reverse-Transcriptase-quantitative PCR) to measure changes in mRNA levels. Targets for this analysis included antioxidant enzyme and pro-inflammatory cytokine transcripts. These experiments were selected with the goal of supporting data obtained by Western blot and/or identifying additional activities that may be occurring independent of the selected protein targets.

4.5.1 Effects of Tundra Haskap Phenolics and C3G on Population Growth and Viability

After 72 h treatment with haskap phenolics and C3G, 2DD and NB1 hTERT fibroblasts were counted and population doubling times were calculated. This was used as an initial assessment of these haskap phenolic (and C3G) treatments, because changes (i.e. increases) in population doubling time can indicate an extension in lifespan due to slowed growth/cell divisions, which has been observed when SIRT1 is overexpressed in model organisms (Kaeberlein, 2010; Rogina and Helfand, 2004). Therefore, increases in population doubling times could indicate impacts in the pathways of interest for this project along with general improvements in metabolic efficiency and cellular recycling/reuse of materials (i.e. autophagy), justifying more extensive experiments related to SIRT1 and its activities (Gillespie et al., 2016). In addition to cell counts, Trypan blue dye was used to identify deceased cells and percent cell survival was calculated to determine if any treatment led to increased cell death. Population doubling times for 2DD and NB1 hTERT fibroblasts after 72 h Tundra variety haskap phenolic treatments and C3G are shown in Figure 4.17A followed by percent cell survival in Figure 4.17B.
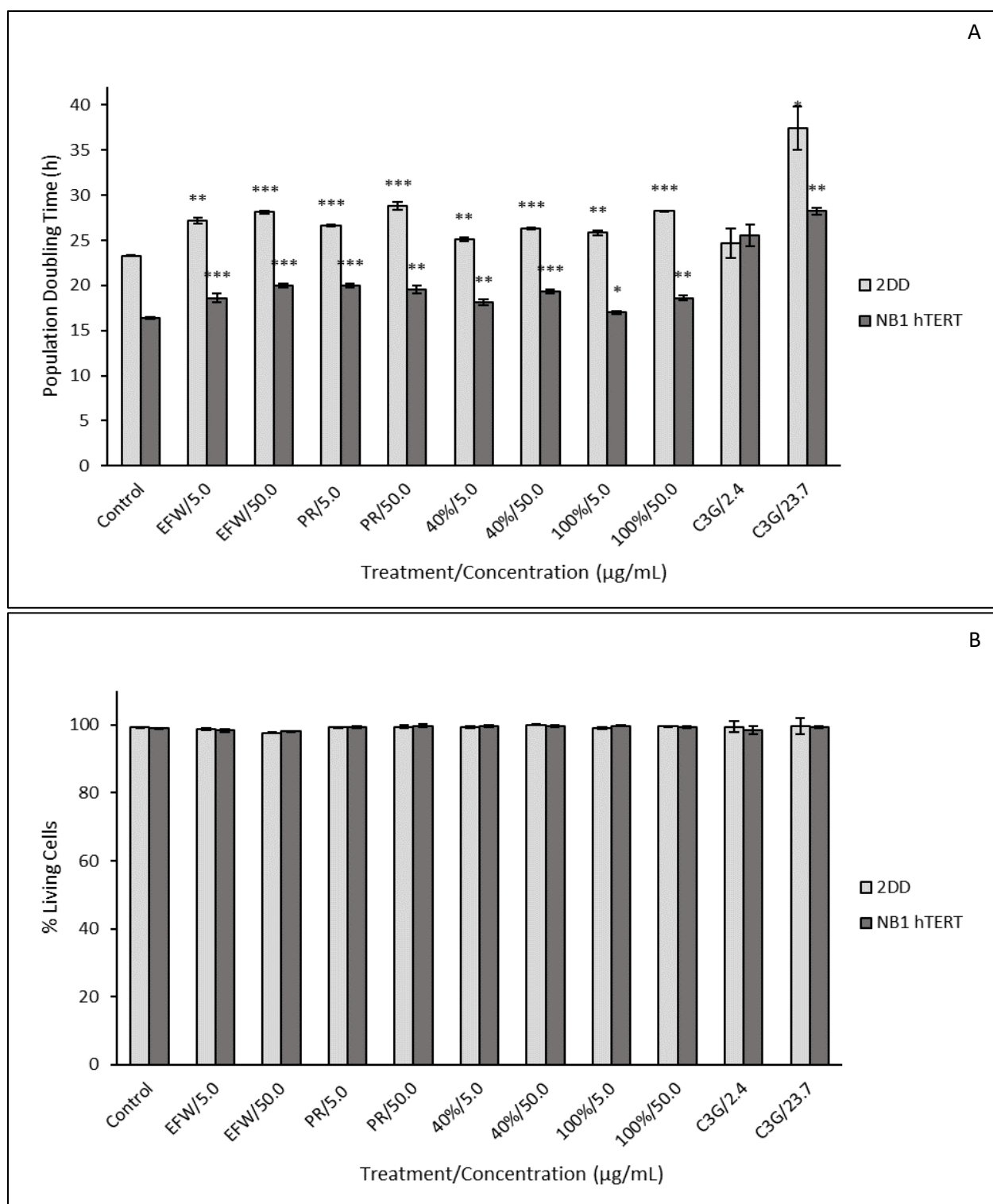
Figure 4.17 Population doubling times (A) and cell survival (B) for 2DD and NB1 hTERT fibroblasts after 72 h treatment with Tundra variety haskap phenolic extracts and C3G. Treatment abbreviations: EFW, ethanol:formic acid:water extract; PR, phenolic rich extract; 40%, 40% ethanol fraction; 100%, 100% ethanol fraction; C3G, cyanidin-3-*O*-glucoside. *p<0.10, **p<0.05, ***p<0.01

Population doubling times increased significantly ($p<0.10$) for both 2DD and NB1 hTERT fibroblasts compared to untreated control cells for all but one of the phenolic treatments. For 2DDs, increases in population doubling time ranged from 1.4-14.2 h (minimum and maximum values for C3G at 2.4 and 23.7 µg/mL, respectively) with a mean 4.3 h greater than the untreated control (Figure 4.17A). The only treatment without a significant increase ($p<0.10$) was C3G at 2.4 µg/mL (1.4 h increase; Figure 4.17A). All other treatments had population doubling time increases >1.8 h. The 2DDs showed no significant changes ($p<0.10$) in percent cell survival (i.e. viability) after phenolic treatments (Figure 4.17B).

NB1 hTERT fibroblasts also showed significant increases ($p<0.10$) in population doubling times for all treatments except C3G at 2.4 µg/mL (0.6 h increase; Figure 4.17A). Increases ranged from 0.6-11.8 h (minimum and maximum values for C3G at 2.4 and 23.7 µg/mL, respectively) with a mean 4.1 h greater than the untreated control (Figure 4.17A). In addition, NB1 hTERT fibroblasts showed no significant changes ($p<0.10$) in percent cell survival (i.e. viability) after phenolic treatments (Figure 4.17B). In both cell lines, the only treatment which did not increase population doubling times was C3G at 2.4 µg/mL, which is likely due to its concentration which was less than half of the lowest concentration (5.0 µg/mL) used for the other treatments.

These results are consistent with previous *in vitro* studies using plant phenolics including: (a) 10 and 100 µg/mL treatments of a pummelo fruit extract (*Citrus maxima* Merr.) which lengthened population doubling times by ~2 and ~4 h, respectively, for treatments that lasted 40 days (increases were first seen at 15 days) (Buachan et al., 2014); and (b) 50-100 µM treatments of avenanthramide C, an oat phenolic, increased population doubling times >5 h for 2DD fibroblasts after 48 h and no increase in cell death was observed (Wang and Eskiw, 2019). Buachan and colleagues (2014) did not observe increased population doubling time until after 15 days of treatment which could be explained by their method of extraction which involved pressing the fruit then filtering and freeze-drying the resulting juice. This juice would likely contain high levels of carbohydrates and organic acids, leading to relatively low concentrations of phenolics in the freeze-dried treatments. A contradicting report by Caprioli et al. (2016) in which human fibroblasts were treated with wild haskap (kamtschatika variety) phenolic extracts at concentrations of 50-200 µg/mL for 12-72 h, showed no changes in cell proliferation. Possible reasons for these observations

include the different haskap variety and phenolic extraction method (water-extracted), which could lead to differences in phenolic composition of the applied treatments.

Extensions in population doubling time *in vitro* can be an indicator of nutraceutical potential through the action of SIRT1 as seen with caloric restriction and phenolics such as resveratrol (Gillespie, et al. 2016; Taormina and Mirisola, 2014; Azorín-Ortuño et al., 2012; Kaeberlein, 2010). These initial results justified the pursuit of haskap phenolic activities *in vitro,* along with the focus on SIRT1 for mechanistic purposes due its importance in aging/lifespan determination.

4.5.2 Effects of Tundra Haskap Phenolics and C3G on SIRT1 and Related Proteins

We hypothesized that haskap phenolics would increase the levels and function of proteins that promote cellular health and mediate cellular stress. To investigate this, we performed semi-quantitative western blotting to evaluate levels of protein or phosphorylation of the following: (a) SIRT1, a protein deacetylase with roles in cellular health such as anti-inflammatory activities (De Boer et al., 2006); (b) phospho-NF-κB p65, the active (phosphorylated) p65 subunit of NF-κB (substrate of SIRT1) involved in pro-inflammatory signaling (Rahman and Islam, 2011; Maiese et al., 2008; Guarente, 2007); (c) phospho-mTOR, the active (phosphorylated) subunit of the mTORC1 and mTORC2 protein complexes (downregulated by SIRT1) for regulation of cellular proliferation (Giovannini and Bianchi, 2017); and (d) Nrf2, a cofactor (upregulated by SIRT1) which modulates the transcription of antioxidant enzymes (Zhang et al., 2018).

It is essential to ensure that equal protein concentrations are loaded in western blot assays. To ensure this, the total protein in each cellular extract was quantified using a NanoDrop™, and this measurement was used to dilute the extracts equally prior to loading. Secondly, β-actin was used as a load control. This is required to ensure that protein quantification was accurate and that equal volumes of protein extract were loaded onto the gels. Semi-quantitative results were then determined by normalizing densitometry to the β-actin results. Representative Western blots and densitometry results for phospho-NF-κB p65, phospho-mTOR, Nrf2, SIRT1, and β-actin in 2DDs are shown in Figure 4.18, followed by NB1 hTERT results in Figure 4.19. Western blot results for both cell lines will be discussed following Figure 4.19.
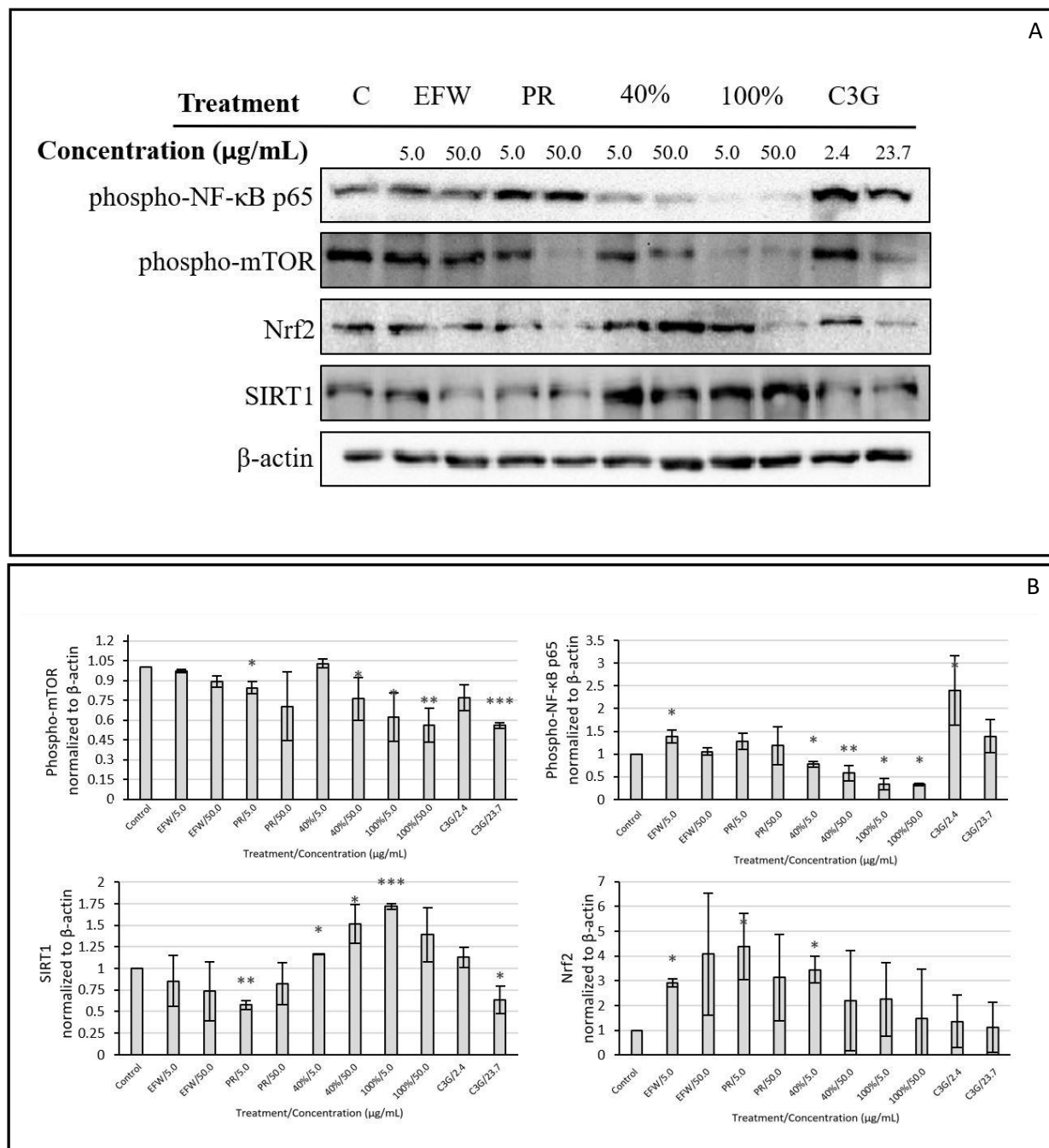
Figure 4.18 Representative Western blots (A) and normalized densitometry results (B) for protein levels of phospho-NF-κB p65, phospho-mTOR, Nrf2, SIRT1, and β-actin in 2DD whole cell protein lysates after 72 h treatment with Tundra variety haskap phenolic extracts and C3G. Treatment abbreviations: EFW, ethanol:formic acid:water extract; PR, phenolic rich extract; 40%, 40% ethanol fraction; 100%, 100% ethanol fraction; C3G, cyanidin-3-O-glucoside. *p<0.10, **p<0.05, ***p<0.01

Figure 4.19 Representative Western blots (A) and normalized densitometry results (B) for protein levels of phospho-NF-κB p65, phospho-mTOR, Nrf2, SIRT1, and β-actin in NB1 hTERT whole cell protein lysates after 72 h treatment with Tundra variety haskap phenolic extracts and C3G. Treatment abbreviations: EFW, ethanol:formic acid:water extract; PR, phenolic rich extract; 40%, 40% ethanol fraction; 100%, 100% ethanol fraction; C3G, cyanidin-3-*O*-glucoside. *p<0.10, **p<0.05
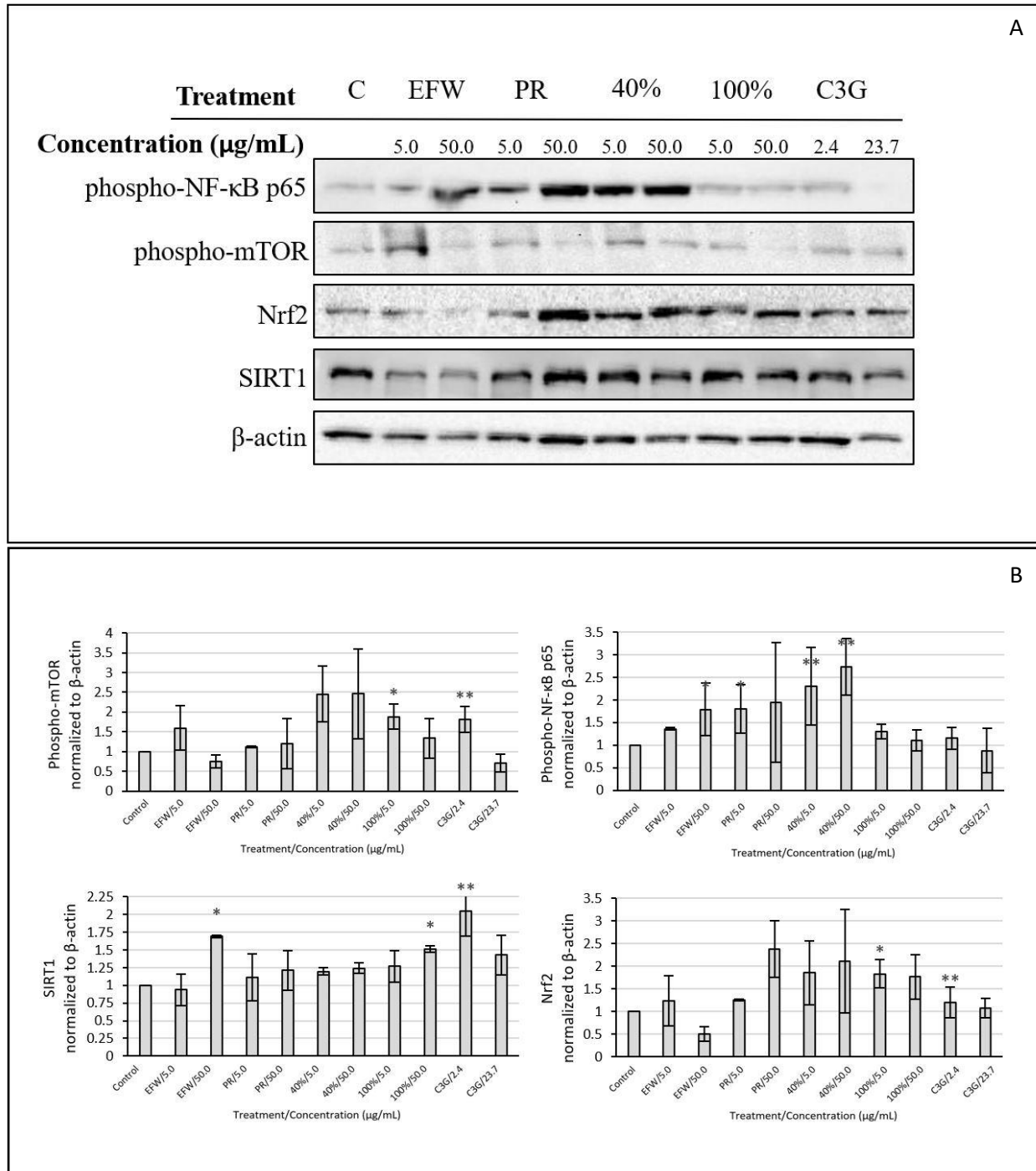
Normalized SIRT1 ratios (Figure 4.18B) for 2DD protein extracts demonstrated a range of changes in protein levels with significant increases ($p < 0.10$) seen for 40% at 5.0 and 50.0 µg/mL, and 100% at 5.0 µg/mL with ratios of 1.2, 1.5, and 1.7, respectively. Other results for 2DD fibroblasts (Figures 4.18A and B) included: (a) both fraction treatments (40 and 100%) decreased phosphorylation of NF-κB p65 levels significantly ($p < 0.10$) with an average ratio of 0.7 for the 40% and 0.3 for the 100% treatments; (b) mTOR phosphorylation was decreased for most treatments and was significantly lower in response to PR at 5.0 µg/mL, 40% at 50.0 µg/mL, 100% at 5.0 and 50.0 µg/mL, and C3G at 23.7 µg/mL (ratios of 0.6-0.8); and (c) Nrf2 levels showed significant increases for EFW, PR, and 40% at 5.0 µg/mL. Western blot results for 2DD fibroblasts showed the most changes in protein levels in response to fraction treatments (40 and 100%), specifically with increases in SIRT1 and concomitant decreases in phosphorylation of mTOR and the pro-inflammatory NF-κB p65. These *in vitro* results demonstrated that phenolic fractions from the Tundra variety influenced levels of SIRT1 and related proteins (or active protein forms) in primary 2DD fibroblasts.

NB1 hTERT fibroblast results (Figures 4.19A and B) corresponded with 2DD results for SIRT1, with increased levels (mean ratio of 1.4) for all but one treatment (EFW at 5.0 µg/mL), and significant increases ($p < 0.10$) for three treatments: 100% at 50.0 µg/mL, EFW at 50.0 µg/mL, and C3G at 2.4 µg/mL (ratios of 1.5, 1.6, and 2.1, respectively). NB1 hTERT fibroblasts showed significant increases in phosphorylation of NF-κB p65 for EFW at 50.0 µg/mL, PR at 5.0 µg/mL, and 40% at 5.0 and 50.0 µg/mL, with ratios of 1.8-2.7, while other treatments resulted in decreased levels of NF-κB p65 phosphorylation. Significant increases in phosphorylation of mTOR were observed for C3G at 2.4 µg/mL and 100% at 5.0 µg/mL with ratios of 1.8 and 1.9, with parallel increases ($p < 0.10$) in Nrf2 levels for the same two treatments. Overall, NB1 hTERT fibroblasts showed increases in SIRT1 protein levels and phosphorylation of NF-κB p65, with few changes in Nrf2 or phosphorylation of mTOR. Increases in phosphorylation of NF-κB p65 were unexpected in comparison to 2DD results, however, phosphorylation of NF-κB is independent of SIRT1 deacetylation (Rahman and Islam, 2011; Guarente, 2007).

Unanticipated differences in protein level changes were observed between primary and immortalized fibroblast cell lines. Although population doubling times increased for both, SIRT1 protein level changes in response to phenolic extracts were divergent. Western blot data showed

that 2DDs were more responsive to fraction treatments and more significant changes were observed, however, NB1s were responsive to a wider range of treatments (Figures 4.18 and 4.19). The immortalization of NB1s may have led to different experimental results after exposure to haskap phenolics, however, further tests would need to be performed to confirm this hypothesis. Literature reports have shown that fibroblasts immortalized using hTERT have differential gene expression in later passages (~passage 50) including changes in microRNA (miRNA) expression such as: (a) an up to ten fold increase in miR146 which can boost inflammatory responses and could potentially lead to altered responses related to inflammatory markers (e.g. phosphorylation of NF-κB p65) which is supported by the results observed; and (b) the oncogenic miR155 showed three fold increases, which could lead to cancer-like gene expression which is often unpredictable or inconsistent in comparison to normal cells (Bonifacio and Jarstfer, 2010). These genetic changes could be contributing factors to the results seen for NB1 hTERT fibroblasts in this work.

Results for 2DD fibroblasts aligned with the hypothesis that haskap phenolics would be able to stimulate cellular pathways involved in stress mediation and lifespan regulation. 2DD fibroblasts showed increases in SIRT1 and Nrf2 levels with concomitant decreases in phosphorylation of mTOR and NF-κB p65 in response to phenolic treatments. The observed 2DD fibroblast results are supported by previous reports employing similar concentrations of phenolic compounds. As examples, phenolics that have been reported to increase SIRT1 protein levels *in vitro* include catechins, delphinin-3-*O*-glucoside, ferulic acid, malvidin, quercetin, and resveratrol, at a wide range of concentrations (~5-200 µM) (Giovannini and Bianchi, 2017; Forbes-Hernández et al., 2014; Jin et al., 2014; Chung et al., 2010). mTOR activity has been reported as being downregulated following phenolic treatments, with resveratrol as a popular focus. One such study showed that resveratrol (10-50 µM) treatments led to significant decreases of mTOR activity in HEK293 kidney cells (Park et al., 2019). Active NF-κB levels have also been reported as being downregulated after phenolic treatments in response to 10 mg intravenous haskap phenolic treatments of lipo-polysaccharide-injected mice where eye tissues were tested (Jin et al., 2006). Nrf2 investigations have demonstrated increased protein levels after treatment with apple pomace phenolic extracts (mouse liver cells), olive oil phenolic extracts (mice *in vivo*), and quercetin and resveratrol (HepG2 cells) (Sharma et al., 2016; Bayram et al., 2012; Suchankova et al., 2009). These examples demonstrate parallel observations seen with haskap phenolic extracts and fractions treatments, and the selected pathways of interest.

126

To the best of the author's knowledge, only one recent study has linked haskap phenolics specifically to SIRT1 *in vitro*. Liu et al. (2019) showed that treatments (20-80 µg/mL) with wild Chinese haskap phenolics (80% ethanol:0.1% HCl (v:v) extract) could ameliorate the observed decrease in SIRT1 levels in response to oxidized low-density lipoprotein (ox-LDL) exposure in RAW 264.7 mouse macrophages. Our observations differed in that whole haskap extracts were mostly ineffective. However, different haskap varieties, cell lines, and treatment methods (Liu and colleagues used ox-LDL to induce stress prior to treatment) were employed in comparison to this research. To test the efficacy of the phenolics from these Canadian haskap varieties (e.g. Tundra) under similar conditions as Liu and colleagues (i.e. cells under stress), a stressor such as TNF-α could be introduced during treatment.

The most significant impacts observed in this work were for the Tundra haskap 40% and 100% phenolic fractions. These fractions had very different phenolic compositions as shown by HPLC-PDA and HPLC-MS/MS results (Section 4.3). The 40% fraction was comprised of 76.8% anthocyanins, 12.1% flavanols, and <6% for each other subclass (Section 4.3.2.3), while the 100% fraction was primarily flavanols (46.2%) and flavonols (35.7%), with only 3% anthocyanins (Section 4.3.2.3). Despite these differences in composition, both fractions were more effective in increasing SIRT1 protein levels (and decreasing phosphorylation of NF-κB p65 and mTOR) than the whole extracts.

Our initial hypothesis was that anthocyanins would be responsible for haskap phenolic impacts *in vitro* due to their high concentration in this fruit (276.2-501.3 mg/100 g FW; Section 4.3.4). Results for the 40% fraction supported this theory, as this treatment was anthocyanin rich and more significant changes (via Western blot) were associated with this treatment than others with lower anthocyanin concentrations. However, treatments of C3G (the major anthocyanin in haskaps), did not show equivalent responses to the fractions (via Western blot), indicating that C3G is not independently responsible for the observed cellular impacts. This conclusion is supported by the results for the 100% fraction, which had very low levels of anthocyanins, and showed similar changes in protein levels to the 40% fraction, meaning that diverse phenolic structures (e.g. flavonols) and synergistic effects (e.g. anthocyanins and flavonols) could result in SIRT1 level increases.

The ability to increase SIRT1 levels and decrease phosphorylation of mTOR and NF-κB p65 *in vitro* demonstrates that select haskap phenolic fractions can modulate cellular stress responses and supports their potential as nutraceutical agents. Based on these results, 2DD fibroblasts were selected as the cell line of interest for SIRT1 activity and mRNA transcript level analysis (RT-qPCR). The relationship between phenolic structures and their *in vitro* effects will be further discussed in Section 4.6.

4.5.3 Effects of Tundra Haskap Phenolics and C3G on Fibroblasts with Knockdown of SIRT1

To further investigate the role of SIRT1 and its level of importance in haskap phenolic activities *in vitro,* SIRT1 knockdown was used in both 2DD and NB1 hTERT cells. If SIRT1 is one of the key enzymes in mediating the impact of haskap phenolics, then removal or greatly reduced levels should eliminate downstream effects. One method of *in vitro* knockdown is a lentiviral transduction which results in permanent gene expression of short hairpin RNAs (shRNAs). The expression of the shRNA will be passed on through cell division and allow long term studies of gene knockdown through multiple generations (Yang et al., 2017). Studies often include multiple cell lines with shRNA sequences targeted at different regions of the mRNA to provide evidence that experimental results are not a byproduct of the lentiviral transduction. An alternate knockdown technique involves the silencing power of small interfering RNAs (siRNAs) which can temporarily be introduced into a cell (transient transfection), leading to short-term loss of gene expression. This is a rapid method that leads to knockdown within hours of siRNA introduction (Yang et al., 2017). siRNA transfections are performed by forcing the cells to take in siRNAs which also target mRNA transcripts for degradation, preventing translation (Yang et al., 2017). Commercial siRNA mixtures typically contain multiple target sequences mixed into one treatment to increase efficiency of the knockdown. Both forms of knockdown were used to target SIRT1 in this research.

4.5.3.1 NB1 hTERT Lentiviral SIRT1 Knockdowns

NB1 hTERT lentiviral SIRT1 knockdown cell lines were obtained as a kind gift from Dr. Franco Vizeacoumar (Saskatchewan Cancer Agency) and were used to determine whether the

observed protein level changes in Western blots (e.g. changes in phosphorylation of NF-κB p65) were dependent on SIRT1. Cell lines included a scramble control (no knockdown of SIRT1) alongside three hairpins targeted at different regions of the SIRT1 mRNA transcript: hairpin 1 (HP1), hairpin 2 (HP2), and a combination (HP1/2). Population doubling times for the HP2 knockdown cells are shown in Figure 4.20A followed by viability (percent cell survival) in Figure 4.20B. Representative Western blots and densitometry results for phospho-NF-κB p65 and β-actin in HP2s are shown in Figures 4.21A and B, respectively.
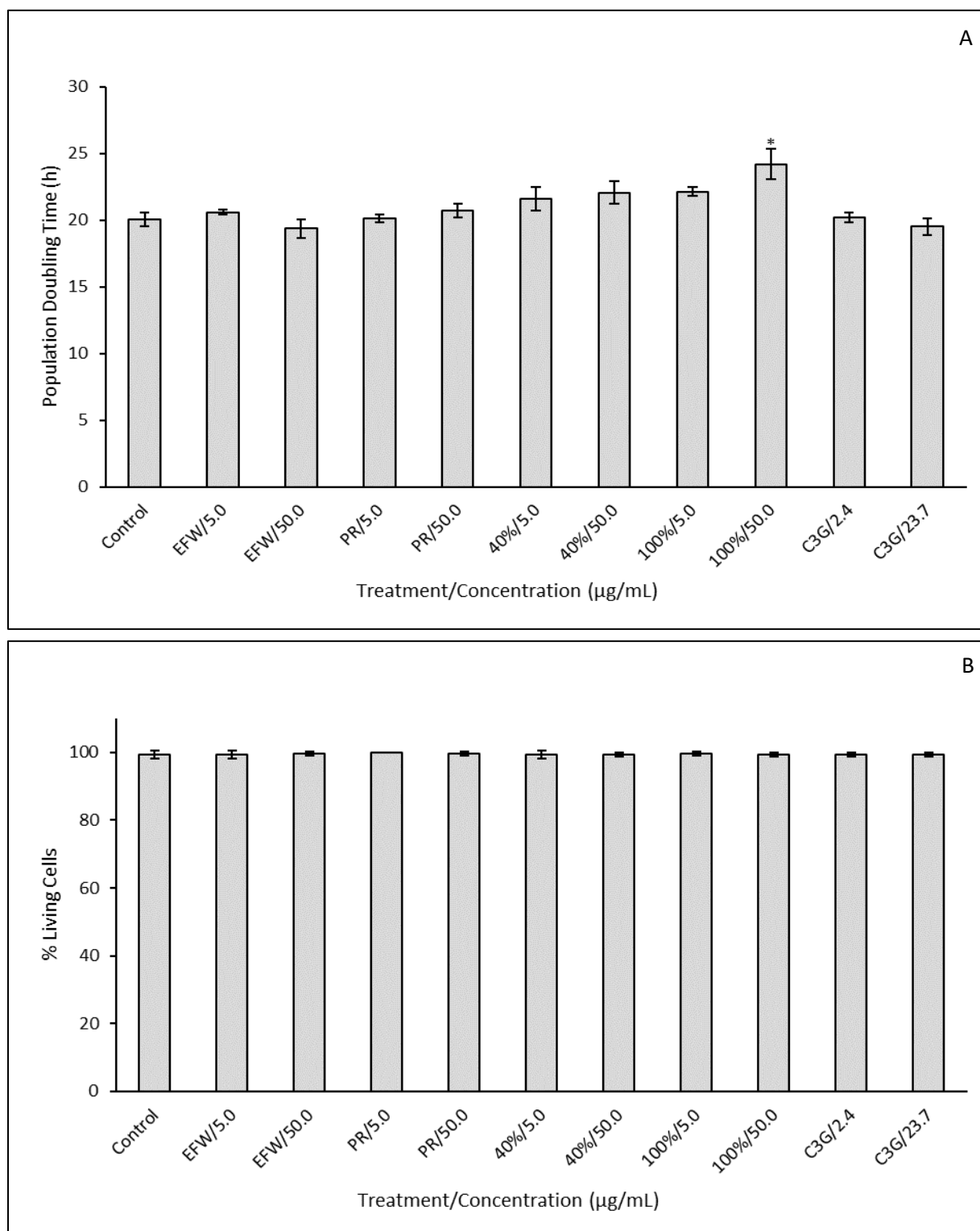
Figure 4.20 Population doubling times (A) and cell survival (B) of lentiviral NB1 hTERT HP2 SIRT1 knockdown after 72 h treatment with Tundra variety haskap phenolic extracts and C3G. Treatment abbreviations: EFW, ethanol:formic acid:water extract; PR, phenolic rich extract; 40%, 40% ethanol fraction; 100%, 100% ethanol fraction; C3G, cyanidin-3-*O*-glucoside. *p<0.10

130
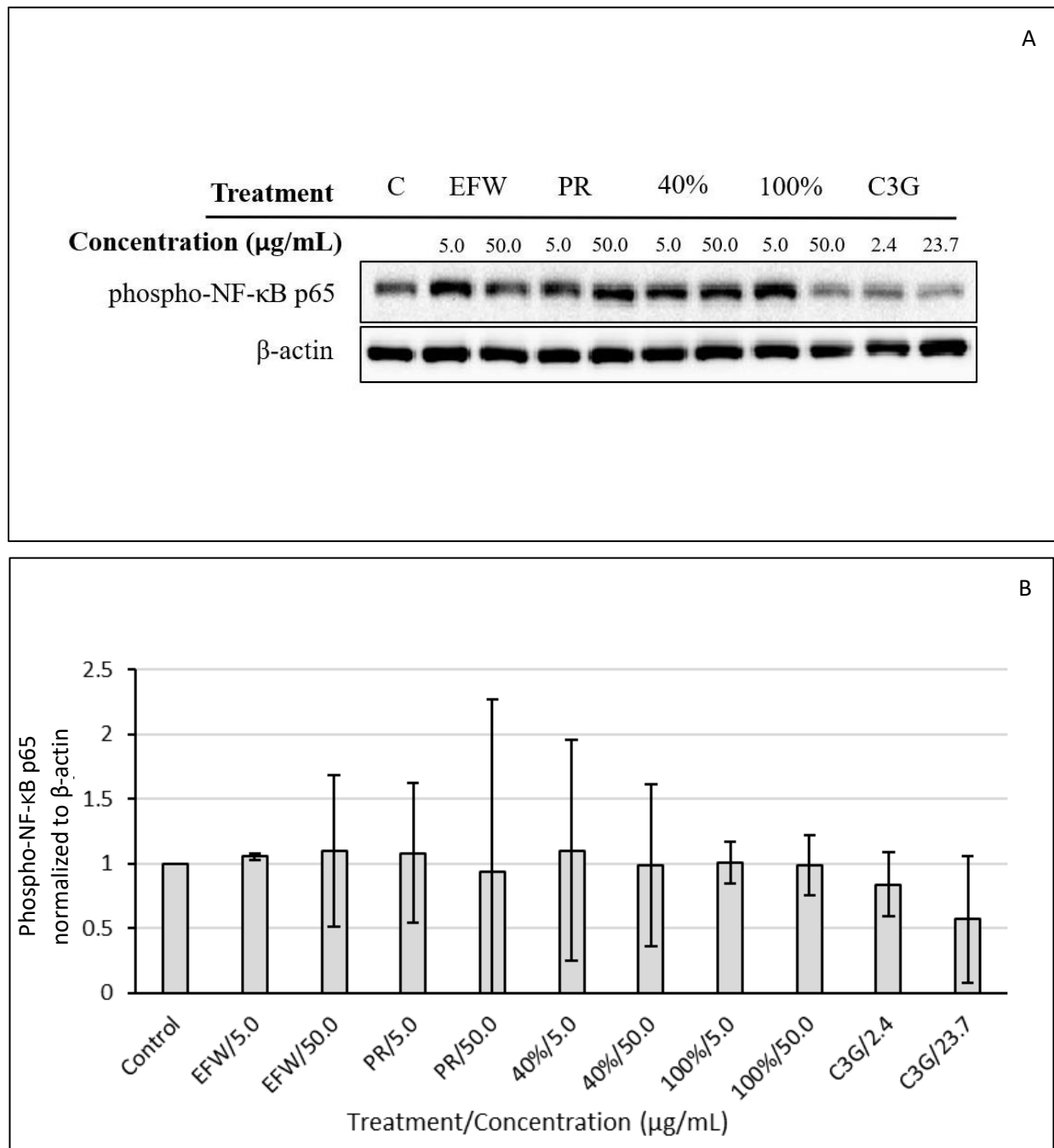
Figure 4.21 Representative Western blots (A) and densitometry results (B) for phospho-NF-κB p65 and β-actin in whole cell protein lysates of NB1 hTERT fibroblasts with HP2 SIRT1 knockdown after 72 h treatment with Tundra variety haskap phenolic extracts and C3G. Treatment abbreviations: EFW, ethanol:formic acid:water extract; PR, phenolic rich extract; 40%, 40% ethanol fraction; 100%, 100% ethanol fraction; C3G, cyanidin-3-O-glucoside.

Changes in population doubling time (Figure 4.20A) for NB1 HP2 cells when compared to the untreated control varied with a mean increase of 1.0 h. These changes were not significant ($p<0.10$) except for 100% at 50.0 µg/mL (increase of 4.1 h) with all other treatments having increases <2.1 h. Cell survival (Figure 4.20B) was not significantly impacted ($p<0.10$) by haskap phenolic treatments.

Results for Western blotting of phospho-NF-κB p65 in NB1 HP2 cells (Figures 4.21A and B) did not show any significant changes ($p<0.10$). Previously, NB1 hTERT cells with normal levels of SIRT1 had shown increases in phosphorylation of NF-κB p65 (Figures 4.19A and B) with a mean ratio of 1.6 and four treatments showed significant increases (EFW at 50.0 µg/mL, PR at 5.0 µg/mL, and 40% at 5.0 and 50.0 µg/mL; Figure 4.19B). These *in vitro* results indicate that SIRT1 plays a significant role in the activity of Tundra haskap phenolics on NB1 hTERT cells. Similar results were seen for NB1 HP1/2 (data not shown), and NB1 HP1 did not successfully knockdown SIRT1 (data not shown) and was not included in further experiments. A discussion of SIRT1 knockdown results is presented in Section 4.5.3.3.

4.5.3.2 2DD Lentiviral SIRT1 Knockdowns

An attempt to grow 2DD lentiviral SIRT1 knockdown cell lines was also made, however, cells immediately displayed stressed phenotypes. These cells did not proliferate successfully and very quickly died or became senescent. These results were not unprecedented, as long-term knockdown of SIRT1 was expected to speed the cellular aging process, and this may be more extreme in primary cell lines (i.e. not immortalized). Other *in vitro* studies have shown similar results in mammalian cells such as in lentiviral SIRT1 knockdown mouse adipocytes (3T3L1), which displayed senescence and other characteristics of aging such as decreased expression of the mitochondria Complex 1 protein, one of the key complexes involved in basic metabolism via the electron transport chain (Lan et al., 2010). Although not investigated further and beyond the scope of this thesis, these observations further indicate the importance of SIRT1 function in primary cells and the aging process.

4.5.3.3 2DD siRNA SIRT1 Knockdowns

Following the death of the lentiviral knockdown cells, siRNA knockdown of SIRT1 was employed in 2DDs as it is a transient (short-term) transfection. The purpose of this experiment was to determine whether the presence/normal levels of SIRT1 was required for haskap phenolics to have an impact on normal fibroblasts. To test this, 2DD fibroblasts were transfected with SIRT1 siRNAs and then treated with haskap phenolics and C3G (Section 3.8.10). Due to the cost of the components needed for siRNA transfection, the 50.0 µg/mL concentration (23.7 µg/mL for C3G) was used for each treatment and one replicate was made. Whole cell protein lysates were harvested after the 72 h treatment period to be assessed by Western blot. A control scramble siRNA was also used to ensure that changes seen in SIRT1 knockdowns were not as a result of siRNA transfection. Representative Western blots for phospho-NF-κB p65, phospho-mTOR, SIRT1, Nrf2, and β-actin in 2DD siRNA knockdown cells are shown in Figure 4.22A followed by densitometry results in Figure 4.22B.
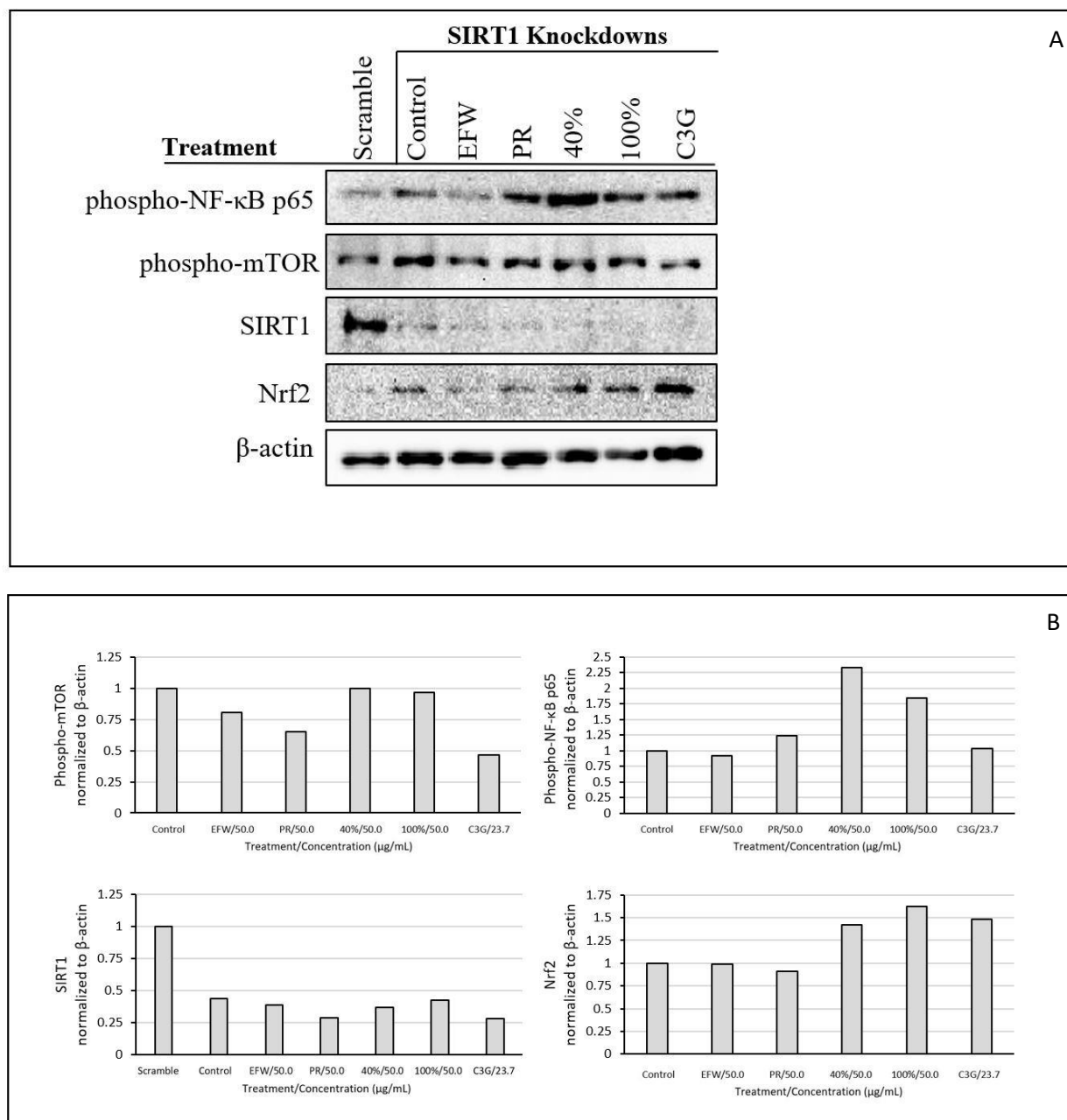
Figure 4.22 Representative Western blots (A) and normalized densitometry results (B) for protein levels of phospho-NF-κB p65, phospho-mTOR, SIRT1, Nrf2, and β-actin in whole cell protein lysates of 2DD fibroblasts with siRNA knockdown of SIRT1 after 72 h treatment with Tundra variety haskap phenolic extracts and C3G. Treatment abbreviations: EFW, ethanol:formic acid:water extract; PR, phenolic rich extract; 40%, 40% ethanol fraction; 100%, 100% ethanol fraction; C3G, cyanidin-3-*O*-glucoside.

Western blot results demonstrated the successful knockdown of SIRT1 (Figures 4.22A and B) as compared to the untreated scramble control siRNA. Densitometry results for the scramble control are only shown for SIRT1 (Figure 4.22B). The primary difference in response between SIRT1 knockdown (Figure 4.22) and SIRT1 normal cells (Figure 4.18) was seen for phospho-NF-κB p65. Phosphorylation of NF-κB p65 in cells with normal SIRT1 levels decreased significantly ($p < 0.10$) in response to both fraction treatments (40 and 100%) with ratios of 0.7 and 0.3, respectively, when compared to untreated control cells (Figure 4.18). Knockdown of SIRT1 reversed this trend, resulting in increased levels of phosphorylation for the 40 and 100% treatments (ratios of 2.3 and 1.8, respectively) (Figure 4.19B). In addition, decreases in mTOR phosphorylation occurred for PR at 50.0 µg/mL and C3G at 23.7 µg/mL, and increases in Nrf2 were seen for the 40%, 100%, and C3G treatments.

Western blot results and literature precedence led to the hypothesis that haskap phenolic treatments would not be effective following SIRT1 knockdown which was supported by results for 2DD (using siRNA) and NB1 hTERT (lentiviral) knockdown fibroblasts (based on changes in phosphorylation of NF-κB p65 seen by Western blot). Reports on the loss/alteration of cellular function due to *in vitro* plant phenolic treatment following knockdown of SIRT1 have been published including: (a) siRNA knockdown of SIRT1 in mouse myoblast (C2C12) cells negated the effects of 10 µM resveratrol, which prior to knockdown showed the ability to counteract antimycin A-induced ROS generation and cell death (Hori et al., 2013); and (b) after 24 h treatment of hydroxytyrosol (25-100 µM), an olive oil phenolic, rat vascular adventitial fibroblasts (VAFs) showed reduced levels of IL-1β and IL-6 in response to TNF-α stimulation; this reduction in pro-inflammatory cytokines was lost after siRNA knockdown of SIRT1 (Wang et al., 2017).

These results clearly show that SIRT1 activity was impacted by haskap phenolic extracts and fractions and also that haskap phenolic treatments require SIRT1 in order to change other protein levels (or active protein forms) within cells. It can be hypothesized that the mechanism(s) of action for Tundra haskap phenolic extracts and fractions are similar to those of other studied phenolics (e.g. resveratrol) which have been shown to work through SIRT1 in literature. Treatment-specific results (i.e. based on phenolic structure) will be discussed in Section 4.6.

4.5.4 Effects of Tundra Haskap Phenolics and C3G on 2DD SIRT1 Activity

To investigate changes in deacetylation activity of SIRT1 as a function of haskap phenolics, and also to test whether these compounds interact directly with SIRT1, a SIRT1 activity assay (Abcam, Cat #: ab156065) was selected. The assay employed a fluoro-substrate peptide which produces fluorescence after deacetylation by SIRT1. To prevent false positives caused by deacetylation activity of other proteins, trichostatin A, a selective histone deacetylase (HDAC) inhibitor, which SIRT1 is resistant to, was added to the reaction medium. The following experiments were performed to answer three different research questions: (a) the activity of recombinant SIRT1 (purified enzyme) was measured in the presence and absence of haskap phenolics and C3G to test whether they interact with SIRT1 directly; (b) SIRT1 activity in untreated whole cell lysates was measured in the presence and absence of haskap phenolics and C3G to investigate if it is activated through another cellular component independent of cellular metabolism; and (c) SIRT1 activity was measured in lysates of cells that were treated with haskap phenolics and C3G to assess changes in its activity during normal cellular metabolism (when SIRT1 levels were seen to increase via Western blot).

For all reactions, SIRT1 activity was assessed by comparing the fluorescence readings from untreated (i.e. DMSO-only as the control) to phenolic-treated reactions/lysates. Results were then normalized to the control sample values and were reported in arbitrary fluorescence units. Figure 4.23A shows SIRT1 activity results for recombinant SIRT1 in the presence of haskap phenolics and C3G (23.7 µg/mL), followed by SIRT1 activity in untreated 2DD whole cell protein lysates in the presence of haskap phenolics and C3G (Figure 4.23B), and SIRT1 activity in lysates of haskap phenolic and C3G-treated 2DDs (Figure 4.23C). The 50.0 µg/mL concentration was used for all phenolic treatments of cells (in DMEM). When phenolics were added directly to the fluorescence reaction, the final phenolic concentration was 50.0 µg/mL in each well. One biological replicate was used for each of these experiments.
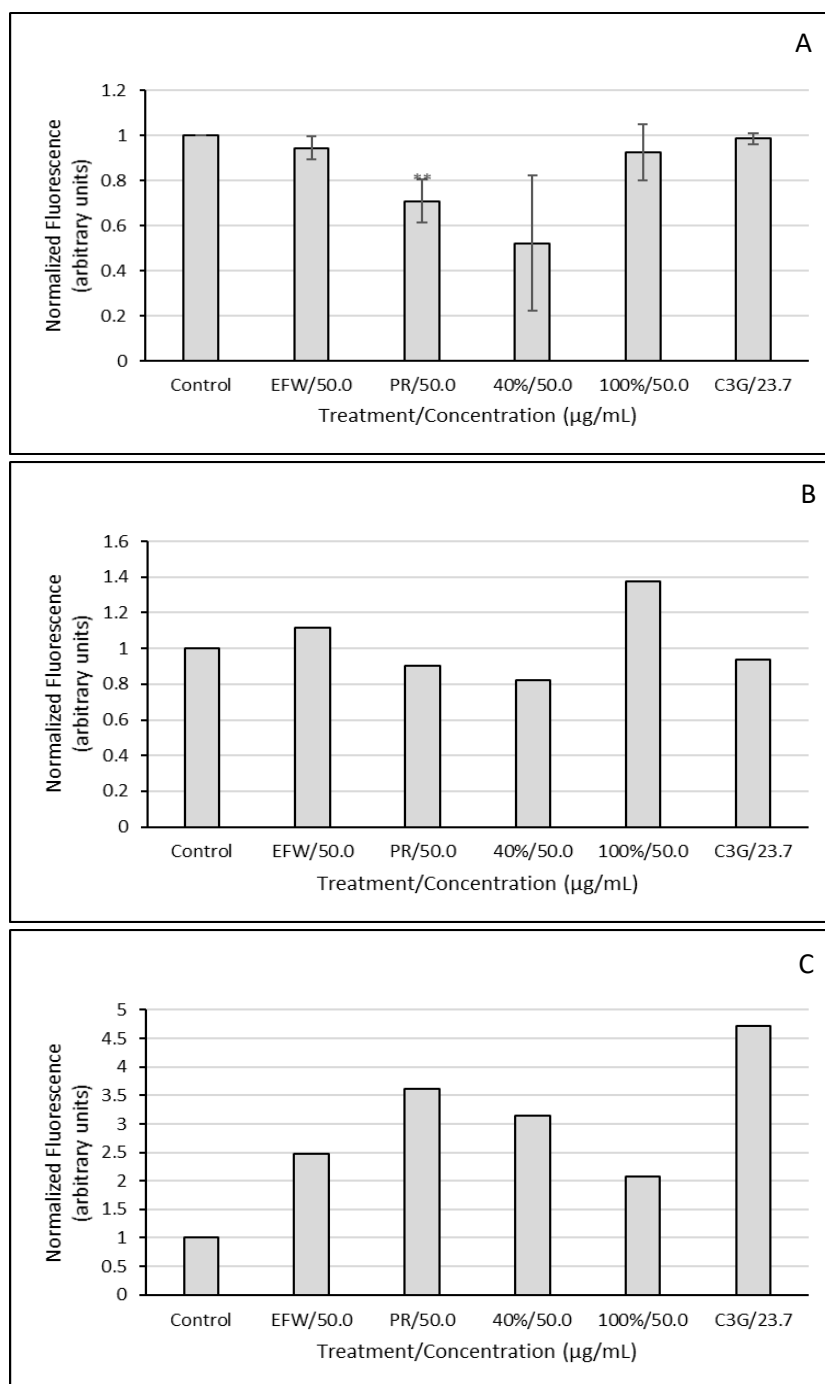
Figure 4.23 Recombinant SIRT1 activity in the presence of Tundra variety haskap phenolics and C3G (A), SIRT1 activity in untreated 2DD whole cell protein lysates in the presence of haskap phenolics and C3G (B), and SIRT1 activity in 2DD whole cell protein lysates after treatment with haskap phenolics and C3G (C). Treatment abbreviations: EFW, ethanol:formic acid:water extract; PR, phenolic rich extract; 40%, 40% ethanol fraction; 100%, 100% ethanol fraction; C3G, cyanidin-3-*O*-glucoside. **$p < 0.05$

Small decreases (including a significant decrease for PR at 50.0 µg/mL) in recombinant SIRT1 activity were observed after the addition of haskap phenolics to the reaction mixtures with normalized fluorescence ranging from 0.52-0.99 (where the control=1.0) and a mean of 0.82 (Figure 4.23A). If haskap phenolics could activate SIRT1 directly (in the absence of any other molecules/cellular materials), these reactions would have shown increases in activity for the treated reactions. The minor changes (decreases) observed do not support a direct activation mechanism of SIRT1 by haskap phenolics. After the addition of haskap phenolics to untreated 2DD cell lysates, normalized fluorescence had a mean of 1.04 (range of 0.82-1.38) for the five treatments (Figure 4.23B). This indicates that haskap phenolic activation of SIRT1 is both indirect and can only occur during more complex metabolic processes, since mixing the phenolics with cellular lysate did not increase SIRT1 activities.

These results are supported by studies for other plant phenolics, primarily resveratrol, which was initially implicated as a direct activator of SIRT1 (Borra et al., 2005). However, other literature results have reported that the observed direct activation was an artifact of an interaction between resveratrol and the fluoro-substrate used in the assay (Pacholec et al., 2010; Beher et al., 2009). When native SIRT1 substrates (e.g. p53) were tested, resveratrol did not promote direct deacetylation (Pacholec et al., 2010; Tang, 2010; Beher et al., 2009). This phenomenon was not observed in these experiments, as deacetylation activity of the fluoro-substrate by recombinant SIRT1 was not increased in the presence of haskap phenolics.

The final set of experiments measured changes in SIRT1 activity after haskap phenolic and C3G treatment of 2DDs. Results showed increases in SIRT1 activity associated with all phenolic treatments with a normalized fluorescence range of 2.08-4.72 and mean of 3.20 (Figure 4.23C). This data aligned with Western blot experimental results where SIRT1 protein levels were shown to increase, and phosphorylation of NF-κB p65 was shown to decrease for certain treatments. This also coincides with observed decreases in levels of pro-inflammatory cytokine transcripts regulated by NF-κB (by RT-qPCR; Section 4.5.5), which could result from increased SIRT1 activity. The primary study linking SIRT1 to haskap phenolics also reported increased activity, however their analysis was actually focused on protein level changes (Western blot) and did not contain further data on SIRT1 activity for comparison (Liu et al., 2019). As described previously, it is known that changes in protein levels are not always parallel with changes in activity. To the

best of the author's knowledge, no other literature sources have tested haskap phenolic activation of SIRT1 in this way.

These results match the increases in population doubling times that were seen for all treatments in initial testing and are in agreement with literature that plant phenolics, such as resveratrol, indirectly increase SIRT1 activity levels in cells (Chung et al., 2010; Kaeberlein, 2010). As such, haskap phenolics and C3G may be able to mediate cellular stress through the indirect activation of SIRT1 parallel to resveratrol (Pacholec et al., 2010; Tang, 2010; Beher et al., 2009). This assay showed that in addition to the increase in SIRT1 protein levels, there was an increase in its associated function, thus demonstrating a significant biological impact.

4.5.5 Effects of Tundra Haskap Phenolics and C3G on 2DD mRNA Levels

Due to our interest in stress mediation through anti-inflammatory and antioxidant activities, additional experiments were performed employing RT-qPCR (Reverse-Transcriptase-quantitative PCR) to measure changes in mRNA transcript levels. Transcript levels (mRNA) of antioxidant enzymes and pro-inflammatory cytokines in 2DD fibroblasts were assessed using RT-qPCR after 72 h treatment with haskap phenolics and C3G. Transcript levels do not always equate to changes at the protein level; however, previous data from the Eskiw laboratory shows consistent results with other treatments that the changes in transcript levels of these genes lead to changes in protein levels (Gillespie et al, 2015). Following RT-qPCR, the $\Delta\Delta$Ct method was used to calculate fold changes for treated *vs.* untreated cells. Fold change results are shown in Figure 4.24 for the following antioxidant enzymes: catalase (CAT; Figure 4.24A); glutathione peroxidase 1 (GPx1; Figure 4.24B); glutathione synthetase (GSS; Figure 4.24C); heme oxygenase I (HMOX1; Figure 4.24D); superoxide dismutase 1 (SOD1; Figure 4.24E); and for pro-inflammatory cytokines: interleukin-1β (IL-1β; Figure 4.24F); interleukin-6 (IL-6: Figure 4.24G); interleukin-8 (IL-8; Figure 4.24H); and tumor necrosis factor-α (TNF-α; Figure 4.24I).

C

Treatment/Concentration (µg/mL)

Glutathione synthetase Transcript Fold Change

D

Treatment/Concentration (µg/mL)

Heme oxygenase 1 Transcript Fold Change

G

H
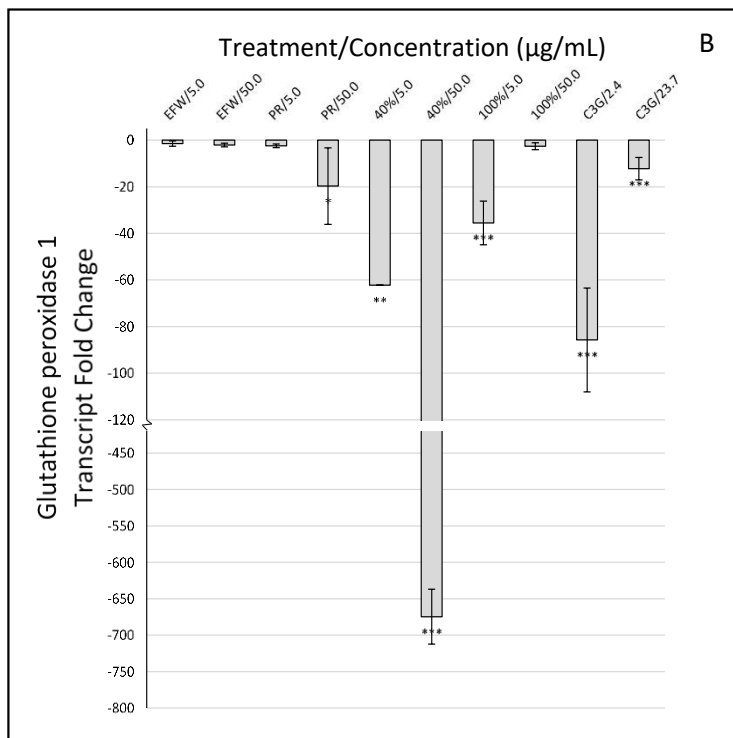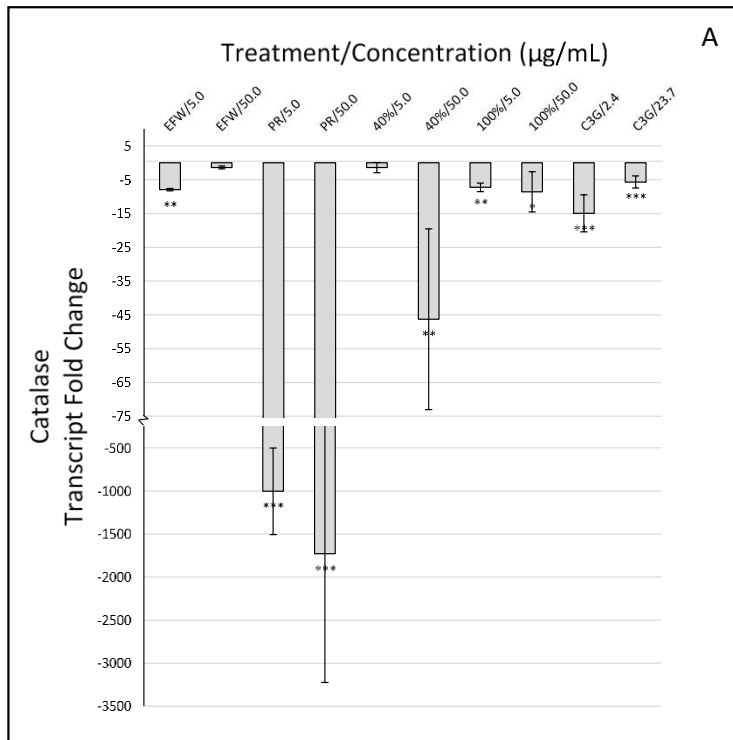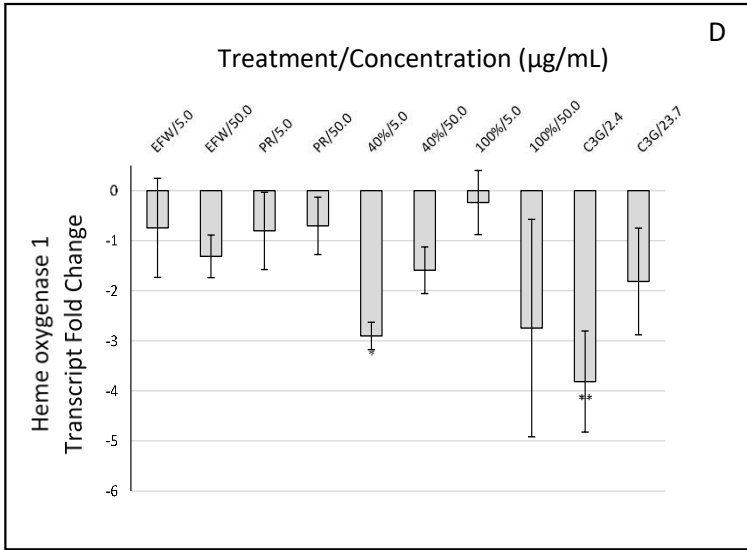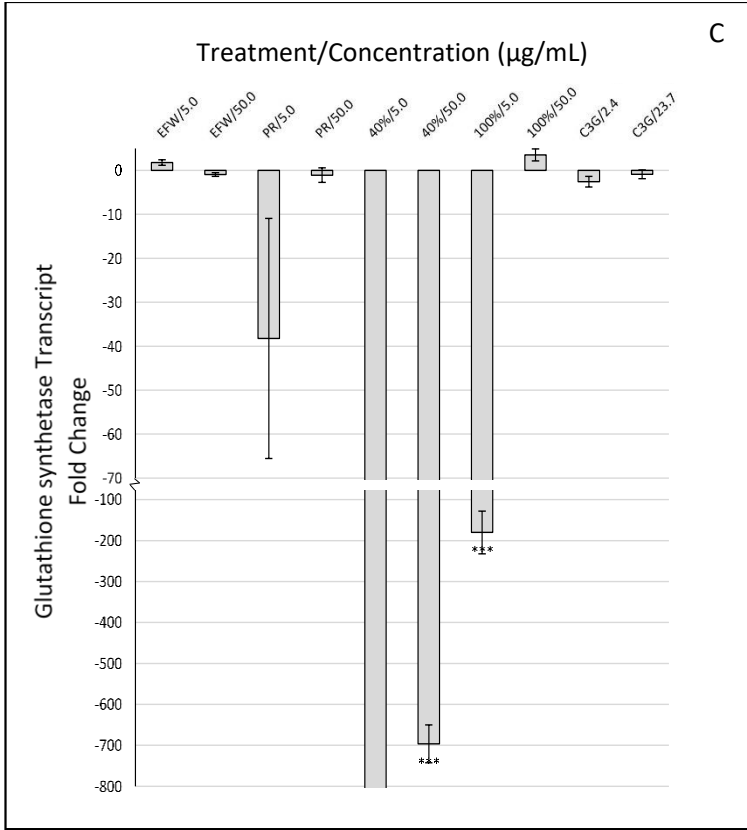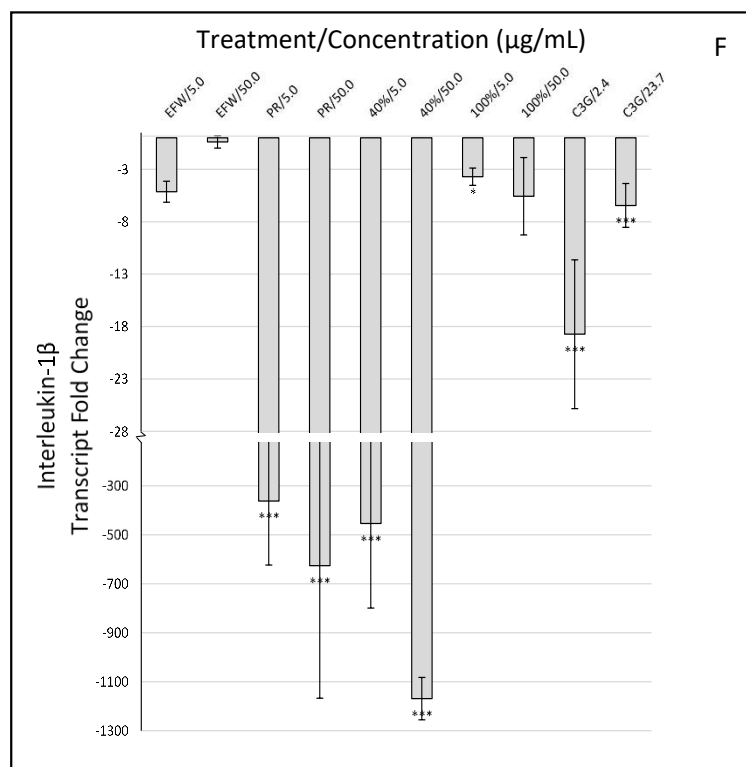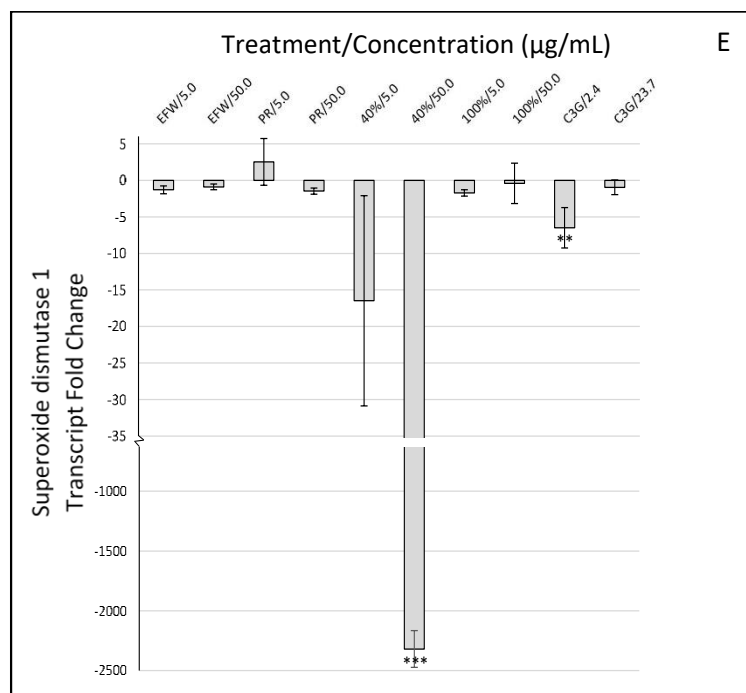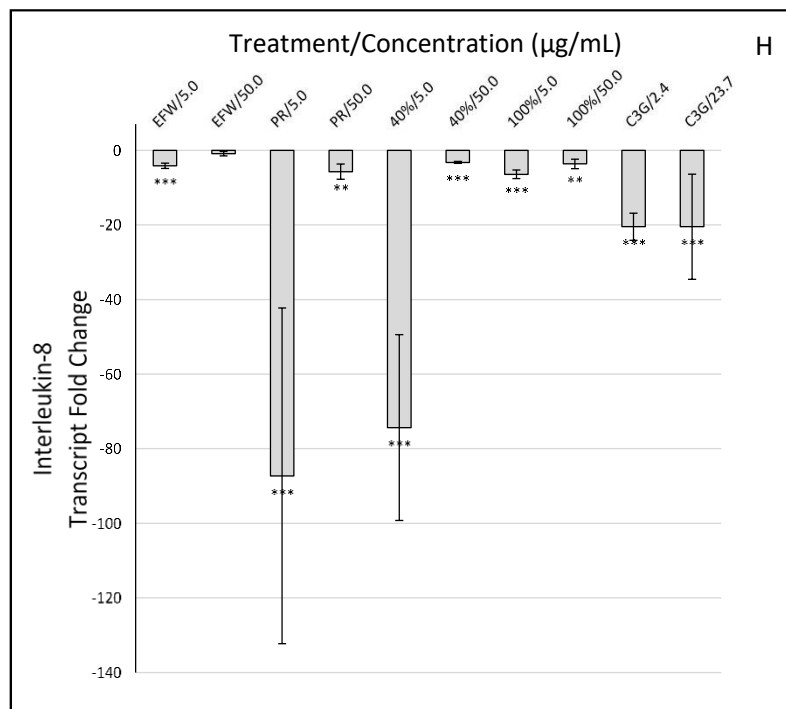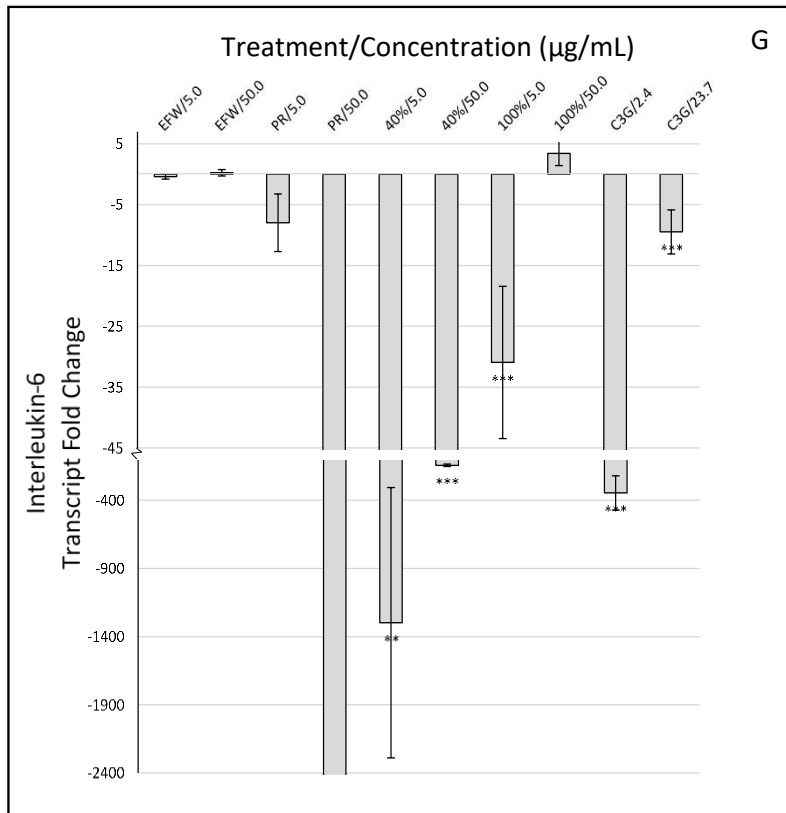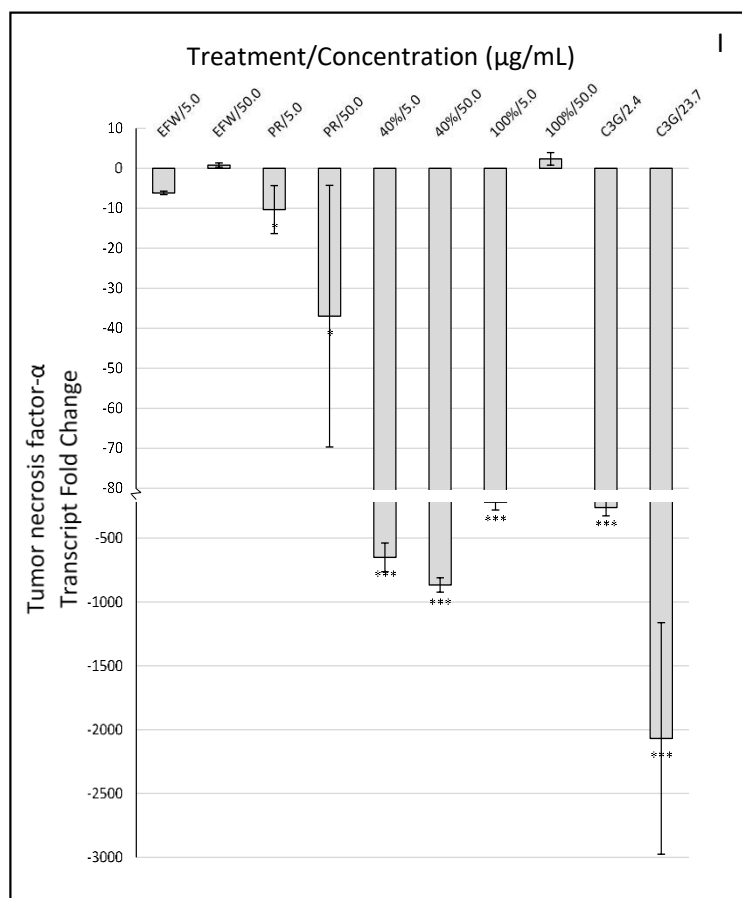
Figure 4.24 2DD fibroblast mRNA fold change results after 72 h treatment with Tundra variety haskap phenolics and C3G. Figure identification for antioxidant enzymes: A. catalase (CAT); B. glutathione peroxidase 1 (GPx1); C. glutathione synthetase (GSS); D. heme oxygenase I (HMOX1); and E. superoxide dismutase 1 (SOD1). For cytokines: F. interleukin-1β (IL-1β); G. interleukin-6 (IL-6); H. interleukin-8 (IL-8); and I. tumor necrosis factor-alpha (TNF-α). Treatment abbreviations: EFW, ethanol:formic acid:water extract; PR, phenolic rich extract; 40%, 40% ethanol fraction; 100%, 100% ethanol fraction; C3G, cyanidin-3-*O*-glucoside. *p<0.10, **p<0.05, ***p<0.01

The 2DD fibroblasts showed significant decreases in transcript levels for all cytokines and some antioxidant enzymes in response to Tundra haskap phenolics and C3G (Figures 4.24A-I). In two cases (Figures 4.24C and G), transcript levels were too low to be amplified by RT-qPCR, resulting in extremely high (negative) fold change values that are shown as off-scale bars for GSS with 40% at 5.0 µg/mL treatment (Figure 4.24C) and IL-6 with PR at 50.0 µg/mL treatment (Figure

4.24G). These results signify an extreme decrease in fold change for GSS and IL-6 mRNA transcript levels in response to these two haskap phenolic treatments.

It was hypothesized that in addition to increases in SIRT1 levels and activity, haskap phenolics would also have radical scavenging abilities within cells, leading to a decreased cellular requirement for antioxidant enzymes. Fibroblast transcript levels of antioxidant enzymes in 2DDs showed significant changes for select haskap phenolic treatments including: (a) fold changes for CAT (Figure 4.24A) were largest for PR treatments (-1003.6x or greater), and all other treatments had fold changes of -46.3x or less; (b) GPx1 (Figure 4.24B) showed the most significant fold changes for the 40% and C3G treatments (at both concentrations) with an average of -208.7x; (c) GSS (Figure 4.24C) fold changes were significant ($p<0.10$) for both the 40% and 100% at 5.0 µg/mL treatments, showing decreases -180.2x or greater; (d) HMOX1 (Figure3.D) was mainly unresponsive to haskap phenolic treatments with a maximum fold change of -3.8x for C3G at 2.4 µg/mL; and (e) SOD1 (Figure 4.24E) showed a large decrease of -2320.1x for the 40% at 50.0 µg/mL treatment, with all others having decreases -16.5x or less.

The antioxidant enzyme transcript levels that responded to the widest range of treatments (i.e. EFW, PR, and fraction treatments) were CAT and GSS (Figures 4.24A and C, respectively) while GPx1 and SOD1 (Figures 4.24B and E, respectively) were primarily responsive to the 40% and C3G treatments, suggesting anthocyanin structure-specific activities. The least responsive were HMOX1 and SOD1 (Figures 4.24D and E, respectively) which each had only two treatments resulting in significant decreases.

As we had observed increased SIRT1 function and decreased phospho-NF-κB p65, it was hypothesized that this would lead to decreased inflammatory responses seen as decreases in pro-inflammatory cytokine production. RT-qPCR data demonstrated significant decreases in fold change values for several pro-inflammatory cytokines following haskap phenolic treatments. Results were as follows: (a) IL-1β (Figure 4.24F) showed at least one significant decrease for each treatment except for EFW with a maximum decrease of -1169.5x for 40% at 50.0 µg/mL; (b) IL-6 (Figure 4.24G) showed the largest decreases for the 40% and PR treatments at 50.0 µg/mL with fold changes greater than -449.3x; (c) IL-8 (Figure 4.24H) had the least extreme response of the tested cytokines with a maximum decrease of -87.3x for PR at 5.0 µg/mL, however, all treatments had at least one significant decrease; and (d) TNF-α (Figure 4.24I) showed significant ($p<0.10$)

decreases for all except three treatments (EFW at both concentrations and 100% at 5.0 µg/mL) with the 40% and C3G treatments (at both concentrations) having fold changes -260.5x or greater.

Overall, the tested antioxidant enzyme and pro-inflammatory cytokine transcript levels were significantly downregulated in response to haskap phenolic treatments and C3G. Certain cytokines (e.g. IL-1β) and enzymes (e.g. SOD1) were more responsive (i.e. more significant fold changes) to specific structures such as anthocyanins in the 40% fraction and C3G. Cytokines were generally more impacted by phenolic treatments with all four showing significant decreases ($p<0.10$) for at least seven of the ten treatments/concentrations. Antioxidant enzymes were less responsive with three of the measured enzymes (GSS, HMOX1, and SOD1) responding to three or fewer treatments/concentrations.

The results obtained for cytokine transcript levels as a function of Tundra phenolic treatments were consistent with multiple literature reports for haskap phenolics showing anti-inflammatory activities, including: (a) phenolic extracts of the Canadian haskap cultivar Borealis at 100 µg/mL inhibited TNF-α and IL-6 by 55 and 50%, respectively, when applied to human THP-1 monocytes (Rupasinghe et al., 2015); (b) phenolic extracts of native Japanese haskaps (100 µg/mL) inhibited the LPS-dependent elevation of TNF-α in mouse RAW 264.7 macrophages (Jin et al., 2006); and (c) mice fed a high-fat diet with 0.5-1% haskap phenolics showed lower levels of lipid peroxidation and pro-inflammatory cytokines (e.g. IL-1β, IL-6, and IL-10) following exposure to carbon tetrachloride (CCl_4) (Wu et al., 2016).

Antioxidant and cytokine transcript fold changes supported 2DD Western blot data which showed decreases in phosphorylation of NF-κB p65 (Figure 4.18), indicating decreases in the activated form of this transcription factor, which is involved in pro-inflammatory cytokine expression. The most extreme results in transcript level changes found by RT-qPCR were in response to the 40% and PR treatments. The results for the PR treatments were unexpected, as PR treatments did not give significant data by western for phospho-NF-κB p65 but there was still an observed decrease in cytokine transcripts by RT-qPCR.

Antioxidant enzyme transcripts consistently decreased in response to select treatments. These decreases could be the result of phenolic radical scavenging abilities which may decrease the cellular requirement for these enzymes. Experimental results were in agreement with literature

reports for plant phenolic treatments *in vitro.* As an example, avenanthramide C, an oat phenolic, significantly decreased levels of GPx1, GSS, and SOD1 transcripts after 48 h treatment (100 and 200 µM) in 2DD fibroblasts (Wang and Eskiw, 2019). The RT-qPCR results also demonstrate another facet of the stress-mediating abilities haskap phenolics have shown *in vitro,* which is the ability to downregulate these cytokine transcripts. This downregulation can then have widespread biological effects in ameliorating inflammation.

4.6 Tissue Culture Results and Phenolic Structure and Concentration

To understand the impact of haskap phenolics on human fibroblasts *in vitro*, cells were exposed to one of four haskap phenolic treatment conditions (EFW, PR, 40%, 100%) or C3G for 72 h. Following this, population doubling times and cell viability, intracellular levels of protein or phosphorylation, SIRT1 protein activity, and transcript levels in normal, immortalized, and SIRT1 knockdown cells were examined. Experimental results showed that the haskap phenolic treatments having the greatest impact on the aforementioned were the 40% and 100% fractions. This section will discuss the relationship between the phenolic structures and concentrations present in these treatments and their impacts *in vitro*.

4.6.1 Treatment Molarities

To examine the impact of haskap phenolics on human fibroblasts, analytical data from TPCI experiments (Section 4.3.2) was used to calculate the molarity of each subclass in the two fraction treatments (40% and 100%) and the PR extract. This was done because molarity describes the number of phenolic molecules in each treatment which could help explain tissue culture results. During phenolic treatments, the same dry weight of each treatment was used, however, this weight would contain different numbers of phenolic molecules in each treatment due to variation in molecular weight of each specific compound.

To perform these calculations, molar masses for representative compounds in each subclass were as follows: hydroxybenzoic acids as gallic acid; flavanols as catechin; hydroxycinnamic acids as chlorogenic acid; flavonols as quercetin-3-*O*-glucoside; flavanones as naringenin; and anthocyanins as cyanidin-3-*O*-glucoside. These were the same representative compounds used for TPCI quantitation with the exception of the flavonol subclass which used rutin (quercetin-3-*O*-

rutinoside). For molarity calculations, quercetin-3-O-glucoside was selected in place of rutin, because the majority of phenolics in these fractions were mono-glycosylated as identified by HPLC-MS/MS (Section 4.3.3-5). The EFW extract was not included in this table as the presence of nonphenolics would contribute to the dry weight (DW) measurement, making the calculation inaccurate for this treatment. For this reason, molarity was not used as the original concentration designation in this work. The calculated molarities (µM) of each major subclass in the 50.0 µg/mL PR, 40%, and 100% Tundra haskap phenolic treatments are shown in Table 4.18.

Table 4.18 Calculated molarity (µM) for the six major phenolic subclasses for EFW, PR, 40%, and 100% Tundra variety haskap phenolic treatments at 50.0 µg/mL.

Phenolic Subclass	PR	40%	100%
Hydroxybenzoic acids	6.2[1]	5.0	45.0
Flavanols	26.9	16.0	82.3
Hydroxycinnamic acids	14.8	7.2	ND[2]
Flavonols	11.7	6.1	39.8
Flavanones	ND	3.1	ND
Anthocyanins	71.0	77.6	3.3
Total treatment[3]	130.6	115.0	170.4

[1]µM.
[2]ND represents not detected by HPLC-PDA for TPCI with no phenolic subclass peak with a height greater than the qualitative detection limit (<3x s/n).
[3]Sum of molarities for each phenolic subclass.

Despite the equal dry weight (DW)/mL media used in tissue culture experiments, the total molarities for these three 50.0 µg/mL treatments ranged from 115.0-170.4 (minimum and maximum for the 40% and 100% fractions, respectively) with a mean of 138.7 µM (Table 4.18). Total molarity of the phenolic treatment is an important factor in understanding and explaining the *in vitro* experimental results obtained in this study. Molarity calculations also showed that select

subclasses that appeared minor by TPCI measurement were prevalent in terms of molarity as illustrated by the hydroxybenzoic acids in the 100% fraction.

The 100% fraction had the highest phenolic molarity and was one of the most effective treatments *in vitro.* This is supported by 2DD results showing significant increases in population doubling times (without a change in cell viability), significant decreases in phospho-NF-κB p65 and phospho-mTOR with increases in SIRT1 protein levels, increases in SIRT1 activity, and significant decreases in three of the five (CAT, GPx1, and GSS) tested antioxidant enzyme transcript levels along with all four (IL-1β, IL-6, IL-8, and TNF-α) of the tested cytokine transcript levels. The total molarity of the 100% treatment was ~40 µM higher than the next highest treatment (PR; Table 4.18) and ~55 µM higher than the lowest treatment (40%; Table 4.18). This indicates that more phenolic molecules were present and available to cells with the 100% fraction treatment. Despite its lower molar concentration, the 40% fraction treatment also resulted in measurable differences when compared to untreated fibroblasts in many of the *in vitro* experiments. Findings for the 40% fraction were similar to those of the 100% fraction, with the addition of decreases in the antioxidant enzymes HMOX1 and SOD1 for at least one of the treatment concentrations. It is hypothesized that some intracellular phenolic mechanisms were more important than the total molarity of the phenolics for the 40% treatment.

4.6.2 Phenolic Structural Interactions

It is well-established that interactions between phenolics are influential in cellular responses to their treatments. The structural complexity of haskap phenolic mixtures means that many different molecular interactions between phenolics could occur. Types of molecular interactions that have been reported amongst phenolics include addition, antagonism, interference, potentiation, and synergism (Phan et al., 2018; Hajimehdipoor et al., 2014). This section will focus on the potential of antagonism and synergism in explaining the *in vitro* cellular experimental results. A synergistic relationship occurs when the effects of the combined phenolic class(es)/subclass(es) is greater (i.e. more positive) than the sum of the effects of the individual phenolic class(es)/subclass(es) (Hajimehdipoor et al., 2014; Hidalgo et al., 2010). An antagonistic relationship occurs when phenolic class(es)/subclass(es) result in a decrease in tissue culture

response when combined compared to as individual treatments (Hajimehdipoor et al., 2014; Hidalgo et al., 2010).

Structural interactions between phenolic subclasses could be responsible for the 40% fraction influencing fibroblasts similarly to the 100% fraction despite its lower molarity. The 40% treatment was primarily anthocyanins (67.5% based on molarity; Table 4.18) which have been reported to have synergistic effects *in vitro*. As an example, treatments of bilberry and blackcurrent anthocyanin mixtures (of 17 different anthocyanins) showed greater decreases in pro-inflammatory cytokine production in HepG2 cells than treatments of isolated cyanidin-3-*O*-glucoside or delphenidin-3-*O*-glucoside (after stimulation with IL-6 and IL-1β) (Zhu et al., 2013). Anthocyanin synergism could have led to the substantial tissue culture effects observed in this work for the 40% fraction treatment, counteracting its lower molarity. Example mechanisms of synergy described in literature for phenolic compounds include: (a) one phenolic can regenerate another after it has become oxidized (i.e. acted as an antioxidant by donating hydrogen atom or electrons); (b) antioxidants can protect each other when they work through different antioxidative mechanisms; and (c) sacrificial oxidation can occur when one oxidation reaction protects another phenolic from becoming oxidized (Phan et al., 2018).

Interactions between phenolics could also explain PR treatment results which had a similar total molarity to the 40% fraction but showed fewer effects *in vitro*. There have been reports of antagonistic relationships for combinations of hydrophilic and hydrophobic phenolics during *in vitro* tissue culture experiments. As an example, 50 µM combinations of quercetin (hydrophobic flavonol) with epicatechin or catechin (hydrophilic flavanols) resulted in fewer anti-inflammatory activities (measured by RT-qPCR of the mRNA transcript for Nos2, which is linked to NO production) in LPS-stimulated RAW264.7 cells when compared to the same compounds used individually (Murakami et al., 2015). A mixture of hydrophilic and hydrophobic phenolics were present in the PR treatment; for example, epicatechin, catechin, and quercetin derivatives (e.g. quercetin-3-*O*-glucoside) were identified using HPLC-MS/MS (Sections 4.3.3-5). Whereas, the 40% and 100% fractions contained mostly hydrophilic or mostly hydrophobic phenolic compounds, respectively. One mechanism (based on chemical *in vitro* reactions) that has been proposed to cause antagonism among phenolic structures is intramolecular hydrogen bonding between hydroxyl groups, which can limit the activities of the bonded compounds (Hidalgo et al.,

2010). Some research has also indicated interference in absorption between hydrophilic and hydrophobic phenolics leading to decreased bioavailability (Phan et al., 2018). It is hypothesized that the most influential antagonistic interactions for the PR extract involved the flavanol subclass which was much lower in the 40% treatment (10.9 µM lower, 59.5% less; Table 4.18). The 40 and 100% phenolic fractions showed the most potential in stress mediation involving SIRT1. The success of these fractions *in vitro* can be linked to synergism, overall molar concentration, and limiting interference and antagonism.

4.6.3 Additional Mechanistic Considerations

In addition to the mechanisms discussed, many other factors can impact haskap phenolic treatment of human fibroblasts *in vitro*. One of these is bioavailability which may be determined by how well molecules cross cellular membranes during *in vitro* experiments. Glycosylated phenolics can actively enter cells through glucose transporters 1 and 2 (GLUT-1 and GLUT-2) in most cell types, which is likely an important factor for haskap extracts because of their high content of glycoslyated phenolics (e.g. anthocyanins) (Tarahovsky et al., 2014). Deglycosylated phenolics (more hydrophobic) are theorized to diffuse through the cellular membrane (i.e. passive transport) as they interact more readily with the phospholipid bilayer (Tarahovsky et al., 2014). The exact structural features that determine where and how a specific phenolic enters a cell are not well understood, however, there is an inverse relationship between the number of hydroxyl groups on a phenolic molecule and its ability to diffuse across the cell membrane (Phan et al., 2018). The treatment concentrations used in this research were higher than predicted physiological levels for many peripheral tissues (following human consumption) as complex digestive mechanisms determine the bioavailability of these molecules *in vivo* (Hussain et al., 2019; Manach et al., 2003). However, the dermal fibroblast model and treatment concentrations were selected to explore mechanisms of action and also because fibroblasts found along the digestive tract in humans would be exposed to high concentrations after consumption of phenolic rich haskaps, making these conditions an appropriate *in vitro* model (Roulis and Flavell, 2016; Higuchi et al., 2015).

Other factors to consider include: (a) phenolic structural stability in the media over time or the possibility of phenolic interaction(s) with the media; (b) the impact of phenolic molecule size and charge on its ability to cross the membrane; and (c) the impact of the treatment vehicle

(DMSO) on the cellular mobility of phenolic structures. The specific molecular interactions between phenolics and intracellular molecules or structures (e.g. enzymes or free radicals) that led to each of the observed effects in the human fibroblast *in vitro* studies (e.g. protein level changes, increases in population doubling time) cannot be determined based solely on this data. Targeted exploration coupled with experimental design would be needed to begin elucidating haskap phenolic mechanisms at the cellular level in more detail. This research accomplished the first steps in assessing the potential of unique Tundra variety haskap phenolic fractions to mediate cellular stress *in vitro* in human fibroblasts through the activity of SIRT1.

5.0 GENERAL CONCLUSIONS

The overarching goals of this project were to determine the chemical composition and physicochemical properties of five Saskatchewan-bred haskap varieties and to extract, fractionate, and characterize their phenolics. We further aimed to evaluate the ability of haskap phenolic extracts and fractions to mediate cellular stress *in vitro*. These five varieties were selected, because they were developed and grown at the UofS (Horticulture Field Laboratory) and were only recently released to the public. An in-depth analysis of these varieties' chemical composition and physicochemical properties adds to currently available information on other haskap varieties and educates industrial growers and food processors about their potential as a berry crop and as a nutraceutical.

For Objective 1, the physicochemical properties and chemical composition of physically pressed juices from Aurora, Blizzard, Honey Bee, Indigo Gem, and Tundra haskap varieties were determined. Tristimulus colour values were L* (5.03-8.34), a* (2.45-11.94), and b* (0.44-4.95), indicating a deep purple colour, with calculated chroma and hue ranges of 2.49-12.02 and 10.61-22.49, respectively. Juice pH values ranged from 2.99-3.31 (for Tundra and Blizzard, respectively), and °Brix values ranged from 13.70-17.05 (for Honey Bee and Indigo Gem, respectively). The diameters of the berries ranged from 9.35-11.97 mm (for Honey Bee and Blizzard, respectively) with lengths of 17.41-23.49 mm (for Tundra and Aurora, respectively). Chemical composition analyses included HPLC-RI and HPAE-PAD analysis of major carbohydrates and polyols/sucrose, respectively. Major carbohydrates identified were fructose (5.12-6.10%; for Tundra and Indigo Gem, respectively) and glucose (4.09-5.88%; for Honey Bee and Indigo Gem, respectively), with no sucrose detected (detection limit of 5 mg/L by HPAE-PAD). Minor polyols identified in all five varieties included inositol and sorbitol, with arabitol identified in all varieties except Tundra; the combined concentrations for these three polyols did not exceed 0.69% in any variety. Organic acids analysis (HPLC-PDA) identified citric (1729.8-2543.1 mg/100g FW; for Honey Bee and Tundra, respectively), malic (343.6-988.6 mg/100 g FW;

for Blizzard and Honey Bee, respectively), and quinic acids (83.4-113.2 mg/100 g FW; for Blizzard and Indigo Gem, respectively) as the major components. Other organic acids identified chromatographically were acetic, malonic, oxalic, and shikimic acids. The ascorbic acid content for each variety was determined due to its biological importance with a range of 3.2-9.5 mg/100 g FW (for Aurora and Tundra, respectively). To the best of the author's knowledge, neither arabitol nor acetic acid were previously reported in haskaps. This compositional data allows for identification of potential uses for these berries including: (a) the deep purple-coloured juices have potential as a natural colourant; (b) their high organic acid content and low pH values mean they could be used as acidulants in food products; and (c) the high carbohydrate content of these berries (similar to other commercial fruits such as apple and pear) suggests that they could also be used in stand-alone products such as haskap juices. This data on these five new Saskatchewan haskap varieties is a significant contribution to currently available scientific information on haskap varieties worldwide.

For Objectives 2 and 3, phenolic extraction and structural characterization were accomplished along with the production of phenolic rich extracts and fractions for *in vitro* experiments (Objective 4). Phenolics were extracted from macerated whole fruits using EFW as the solvent to produce the starting material for solid phase extraction and structural studies. Total phenolic content results for EFW extracts ranged from 451.5-778.9 mg GAE/100 g FW, and total phenolic chromatographic index (TPCI; HPLC-PDA) results ranged from 442.5-727.0 mg/100 g FW. Tundra and Aurora had the highest and lowest values for these two ranges, respectively. Major phenolic subclasses identified by HPLC-PDA included anthocyanins (249.2-429.4 mg/100 g FW), flavanols (23.6-143.1 mg/100 g FW), flavonols (29.8-90.7 mg/100 g FW), and hydroxycinnamic acids (46.5-80.2 mg/100 g FW). The less prevalent subclasses were the hydroxybenzoic acids and flavanones. Further chromatographic investigation on anthocyanin composition was performed (HPLC-PDA) and showed cyanidin-3-*O*-glucoside (227.3-361.6 mg/100 g FW) to be the most abundant compound, making up 72.5-82.1% of the total anthocyanin contents. Other major anthocyanins identified were cyanidin-3,5-*O*-diglucoside (17.5-48.1 mg/100 g FW), cyanidin-3-*O*-rutinoside (13.2-32.4 mg/100 g FW), and peonidin-3-*O*-glucoside (11.8-31.8 mg/100 g FW). The Indigo Gem variety was found to have the highest anthocyanin and cyanidin-3-*O*-glucoside contents of 501.3 and 396.3 mg/100 g FW, respectively.

To remove nonphenolic compounds (e.g. carbohydrates and organic acids) from the EFW extracts and separate phenolics by subclass, solid phase extraction was used. A concentrated EFW extract (from each variety) was applied to Amberlite® XAD16N resin and then subjected to water treatment followed by 100% ethanol elution. The resulting phenolic rich (PR) extract had the majority of nonphenolics removed (i.e. final concentrations of <0.03% carbohydrates and <0.2% organic acids, respectively) and also had a similar phenolic composition (TPCI: 381.7-663.3 mg/100 g FW) to the original EFW extract. This resin was also used in conjunction with aqueous ethanol to produce five phenolic fractions (water, 20% ethanol, 40% ethanol, 70% ethanol, and 100% ethanol) with their phenolic compositions identified chromatographically (HPLC-PDA). This analysis showed that the 40% and 100% fractions had the best subclass separation with the 40% fractions containing mostly anthocyanins (55.9-84.0%) and the 100% fractions containing primarily flavanols (46.2-75.6%) and flavonols (14.5-35.7%). The successful fractionation of haskap phenolic extracts was an important achievement, as it resulted in unique experimental materials for *in vitro* experiments (Objective 4) which allowed comparison of the activities of specific phenolic subclasses with the whole extracts.

More detailed phenolic data was also obtained on the Tundra variety using HPLC-MS/MS to identify specific phenolics (i.e. structures) present in the fractions. This analytical platform identified previously unreported phenolics including two anthocyanins: delphinidin-sambubioside and peonidin-pentoside; and one flavonol: kaempferol-rutinoside. The identification of these compounds adds novel data to the known composition of haskaps; this information could be important for future *in vitro* or *in vivo* research and/or to identify compositional variations between haskap cultivars. To complete Objectives 2 and 3, two *in vitro* free radical scavenging assays (ABTS and DPPH) were performed on all extracts and fractions, and this data was used to select the Tundra variety for *in vitro* tissue culture experiments (Objective 4) due to its significantly higher phenolic content and free radical scavenging abilities.

For Objective 4, the impact of haskap phenolics and cyanidin-3-*O*-glucoside (C3G) on the mediation of cellular stress was investigated. Tundra haskap extracts (EFW and PR), fractions (40 and 100%), and C3G (at the concentration present in EFW extracts), were applied to two human fibroblast cells lines: 2DD (primary) and NB1 hTERT (immortalized) for 72 hours. Phenolic concentrations of 5.0 and 50.0 µg/mL (2.4 and 23.7 µg/mL for C3G) were shown to significantly

(p<0.10) increase cell population doubling times (i.e. slow growth/extend lifespan), comparable to the health-promoting phenolic, resveratrol, without increasing cell death. Selected *in vitro* experiments showed the 40 and 100% fractions to have the ability to increase levels of SIRT1 and Nrf2 proteins in 2DD fibroblasts while decreasing levels of phosphorylated NF-κB p65 and mTOR. Following knockdown of SIRT1, both cell lines showed a loss of responses to treatments in terms of phospho-NF-κB p65, though SIRT1-independent increases in Nrf2 were observed in 2DD knockdown fibroblasts. This experiment demonstrated that haskap phenolic function depended on SIRT1. In addition to SIRT1 protein levels, changes in SIRT1 activity were also examined. Purified SIRT1 exposed to haskap phenolics showed no changes in activity, indicating they do not interact directly with SIRT1. In addition, SIRT1 activity was not altered in cell extracts incubated with phenolic extracts, indicating that metabolic activity is required for haskap phenolics to indirectly activate SIRT1. Measurements of SIRT1 activity in treated 2DD cell lysates showed that all haskap phenolic treatments (50.0 µg/mL) and C3G (23.7 µg/mL) increased SIRT1 activity >2.1x the untreated control. These experiments showed that haskap phenolic treatments led to increases in SIRT1 protein levels and activity through an indirect mechanism.

Additional markers related to cellular stress were measured in 2DD fibroblasts including transcript levels of select pro-inflammatory cytokines and antioxidant enzymes. The 40 and 100% fraction treatments led to decreased levels of pro-inflammatory cytokine transcripts including: IL-1β, IL-6, IL-8, and TNF-α, along with antioxidant enzymes: CAT, GSS, GPx1, and SOD1. These experimental results suggested that along with decreasing inflammatory responses through NF-κB, haskap phenolics were scavenging sufficient free radicals to decrease the cellular requirement for antioxidant enzymes. This could also be a result of decreased cellular stress due to increased SIRT1 (and decreased NF-κB) activities.

In conclusion, select Tundra haskap phenolics showed *in vitro* activities in human fibroblasts through an indirect interaction with SIRT1, including increases in population doubling times without increases in cell death, increases in SIRT1 protein and activity levels, and decreases in phospho-NF-κB p65 and phospho-mTOR. Decreases in inflammatory responses and cellular requirement for antioxidant defense mechanisms were also observed via changes in transcript levels. The phenolic treatments which showed the greatest impacts *in vitro* were the 40 and 100% fractions, while the EFW and PR extract treatments showed few changes. C3G treatments showed

that it was not the primary functional component in haskap phenolic treatments. Nonphenolics found in the EFW extract likely interfered with phenolic activities and also led to lower phenolic concentrations in the treatment. The PR extract was hypothesized to contain high levels of antagonistic compounds, specifically combinations of hydrophilic flavanols and hydrophobic flavonols. The fraction treatments contained subclasses separated by their hydrophobicity, meaning that these antagonistic combinations were avoided. The 100% treatment also contained high levels of hydroxybenzoic acids (in terms of molarity) in comparison to the other treatments, suggesting that synergism with this subclass may have also been a factor. The exact mechanisms that lead to these effects and how phenolic interactions contribute to results would need further exploration as they cannot be determined based solely on this data.

These *in vitro* tissue culture experiments successfully identified select haskap phenolics (i.e. fractions) that had the ability to mediate cellular stress in human fibroblasts through the action of SIRT1 and also demonstrated their impacts on inflammatory and antioxidant pathways. This research showed the potential value for Canadian haskap berries beyond commercial sales and justified the pursuit and further exploration of haskap phenolics as nutraceuticals.

6.0 FUTURE DIRECTIONS

This research investigated the physicochemical properties, chemical composition (specifically phenolics), and *in vitro* cellular stress mediation potential of these five new Saskatchewan-bred haskap varieties. Future work could address additional questions about each of these topics, with a focus on chemical composition (carbohydrate, organic acids, and phenolics) and *in vitro* health effects.

Literature has shown significant variation in composition for haskap berries based on variety, geographic location, growing conditions, and seasonal changes. The data collected in this project focused on varietal differences, as berries of different varieties from the same year and region (i.e. same geographic location, growing conditions, and season) were used for analysis. Further research investigating these alternate factors would be an important addition to current knowledge for these five varieties. Industrial processors and commercial growers would need this information for product consistency and to make intelligent use of their haskap berries year to year. For commercial purposes, organic acids and carbohydrate analysis should be the focus to yield further data about shifts in flavour and organoleptic properties. However, changes in phenolic composition would be more important for the development of value-added products, such as haskap phenolic supplements or encapsulated haskap phenolics. A greater understanding of the how these factors impact chemical composition would make haskaps a more valid option for future commercial development.

In vitro experiments showed the abilities of haskap phenolic fractions to mediate cellular stress through SIRT1, phospho-NF-κB p65, phospho-mTOR, and Nrf2. Results showed that SIRT1 activation was not through a direct interaction, leading first to questions about the mechanism(s) by which these phenolics are upregulating SIRT1 protein levels and activity. Additional knockdown (siRNA) experiments of upstream pathways related to SIRT1 could be pursued. This could include AMPK and also mTORC1 and 2 (due to their reciprocal relationship

with SIRT1), which could help identify if other cellular targets are potentially interacting with haskap phenolics directly. The impact of haskap phenolic treatments on these cellular targets could also be analyzed after treatment with a cellular stressor such as TNF-α or lipopolysaccharide (LPS) since many studies have shown the ability of fruit phenolics to rescue stressed phenotypes.

Further experiments involving Nrf2 could also be pursued, as this protein showed unique increases in response to haskap treatments that were independent of SIRT1 (increases were seen for pre- and post- SIRT1 knockdown cells). Nrf2 is involved in the transcription of antioxidant enzymes, one of the most common being heme oxygenase 1 (HMOX1). HMOX1 transcript levels were not significantly impacted by haskap phenolics in this work, however, Nrf2 regulates many other potential targets. To investigate the activities of Nrf2 after haskap phenolic-mediated upregulation, a chromatin immunoprecipitation (ChIP) assay could be performed to analyze protein/DNA interactions between Nrf2 and its other regulatory targets in the genome. ChIP could also be performed to investigated promoter binding of NF-κB to its pro-inflammatory gene targets. This analysis could show additional impacts of haskap phenolics that were not revealed through experiments in this project.

One of the most important questions to pursue regarding *in vitro* activities is why haskap phenolic whole extracts were ineffective in comparison to the fraction treatments. To investigate this, synergistic treatments could be tested to recreate combinations/concentrations of the haskap phenolics that are found in the respective treatments. For example, C3G combined with chlorogenic acid could be tested at the concentrations it is found in both the PR extract and the 40% fraction, to determine if differences in responses are a result of nuanced combinations and concentrations of these two compounds. Another treatment could be tested combining groups of flavonol standards at the concentrations they are found in the 100% fraction. Answering this question presents a significant research challenge, as the *in vitro* effects are likely to be the result of many complex interactions. Another possibility would be to sequentially increase the concentrations of EFW and PR treatments. If higher concentrations begin to show similar effects to fraction treatments, the phenolic composition in each could be compared to determine what elements are most aligned at that concentration. This would hopefully allow for the selection of a few key compounds or combinations.

This research answered many initial questions about the cellular stress mediation potential of these berries, along with identifying unique and novel compositional details. Further research on a variety of topics would build on this data to yield a full profile of these new Saskatchewan haskap varieties for a better understanding of their full economic and nutraceutical potential.

7.0 REFERENCES

Abdulkhaleq, L. A, Assi, M. A., Abdullah, R., Zamri-Saad, M., Taufiq-Yap, Y. H., and Hezmee, M. N. M. (2018). The crucial roles of inflammatory mediators in inflammation: a review. *Veterinary World, 11:* 627-635.

Ambriz-Pérez, D. L., Leyva-López, N., Gutierrez-Grijalva, E. P., and Heredia, J. B. (2016). Phenolic compounds: natural alternative in inflammation treatment. A Review. *Cogent Food & Agriculture*, *2*: 1-14.

Armenta, S., Alcala, M., and Blanco, M. (2011). A review of recent, unconventional applications of ion mobility spectrometry (IMS). *Analytica Chimica Acta, 703*: 114-123.

Aruoma, O. I., Grootveld, M., and Bahorun, T. (2006). Free radicals in biology and medicine: from inflammation to biotechnology. *BioFactors, 27:* 1–3.

Auzanneau, N., Weber, P., Kosińska-Cagnazzo, A., Andlauer, W. (2018). Bioactive compounds and antioxidant capacity of *Lonicera caerulea* berries: comparison of seven cultivars over three harvesting years. *Journal of Food Composition and Analysis, 66:* 81-89.

Azorín-Ortuño, M., Yañéz-Gascón, M. J., Pallarés, F. J., Rivera§, J., González-Sarrías, A., Larrosa, M., Vallejo, F., García-Conesa, M. T., Tomás-Barberán, F., and Espín, C. (2012). A dietary resveratrol-rich grape extract prevents the developing of lesions in the aorta of pigs fed an atherogenic diet. *Journal of Agricultural and Food Chemistry, 60:* 5609-5620.

Bakowska-Barczak, A. M., Marianchuk, M., and Kolodziejckz, P. (2007). Survey of bioactive components in Western Canadian berries. *Canadian Journal of Physiology and Pharmacology, 85:* 1139-1152.

Balasundram, N., Sundram, K., and Samman, S. (2006). Phenolic compounds in plants and agri-industrial by-products: antioxidant activity, occurrence, and potential uses. *Food Chemistry*, *99:* 191–203.

Balogh, M. P. (2004). Debating resolution and mass accuracy in mass spectrometry. *Spectroscopy, 19:* 34-40.

Bayram, B., Ozcelik, B., Grimm, S., Roeder, T., Schrader, C., Ernst, I. M. A., Wagner, A. E., Grune, T., Frank, J., and Rimbach, G. (2012). A diet rich in olive oil phenolics reduces oxidative stress in the heart of SAMP8 mice by induction of Nrf2-dependent gene expression. *Rejuvenation Research, 15:* 71-81.

Beher, D. B., Cumine, S., Kim, K. W., Lu, S., Atangan, L., and Wang, M. (2009). Resveratrol is not a direct activator of SIRT1 enzyme activity. *Chemical Biology & Drug Design, 74:* 619-624.

Bell, L., and Williams, C. M. (2018). A pilot dose-response study of the acute effects of haskap berry extract (*Lonicera caerulea* L.) on cognition, mood, and blood pressure in older adults. *European Journal of Nutrition, 1:* 1-10.

Bhattacharya, A., Sood, P., and Citovsky, V. (2010). The roles of plant phenolics in defence and communication during *Agrobacterium* and *Rhizobium* infection. *Molecular Plant Pathology, 11:* 705-719.

Bodnar, A. G., Ouellette, M., Frolkis, M., Holt, S. E., Chiu, C. P., Morin, G., B., Harley, C. B., Shay, J. W., Lichtsteiner, S., and Wright, W. E. (1998). Extension of life-span by introduction of telomerase into normal human cells. *Science, 279:* 349-352.

Bonifacio, L. N., and Jarstfer, M. B. (2010). MiRNA profile associated with replicative senescence, extended cell culture, and ectopic telomerase expression in human foreskin fibroblasts. *PLoS ONE, 5:* 1-12.

Borra, M. T., Smith, B. C., and Denu, J. M. (2005). Mechanism of human SIRT1 activation by resveratrol. *Journal of Biological Chemistry, 280:* 17187-17195.

Bors, B. (2007). Growing haskap in Canada. Department of Plant Sciences, University of Saskatchewan. Available at http://www.fruit.usask.ca/haskap.html (Accessed July 5, 2018).

Bors, B. (2018). Haskap Presentations. Haskap School, University of Saskatchewan Fruit Program. (Presented July 5, 2018).

Brenton, A. G., and Godfrey, A. R. (2010). Accurate mass measurement: terminology and treatment of data. *Journal of the American Society for Mass Spectrometry, 21:* 1821-1835.

Bridger, J. M., Kill, I. R., O'Farrell, M. and Hutchison, C. J. (1993). Internal lamin structures within G1 nuclei of human dermal fibroblast. *Journal of Cell Science, 104*: 297-306.

Brown, A. H. D. (1967). Correlation between brix in juice and fibre in commercial hybrid sugar cane populations. Proceedings 12th Congress of International Society of Sugarcane Technologists. Available at https://www.researchgate.net/publication/280058736 _Correlation_between_Brix_in_juice_and_fibre_in_commercial_hybrid_sugar_cane_pop ulations (Accessed June 19, 2018).

Buachan, P., Chularojmontri, L., and Wattanapitayakul, S. K. (2014). Selected activities of *Citrus maxima* Merr. fruits on human endothelial cells: enhancing cell migration and delaying cellular aging. *Nutrients, 6:* 1618-1634.

Buehler, B. A. (2012). The free radical theory of aging and antioxidant supplements: a systematic review. *Journal of Evidence-Based Complementary & Alternative Medicine*, *17*: 218–220.

Caprioli, G., Iannarelli, R., Innocenti, M., Bellumori, M., Fiorini, D., Sagratini, G., Vittori, S., Buccioni, M., Santinelli, C., Bramucci, M., Quassinti, L., Lupidi, G., Vitali, L. A. Petrelli, D., Behelli, D., Cavallucci, C., Bistoni, O., Trivisonno, A., and Maggi, F. (2016). Blue honeysuckle fruit (*Lonicera caerulea* L.) from eastern Russia: phenolic composition, nutritional value and biological activities of its polar extracts. *Food & Function, 7:* 1892-1903.

Celli, G. B., Ghanem, A., and Brooks, M. S. L. (2014). Haskap berries (*Lonicera caerulea* L.)-a critical review of antioxidant capacity and health-related studies for potential value-added products. *Food and Bioprocess Technology, 7:* 1541–1554.

Chaovanalikit, A., Thompson, M. M., and Wrolstad, R. (2004). Characterization and quantification of anthocyanins and polyphenolics in blue honeysuckle (*Lonicera caerulea* L.). *Journal of Agricultural and Food Chemistry, 52:* 848-852.

Cheynier, V. (2012). Phenolic compounds: from plants to foods. *Phytochemistry Reviews, 11:* 153-177.

Chung, S., Yao, H., Caito, S., Hwang, J., Arunachalam, G., and Rahman, I. (2010). Regulation of SIRT1 in cellular functions: role of polyphenols. *Archives of Biochemsitry and Biophysics, 510:* 79-90.

Corradini, E., Foglia, P., Giansanti, P., Gubbiotti, R., Samperi, R., and Lagana, A. (2011). Flavonoids: chemical properties and analytical methodologies of identification and quantitation in foods and plants. *Natural Product Research*, *25*: 469-495.

Costamagna, M. S., Zampini, I. C., Alberto, M. R., Cuello, S., Torres, S., Pérez, Quispe, C., Schmeda-Hirschmann, G., and Isla, M. I. (2016). Polyphenols rich fraction from *Geoffroea decorticans* fruits flour affects key enzymes involved in metabolic syndrome, oxidative stress and inflammatory process. *Food Chemistry, 190:* 392-402.

De Boer, V. C. J., de Goffau, M. C., Arts, I. C. W., Hollman, P. C. H., and Keijer, J. (2006). SIRT1 stimulation by polyphenols is affected by their stability and metabolism. *Mechanisms of Ageing and Development, 127:* 618-627.

Del Rio, D., Borges, G., and Crozier, A. (2010). Berry flavonoids and phenolics: bioavailability and evidence of protective effects. *British Journal of Nutrition*, *104:* S67–S90.

El-Aneed, A., Cohen, A., and Bahoub, J. (2009). Mass spectrometry, review of the basics: electrospray, MALDI, and commonly used mass analyzers. *Applied Spectroscopy Reviews, 44:* 210-230.

Escarpa, A., and Gonzalez, M. (2001). Approach to the content of total extractable phenolic compounds from different food samples by comparison of chromatographic and spectrophotometric methods. *Analytica Chimica Acta, 427:* 119-127.

Escobar, K. A., Cole, N. H., Mermier, C. M., and VanDusseldorp, T. A. (2019). Autophagy and aging: maintaining the proteome through exercise and caloric restriction. *Aging Cell, 18:* 1-8.

Folin, O., and Ciocalteu, V. (1927). On tyrosine and tryptophan determinations in proteins. *Journal of Biological Chemistry, 73:* 627-650.

Forbes-Hernández, T. Y., Giampieri, F., Gasparrini, M., Mazzoni, L., Quiles, J. L., Alvarez Suarez, J. M., and Battino, M. (2014). The effects of bioactive compounds from plant foods on mitochondrial function: a focus on apoptotic mechanisms. *Food and Chemical Toxicology, 68:* 154-182.

García-Martínez, E., Andújar, I., del Carmen, A. Y., Prohens, J., and Martínez-Navarrete, N. (2017). Antioxidant and anti-inflammatory activities of freeze-dried grapefruit phenolics as affected by gum Arabic and bamboo fibre addition and microwave pretreatment. *Journal of the Science of Food and Agriculture, 98:* 1-9.

García-Salas, P., Morales-Soto, A., Segura-Carretero, A., and Fernández-Gutiérrez, A. (2010). Phenolic compound extraction systems for fruit and vegetable samples. *Molecules, 15:* 8813-8826.

Gasparrini, M., Forbes-Hernandez, T. Y., Giampieri, F., Afrin, S., Alvarez-Suarez, J. M., Mazzoni, L., Mezzetti, B., Quiles, J. L, and Battino, M. (2017). Anti-inflammatory effect of strawberry extract against LPS-induced stress in RAW 264.7 macrophages. *Food and Chemical Toxicology, 102:* 1-10.

Gazdik, Z., Reznicek, V., Adam, V., Zitka, O., Jurikova, T., Krska, B., Matuskovic, J., Plsek, J., Saloun, J., Horna, A., and Kizek, R. (2008). Use of liquid chromatography with electrochemical detection for the determination of antioxidants in less common fruits. *Molecules, 13:* 2823–2836.

Ghosh, H. S., McBurney, M., and Robbins, P. D. (2010). SIRT1 negatively regulates the mammalian target of rapamycin. *PLoS ONE, 5:* 1-8.

Giada, M. D. L. R. (2013). Food Phenolic Compounds: Main Classes, Sources and their Antioxidant Power. In: *Oxidative Stress and Chronic Degenerative Diseases - A Role for Antioxidants.* Morales-González, J. A. (Ed.). InTech, pp. 87-112.

Giampieri, F., Forbes-Hernandez, T. Y., Gasparrini, M., Afrin, S., Cianciosi, D., Reboredo Rodriguez, P., Varela-Lopez, A., Quiles, J. L., Mezzeti, B., and Battino, M. (2017). The healthy effects of strawberry bioactive compounds on molecular pathways related to chronic diseases. *Annals of the New York Academy of Sciences, 1398:* 1-8.

Gillespie, Z. E., Mackay, K., Sander, M., Trost, B., Dawicki, W., Wickramarathna, A., Gordon, J., Eramian, M., Kill, I. R., Bridger, J. M., Kusalik, A., Mitchell, J. A., and Eskiw, C. H. (2015). Rapamycin reduces fibroblast proliferation without causing quiescence and induces STAT5A/B-mediated cytokine production. *Nucleus, 6:* 490-506.

Gillespie, Z. E., Pickering, J., and Eskiw, C. H. (2016). Better living through chemistry: caloric restriction (CR) and CR mimetics alter genome function to promote increased health and lifespan. *Frontiers in Genetics, 7:* 142-153.

Giovannini, L., and Bianchi, S. (2017). Role of nutraceutical SIRT1 modulators in AMPK and mTOR pathway: evidence of a synergistic effect. *Nutrition, 34:* 82-96.

Government of Canada Food and Drug Regulations (2018). Justice Laws Website. Available at: http://laws.justice.gc.ca/eng/regulations/c.r.c.,_c._870/page-60.html (Accessed June 10, 2018).

Grace, M. H., Xiong, J., Esposito, D., Ehlenfeldt, M., and Lila, M. A. (2019). Simultaneous LC MS quantification of anthocyanins and non-anthocyanin phenolics from blueberries with widely divergent profile and biological activities. *Food Chemistry, 277:* 336-346.

Granato, D., Shahidi, F., Wrolstad, R., Kilmartink, P., Melton, L. D., Hidalgo, F. J., Miyashita, K., Van Camp, J., Alasalvar, C., Ismail, A. B., Elmore, S., Birch, G. G., Charalampopoulos, D., Astley, S. B., Pegg, R., Zhou, P. and Finglas, P. (2018).

Antioxidant activity, total phenolics and flavonoids contents: should we ban *in vitro* screening methods? *Food Chemistry*, *264*: 471-475.

Green, R. (2007). Physicochemical properties and phenolic composition of selected Saskatchewan fruits: buffaloberry, chokecherry and sea buckthorn. PhD thesis, University of Saskatchewan, July 2007.

Green, R. C., and Low, N. H. (2013). Physicochemical composition of buffaloberry (*Shepherdia argentea*), chokecherry (*Prunus virginiana*) and sea buckthorn (*Hippophae rhamnoides)* fruit harvested in Saskatchewan, Canada. *Canadian Journal of Plant Science, 93:* 1143-1153.

Gruia, M. I., Oprea, E., Gruia, I., Negoita, V., and Farcasanu, I. C. (2008). The antioxidant response induced by *Lonicera caerulaea* berry extracts in animals bearing experimental solid tumors. *Molecules, 13*: 1195–1206.

Guarente, L. (2007). Sirtuins in aging and disease. *Cold Spring Harbor Symposia on Quantitative Biology, 72:* 483-488.

Hajimehdipoor, H., Shahrestani, R., and Shekarchi, M. (2014). Investigating the synergistic antioxidant effects of some flavonoid and phenolic compounds. *Research Journal of Pharmacognosy, 1:* 35-40.

Haminiuk, C. W. I., Maciel, G. M., Plata-Oviedo, M. S. V., and Peralta, R. M. (2012). Phenolic compounds in fruits – an overview. *International Journal of Food Science & Technology*, *47:* 2023–2044.

Hassimotto, N. M., Moreira, V., do Nascimento, N. G., Souto, P. C., Teixeira, C. and Lajolo, F. M. (2013). Inhibition of carrageenan-induced acute inflammation in mice by oral administration of anthocyanin mixture from wild mulberry and cyanidin-3-glucoside. *BioMed Research Internationa*l, *2013:* 1-10.

Heim, K. E., Tagliaferro, A. R., and Bobilya, D. J. (2002). Flavonoid antioxidants: chemistry, metabolism and structure-activity relationships. *Journal of Nutritional Biochemistry*, *13*: 572-584.

Hidalgo, M., Sánchez-Moreno, C., and Pascual-Teresa, S. (2010). Flavonoid-flavonoid interaction and its effect on their antioxidant activity. *Food Chemistry, 121:* 691-696.

Higuchi, Y., Kojima, M., Ishii, G., Aoyagi, K., Sasaki, H., and Ochiai, A. (2015). Gastrointestinal fibroblasts have specialized, diverse transcriptional phenotypes: a comprehensive gene expression analysis of human fibroblasts. *PLoS ONE, 10:* 1-9.

Hori, Y. S., Kuno, A., Hosoda, R., and Horio, Y. (2013). Regulation of FOXOs and p53 by SIRT1 modulators under oxidative stress. *PLoS ONE, 8:* 1-9.

Huang, D., Ou, B., and Prior, R. L. (2005). The chemistry behind antioxidant capacity assays. *Journal of Agricultural and Food Chemistry, 53:* 1841-1856.

Hussain, M. B., Hassan, S., Waheed, M., Javed, A., Farooq, M. A., and Tahir, A. (2019). Bioavailability and metabolic pathway of phenolic compounds. In: *Plant Physiological Aspects of Phenolic Compounds.* Soto-Hernández, M., García-Mateos, R., and Palma Tenango, M. (Eds). Intechopen, pp. 425-662.

Ignat, I., Volf, I., and Popa, V. I. (2011). A critical review of methods for characterisation of polyphenolic compounds in fruits and vegetables. *Food Chemistry*, *126:* 1821–1835.

Imai, S. (2009). Nicotinamide phosphoribosyltransferase (Nampt): A link between NAD biology, metabolism, and diseases. *Current Pharmaceutical Design, 15:* 20-28.

Jin, X. H., Ohgami, K., Shiratori, K., Suzuki, Y., Koyama, Y., Yoshida, K., Ilieva, I., Tanaka, T., Onoe, K., and Ohno, S. (2006). Effects of blue honeysuckle (*Lonicera caerulea L.*) extract on lipopolysaccharide-induced inflammation *in vitro* and *in vivo*. *Experimental Eye Research, 82:* 860–867.

Jin, X., Chen, M., Yi, L., Chang, H., Zhang, T., Wang, L., Ma, W., Peng, X., Zhou, Y., and Mi, M. (2014). Delphinidin-3-glucoside protects human umbilical vein endothelial cells against oxidized low-density lipoprotein-induced jury by autophagy upregulation via the AMPK/SIRT1 signaling pathway. *Molecular Nutrition & Food Research, 58:* 1-8.

Jurikova, T., and Matuškovič, J. (2007). The study of irrigation influence on nutritional value of *Lonicera kamtschatica-* cultivar Gerda 25 and *Lonicera edulis* berries under the Nitra conditions during 2001-2003. *Horticultural Science, 34:* 11-16.

Jurikova, T., Rop, O., Mlček, J., Sochor, J., Balla, S., Szekeres, L., Hegedusova, A., Hubalek, J., Adam, V., and Kizek, R. (2012a). Phenolic profile of edible honeysuckle berries (Genus *Lonicera*) and their biological effects. *Molecules, 17*: 61-79.

Jurikova, T., Sochor, J., Rop, O., Mlček, J., Balla, S., Szekeres, L., Žitny, R., Zitka, O., Adam, V., and Kizek, R. (2012b). Evaluation of polyphenolic profile and nutritional value of non-traditional fruit species in the Czech Republic-a comparative study. *Molecules, 17:* 8968-8981.

Kaeberlein, M. (2010). Resveratrol and rapamycin: are they anti-aging drugs? *BioEssays, 32:* 96-99.

Kähkönen, M. P, and Heinonen, M. (2003). Antioxidant activity of anthocyanins and their aglycons. *Journal of Agricultural and Food Chemistry, 51*: 628-633.

Khattab, R., Brooks, M. S., and Ghanem, A. (2015). Phenolic analyses of haskap berries (*Lonicera caerulea* L.): spectrophotometry versus high performance liquid chromatography. *International Journal of Food Properties, 19:* 1708-1725.

Khattab, R., Ghanem, A., and Brooks, M. S. (2016). Quality of dried haskap berries (*Lonicera caerulea* L.) as affected by prior juice extraction, osmotic treatment, and drying conditions. *Drying Technology, 35:* 375-391.

Khoddami, A., Wilkes, M. A., and Roberts, T. H. (2013). Techniques for analysis of plant phenolic compounds. *Molecules, 18*: 2328-2375.

Kleiner, D. E., and Stetler-Stevenson, W. G. (1999). Matrix metalloproteinases and metastasis. *Cancer Chemotherapy and Pharmacology, 43:* 42-51.

Kong, J., Chia, L., Goh, N., Chia., T., and Brouillard, R. (2003). Analysis and biological activities of anthocyanins. *Phytochemistry, 64:* 923-933.

Kucharska, A., Sokół-Łętowska, A., Oszmiański, J., Piórecki, N., and Fecka, I. (2017). Iridoids, phenolic compounds and antioxidant activity of edible honeysuckle berries (*Lonicera caerulea* var. *kamtschatica Sevast.). Molecules, 22:* 405-412.

Kumar, S. and Pandey, A. K. (2013). Chemistry and biological activities of flavonoids: an overview. *The Scientific World Journal*, *2013:* 1-16.

Kusznierewicz, B., Piekarska, A., Mrugalska, B., Konieczka, P., Namiesnik, J., and Bartoszek, A. (2012). Phenolic composition and antioxidant properties of Polish blue-berried honeysuckle genotypes by HPLC-DAD-MS, HPLC postcolumn derivatization with ABTS or FC, and TLC with DPPH visualization. *Journal of Agricultural and Food Chemistry, 60:* 1755-1763.

Lan, F., Cacicedo, J., and Ruderman, N. (2010). Sirt1 knockdown promotes senescence-like phenotype in 3T3L1 adipocyte, that is prevented by Sirt1-independent active LKB1 expression. *Diabetes, 59:* 1-8.

Lee, H. J., Suh, D. H., Jung, E. S., Park, H. M., Jung, G., Do, S., and Lee, C. H. (2015). Metabolomics of *Lonicera caerulea* fruit during ripening and its relationship with color and antioxidant activity. *Food Research International, 78:* 343-351.

Lee, K. M., Choi, K. H., and Ouellette, M. M. (2004). Use of exogeneous hTERT to immortalize primary human cells. *Cytotechnology, 45:* 33-38.

Li, A., Li, S., Zhang, Y., Xu, X., Chen, Y., and Li, H. (2014). Resources and biological activities of natural polyphenols. *Nutrients, 6:* 6020-6047.

Li, D., Wang, P., Luo, Y., Zhao, M., and Chen, F. (2017). Health benefits of anthocyanins and molecular mechanisms: update from recent decade. *Critical Reviews in Food Science and Nutrition, 57:* 1729–1741.

Lin, D., Xiao, M., Zhao, J., Li., Z., Xing, B., Li, X., Kong, M., Li, L., Zhang, Q., Liu, Y., Chen, H., Qin, W., Wu, H., and Chen, S. (2016). An overview of plant phenolic compounds and their importance in human nutrition and management of type 2 diabetes. *Molecules, 21:* 1-19.

Liu, S., Sui, Q., Zhao, Y., and Chang, X. (2019). *Lonicera caerulea* berry polyphenols activate SIRT1, enhancing inhibition of Raw264.7 macrophage foam cell formation and promoting cholesterol efflux. *Journal of Agricultural and Food Chemistry, 67:* 7157-7166.

170

Maiese, K., Chong, Z. Z., Shang, Y. C., and Hou, J. (2008). FoxO proteins: cunning concepts and considerations for the cardiovascular system. *Clinical Science, 116:* 191-203.

Manach, C., Scalbert, A., Morand, C., Rémésy, C., and Jiménez, L. (2003). Polyphenols: food sources and bioavailability. *American Journal of Clinical Nutrition, 79*: 727-747.

Maniyar, S. A., Jargar, J. G., Das, S. N., Dhunsasi, S. A., and Das, K. K. (2012). Alteration of chemical behavior of L-ascorbic acid in combination with nickel sulfate at different pH solutions *in vitro*. *Asian Pacific Journal of Tropical Biomedicine, 2*: 220-232.

Matchett, M. D., MacKinnon, S. L., Sweeney, M. I., Gottschall-Pass, K. T., and Hurta, R. A. (2006). Inhibition of matrix metalloproteinase activity in DU145 human prostate cancer cells by flavonoids from lowbush blueberry (*Vaccinium angustifolium*): possible roles for protein kinase C and mitogen-activated protein-kinase-mediated events. *Journal of Nutritional Biochemistry, 2:* 117– 125.

Mathew, S., Abraham, T. A., and Zakaria, Z. A. (2015). Reactivity of phenolic compounds towards free radicals under in vitro conditions. *Journal of Food Science and Technology, 52*: 5790-5798.

McDougall, G. J., Ross, H. A., Ikeji, M., and Stewart, D. (2008). Berry extracts exert different antiproliferative effects against cervical and colon cancer cells grown *in vitro. Journal of Agricultural and Food Chemistry, 56:* 3016-3023.

Merken, H. M., and Beecher, G. R. (2000). Measurement of food flavonoids by hig performance liquid chromatography: a review. *Journal of Agricultural and Food Chemistry, 48:* 577-599.

Mikulic-Petkovsek, M., Schmitzer, V., Slatnar, A., Stampar, F., and Veberic, R. (2012). Composition of sugars, organic acids, and total phenolics in 25 wild or cultivated berry species. *Journal of Food Science, 77:* 1064-1070.

Murakami, Y., Kawata, A., Ito, S., Katayama, T., and Fujisawa, S. (2015). Radical-scavenging and anti-inflammatory activity of quercetin and related compounds and their combinations against RAW264.7 cells stimulated with *Porphyromonas gingivalis* Fimbriae. Relationships between anti-inflammatory activity and quantum chemical

parameters. *In vivo: International Journal of Experimental and Clinical Pathophysiology and Drug Research, 29:* 701-710.

National Center for Biotechnology Information (2018). US National Library of Medicine. Available at https://pubchem.ncbi.nlm.nih.gov/compound/malic_acid#section=Top (Accessed July 30, 2018).

Ochmian, I. Skupień, K., Grajkowski, J., Smolik, M., and Ostrowska, K. (2012). Chemical composition and physical characteristics of fruits of two cultivars of blue honeysuckle (*Lonicera caerulea* L.) in relation to their degree of maturity and harvest date. *Notulae Botanicae Horti Agrobotanici Cluj-Napoca, 40:* 155-162.

Oszmianski, J., Wojdylo, A., and Lachowicz, S. (2016). Effect of dried powder preparation process on polyphenolic content and antioxidant activity of blue honeysuckle berries (*Lonicera caerulea* L. var. *kamtschatica*). *LWT – Food Science and Technology, 67:* 214-222.

Ozga, J. A., Saeed, A., and Reinecke, D. M. (2006). Anthocyanins and nutrient components of Saskatoon fruits (*Amelanchier alnifolia* Nutt.*). Canadian Journal of Plant Science, 86:* 193-197.

Pacholec, M., Bleasdale, J. E., Chrunyk, B., Cunningham, D., Flynn, D., Garofalo, R. S., Griffith, D., Griffor, M., Loulakis, P., Pabst, B., Qiu, X., Stockman, B., Thanabal, V., Alison Varghese, Ward, J., Withka, J., and Ahn, K. (2010). SRT1720, SRT2183, SRT1460, and resveratrol are not direct activators of SIRT1. *The Journal of Biological Chemistry, 285:* 8340-8351.

Palíková, I., Heinrich, J., Bednář, P, Marhol, P., Křen, V., Cvak, L., Valentová, K., Růžička, F., Holá, V., Kolář, M., Šimánek, V., and Ulrichová, J. (2008). Constituents and antimicrobial properties of blue honeysuckle: a novel source for phenolic antioxidants. *Journal of Agricultural and Food Chemistry, 56:* 11883-11889.

Pandey, K. B. and Rizvi, S. I. (2009). Plant polyphenols as dietary antioxidants in human health and disease. *Oxidative Medicine and Cellular Longevity*, *2*: 270-278.

Park, D., Jeong, H., Lee, M. N., Koh, A., Kwon, O., Yang, Y. R., Noh, J., Suh, P., Park, H., and Ryu, S. H. (2016). Resveratrol induces autophagy by directly inhibiting mTOR through ATP competition. *Scientific Reports, 6:* 1-9.

Park, M., Yoo, J., Lee, Y., and Lee, H. (2019). *Lonicera caerulea* extract attenuates non-alcoholic fatty liver disease in free fatty acid-induced HepG2 hepatocytes and in high fat diet-fed mice. *Nutrients, 11*: 494-500.

Phan, M., Paterson, J., Bucknall, M., and Arcot, J. (2018). Interactions between phytochemicals from fruits and vegetables: effects on bioactivities and bioavailability. *Critical Reviews in Food Science and Nutrition, 24:* 1310-1329.

Prior, R. L. and Wu, X. (2006). Anthocyanins: structural characteristics that result in unique metabolic patterns and biological activities. *Free Radical Research*, *40*: 1014–1028.

Rahman, S. and Islam, R. (2011). Mammalian Sirt1: insights on its biological functions. *Cell Communication and Signaling, 9:* 1-12.

Raudsepp, P., Anton, D., Roasto, M., Meremäe, K., Pedastsaar, P., Mäesaar, M., Raal, A., Laikoja, K., and Püssa, T. (2013). The antioxidative and antimicrobial properties of the blue honeysuckle (*Lonicera caerulea* L.), Siberian rhubarb (*Rheum rhaponticum* L.) and some other plants, compared to ascorbic acid and sodium nitrite. *Food Control, 31:* 129-135.

Ribeiro de Souza, D. (2017). Chemical composition of select saskatoon berry varieties with an emphasis on phenolics. MSc thesis, University of Saskatchewan, September 2017.

Ribeiro de Souza, D., Willems, J. L., and Low, N. H. (2019). Phenolic composition and antioxidant activities of saskatoon berry fruit and pomace. *Food Chemistry, 290*: 168-177.

Rice-Evans, C. A., Miller, N. J., and Paganga, G. (1996). Structure-antioxidant activity relationships of flavonoids and phenolic acids. *Free Radical Biology and Medicine, 20*: 933-956.

Rios de Souza, V., Pereira, P., Silva, T., Lima, L., Pio, R., and Quieroz, F. (2014). Determination of the bioactive compounds, antioxidant activity and chemical composition of Brazilian

blackberry, red raspberry, strawberry, blueberry and sweet cherry fruits. *Food Chemistry, 156:* 362-368.

Rogina, B. and Helfand, S. L. (2004). Sir2 mediates longevity in the fly through a pathway related to calorie restriction. *Proceedings of the National Academy of Sciences, 101:* 15998-16003.

Roulis, M., and Flavell, R. A. (2016). Fibroblasts and myofibroblasts of the intestinal lamina propia in physiology and disease. *Differentiation, 92:* 116-131.

Rupasinghe, H. P. V., Yu, L. J., Bhullar, K. S., and Bors, B. (2012). Short communication: haskap (*Lonicera caerulea*): a new berry crop with high antioxidant capacity. *Canadian Journal of Plant Science, 92:* 1311-1317.

Rupasinghe, H. P. V., Boehm, M. M. A., Sekhon-Loodu, S., Parmar, I., Bors, B., and Jamieson, A. R. (2015). Anti-inflammatory activity of haskap cultivars is polyphenols-dependent. *Biomolecules, 5:* 1079-1098.

Rupasinghe, H. P. V., Arumuggam, N., Amararathna, M., and De Silva, A. B. K. H. (2018). The potential health benefits of haskap (*Lonicera caerulea* L.): role of cyanidin-3-*O*-glucoside. *Journal of Functional Foods, 44:* 24-39.

Seeram, N. P. (2008). Berry fruits for cancer prevention: current status and future prospects. *Journal of Agricultural and Food Chemistry*, 56: 630–635.

Senica, M., Bavec, M., Stampar, F., and Mikulic-Petkovsek, M. (2017). Blue honeysuckle (*Lonicera caerulea* subsp. *Edulis* (Turcz. ex Herder) Hultén) berries and changes in their ingredients across different locations. *Journal of the Science of Food and Agriculture, 98:* 1-8.

Senica, M., Stampar, F., and Mikulic-Petkovsek, M. (2018). Blue honeysuckle (*Lonicera caerulea* L. subs. *edulis*) berry: a rich source of some nutrients and their differences among four different cultivars. *Scientia Horticulturae, 238:* 215-221.

Sharma, S., Rana, S., Patial, V., Gupta, M., Bhushan, S., and Padwad, Y. S. (2016). Antioxidant and hepatoprotective effect of polyphenols from apple pomace extract via apoptosis

inhibition and Nrf2 activation in mice. *Human & Experimental Toxicology, 35:* 1264-1275.

Srivastava, A., Akoh, C. C., Fischer, J., and Krewer, G. (2007). Effect of anthocyanin fractions from selected cultivars of Georgia-grown blueberries on apoptosis and phase II enzymes. *Journal of Agricultural and Food Chemistry*, *55:* 3180–3185.

Suchankova, G., Nelson, L. E., Gerhart-Hines, Z., Kelly, M., Gauthier, M., Saha, A. K., Ido, Y., Puigserver, P., and Ruderman, N. B. (2009). Concurrent regulation of AMP-activated protein kinase and SIRT1 in mammalian cells. *Biochemical and Biophysical Research Communications, 378:* 836-841.

Tang, B. L., (2010). Resveratrol is neuroprotective because it is not a direct activator of Sirt1-A hypothesis. *Brain Research Bulletin, 3:* 359-361.

Taormina, G., and Mirisola, M. G. (2014). Calorie restriction in mammals and simple model organisms. *BioMed Research International, 2014:* 1-10.

Tarahovsky, Y. S., Kim, Y. A., Yagolnik, E. A., and Muzafarov, E. N. (2014). Flavonoid membrane interactions: involvement of flavonoid-metal complexes in raft signaling. *Biochimica et Biophysica Acta-Biomembranes, 1838:* 1235-1246.

Taverniti, V., Fracassetti, D., Del Bo', C., Lanti, C., Minuzzo, M., Klimis-Zacas, D., Riso, P. and Guglielmetti, S. (2014). Immunomodulatory effect of a wild blueberry anthocyanin-rich extract in human Caco-2 intestinal cells. *Journal of Agricultural and Food Chemistry*, *62*: 8346–8351.

Todorova, I. T., Batovska, D. I., Stamboliyska, B. A., and Parushev, S. P. (2010). Evaluation of the radical scavenging activity of a series of synthetic hydroxychalcones towards the DPPH radical. *Journal of the Serbian Chemical Society, 76*: 491-497.

Tsuda, T., Horio, F., and Osawa, T. (2002). Cyanidin 3-*O*-beta-D-glucoside suppresses nitric oxide production during a zymosan treatment in rats. *Journal of Nutritional Science and Vitaminology*, *48:* 305–310.

United States Department of Agriculture. (2013). USDA Database for the Flavonoid Content of Selected Foods. *Agricultural Research Service.* Available at: https://www.ars.usda.gov/ARSUse rFiles/80400525/Data/Flav/Flav_R03-1.pdf (Accessed August 3, 2017).

United States Department of Agriculture, Agriculture Research Service. (2018). National Nutrient Database for Standard Reference Legacy Release. Available at: https://ndb.nal.usda.gov/ndb/foods/ (Accessed June 25, 2018).

Vermerris, W., and Nicholson, R. (2006). Families of phenolic compounds and means of classification. In: *Phenolic Compound Biochemistry*. Vermerris, W. and Nicholson, R. (Eds). Springer, pp. 1-34.

Vuong, Q. V., Hirun, S., Phillips, P. A., Chuen, T. L. K., Bowyer, M. C., Goldsmith, C. D., and Scarlett, C. J. (2014). Fruit-derived phenolic compounds and pancreatic cancer: perspectives from Australian native fruits. *Journal of Ethnopharmacology, 152*: 227-242.

Wang, H., Cao, G., and Prior, R. L. (1997). Oxygen radical absorbing capacity of anthocyanins. *Journal of Agricultural and Food Chemistry, 45*: 304-309.

Wang, S., Chen, C., Sciarappa, W., Wang, C., and Camp, M. (2008). Fruit quality, antioxidant capacity, and flavonoid content of organically and conventionally grown blueberries. *Journal of Agricultural and Food Chemistry, 56:* 5788-5794.

Wang, N. S. (2017). Wine Fermentation. Department of Chemical & Biomolecular Engineering, University of Maryland. Available at: https://eng.umd.edu/~nsw/ench485/lab12.htm (Accessed June 21, 2018).

Wang, W., Jin, T., Yan, X., He, Y., Wang, B., Xiao, Y., Shang, C., Jiye, Z., and Lin, R. (2017). Hydroxytyrosol regulates the autophagy of vascular adventitial fibroblasts through the SIRT1-mediated signaling pathway. *Canadian Journal of Physiology and Pharmacology, 96:* 88-96.

Wang, C., and Eskiw, C. H. (2019). Cytoprotective effects of avenanthramide C against oxidative and inflammatory stress in normal human dermal fibroblasts. *Scientific Reports, 9:* 1-8.

Welch, C. R., Wu, Q., and Simon, J. E. (2008). Recent advances in anthocyanin analysis and characterization. *Current Analytical Chemistry*, *4:* 75-101.

Willems, J., and Low, N.H. (2012). Major carbohydrate, polyol, and oligosaccharide profiles of agave syrup. Application of this data to authenticity analysis. *Journal of Agricultural and Food Chemistry, 60:* 8745-8754.

Willems, J. L., Khamis, M. M., Saeid, W. M., Purves, R. W., Katselis, G., Low, N. H., and El-Aneed, A. (2016). Analysis of a series of chlorogenic acid isomers using differential ion mobility and tandem mass spectrometry. *Analytica Chimica Acta, 933:* 164-174.

Wojdylo, A., Jáuregui, P. N. N., Carbonell-Barrachina, A. A., Oszmiański, J., and Golis. T. (2013). Variability of phytochemical properties and content of bioactive compounds in *Lonicera caerulea* L. var. *kamtschatica* berries. *Journal of Agricultural and Food Chemistry, 61:* 12072-12084.

Wood, J. G., Rogina, B., Lavu, S., Howitz, K., Helfand, S. L, Tatar, M., and Sinclair, D. (2004). Sirtuin activators mimic caloric restriction and delay ageing in metazoans. *Nature, 430:* 686-689.

Wright, J. S., Johnson, E. R., and Di Labio, G. A. (2001). Predicting the activity of phenolic antioxidants: theoretical method, analysis of substituent effects, and application to major families of antioxidants. *Journal of the American Chemical Society*, *123:* 1173-1183.

Wu, S., Yano, S., Hisanaga, A., He, X., He, J., Sakao, K., and Hou, D. (2016). Polyphenolics from *Lonicera caerulea* L. berry attenuate experimental nonalcoholic steatohepatitis by inhibiting proinflammatory cytokines productions and lipid peroxidation. *Molecular Nutrition & Food Research, 61:* 1-9.

Yamagami, C., Akamatsu, M., Motohashi, N., Hamada, S., and Tanahashi, T. (2005). Quantitative structure-activity relationship studies for antioxidant hydroxybenzalacetones by quantum chemical- and 3-D-QSAR(CoMFA) analyses. *Bioorganic & Medicinal Chemistry Letters, 15*: 2845-2850.

Yamamoto, Y., Hoshino, Y., Masago, H., and Kawano, T. (2014). Attempt for postharvest ripening of immature fruit of haskap (*Lonicera caerulea* L. var. *emphyllocalyx* Nakai), an emerging fruit in Northern Japan. *Advances in Horticultural Science, 28:* 244-249.

Yang, C. S., Landau, J. M., Huang, M., and Newmark, H. L. (2001). Inhibition of carcinogenesis by dietary polyphenolic compounds. *Annual Review of Nutrition*, *21:* 381–406.

Yang, C., Qiu, L., and Xu, Z. (2017). Specific gene silencing using RNAi in cell culture. *Methods in Molecular Biology, 793:* 457-477.

You, Q., Wang, B., Chen, F., Huang, Z., Wang, X., and Luo, P. G. (2011). Comparison of anthocyanins and phenolics in organically and conventionally grown blueberries in selected cultivars. *Food Chemistry, 125:* 201-208.

Zadernowski, R., Naczk, M., and Nesterowicz, J. (2005). Phenolic acid profiles in some small berries. *Journal of Agricultural and Food Chemistry, 53:* 2118-2124.

Zhang, L., Chen, Z., Gong, W., Zou, Y., Xu, F., Chen, L., and Huang, H. (2018). Peonol ameliorates diabetic renal fibrosis through promoting the activation of the Nrf2/ARE pathway via up-regulating SIRT1. *Frontiers in Pharmacology, 9:* 1-12.

Zhu, Y., Ling, W., Guo, H., Song, F., Ye, Q., Zou, T., Li, D., Zhang, Y., Li, G., Xiao, Y., Liu, F., Li, Z., Shi, Z., and Yang, Y. (2013). Anti-inflammatory effect or purified dietary anthocyanin in adults with hypercholesterolemia: a randomized controlled trial. *Nutrition, Metabolism, and Cardiovascular Diseases, 23:* 843-849.

Zunino, S. J., Zhang, Y., Seeram, N. P., and Storms, D. H. (2010). Berry fruit extracts inhibit growth and induce apoptosis of high-risk acute lymphoblastic leukemia cells *in vitro. Journal of Functional Foods, 2:* 187-195.
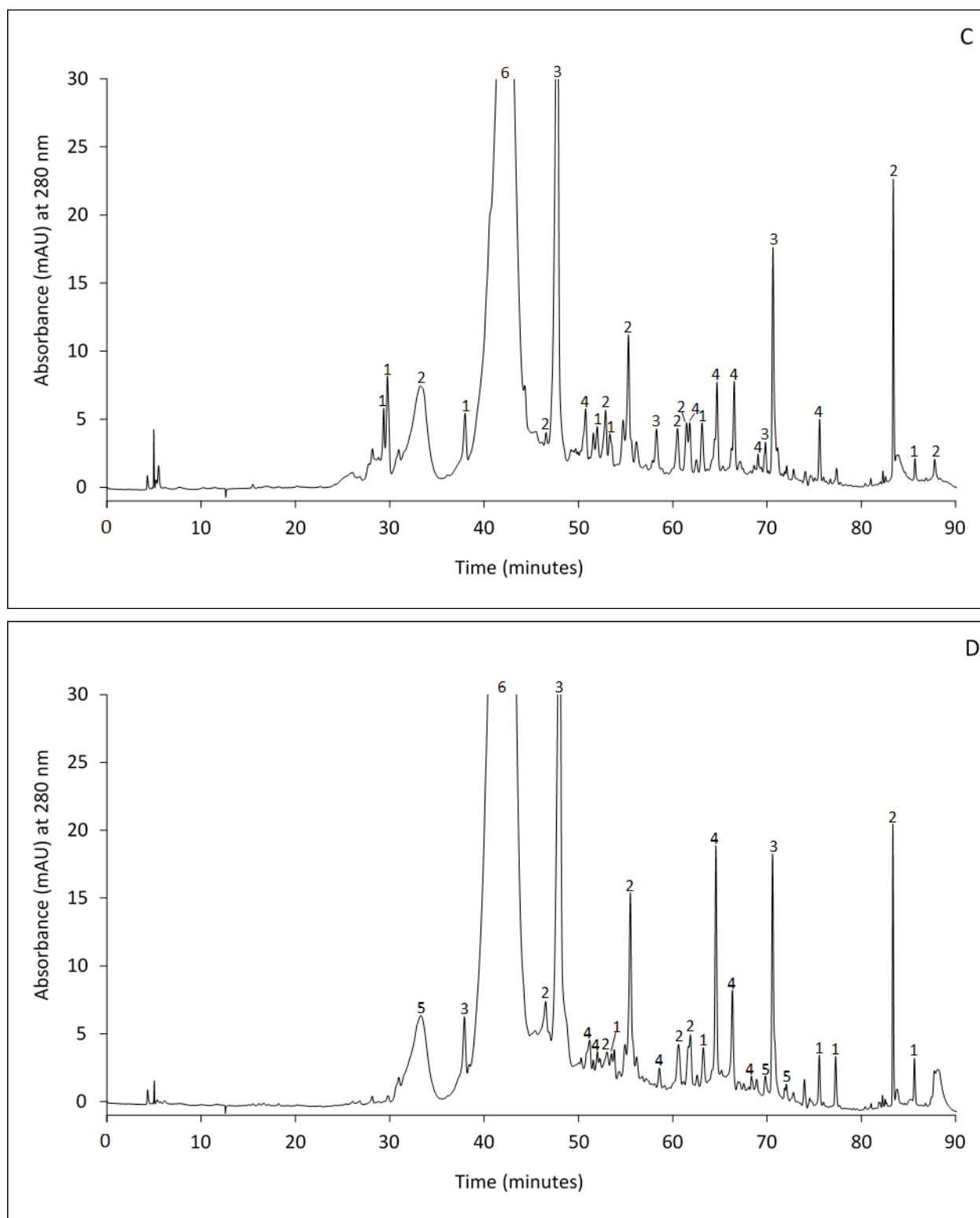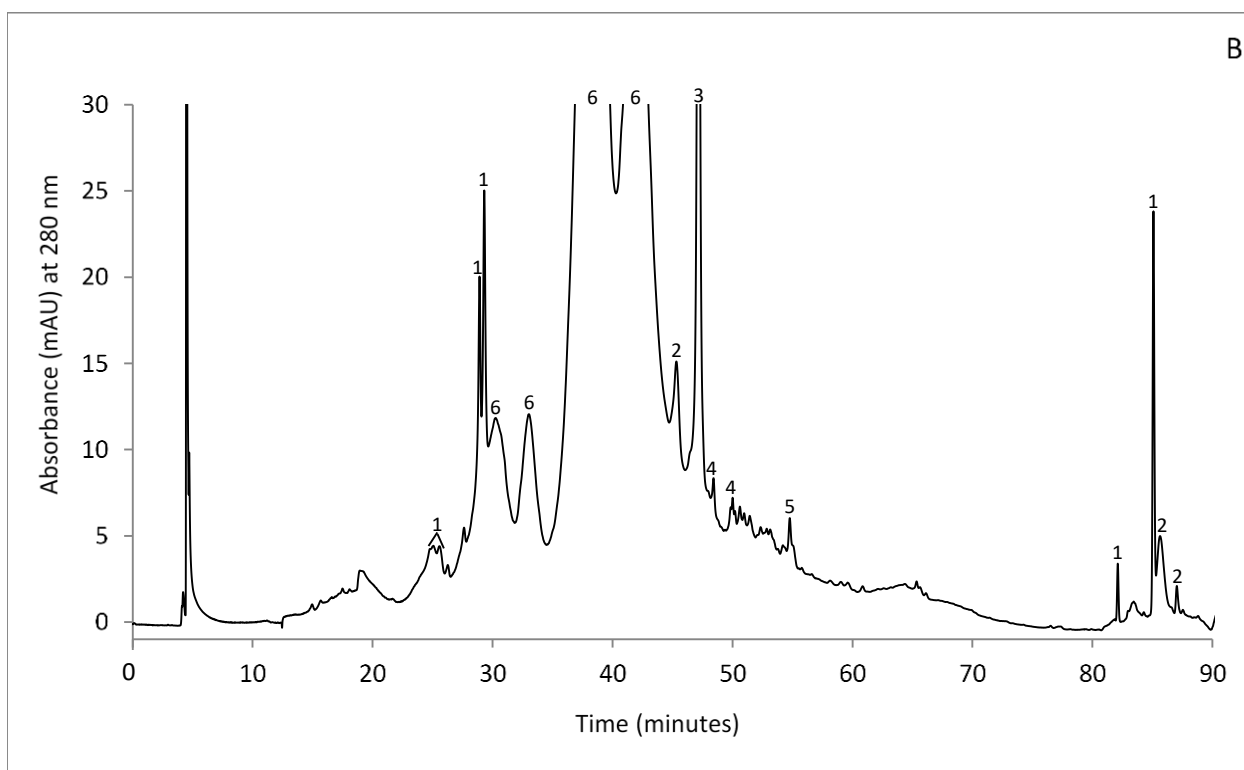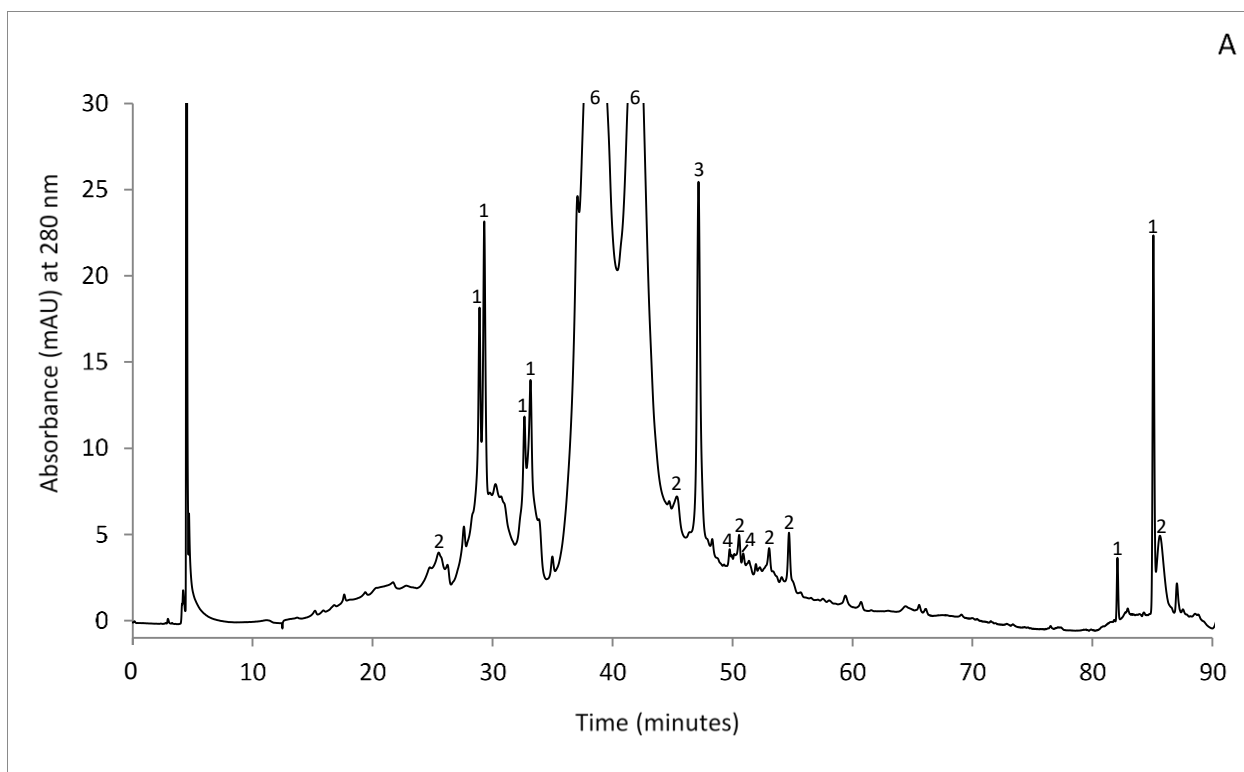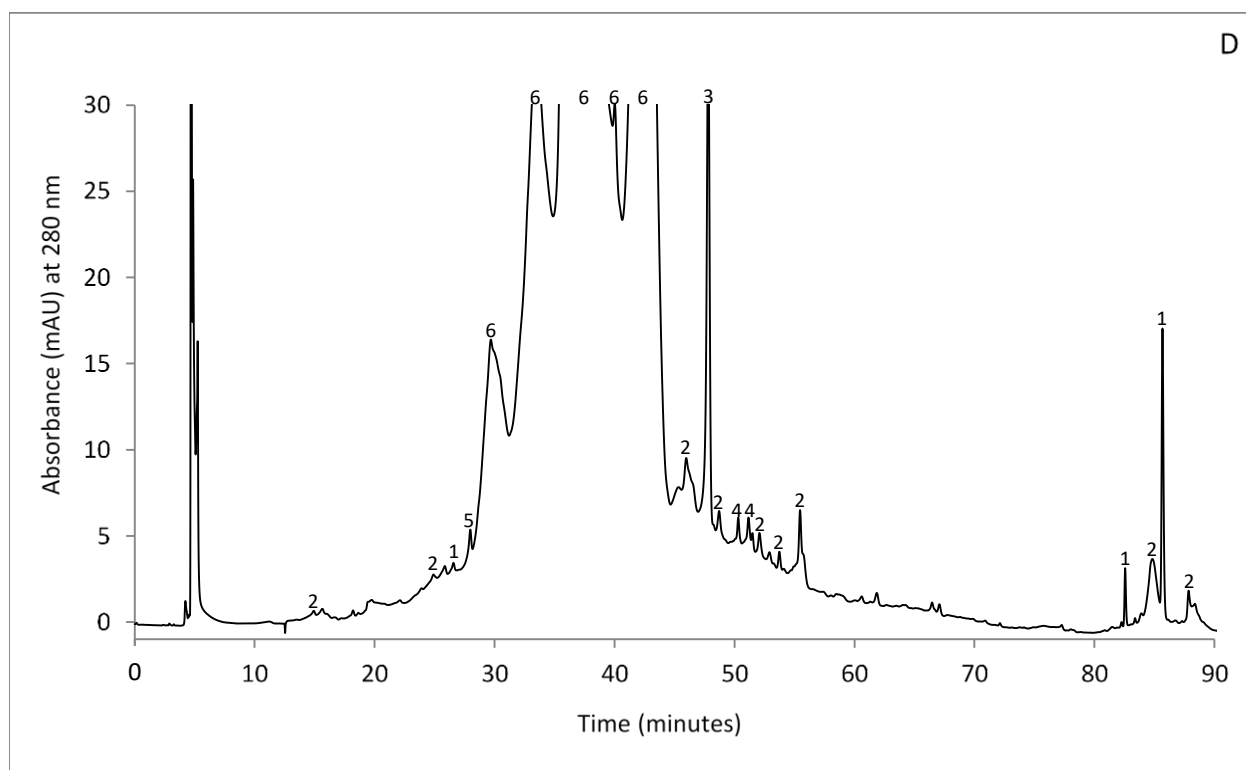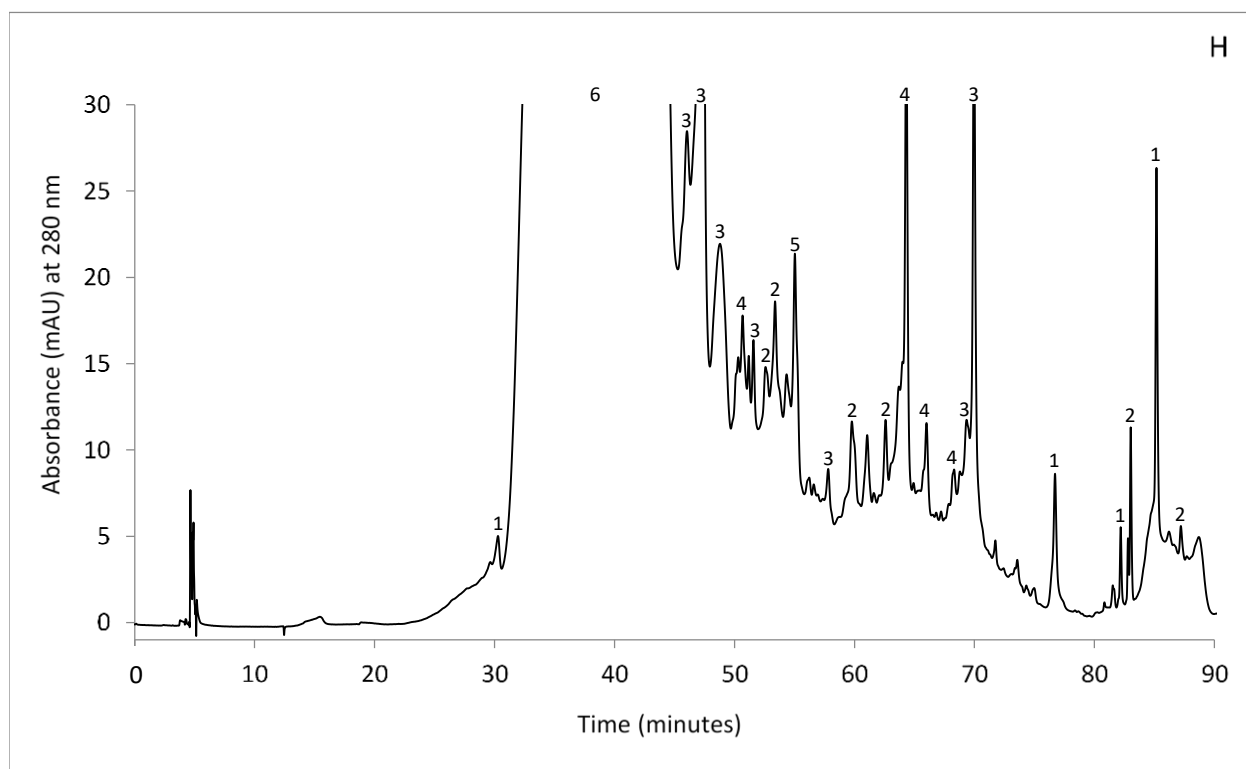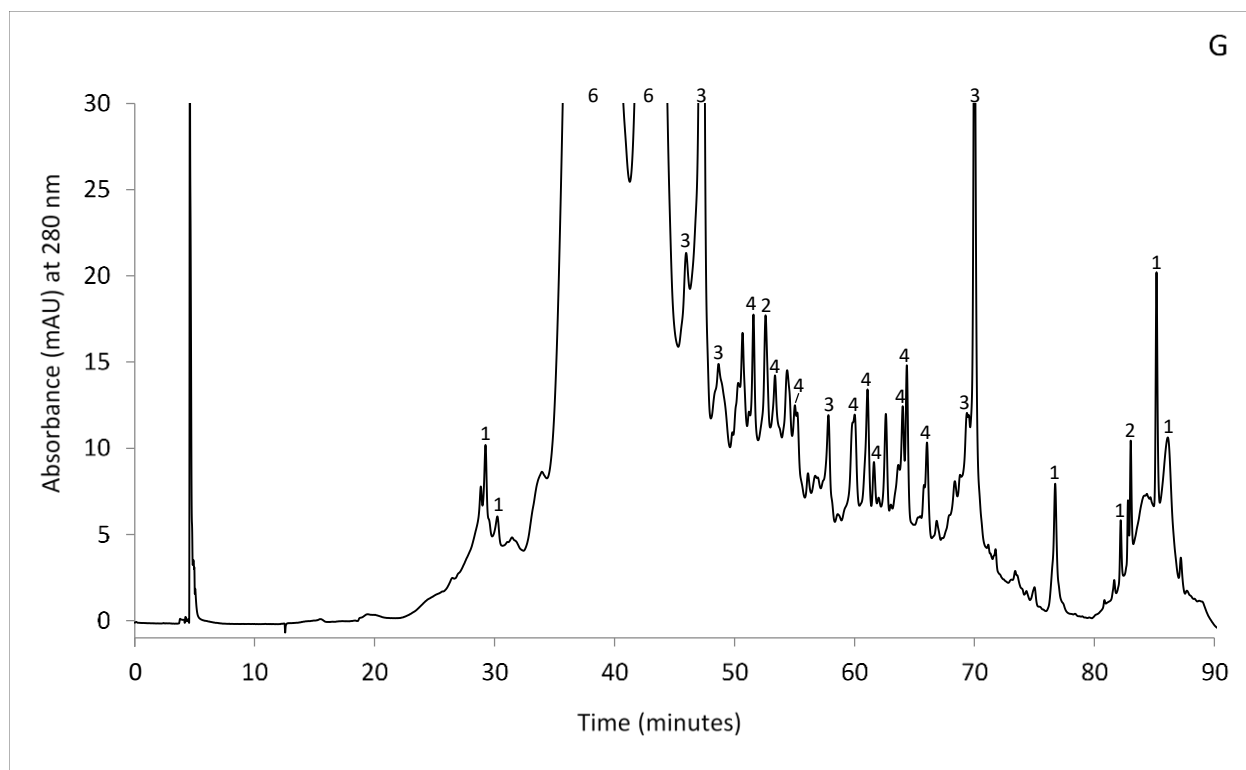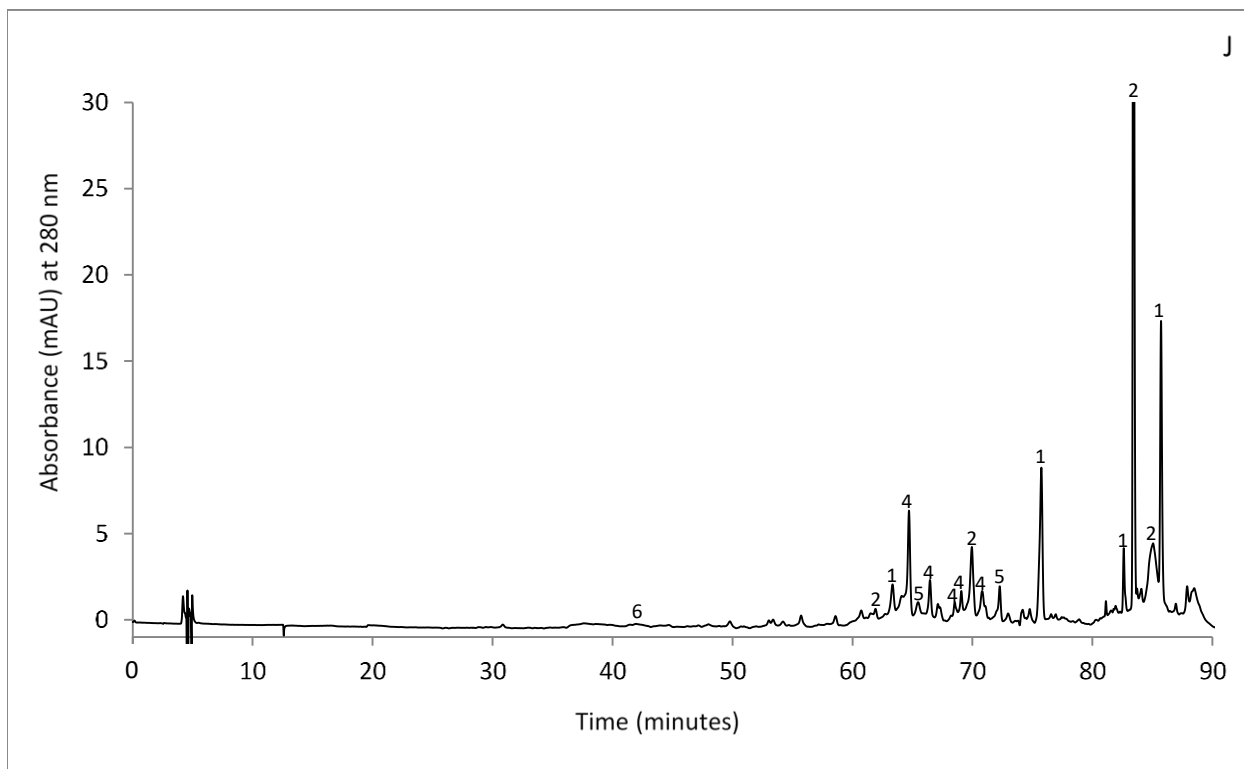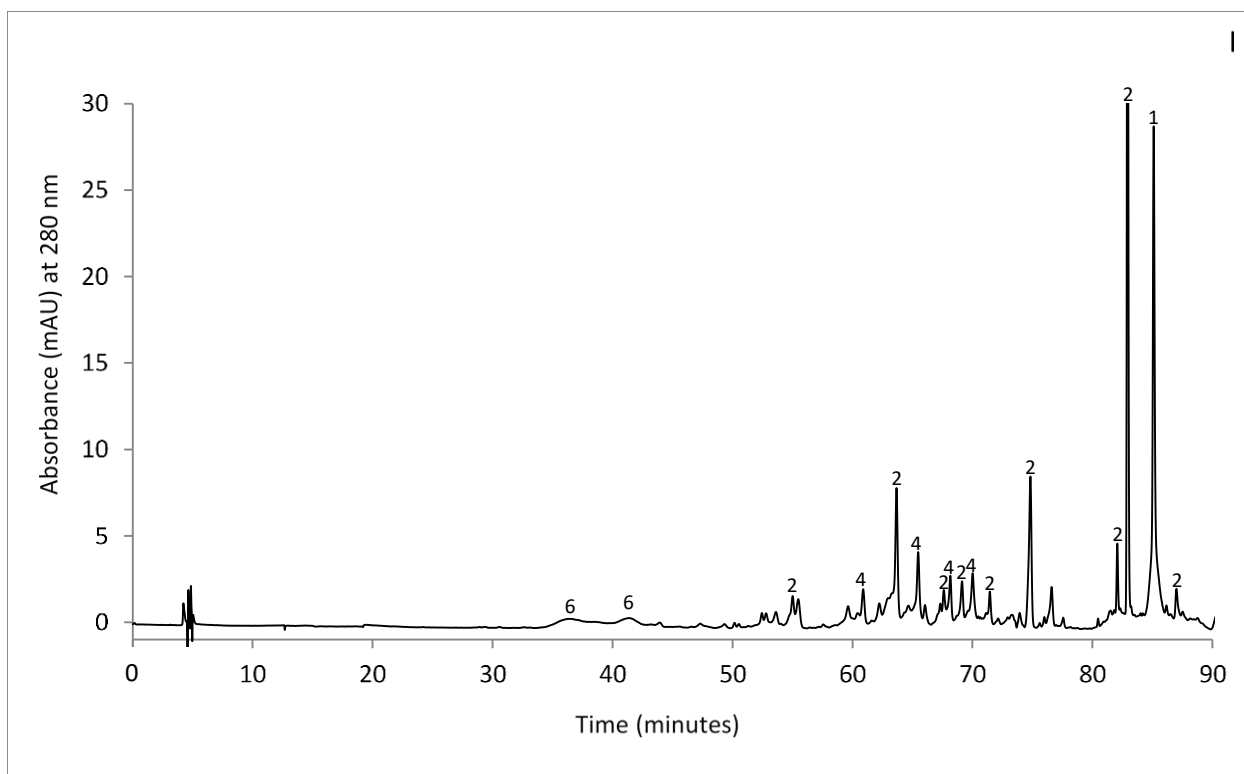
8.0 APPENDIX
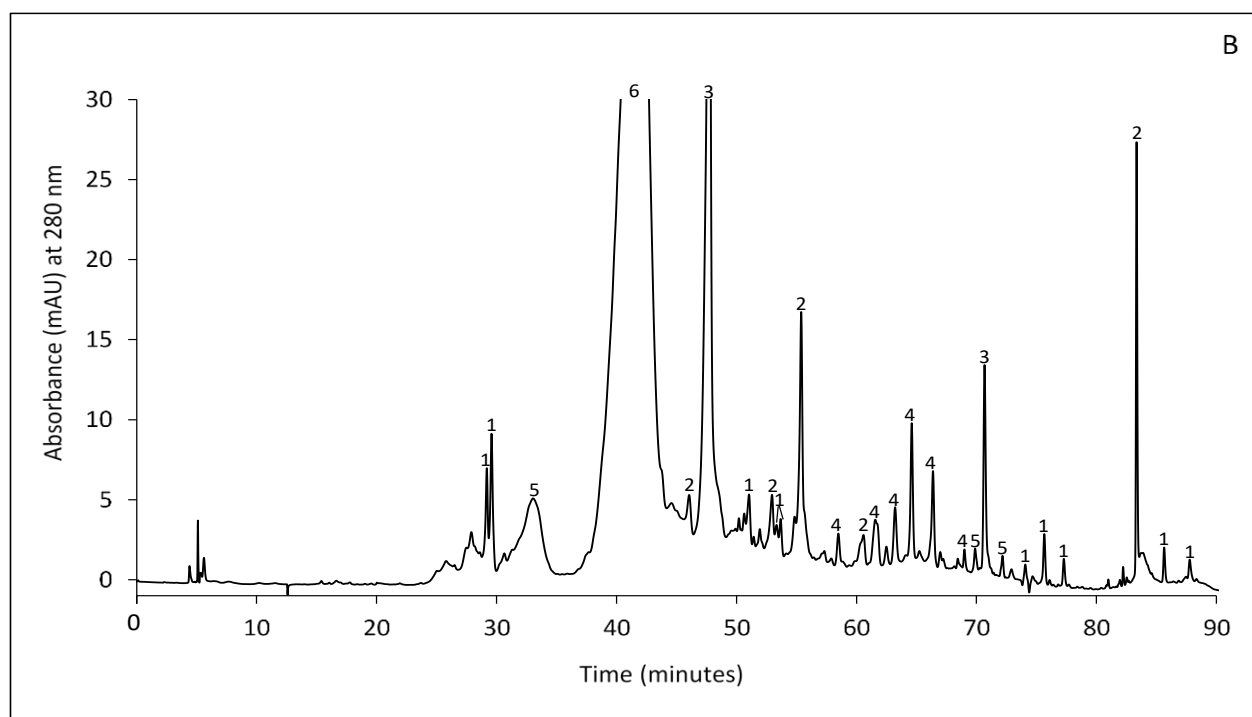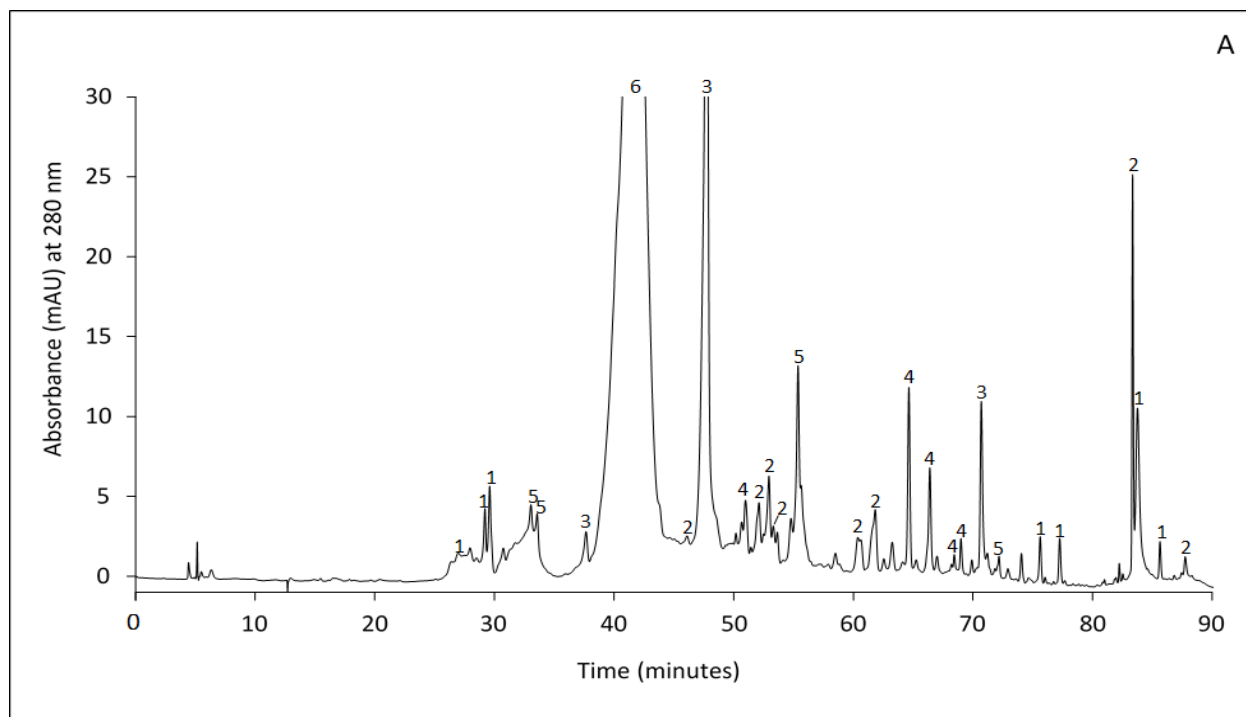
Figure 8.1 HPLC-PDA chromatograms of PR extracts. Chromatogram identification: A. Aurora; B. Blizzard; C. Honey Bee; and D. Indigo Gem. Peak phenolic subclass assignments: 1. hydroxybenzoic acids; 2. flavanols; 3. hydroxycinnamic acids; 4. flavonols; 5. flavanones; and 6. anthocyanins.
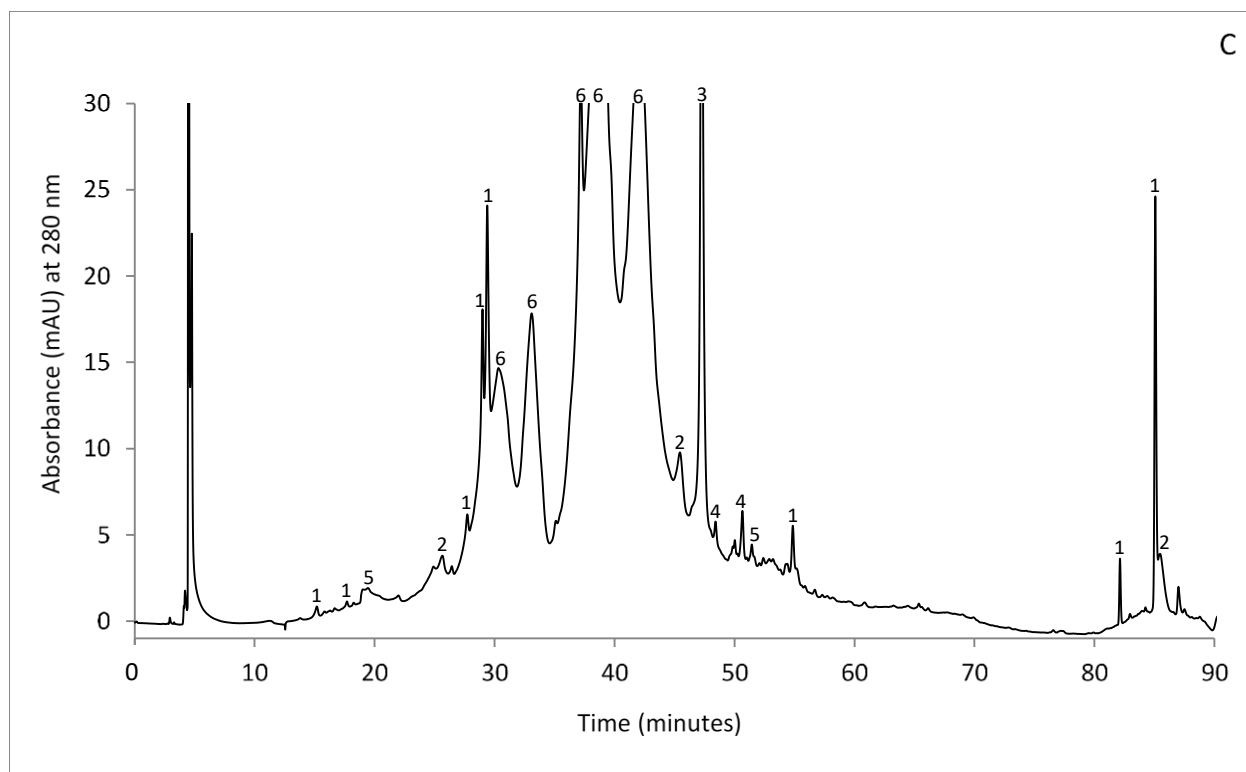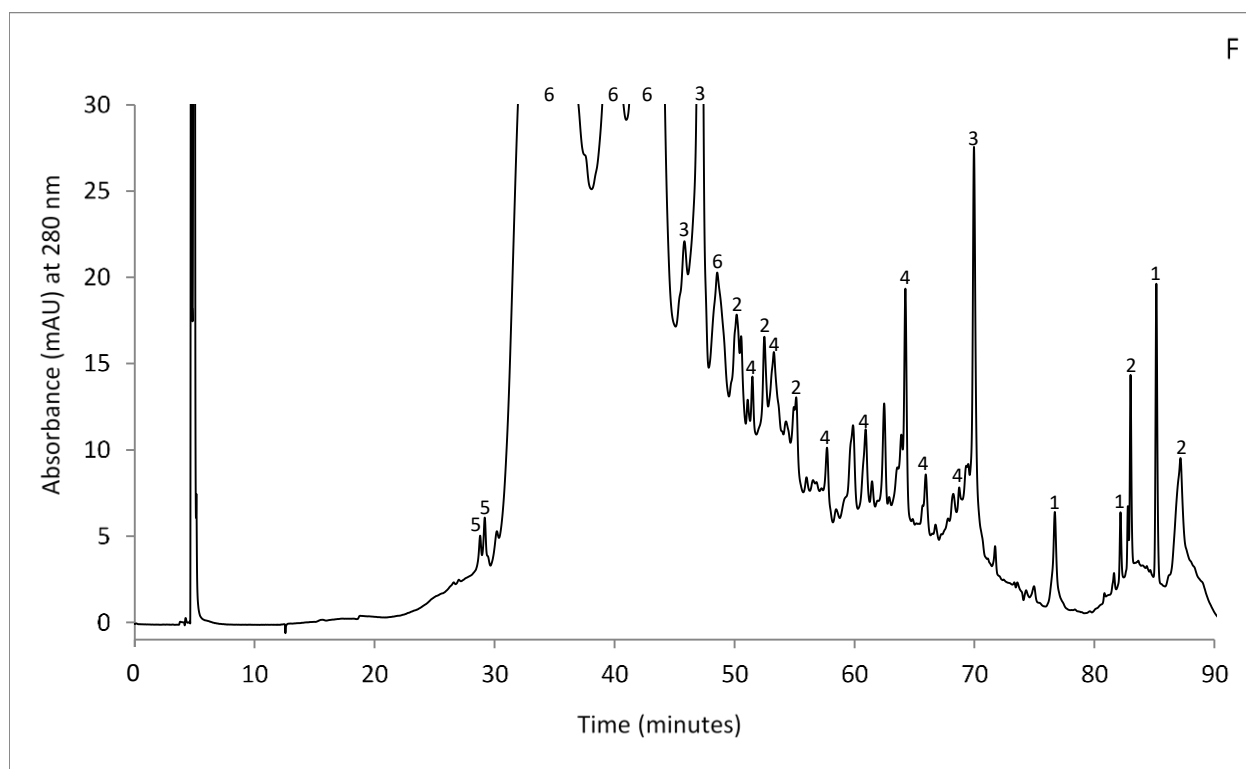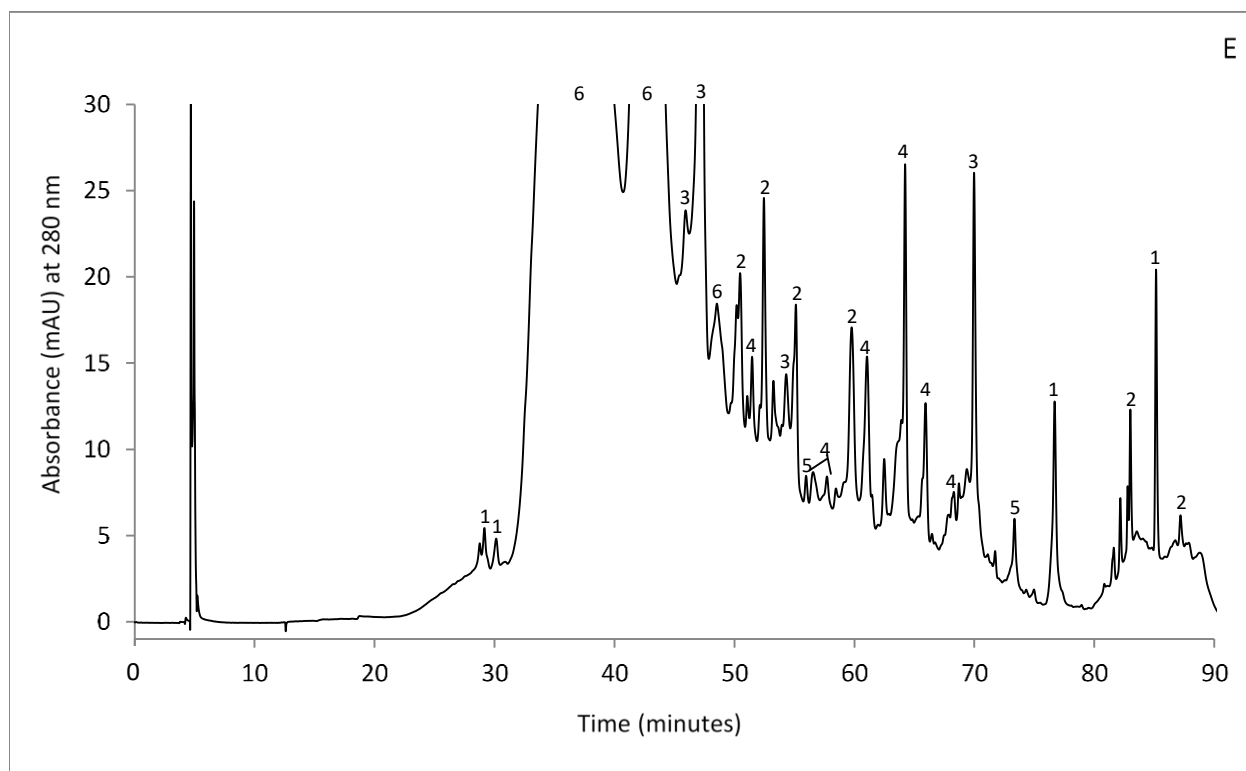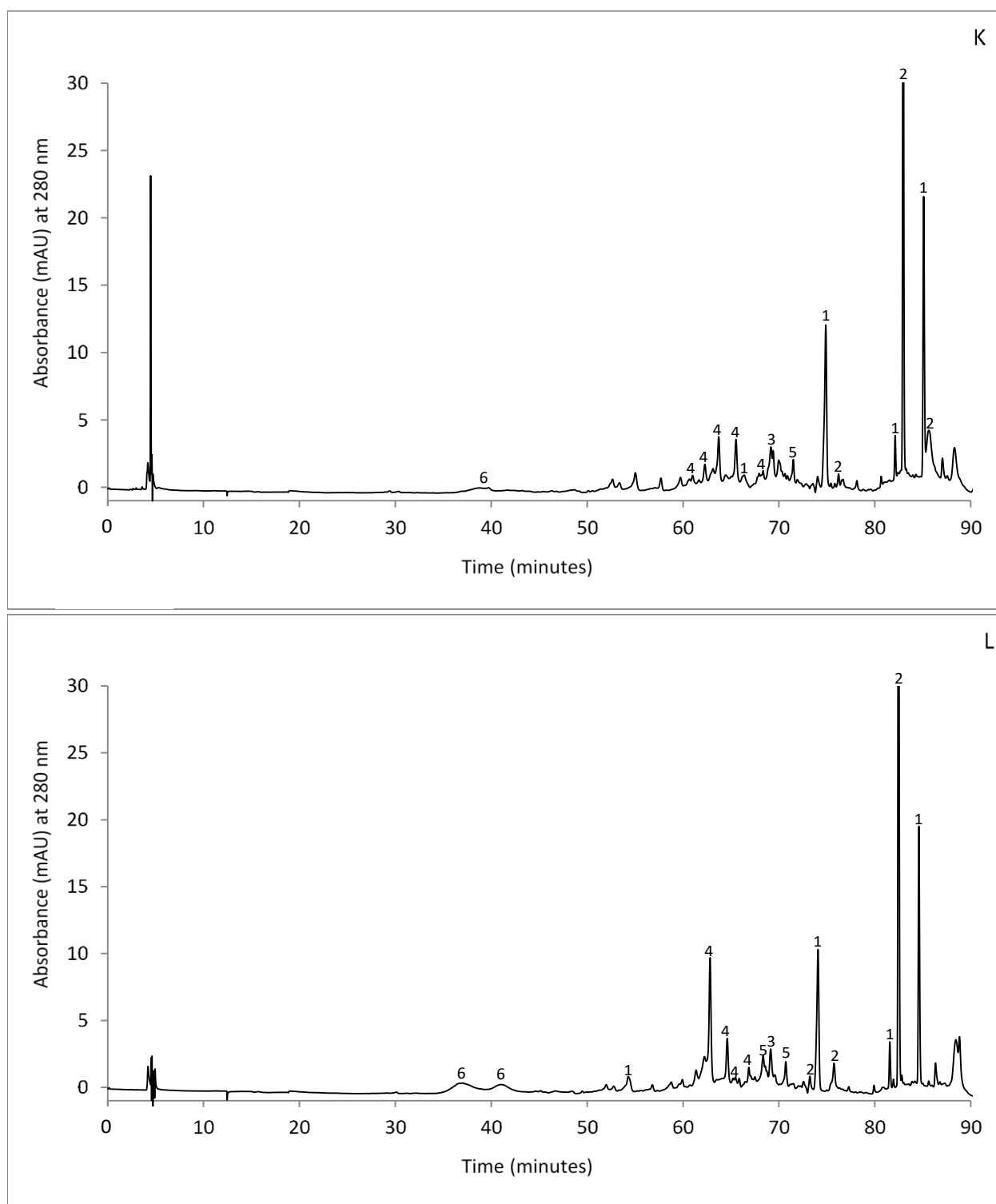
Figure 8.2 HPLC-PDA chromatograms of fractions. Chromatogram identification: A.-D. 40% fractions, A. Aurora; B. Blizzard; C. Honey Bee; D. Indigo Gem; E.-H. 70% fractions, E. Aurora; F. Blizzard; G. Honey Bee; H. Indigo Gem; I.-L. 100% fractions, I. Aurora; J. Blizzard; K. Honey Bee; and L. Indigo Gem. Phenolic subclass assignments: 1. hydroxybenzoic acids; 2. flavanols; 3. hydroxycinnamic acids; 4. flavonols; 5. flavanones; and 6. anthocyanins.

Table 8.1 HPLC-MS/MS precursor and product ion *m/z* values and phenolic identification for the Tundra variety 40% ethanol fraction.

Peak No.[1]	RT[2]	Precursor [M-H]⁻ (*m/z*)	Other Product Ions (*m/z*)	Compound Identification
5a	33.98	627.2	465.1, 447.1, 355.1, 303.1, 285.1, 267.0	Taxifolin-dihexoside
3a	38.94	353.1	191.0, 179.0, 173.1, 151.1, 135.0	3-*O*-caffeoylquinic acid*
6a	42.65	465.1	329.1, 285.0, 241.1, 199.1, 166.0, 149.0, 125.0	Anthocyanins*
3b	49.38	353.1	191.1	5-*O*-caffeoylquinic acid*
5b	52.42	465.1	329.1, 285.0, 303.0, 241.1, 217.0	Taxifolin-hexoside
4a/4b	66.76	463.1	387.1, 381.0, 301.0, 257.0	Quercetin-3-*O*-glucoside*/galactoside*

[1] Peak number matched to peak label of Figure 8.2.
[2] Retention time (min).
* Compound identification confirmed using standards.

Table 8.2 HPLC-MS/MS precursor and product ion *m/z* values and phenolic identification for the Tundra variety 70% ethanol fraction.

Peak Number[1]	RT[2]	Precursor [M-H]⁻ *m/z* values	Product Ion *m/z* values	Compound Identification
6a	42.17	465.1	447.1, 285.0, 241.1, 199.0, 166.0, 139.0	Anthocyanins[*]
7a	46.02	447.0	357.0, 327.0, 299.0, 284.0, 241.0, 133.0	Luteolin-hexoside
3b	48.95	353.1	191.1	5-*O*-caffeoylquinic acid[*]
5a	51.93	465.1	329.1, 303.0, 285.0, 199.0, 166.0	Taxifolin-hexoside
2b	53.80	289.1	254.1, 203.1	Epicatechin[*]
4a	62.71	595.1	300.0, 271.0, 255.0	Quercetin-vicianoside
4b	65.51	609.1	301.0, 271.0, 257.0	Quercetin-3-*O*-rutinoside[*]
4c/4d	67.08	463.1	301.0, 271.0, 257.0	Quercetin-3-*O*-glucoside[*]/ galactoside[*]
3d	71.19	515.1	353.1, 191.1, 179.0	Dicaffeoylquinic acid

[1]Peak number matched to peak label of Figure 8.2.
[2] Retention time (min).
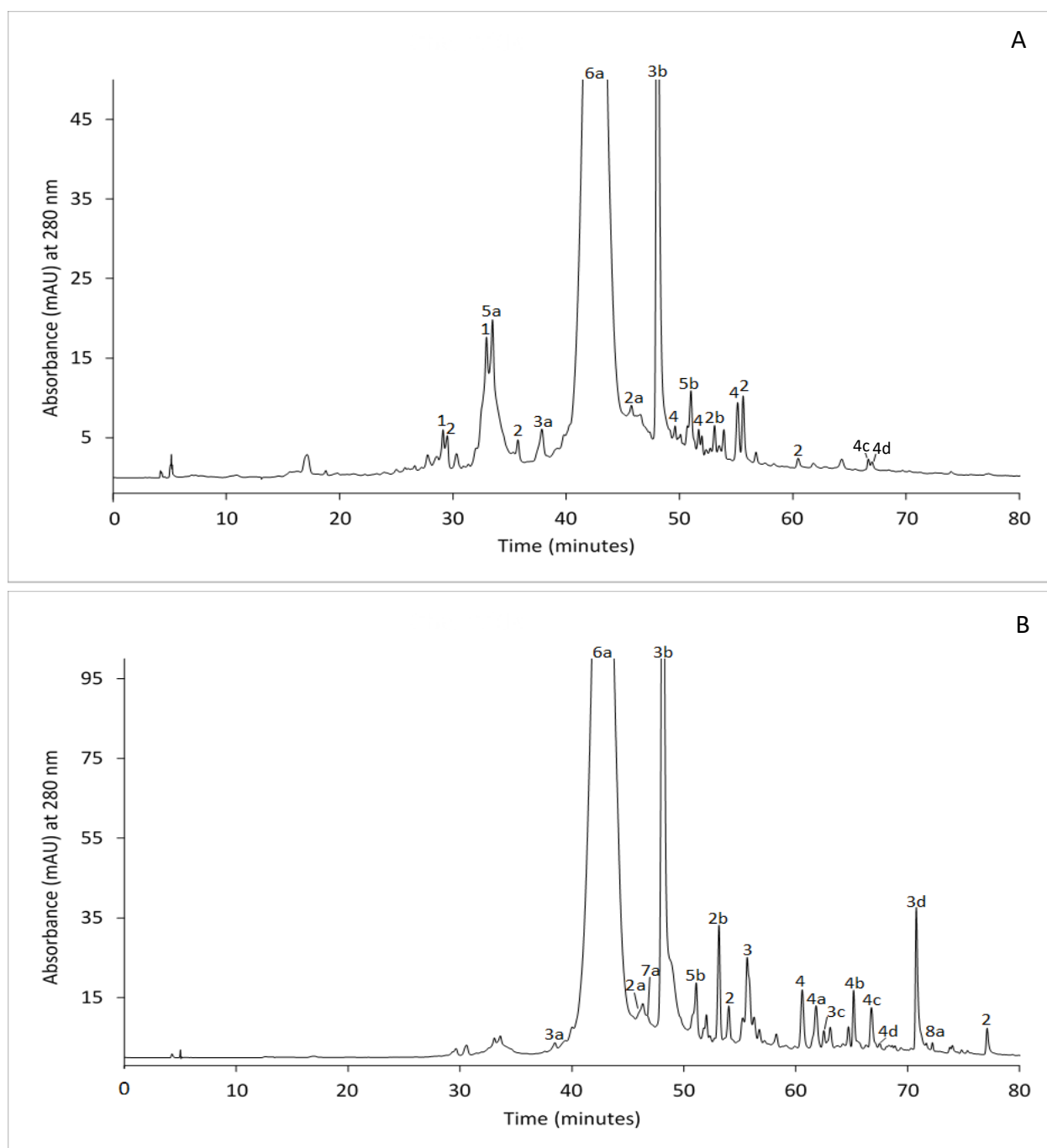[*]Compound identification confirmed using standards.

Figure 8.3 HPLC-PDA chromatograms of Tundra fractions labeled with HPLC-MS/MS results. Chromatogram identification: A. Tundra 40% ethanol fraction; and B. Tundra 70% ethanol fraction. Phenolic subclass assignments: 1. hydroxybenzoic acids; 2. flavanols; 3. hydroxycinnamic acids; 4. flavonols; 5. flavanones; 6. anthocyanins; 7. flavones; and 8. chalcones. Compound identification: 2a. catechin*; 2b. epicatechin*; 3a. 5-O-caffeoylquinic acid*; 3b. 3-O-caffeoylquinic acid*; 3c. ferulic acid*; 3d. dicaffeoylquinic acid; 4a. quercetin-vicianoside; 4b. quercetin-3-O-rutinoside*; 4c. quercetin-3-O-glucoside*; 4d. quercetin-3-O-galactoside*; 5a. taxifolin-dihexoside; 5b. taxifolin-hexoside; 6a. anthocyanins; 7a. luteolin-hexoside; and 8a. phloridzin*. *confirmed using standards.